

SOLID STATE NUCLEAR MAGNETIC RESONANCE METHODOLOGY
AND APPLICATIONS TO STRUCTURE DETERMINATION
OF
PEPTIDES, PROTEINS AND AMYLOID FIBRILS

by

Christopher Peter Jaroniec

B.S. Chemistry
Kent State University (1997)

SUBMITTED TO THE DEPARTMENT OF CHEMISTRY
IN PARTIAL FULFILLMENT OF THE REQUIREMENTS FOR THE DEGREE OF

DOCTOR OF PHILOSOPHY IN CHEMISTRY
AT THE
MASSACHUSETTS INSTITUTE OF TECHNOLOGY

FEBRUARY 2003

© 2003 Massachusetts Institute of Technology. All rights reserved.

Signature of Author_____

Department of Chemistry
December 2, 2002

Certified by_____

Professor Robert G. Griffin
Thesis Supervisor

Accepted by_____

Professor Robert W. Field
Chairman, Departmental Committee on Graduate Students

This Doctoral thesis has been examined by a Committee of the Department of Chemistry as follows:

Professor Mounji G. Bawendi _____
Chairman

Professor Robert G. Griffin _____
Thesis Supervisor

Professor Andrei Tokmakoff _____

**Solid State Nuclear Magnetic Resonance
Methodology and Applications to Structure Determination
of
Peptides, Proteins and Amyloid Fibrils**

by
Christopher Peter Jaroniec

Submitted to the Department of Chemistry
on December 2, 2002 in Partial Fulfillment of the
Requirements for the Degree of Doctor of Philosophy in Chemistry

ABSTRACT

Several methodological developments and applications of multidimensional solid-state nuclear magnetic resonance to biomolecular structure determination are presented. Studies are performed in uniformly ^{13}C , ^{15}N isotope labeled samples with magic-angle spinning for optimal resolution and sensitivity.

Frequency selective rotational-echo double-resonance (FSR) and three-dimensional transferred-echo double-resonance (3D TEDOR) methods for carbon-nitrogen distance measurements in (^{13}C , ^{15}N)-labeled peptides and proteins are described. FSR employs frequency selective Gaussian pulses in combination with broadband REDOR recoupling to measure dipolar couplings based on the isotropic chemical shifts of the selected ^{13}C - ^{15}N spin pairs. The experiment is demonstrated in model peptides, N-acetyl-L-Val-L-Leu and N-formyl-L-Met-L-Leu-L-Phe, where multiple distances in the 3-6 Å range are determined with high precision, and in a membrane protein, bacteriorhodopsin, where the distances between aspartic acids Asp-85 and Asp-212 and the retinal Schiff base nitrogen are measured in the active site. The 3D TEDOR methods employ ^{13}C and ^{15}N chemical shift dimensions for site-specific resolution and encode the distance information in the buildup of cross-peak intensities, allowing multiple distances to be measured simultaneously. The methods are demonstrated in N-acetyl-L-Val-L-Leu and N-formyl-L-Met-L-Leu-L-Phe, where 20 and 26 distances up to 6 Å are determined, respectively.

The molecular conformation of peptide fragment 105-115 of transthyretin in an amyloid fibril is investigated. Complete sequence-specific ^{13}C and ^{15}N backbone and side-chain resonance assignments are obtained using two-dimensional ^{13}C - ^{13}C and ^{15}N - ^{13}C - ^{13}C chemical shift correlation experiments. Backbone torsion angles are measured directly using three-dimensional dipolar-chemical shift correlation experiments, which report on the relative orientations of ^{13}C - ^{15}N , ^{13}C - ^1H and ^{15}N - ^1H dipolar tensors, and intramolecular ^{13}C - ^{15}N distances in the 3-5 Å range are determined using 3D TEDOR, resulting in about 60 constraints on the peptide structure. An atomic-resolution structure of the peptide consistent with the NMR constraints is calculated using simulated annealing molecular

dynamics, and the results indicate that the peptide adopts an extended β -strand conformation in the fibril.

Thesis Supervisor: Robert G. Griffin
Title: Professor of Chemistry
Director of the Francis Bitter Magnet Laboratory

DEDICATION

This thesis is dedicated to Simone.

CONTENTS

ABSTRACT	3
DEDICATION	5
CONTENTS	7
LIST OF FIGURES	10
LIST OF TABLES	12
ABBREVIATIONS	13
ACKNOWLEDGMENTS	15
CHAPTER 1. INTRODUCTION TO SOLID STATE NMR	19
1.1 PREFACE	19
1.2 NUCLEAR SPIN INTERACTIONS AND SPIN DYNAMICS	27
1.2.1 <i>The Nuclear Spin Hamiltonian</i>	27
1.2.1.1 Zeeman Interaction	28
1.2.1.2 Internal Interactions	29
1.2.1.3 Interaction with Radiofrequency Fields	35
1.2.2 <i>Nuclear Spin Dynamics</i>	36
1.2.2.1 Time Evolution of the Density Operator	36
1.2.2.2 Average Hamiltonian Theory	37
1.3 MAGIC-ANGLE SPINNING NMR	39
1.3.1 <i>Powder Spectra</i>	39
1.3.2 <i>Internal Hamiltonians as Products of Spherical Tensors</i>	41
1.3.3 <i>Internal Hamiltonians under MAS</i>	45
REFERENCES	50
CHAPTER 2. REDOR NMR AT HIGH MAS FREQUENCIES	71
ABSTRACT	71
2.1 INTRODUCTION	72
2.2 THEORY	73
2.3 EXPERIMENTAL	79
2.4 RESULTS AND DISCUSSION	81
2.5 CONCLUSIONS	89
ACKNOWLEDGMENTS	90
REFERENCES	91
CHAPTER 3. J-DECOUPLED REDOR: CARBON-NITROGEN DISTANCE MEASUREMENTS IN U-¹³C LABELED SOLIDS	97
ABSTRACT	97
3.1 INTRODUCTION	98
3.2 RESULTS AND DISCUSSION	99
3.3 CONCLUSIONS	106
ACKNOWLEDGMENTS	107
REFERENCES	108
CHAPTER 4. FREQUENCY SELECTIVE REDOR: ACCURATE CARBON-NITROGEN DISTANCE MEASUREMENTS IN U-¹³C, ¹⁵N-LABELED PEPTIDES	111
ABSTRACT	111
4.1 INTRODUCTION	112
4.2 EXPERIMENTAL	117
4.2.1 <i>NMR Experiments</i>	117
4.2.2 <i>Internuclear Distance Measurements</i>	120

4.2.3 ^{13}C , ^{15}N -Labeled Model Systems	122
4.3 THEORY	123
4.3.1 Broadband Recoupling in Multispin Systems	123
4.3.2 Selective Recoupling in Multispin Systems	126
4.4 RESULTS AND DISCUSSION.....	128
4.4.1 Selective Recoupling in [U - ^{13}C , ^{15}N]Asparagine.....	128
4.4.2 Internuclear Distance Measurements in U - ^{13}C , ^{15}N -Labeled Peptides	136
4.4.3 Effect of ^1H Decoupling on REDOR Experiments	145
4.4.4 Effect of ^{15}N CSA on REDOR Experiments.....	150
4.5 CONCLUSIONS.....	152
ACKNOWLEDGMENTS	154
SUPPORTING INFORMATION.....	155
REFERENCES	157
CHAPTER 5. FREQUENCY SELECTIVE REDOR DISTANCE MEASUREMENTS IN THE ACTIVE SITE OF BACTERIORHODOPSIN.....	167
ABSTRACT	167
5.1 INTRODUCTION	168
5.2 EXPERIMENTAL.....	169
5.2.1 Preparation of Light-Adapted [U - ^{13}C , ^{15}N]Bacteriorhodopsin.....	169
5.2.2 NMR Spectroscopy.....	169
5.2.3 Numerical Simulations and Distance Measurements	170
5.3 RESULTS AND DISCUSSION.....	171
5.4 CONCLUSIONS.....	177
ACKNOWLEDGMENTS	177
REFERENCES	178
CHAPTER 6. 3D TEDOR NMR EXPERIMENTS FOR THE SIMULTANEOUS MEASUREMENT OF MULTIPLE CARBON-NITROGEN DISTANCES IN U-^{13}C, ^{15}N-LABELED SOLIDS	185
ABSTRACT	185
6.1 INTRODUCTION	187
6.2 EXPERIMENTAL.....	192
6.2.1 NMR Experiments	192
6.2.2 U - ^{13}C , ^{15}N -Labeled Peptides.....	192
6.3 THEORY	193
6.3.1 3D TEDOR Pulse Sequences	193
6.3.2 Spin Dynamics in U - ^{13}C , ^{15}N Labeled Systems	196
6.3.3 Internuclear Distance Measurements	202
6.3.4 Uncertainties in the Measured Distances	206
6.4 RESULTS AND DISCUSSION.....	211
6.4.1 Distance Measurements in [U - ^{13}C , ^{15}N]N-acetyl-Val-Leu	211
6.4.2 Distance Measurements in N-formyl-[U - ^{13}C , ^{15}N]Met-Leu-Phe.....	218
6.5 CONCLUSIONS.....	224
ACKNOWLEDGMENTS	225
APPENDIX.....	226
REFERENCES	230
CHAPTER 7. MOLECULAR CONFORMATION OF A PEPTIDE FRAGMENT OF TRANSTHYRETIN IN AN AMYLOID FIBRIL.....	239
ABSTRACT	239
7.1 INTRODUCTION	240
7.2 EXPERIMENTAL.....	242
7.2.1 Preparation of Amyloid Fibrils	242
7.2.2 NMR Experiments	244
7.3 RESULTS AND DISCUSSION.....	246

7.4 CONCLUSIONS	258
ACKNOWLEDGMENTS	259
REFERENCES	260
CHAPTER 8. STRUCTURE OF TTR(105-115) IN AN AMYLOID FIBRIL AT ATOMIC RESOLUTION	267
ABSTRACT	267
8.1 TORSION ANGLE MEASUREMENTS.....	268
8.1.1 $3D^{15}N_i-^{13}C_i^{\alpha}-^{13}CO_i-^{15}N_{i+1}$ Spectroscopy	271
8.1.2 $3D^1H_{i+1}^N-^{15}N_{i+1}-^{13}C_i^{\alpha}-^1H_i^{\alpha}$ Spectroscopy.....	278
8.2 CARBON-NITROGEN DISTANCE MEASUREMENTS	284
8.3 ATOMIC-RESOLUTION STRUCTURE OF TTR(105-115).....	288
8.4 CONCLUSIONS.....	291
ACKNOWLEDGMENTS	291
REFERENCES	292
CURRICULUM VITAE.....	297

LIST OF FIGURES

FIGURE 1-1. DEFINITION OF THE EULER ANGLES (α , β , γ).....	31
FIGURE 1-2. SIMULATED NMR SPECTRA FOR THE CHEMICAL SHIELDING AND HETERONUCLEAR DIPOLAR INTERACTIONS IN A POLYCRYSTALLINE SOLID.	41
FIGURE 1-3. REFERENCE FRAMES FOR THE DESCRIPTION OF NMR EXPERIMENTS IN ROTATING SOLIDS.	42
FIGURE 1-4. ^{15}N NMR SPECTRA OF POLYCRYSTALLINE ^{15}N LABELED N-ACETYL-L-VALINE.	49
FIGURE 2-1. REDOR PULSE SEQUENCE.....	74
FIGURE 2-2. COEFFICIENTS IN THE INTERACTION FRAME HAMILTONIAN FOR REDOR.....	76
FIGURE 2-3. COMPARISON OF AVERAGE HAMILTONIAN AND NUMERICAL SIMULATIONS FOR REDOR.	80
FIGURE 2-4. EXPERIMENTAL REDOR $\Delta S/S_0$ CURVES FOR $[1-^{13}\text{C},^{15}\text{N}]$ GLYCINE AND $[2-^{13}\text{C},^{15}\text{N}]$ GLYCINE.	82
FIGURE 2-5. COMPARISON OF EXPERIMENTAL AND PREDICTED DIPOLAR COUPLINGS IN GLYCINE.	85
FIGURE 2-6. EXPERIMENTAL REDOR S_0 CURVES FOR THE C^α RESONANCE IN $[\text{U}-^{13}\text{C},^{15}\text{N}]$ GLYCINE.	88
FIGURE 3-1. REDOR AND J-DECOUPLED REDOR PULSE SEQUENCES.....	100
FIGURE 3-2. REDOR AND J-DECOUPLED REDOR EXPERIMENTS IN GLYCINE.	102
FIGURE 3-3. REDOR AND J-DECOUPLED REDOR EXPERIMENTS IN $[\text{U}-^{13}\text{C},^{15}\text{N}]$ THREONINE.	104
FIGURE 3-4. SELECTIVE INVERSION OF ^{13}C RESONANCES IN $[\text{U}-^{13}\text{C},^{15}\text{N}]$ THREONINE.....	106
FIGURE 4-1. FREQUENCY SELECTIVE REDOR (FSR) PULSE SEQUENCE.	118
FIGURE 4-2. ASPARAGINE NEUTRON DIFFRACTION STRUCTURE AND ^{13}C AND ^{15}N MAS SPECTRA.	130
FIGURE 4-3. SELECTIVE RECOUPLING OF $\text{C}^\beta\text{-N}'$ AND $\text{C}^\beta\text{-N}^{\text{t}62}$ DIPOLAR INTERACTIONS IN $[\text{U}-^{13}\text{C},^{15}\text{N}]$ ASPARAGINE.....	131
FIGURE 4-4. INTERNUCLEAR DISTANCE MEASUREMENTS FOR C^β IN $[\text{U}-^{13}\text{C},^{15}\text{N}]$ ASPARAGINE.	134
FIGURE 4-5. INTERNUCLEAR DISTANCE MEASUREMENTS FOR C^α IN $[\text{U}-^{13}\text{C},^{15}\text{N}]$ ASPARAGINE.	135
FIGURE 4-6. N-ACETYL-L-VAL-L-LEU CRYSTAL STRUCTURE AND ^{13}C AND ^{15}N MAS SPECTRA.	137
FIGURE 4-7. REPRESENTATIVE INTERNUCLEAR DISTANCE MEASUREMENTS IN $[\text{U}-^{13}\text{C},^{15}\text{N}]$ N-ACETYL-L-VAL-L-LEU.....	139
FIGURE 4-8. N-FORMYL-L-MET-L-LEU-L-PHE-OME CRYSTAL STRUCTURE AND N-FORMYL-L-MET-L-LEU-L-PHE ^{13}C AND ^{15}N MAS SPECTRA.....	142
FIGURE 4-9. REPRESENTATIVE INTERNUCLEAR DISTANCE MEASUREMENTS IN N-FORMYL- $[\text{U}-^{13}\text{C},^{15}\text{N}]$ L-MET-L-LEU-L-PHE.....	143
FIGURE 4-10. REPRESENTATIVE DISTANCES MEASURED IN N-FORMYL-L-MET-L-LEU-L-PHE.....	144
FIGURE 4-11. EFFECT OF ^1H DECOUPLING ON REDOR EXPERIMENTS.	146
FIGURE 4-12. EFFECT OF ^1H DECOUPLING ON REDOR EXPERIMENTS.	149
FIGURE 4-13. EFFECT OF ^{15}N CHEMICAL SHIELDING ANISOTROPY ON ^{13}C -OBSERVE REDOR EXPERIMENTS.	151
FIGURE 4-S1. RESONANCE ASSIGNMENTS FOR $[\text{U}-^{13}\text{C},^{15}\text{N}]$ N-ACETYL-L-VAL-L-LEU.	156
FIGURE 5-1. THE ACTIVE SITE OF BACTERIORHODOPSIN.	172
FIGURE 5-2. ONE-DIMENSIONAL ^{15}N MAS SPECTRUM OF LIGHT-ADAPTED BACTERIORHODOPSIN.....	172
FIGURE 5-3. TWO-DIMENSIONAL RFDR ^{13}C - ^{13}C CHEMICAL SHIFT CORRELATION AND FILTERED ONE-DIMENSIONAL ^{13}C MAS SPECTRA OF DARK-ADAPTED $[\text{U}-^{13}\text{C},^{15}\text{N}]$ BACTERIORHODOPSIN.	174
FIGURE 5-4. TWO-DIMENSIONAL EXPERIMENT FOR THE MEASUREMENT OF DIPOLAR COUPLINGS BETWEEN THE RETINAL SB NITROGEN AND ASP C_γ IN $[\text{U}-^{13}\text{C},^{15}\text{N}]$ BR.....	175
FIGURE 5-5. DISTANCE MEASUREMENTS FROM THE SCHIFF BASE LYS216 $\text{N}\zeta$ TO ASP85 C_γ AND ASP212 C_γ IN LIGHT-ADAPTED $[\text{U}-^{13}\text{C},^{15}\text{N}]$ BR.	176
FIGURE 6-1. 3D TEDOR PULSE SEQUENCES.	194
FIGURE 6-2. TEDOR CROSS-PEAK SIMULATIONS.	200
FIGURE 6-3. COMPARISON OF THE APPROXIMATE SIMULATION MODEL WITH AVERAGE HAMILTONIAN SIMULATIONS FOR AN $I\text{-S}_2$ SPIN SYSTEM.....	210
FIGURE 6-4. X-RAY CRYSTAL STRUCTURE OF N-ACETYL-L-VAL-L-LEU.....	211
FIGURE 6-5. REPRESENTATIVE TWO-DIMENSIONAL SLICES FROM BROADBAND 3D TEDOR EXPERIMENTS IN $[\text{U}-^{13}\text{C},^{15}\text{N}]$ N-ACETYL-L-VAL-L-LEU.....	213
FIGURE 6-6. 3D ZF TEDOR CROSS-PEAK BUILDUP CURVES IN $[\text{U}-^{13}\text{C},^{15}\text{N}]$ N-ACETYL-L-VAL-L-LEU.....	214
FIGURE 6-7. REPRESENTATIVE TWO-DIMENSIONAL SLICES FROM THE 3D BASE TEDOR EXPERIMENT FOR ^{13}CO NUCLEI AND CROSS-PEAK BUILDUP CURVES IN $[\text{U}-^{13}\text{C},^{15}\text{N}]$ N-ACETYL-L-VAL-L-LEU.....	215

FIGURE 6-8. SUMMARY OF DISTANCE MEASUREMENTS IN N-ACETYL-L-VAL-L-LEU.	216
FIGURE 6-9. X-RAY CRYSTAL STRUCTURE OF N-FORMYL-L-MET-L-LEU-L-PHE-OME.....	218
FIGURE 6-10. REPRESENTATIVE TWO-DIMENSIONAL SLICES FOR THE 3D ZF TEDOR EXPERIMENT IN N-FORMYL-[U- ¹³ C, ¹⁵ N]L-MET-L-LEU-L-PHE.	219
FIGURE 6-11. 3D ZF TEDOR CROSS-PEAK BUILDUP CURVES IN N-FORMYL-[U- ¹³ C, ¹⁵ N]L-MET-L-LEU-L-PHE.....	220
FIGURE 6-12. REPRESENTATIVE TWO-DIMENSIONAL SLICES FROM THE 3D BASE TEDOR EXPERIMENT FOR ¹³ CO NUCLEI AND CROSS-PEAK BUILDUP CURVES IN N-FORMYL-[U- ¹³ C, ¹⁵ N]L-MET-L-LEU-L-PHE....	221
FIGURE 6-13. SUMMARY OF DISTANCE MEASUREMENTS IN N-FORMYL-L-MET-L-LEU-L-PHE.	223
FIGURE 7-1. AMINO ACID SEQUENCE OF TTR(105-115).	243
FIGURE 7-2. TWO-DIMENSIONAL SPIN DIFFUSION PULSE SEQUENCE.....	245
FIGURE 7-3. TWO-DIMENSIONAL N-C-C PULSE SEQUENCE.	246
FIGURE 7-4. ELECTRON MICROGRAPH OF TTR(105-115) FIBRILS.	247
FIGURE 7-5. 1D ¹³ C AND ¹⁵ N MAS NMR SPECTRA OF (U- ¹³ C, ¹⁵ N)-LABELED TTR(105-115) FIBRILS.....	248
FIGURE 7-6. 2D ¹³ C- ¹³ C CORRELATION SPECTRA OF TTR(105-115) FIBRILS.....	250
FIGURE 7-7. 2D ¹⁵ N- ¹³ C CORRELATION SPECTRA OF TTR(105-115) FIBRILS.....	251
FIGURE 7-8. SECONDARY ¹⁵ N AND ¹³ C CHEMICAL SHIFTS IN TTR(105-115) FIBRILS.....	253
FIGURE 7-9. BACKBONE ¹³ C- ¹⁵ N DISTANCES MEASURED IN SELECTIVELY LABELED TTR(105-115) FIBRILS USING REDOR.....	255
FIGURE 7-10. X-RAY STRUCTURE OF THE PEPTIDE FRAGMENT CORRESPONDING TO RESIDUES 105-115 IN WT TTR AND THE BACKBONE MODEL FOR THE TTR(105-115) PEPTIDE IN THE FIBRILLAR STATE.....	258
FIGURE 8-1. MODEL OF THE PEPTIDE BACKBONE.....	270
FIGURE 8-2. DEPENDENCE OF THE PROJECTION ANGLE Θ BETWEEN ¹⁵ N _i - ¹³ C ^α _i AND ¹³ CO _i - ¹⁵ N _{i+1} BOND VECTORS ON THE MOLECULAR TORSION ANGLE ψ	271
FIGURE 8-3. 3D ¹⁵ N _i - ¹³ C ^α _i - ¹³ CO _i - ¹⁵ N _{i+1} PULSE SEQUENCE FOR THE MEASUREMENT OF ψ _i	272
FIGURE 8-4. DOUBLE QUANTUM-SINGLE QUANTUM CORRELATION SPECTRUM OF TTR(105-115) _{YTIA}	273
FIGURE 8-5. SIMULATED ¹⁵ N _i - ¹³ C ^α _i - ¹³ CO _i - ¹⁵ N _{i+1} DQ DEPHASING CURVES.....	275
FIGURE 8-6. ¹⁵ N _i - ¹³ C ^α _i - ¹³ CO _i - ¹⁵ N _{i+1} SIMULATIONS IN THE FREQUENCY DOMAIN.....	276
FIGURE 8-7. ¹⁵ N _i - ¹³ C ^α _i - ¹³ CO _i - ¹⁵ N _{i+1} MEASUREMENT OF ψ FOR RESIDUES Y105 AND T106 IN TTR(105-115) _{YTIA} FIBRILS.	277
FIGURE 8-8. DEPENDENCE OF THE PROJECTION ANGLE Θ BETWEEN THE ¹ H ^N _{i+1} - ¹⁵ N _{i+1} AND ¹³ C ^α _i - ¹ H ^α _i BOND VECTORS ON THE MOLECULAR TORSION ANGLE ψ	279
FIGURE 8-9. 3D ¹ H ^N _{i+1} - ¹⁵ N _{i+1} - ¹³ C ^α _i - ¹ H ^α _i PULSE SEQUENCE FOR THE MEASUREMENT OF ψ _i	281
FIGURE 8-10. ¹ H ^N _{i+1} - ¹⁵ N _{i+1} - ¹³ C ^α _i - ¹ H ^α _i MEASUREMENT OF ψ FOR RESIDUES Y105 AND T106 IN TTR(105-115) _{YTIA} FIBRILS.....	283
FIGURE 8-11. 3D ZF TEDOR SPECTRA AND BUILDUP CURVES IN TTR(105-115) _{YTIA} FIBRILS.	285
FIGURE 8-12. SUMMARY OF CARBON-NITROGEN DISTANCE RESTRAINTS IN TTR(105-115) FIBRILS.....	287
FIGURE 8-13. ENSEMBLE OF 30 ATOMIC-RESOLUTION STRUCTURES OF TTR(105-115) IN THE AMYLOID FIBRIL CONSISTENT WITH THE NMR RESTRAINTS.	287
FIGURE 8-14. RAMACHANDRAN PLOT WITH (ϕ , ψ) PAIRS FOR ALL RESIDUES IN THE ENSEMBLE OF 30 CALCULATED STRUCTURES SUPERIMPOSED.	288
FIGURE 8-15. DISTRIBUTIONS OF BACKBONE AND SIDE-CHAIN TORSION ANGLES FOR THE ENSEMBLE OF 30 CALCULATED TTR(105-115) STRUCTURES.	289
FIGURE 8-16. COMPARISON OF EXPERIMENTALLY DETERMINED CARBON-NITROGEN DISTANCES WITH THE CORRESPONDING DISTANCES OBSERVED IN THE ENSEMBLE OF 30 CALCULATED TTR(105-115) STRUCTURES.	290

LIST OF TABLES

TABLE 2-1. EXPERIMENTAL C'-N AND C ^α -N DIPOLAR COUPLINGS IN GLYCINE	84
TABLE 4-1. INTERNUCLEAR DISTANCES IN ASPARAGINE	133
TABLE 4-2. INTERNUCLEAR DISTANCES IN N-ACETYL-L-VAL-L-LEU	140
TABLE 4-3. INTERNUCLEAR DISTANCES IN N-FORMYL-L-MET-L-LEU-L-PHE	145
TABLE 4-S1. SELECTED INTERMOLECULAR C-N DISTANCES UP TO 6 Å IN N-ACETYL-L-VAL-L-LEU	155
TABLE 4-S2. SELECTED INTERMOLECULAR C-N DISTANCES UP TO 6 Å IN N-FORMYL-L-MET-L-LEU-L- PHE-OME	155
TABLE 5-1. DIFFRACTION DISTANCES FROM THE RETINAL SCHIFF BASE NITROGEN IN BR ₅₆₈	173
TABLE 6-1. CARBON-CARBON J-COUPLING CONSTANTS IN N-ACETYL-L-VAL-L-LEU	206
TABLE 6-2. INTERNUCLEAR DISTANCES IN N-ACETYL-L-VAL-L-LEU	217
TABLE 6-3. INTERNUCLEAR DISTANCES IN N-FORMYL-L-MET-L-LEU-L-PHE	224
TABLE 7-1. ¹³ C AND ¹⁵ N CHEMICAL SHIFTS MEASURED IN TTR(105-115) FIBRILS	249
TABLE 7-2. ¹³ C AND ¹⁵ N LINewidthS MEASURED IN TTR(105-115) FIBRILS	249
TABLE 7-3. BACKBONE TORSION ANGLES φ AND ψ IN TTR(105-115) FIBRILS AND IN WT TTR	254
TABLE 7-4. BACKBONE CARBON-NITROGEN DISTANCES IN TTR(105-115) FIBRILS AND IN WT TTR	257
TABLE 8-1. BACKBONE TORSION ANGLES φ AND ψ IN TTR(105-115) FIBRILS PREDICTED USING TALOS AND MEASURED USING 3D DIPOLAR-CHEMICAL SHIFT CORRELATION EXPERIMENTS.	284
TABLE 8-2. CARBON-NITROGEN DISTANCES IN TTR(105-115) FIBRILS	286

ABBREVIATIONS

1D	One-dimensional
2D	Two-dimensional
3D	Three-dimensional
3D TEDOR	Three-dimensional Transferred Echo Double Resonance
3D BASE TEDOR	3D Band Selective TEDOR
3D ZF TEDOR	3D Z-Filtered TEDOR
AHT	Average Hamiltonian Theory
bR	Bacteriorhodopsin
CP	Cross Polarization
CPMAS	Cross Polarization with Magic Angle Spinning
CSA	Chemical Shielding Anisotropy
CW	Continuous Wave
DQ	Double Quantum
FID	Free Induction Decay
FSR	Frequency Selective Rotational Echo Double Resonance
FWHM	Full Width at Half Maximum
MAS	Magic Angle Spinning
MQ	Multiple Quantum
MREV	Mansfield, Rhim, Elleman and Vaughn (Pulse Sequence)
NMR	Nuclear Magnetic Resonance
PAS	Principal Axis System
ppm	parts per million
R ²	Rotational Resonance
R ³	Rotary Resonance Recoupling
REDOR	Rotational Echo Double Resonance
RF	Radio Frequency
RFDR	Radio Frequency Driven Recoupling
RMSD	Root Mean Square Deviation
SB	Schiff Base
SEDRA	Simple Excitation for the Dephasing of Rotational Echoes
SPC-5	Supercycled Permutationally Offset Stabilized C5
SPECIFIC CP	Spectrally Induced Filtering in Combination with CP
SSNMR	Solid State Nuclear Magnetic Resonance
TALOS	Torsion Angle Likelihood Obtained from Shifts and Sequence Similarity
TEDOR	Transferred Echo Double Resonance
TEM	Transmission Electron Microscopy
TPPM	Two Pulse Phase Modulation
T-MREV	Transverse MREV
TTR	Transthyretin
TTR(105-115)	Residues 105-115 of TTR
wt	Wild Type
ZQ	Zero Quantum

ACKNOWLEDGMENTS

The past five years at MIT have been extremely rewarding and enjoyable. First of all, I would like to thank my supervisor, Prof. Robert Griffin, for his encouragement and support and for providing me with numerous opportunities to work on interesting research projects.

I have had the good fortune to collaborate with a number of outstanding individuals in the Griffin laboratory. During my first two years in the lab I have greatly benefited from working with Morten Hohwy, Bernd Reif and Chad Rienstra, who not only provided tremendous research insight but also remain close friends. I am especially grateful to Morten, who introduced me to solid-state NMR and involved me in a number of his research projects. I have very much enjoyed the subsequent collaborations and valuable discussions with many people in the lab. Brett Tounge contributed to the development of frequency selective REDOR, and Brett and Jon Lansing were collaborators on the application of frequency selective REDOR to bacteriorhodopsin. Claudiu Filip provided many ideas and contributed to the exciting collaboration on the development of 3D TEDOR methods. I am grateful to Nathan Astrof, Vik Bajaj, and Mike McMahon for their contributions to the work on amyloid fibril structure. Nathan provided many ideas in the area of sample preparation and contributed to the work on resonance assignments. Vik has been very closely involved in the measurements of distance and torsion angle constraints as well as the structure calculations. Mike contributed to the structure calculation efforts. I would also like to acknowledge many valuable discussions with John Gross and Vlad Ladizhansky about NMR experiments and structure calculations.

The assistance of the Magnet Lab research and technical staff is also very much appreciated. Dave Ruben and Chris Turner provided insight about pulse programming and numerous hints on trouble-shooting spectrometer problems. Peter Allen, Jeff Bryant, Ron Durocher and Ajay Thakkar were very helpful in building, trouble-shooting and repairing equipment.

Prof. Judith Herzfeld from Brandeis University was closely involved in the work described in Chapters 2-5. Prof. Herzfeld provided the bacteriorhodopsin samples and many constructive comments on the experiments.

The research in Chapters 7 and 8 would not have been possible without Cait MacPhee and Prof. Christopher Dobson from the University of Cambridge. Their work on amyloid fibrils introduced me to this fascinating research area and provided the initial motivation for our collaborative work. During the past three years Cait has prepared and characterized numerous fibril samples, and both Cait and Prof. Dobson provided tremendous insight about the design and interpretation of our experiments.

Personally, I would like to thank my parents, Jadwiga and Mieczyslaw Jaroniec, as well as my parents-in-law, Ute and Heinrich Becker, for always being interested in what I was up to, and their constant encouragement and support.

And finally last but not least I would like to thank my wife, Simone Jaroniec, for her constant encouragement and support, and for making the past five years truly enjoyable and memorable.

CHAPTER 1. INTRODUCTION TO SOLID STATE NMR

1.1 Preface

Atomic-level structural information about peptides, proteins and nucleic acids is key to understanding the biological function of these molecules, their intermolecular interactions, and to drug design. The primary approaches to determining three-dimensional molecular structures are X-ray crystallography and solution-state nuclear magnetic resonance (NMR) spectroscopy, and these techniques account for the majority of structures deposited to date in the Protein Data Bank.¹ X-ray crystallography, which relies on the availability of high-quality crystals, is the most successful technique for complete structure determination in biological systems and it has, for example, recently been used to determine the structure of the complete 70S ribosome at 5.5 Å resolution.² The application of solution-state NMR methods to proteins^{3,4} requires solubility at ~0.2-1 mM concentrations, and isotopically ¹³C, ¹⁵N and ²H labeled samples. Structural investigations of proteins with molecular weights up to ~30 kDa are becoming increasingly routine, and new methodology⁵⁻⁷ promises to extend the size of molecules amenable to detailed NMR studies, as demonstrated by a number of recent examples.⁸⁻¹¹

Despite the success of the aforementioned structural methods there are a number of systems of importance in biophysical chemistry and structural biology to which these techniques may not be directly applicable because the systems are non-crystalline, insufficiently soluble or simply too large to tumble rapidly in solution. Important examples of such systems include large peptide-protein complexes,¹² enzyme-inhibitor complexes,¹³⁻¹⁹ surface-associated biomaterials,²⁰⁻²⁴ intermediates of chemical and

photochemical reactions,²⁵⁻²⁹ peptide and protein fibrils often associated with protein deposition diseases,³⁰⁻⁴⁴ and integral membrane proteins.^{25,26,28,29,45-51} Atomic-level structural constraints have been obtained in all of the above systems using solid-state NMR techniques, which do not require soluble or crystalline samples.

Solid-state NMR studies of peptides and proteins require the chemical or biosynthetic incorporation of ¹³C and/or ¹⁵N nuclei at the sites of interest. For each atomic site that gives rise to a resolved resonance line in an NMR spectrum the information about the nuclear spin interactions with electrons and other nuclei can be obtained via the measurements of NMR observables such as the chemical shift and dipolar coupling, and subsequently converted to a three-dimensional structural model. However, in static, unoriented solids NMR lineshapes are severely broadened by the anisotropic chemical shift and dipolar interactions, which depend on the orientation of the molecular fragment with respect to the external magnetic field. As a result, NMR spectra of randomly oriented solids containing more than a few isotopically labeled sites become increasingly difficult to interpret. However, a number of fundamental advances made over the past three decades in solid-state NMR methodology, most notably the development of magic-angle spinning (MAS)^{52,53} and cross-polarization (CP),⁵⁴ have enabled the acquisition of high resolution and sensitivity NMR spectra of solids. Indeed, the CPMAS experiment^{55,56} which involves the combination of cross-polarization⁵⁴ with magic-angle spinning^{52,53} and broadband proton decoupling,⁵⁷⁻⁶¹ provides the basis for structural studies of biological solids.

Magic-angle spinning involves the rotation of the sample about an axis inclined at an angle of $\sim 54.74^\circ$ with respect to the external magnetic field.^{52,53} During MAS the

interactions described by second rank tensors and considered to be inhomogeneous according to the treatment of Maricq and Waugh⁶² (e.g., chemical shielding anisotropies and heteronuclear dipolar couplings among low- γ spins) are averaged to their isotropic values. As a result, at external fields of ca. 10-20 Tesla (^1H Larmor frequencies of ca. 400-800 MHz) and spinning frequencies of 5-25 kHz the ^{13}C and ^{15}N MAS NMR spectra of biological molecules consist primarily of relatively narrow resonances present at the isotropic chemical shifts, and closely resemble solution-state NMR spectra. The isotropic resonances are, in addition, flanked by series of rotational sidebands at integer multiples of the spinning frequency.⁶² The intensities of the rotational sidebands contain information about the anisotropic interactions^{62,63} and they become negligible when the spinning frequency greatly exceeds the magnitude of the anisotropic interaction. Note that MAS alone is not sufficient to provide high-resolution ^1H spectra even at spinning frequencies exceeding 30 kHz due to the fact that the dipole-dipole interactions among the abundant proton spins are both large and homogeneous.⁶² Although MAS greatly enhances the resolution and sensitivity of NMR spectra, it concurrently attenuates the dipole-dipole couplings, which are the primary source of structural information. Thus, it is necessary to “recouple” these interactions during indirect dimensions of multidimensional NMR experiments, using radiofrequency pulse sequences specifically designed to interfere with the MAS averaging process.

The theoretical developments in coherent averaging (average Hamiltonian) theory^{64,65} and Floquet theory,^{66,67} which have led to the design of pulse sequences for homonuclear⁶⁸⁻⁷⁵ and heteronuclear spin decoupling,^{57,59-61,76} have also inspired the development of pulse sequences for the recoupling of anisotropic interactions under MAS

conditions.⁷⁷⁻⁸⁷ Within the framework of separated local field spectroscopy⁸⁸⁻⁹⁵ these recoupling pulse sequences have been used to measure very precise structural constraints in molecules selectively labeled with pairs of spin-1/2 nuclei.^{85,86,96-98} Such measurements in selectively labeled systems will likely remain the method of choice for providing answers to specific structural questions. However, despite the success of these experiments, there is significant interest in performing analogous measurements in multiply and/or uniformly ¹³C and ¹⁵N labeled samples, where multiple structural constraints can be obtained. Techniques suitable for structural measurements in multiply ¹³C, ¹⁵N labeled molecules have been the focus of research that was initiated in the second half of the last decade and that continues today. Although still in relatively early stages of development, these approaches have already been used to acquire spectra with tens to hundreds of resolved atomic sites, to perform spectral assignments,^{41,44,99-114} to measure internuclear distance^{51,115-121} and torsion angle constraints,¹²²⁻¹³³ and to determine the initial molecular structures.^{134,135} The work presented here has greatly benefited from these recent developments, many of which were made in the Griffin laboratory at MIT.

This thesis addresses the methodology for measuring multiple structural constraints in multiply and uniformly ¹³C, ¹⁵N labeled systems with applications to biomolecular structure determination. The remainder of Chapter 1 introduces the nuclear spin interactions, nuclear spin dynamics, and magic-angle spinning NMR. In Chapters 2-6 several methods for measuring long-range (ca. 3-6 Å) carbon-nitrogen distances in (¹³C,¹⁵N)-labeled molecules are described. Applications of these methods to model peptides and a membrane protein are demonstrated. In Chapters 7 and 8 the molecular conformation of a peptide in an amyloid fibril is determined by using primarily three-

dimensional dipolar-chemical shift correlation experiments to measure internuclear distances and torsion angles in (U - ^{13}C , ^{15}N)-labeled samples. The specific topics addressed are outlined below in more detail.

In Chapter 2 the rotor-synchronized rotational-echo double-resonance (REDOR) dipolar recoupling pulse sequence is investigated theoretically and experimentally in the rapid magic-angle spinning regime. The REDOR recoupling effect was originally derived for isolated heteronuclear spin-1/2 pairs assuming a δ -function pulse approximation. This assumption is strictly valid only for relatively low MAS frequencies (ca. 2–8 kHz), where REDOR has indeed been employed to perform highly accurate and precise distance measurements. However, the studies of (U - ^{13}C , ^{15}N)-labeled molecules typically require the use of high MAS frequencies (ca. 10-30 kHz). Under these conditions the RF pulses occupy a significant fraction of the rotor period and the δ -function pulse approximation breaks down. We demonstrate experimentally, in two model ^{13}C - ^{15}N spin systems, [1 - ^{13}C , ^{15}N] and [2 - ^{13}C , ^{15}N]glycine, that REDOR dipolar dephasing curves acquired at high MAS rates and using relatively long RF pulses are nearly identical to the curve expected in the δ -pulse limit. The only noticeable effect of the finite pulse length on the recoupling is a very minor scaling of the dipolar oscillation frequency. These experimental results are explained using numerical simulations as well as average Hamiltonian theory, which is used to derive analytical expressions for the spin evolution under REDOR recoupling sequences with different pulse phasing schemes. For the relevant xy -4 phase cycling scheme and extensions thereof, it is found that the finite pulses are expected to scale only the dipolar oscillation frequency by a small, well-defined factor, which is in agreement with our experimental observations.

Chapters 3 and 4 address approaches to frequency selective heteronuclear recoupling in uniformly ^{13}C , ^{15}N -labeled solids, which combine REDOR with the selective irradiation of ^{13}C and ^{15}N spectra. In Chapter 3 a J-decoupled REDOR experiment is described for distance measurements between a single ^{15}N nucleus and individual ^{13}C nuclei within a tightly coupled cluster. The ^{13}C - ^{13}C J-coupling interactions are suppressed by applying a rotor-synchronized, frequency selective Gaussian π pulse on resonance with a single ^{13}C spin. The dipolar interaction between this ^{13}C and the ^{15}N spin is recoupled, while the J-couplings to other ^{13}C nuclei are refocused. Failure to refocus the J-couplings among the ^{13}C spins compromises the accurate measurement of ^{13}C - ^{15}N dipole interactions, which are often of similar magnitude (ca. 30-60 Hz). In Chapter 4 the basic ideas presented in Chapter 3 are extended to describe a frequency selective REDOR (FSR) experiment capable of selective measurements of weak ^{13}C - ^{15}N dipolar couplings in uniformly ^{13}C , ^{15}N -labeled solids. In FSR, the application of simultaneous frequency selective Gaussian pulses to a ^{13}C - ^{15}N spin-pair of interest, recouples this dipolar interaction, while concurrently suppressing the remaining ^{13}C - ^{15}N dipolar couplings and all ^{13}C - ^{13}C scalar couplings to the selected ^{13}C . The ^{13}C - ^{15}N coupling of interest is extracted by a least-squares fit of the experimentally observed modulation of the ^{13}C spin-echo intensity to the analytical expression describing the dipolar dephasing in an isolated heteronuclear spin pair under conventional REDOR. The FSR experiment is demonstrated in three uniformly- ^{13}C , ^{15}N -labeled model systems: asparagine, N-acetyl-L-Val-L-Leu and N-formyl-L-Met-L-Leu-L-Phe; in N-formyl-[U- ^{13}C , ^{15}N]L-Met-L-Leu-L-Phe a total of 16 internuclear distances in the 2.5–6 Å range have been determined. In addition, Chapter 4 discusses several experimental challenges associated with the

measurement of weak dipolar couplings, including the choice of proton decoupling scheme during REDOR mixing and the choice of the appropriate xy -type error compensation scheme in the presence of non-negligible ^{15}N chemical shift anisotropy.

In Chapter 5 frequency selective REDOR is used to measure two ^{13}C - ^{15}N distances in the active site of a 248-residue uniformly ^{13}C , ^{15}N labeled membrane protein, light-adapted bacteriorhodopsin in its native purple membrane. The distances from the retinal Schiff base nitrogen to the Asp85 and Asp212 sidechain carboxyl carbons were found to be 4.7 ± 0.3 Å and 4.9 ± 0.5 Å, respectively. The Asp85 distance agrees with the 4.3-5.0 Å distances in recent diffraction structures of light-adapted bacteriorhodopsin, while the Asp212 distance appears to be somewhat longer in the NMR measurement than the 4.0-4.4 Å diffraction values.

In Chapter 6 we present three-dimensional magic-angle-spinning NMR experiments for the simultaneous measurement of multiple carbon-nitrogen distances in uniformly ^{13}C , ^{15}N labeled solids. The approaches employ transferred echo double resonance (TEDOR) for ^{13}C - ^{15}N coherence transfer and ^{15}N and ^{13}C frequency labeling for site-specific resolution, and build on several previous 3D TEDOR techniques. The novel feature of the 3D TEDOR pulse sequences presented here is that they are specifically designed to circumvent the detrimental effects of homonuclear ^{13}C - ^{13}C J-couplings on the measurement of weak ^{13}C - ^{15}N dipolar couplings. In particular, homonuclear J-couplings lead to two undesirable effects: (i) they generate anti-phase and multiple-quantum (MQ) spin coherences, which lead to spurious cross-peaks and phase-twisted lines in the 2D ^{15}N - ^{13}C correlation spectra, and thus degrade the spectral resolution and prohibit the extraction of reliable cross-peak intensities, and (ii) they significantly reduce cross-peak

intensities for strongly J-coupled ^{13}C sites (e.g., CO and C^α). The first experiment employs z -filter periods to suppress the anti-phase and MQ coherences and generates 2D spectra with purely absorptive peaks for all TEDOR mixing times. The second approach uses band-selective ^{13}C pulses to refocus J-couplings between ^{13}C spins within the selective pulse bandwidth and ^{13}C spins outside the bandwidth. The internuclear distances are extracted using a simple analytical model, which accounts explicitly for multiple spin-spin couplings contributing to cross-peak buildup. The experiments are demonstrated in two U- ^{13}C , ^{15}N labeled peptides, N-acetyl-L-Val-L-Leu (N-ac-VL) and N-formyl-L-Met-L-Leu-L-Phe (N-f-MLF), where 20 and 26 ^{13}C - ^{15}N distances up to $\sim 5\text{-}6$ Å were measured, respectively. Of the measured distances, 10 in N-ac-VL and 13 in N-f-MLF are greater than 3 Å and provide valuable structural constraints.

In Chapters 7 and 8 we describe the structural studies of a peptide in an amyloid fibril. Amyloid fibrils are self-assembled aggregates formed by peptides and proteins with a wide variety of structures and functions, and their formation is associated with a number of protein deposition diseases including Alzheimer's disease and the transmissible spongiform encephalopathies. Atomic resolution structural information is inaccessible for most fibrillar systems using traditional methods due to the noncrystalline and insoluble nature of these materials. Hence these materials are ideally suited for solid-state NMR investigations. In Chapter 7 we use MAS solid-state NMR to investigate the molecular conformation of an 11-residue peptide fragment of transthyretin (TTR) corresponding to residues 105-115 and previously shown to form amyloid fibrils *in vitro*. Complete sequence specific backbone and side-chain ^{13}C and ^{15}N resonance assignments were obtained using two-dimensional ^{13}C - ^{13}C and ^{15}N - ^{13}C - ^{13}C correlation experiments.

The resonance assignments indicate that the peptide adopts an extended β -strand conformation in the fibril. Chapter 8 describes the direct NMR measurements of site-specific structural constraints in TTR(105-115) fibrils. The backbone torsion angles are determined using three-dimensional dipolar-chemical shift correlation experiments, which report on the relative orientations of ^{13}C - ^{15}N , ^{13}C - ^1H and ^{15}N - ^1H dipolar tensors, and intramolecular ^{13}C - ^{15}N distances in the 3-5 Å range are determined using the 3D TEDOR methods described in Chapter 6, resulting in a total of about 60 constraints on the peptide structure. An atomic-resolution structure of the peptide in the fibril is calculated using simulated annealing molecular dynamics. The supramolecular organization of the β -strands in the fibril is investigated using experiments, which probe intermolecular dipolar couplings.

1.2 Nuclear Spin Interactions and Spin Dynamics

This section provides an introduction to the nuclear spin interactions and nuclear spin dynamics. Magic-angle spinning NMR is discussed in section 1.3. The reader is encouraged to consult one of the many excellent texts for a thorough introduction to the fundamentals of magnetic resonance and multidimensional NMR experiments.^{4,65,136-142} In addition, the review articles highlighted in the preceding section provide a suitable introduction to some recent research topics.

1.2.1 The Nuclear Spin Hamiltonian

Solid-state NMR spectra are determined by the Hamiltonian:

$$H = H_Z + H_{int} + H_{RF} \quad (1)$$

which consists of the nuclear spin Zeeman interaction with the static magnetic field H_Z , the internal nuclear spin interactions H_{int} , and the interaction with the applied radiofrequency (RF) fields H_{RF} . The various Hamiltonian terms are discussed in detail below.

1.2.1.1 Zeeman Interaction

The Zeeman Hamiltonian is given by

$$H_Z = -\gamma\hbar\mathbf{I} \cdot \mathbf{B}_0 = -\gamma\hbar B_0 I_z \quad (2)$$

where γ is the gyromagnetic ratio, B_0 is the flux density of the static magnetic field, $\hbar = h/2\pi$ where h is Planck's constant, and I_z is the z-component of the nuclear spin angular momentum operator \mathbf{I} . In the final form of eq 2 we have assumed that the static magnetic field \mathbf{B}_0 corresponds to the z-axis of the laboratory frame of reference. Furthermore, for convenience and consistency with the NMR literature all following Hamiltonian terms will given in frequency units (i.e., $H \equiv H/\hbar$).

For a nuclear spin with non-zero spin angular momentum I , the Zeeman interaction generates $2I + 1$ equally spaced energy levels with eigenvalues:

$$E = -\gamma\hbar B_0 m \quad m = I, I-1, \dots, -I \quad (3)$$

The energy difference between two adjacent energy levels is

$$\Delta E = \hbar\omega_0 \quad (4)$$

where the nuclear Larmor frequency, ω_0 , is equal to the precession frequency of the magnetization around the static field. The B_0 fields generated by modern superconducting magnets range from ca. 2.35 to 21.2 Tesla and correspond to ^1H Larmor frequencies of

ca. 100-900 MHz. Most applications of NMR to biomolecular structure determination have greatly benefited from the use of the highest possible B_0 fields, due to the associated increases in sensitivity and spectral resolution.

Note that with the exception of the quadrupolar interaction, the Zeeman interaction is typically three to six orders of magnitude larger than all other nuclear spin interactions discussed below. Therefore, the local field Hamiltonians can be treated as perturbations on the Zeeman interaction. In an interaction frame defined by $H_Z = \omega_0 I_z$ the Hamiltonian terms, which do not commute with the Zeeman interaction become time-dependent. To first-order these non-secular terms are effectively averaged to zero, and only the secular components of H_{int} , i.e., those which commute with H_Z , contribute to the internal Hamiltonian.

1.2.1.2 Internal Interactions

The internal Hamiltonian

$$H_{int} = \sum_{\lambda} H_{\lambda} \quad \lambda = \text{CS, D, J, Q} \quad (5)$$

describes the nuclear spin interactions with the local fields present at each atomic site. The interactions with local fields are crucial in the applications of NMR to the determination of molecular structure. They include the shielding of the static B_0 field by the electrons represented by the chemical shielding (or chemical shift) Hamiltonian H_{CS} , the direct through-space magnetic dipole-dipole interactions H_D , the indirect electron-mediated J-coupling interactions H_J , and the interactions of nuclear electric quadrupole moments with electric field gradients represented by H_Q .

All internal interactions relevant to NMR of diamagnetic solids can in general be expressed as a coupling of two vectors \mathbf{V} and \mathbf{U} by a Cartesian tensor \mathfrak{R} of rank two:¹⁴³

$$H_\lambda \propto \mathbf{V} \cdot \mathfrak{R} \cdot \mathbf{U} \quad (6)$$

where \mathbf{V} is a spin angular momentum operator, and \mathbf{U} may be a vector describing the static magnetic field or another spin operator. The expressions for the internal Hamiltonians are given below:^{138,142}

$$H_{\text{CS}} = \sum_k \gamma_k \mathbf{I}_k \cdot \boldsymbol{\sigma}_k \cdot \mathbf{B}_0 \quad (7)$$

$$H_{\text{D}} = \sum_{k < l} \mathbf{I}_k \cdot \mathbf{D}_{kl} \cdot \mathbf{I}_l \quad (8)$$

$$H_{\text{J}} = 2\pi \sum_{k < l} \mathbf{I}_k \cdot \mathbf{J}_{kl} \cdot \mathbf{I}_l \quad (9)$$

$$H_{\text{Q}} = \sum_k \frac{eQ_k}{2I_k(2I_k - 1)\hbar} \mathbf{I}_k \cdot \mathbf{V}_k \cdot \mathbf{I}_k \quad (10)$$

Here $\boldsymbol{\sigma}_k$, \mathbf{D}_{kl} , \mathbf{J}_{kl} and \mathbf{V}_k are the chemical shielding, direct dipolar coupling, indirect spin-spin coupling, and electric field gradient tensors, respectively, e is the elementary charge and Q is the quadrupole moment. The interaction tensors are defined in the laboratory frame, where the NMR experiment is performed. In the context of NMR studies of (^{13}C , ^{15}N)-labeled biomolecules discussed in this thesis the anisotropic J-coupling terms are negligible and the quadrupolar interactions, which occur only for nuclei with $I > 1/2$, are absent. Therefore, these interactions will not be considered further.

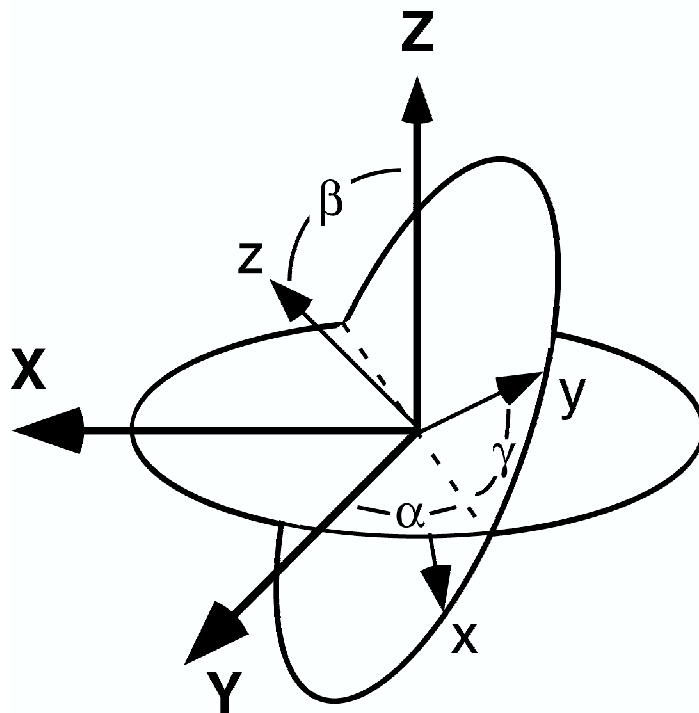


Figure 1-1. Definition of the Euler angles (α , β , γ).

The Euler angles (α , β , γ), defined in the convention of Rose,¹⁴²⁻¹⁴⁴ rotate the (\mathbf{X} , \mathbf{Y} , \mathbf{Z}) coordinate system into the (x , y , z) system. The rotations of the (\mathbf{X} , \mathbf{Y} , \mathbf{Z}) system proceed as follows. The first rotation is about the \mathbf{Z} axis by the angle α , until the \mathbf{Y} axis coincides with the node line (indicated by the dashed line). The second rotation is about the node line by the angle β until the \mathbf{Z} axis coincides with the z axis. The final rotation is about the z axis by the angle γ until the \mathbf{Y} axis coincides with the y axis.

The derivation of the high-field truncated Hamiltonians for the chemical shift and dipole-dipole interactions given below requires the rotation of the interaction tensors σ_k and \mathbf{D}_{kl} (denoted as \mathfrak{R} below) from their principal axis systems (denoted as PAS or P in the following), where the tensors are diagonal, into the laboratory frame (denoted as LAB or L in the following), where the NMR experiment is performed. These transformations are in general achieved by using Euler rotation matrices \mathbf{R} , which specify rotations of coordinate systems by triplets of angles $\Omega = \{\alpha, \beta, \gamma\}$ as follows (Figure 1-1):¹⁴²⁻¹⁴⁴

$$\mathfrak{R}_{\text{LAB}} = \mathbf{R} \cdot \mathfrak{R}_{\text{PAS}} \cdot \mathbf{R}^{-1} \quad (11)$$

with

$$\mathbf{R} = \begin{bmatrix} \cos\alpha \cos\beta \cos\gamma - \sin\alpha \sin\gamma & \sin\alpha \cos\beta \cos\gamma + \cos\alpha \sin\gamma & -\sin\beta \cos\gamma \\ -\cos\alpha \cos\beta \sin\gamma - \sin\alpha \cos\gamma & -\sin\alpha \cos\beta \sin\gamma + \cos\alpha \cos\gamma & \sin\beta \sin\gamma \\ \cos\alpha \sin\beta & \sin\alpha \sin\beta & \cos\beta \end{bmatrix} \quad (12)$$

Chemical Shielding Interaction

The high-field truncated Hamiltonian for the chemical shielding interaction is obtained using equations 7, 11 and 12 with $\Omega = \{\phi, \theta, 0\}$:

$$\begin{aligned} H_{CS} &= \sum_k \gamma_k B_0 \sigma_{zz}^{k,LAB} I_{kz} \\ &= \sum_k \gamma_k B_0 \left(\sigma_{xx}^k \sin^2 \theta_k \cos^2 \phi_k + \sigma_{yy}^k \sin^2 \theta_k \sin^2 \phi_k + \sigma_{zz}^k \cos^2 \theta_k \right) I_{kz} \end{aligned} \quad (13)$$

where $\sigma_{zz}^{k,LAB}$ is the relevant component of the chemical shielding tensor in the laboratory frame, and σ_{xx}^k , σ_{yy}^k , and σ_{zz}^k are the principal values of the chemical shielding tensor σ_k in the PAS. The polar and azimuthal angles, θ_k and ϕ_k , respectively, describe the orientation of \mathbf{B}_0 in the PAS of the chemical shielding tensor.

The chemical shielding Hamiltonian in eq 13 is often reformulated to separate the isotropic and anisotropic contributions to the chemical shielding interaction. This is accomplished by introducing the isotropic chemical shift σ_{iso} , the anisotropy δ , and the asymmetry η parameters as follows:¹⁴²

$$\sigma_{iso} = \frac{1}{3} (\sigma_{xx} + \sigma_{yy} + \sigma_{zz}) \quad (14)$$

$$\delta = \sigma_{zz} - \sigma_{iso} \quad (15)$$

$$\eta = \frac{\sigma_{yy} - \sigma_{xx}}{\delta} \quad (16)$$

The convention typically used¹⁴² is $|\sigma_{zz} - \sigma_{iso}| \geq |\sigma_{xx} - \sigma_{iso}| \geq |\sigma_{yy} - \sigma_{iso}|$ and the resulting expression is:

$$H_{CS} = \sum_k \left\{ \gamma_k B_0 \sigma_{iso}^k + \gamma_k B_0 \frac{1}{2} \delta^k \left[3 \cos^2 \theta_k - 1 - \eta^k \sin^2 \theta_k \cos(2\phi) \right] \right\} I_{kz} \quad (17)$$

In this thesis the chemical shift interaction will be used primarily to provide the spectral resolution in multidimensional experiments. Therefore, only the isotropic chemical shift will be of significant interest.

Dipole-Dipole Interaction

The direct through-space dipole-dipole interaction has no isotropic component (i.e., the dipolar tensor is traceless) and the high-field truncated Hamiltonian is given by:

$$H_D = \sum_{k < l} b_{kl} \frac{1}{2} (3 \cos^2 \theta_{kl} - 1) [3 I_{kz} I_{lz} - \mathbf{I}_k \cdot \mathbf{I}_l] \quad (18)$$

with the dipolar coupling constant b_{kl} in angular units:

$$b_{kl} = -\frac{\mu_0}{4\pi} \frac{\gamma_k \gamma_l \hbar}{r_{kl}^3} \quad (19)$$

Here r_{kl} is the internuclear distance and θ_{kl} is the orientation of the \mathbf{I}_k - \mathbf{I}_l vector relative to \mathbf{B}_0 . The dependence of the dipolar coupling constant on the inverse cube of the internuclear distance makes the dipolar interaction an exquisite probe of three-dimensional molecular structure. A major part of this thesis is devoted to the development of methods for the accurate measurement of dipolar coupling constants.

Note that for heteronuclear (e.g., ^{13}C - ^{15}N) spin-pairs the operator product $\mathbf{I}_k \cdot \mathbf{I}_l$ in eq 18 can be further truncated because the large difference in the resonance frequencies

of the two spin species renders the terms proportional to $I_k^+ I_l^- + I_k^- I_l^+$ (the flip-flop terms) non-secular. The resulting Hamiltonian for the heteronuclear dipole-dipole interaction is:

$$H_D = \sum_{k<l} b_{kl} \frac{1}{2} (3 \cos^2 \theta_{kl} - 1) 2I_{kz} I_{lz} \quad (20)$$

Indirect Spin-Spin Interaction

As noted above, in the context of NMR studies of (U- ^{13}C , ^{15}N)-labeled biomolecules the indirect spin-spin (J-coupling) interactions are typically considered to be isotropic:

$$H_J = \sum_{k<l} 2\pi J_{kl} \mathbf{I}_k \cdot \mathbf{I}_l \quad (21)$$

where J_{kl} the scalar J-coupling constant in hertz. In analogy to the dipole-dipole interaction, the J-coupling Hamiltonian for heteronuclear spin pairs is truncated to the secular term:

$$H_J = \sum_{k<l} 2\pi J_{kl} I_{kz} I_{lz} \quad (22)$$

Equation 22 is also valid for homonuclear spin pairs in the “weak-coupling limit”,¹³⁸ i.e., when the chemical shift difference between the coupled spins greatly exceeds the magnitude of the J-coupling constant. This is often the case for homonuclear ^{13}C - ^{13}C J-couplings in (U- ^{13}C , ^{15}N)-biomolecules, where the chemical shift differences are typically one or two orders of magnitude larger than the J-coupling constants. A truncation process of this type is often referred to as second averaging.¹⁴²

It should be pointed out that in the context of most solid-state NMR experiments ^{13}C - ^{13}C and ^{13}C - ^{15}N J-couplings do not significantly influence the spin dynamics and can therefore be neglected. It is important to note, however, that ^{13}C - ^{13}C J-couplings

complicate the accurate measurements of weak ^{13}C - ^{15}N dipolar couplings (as discussed in Chapters 3 and 4 of this thesis), and in combination with residual dipolar and chemical shift interactions they can lead to significant line broadening in ^{13}C MAS spectra.

1.2.1.3 Interaction with Radiofrequency Fields

The final term in the NMR Hamiltonian (c.f. eq 1) is due to the nuclear spin interaction with applied radiofrequency fields. The interaction has the same general form as the Zeeman interaction, namely:

$$H_{\text{RF}} = -\sum_k \gamma_k \mathbf{I}_k \cdot \mathbf{B}_{\text{RF}}(t) \quad (23)$$

In the usual treatment,^{136-138,142} the linearly oscillatory RF field generated in the NMR coil is decomposed into two components rotating at ω_{rf} and $-\omega_{\text{rf}}$. Only the component rotating with the angular frequency ω_{rf} close to the Larmor frequency ω_0 has an appreciable effect on the nuclear magnetization and is retained. Following the transformation of the spin Hamiltonian to a frame rotating at ω_{rf} the RF term becomes time-independent:

$$H_{\text{RF}} = \sum_k \omega_1^k [I_{kx} \cos\varphi + I_{ky} \sin\varphi] \quad (24)$$

where $\omega_1^k = -\gamma_k B_1$ and φ are the amplitude and phase of the RF field, respectively. The rotating frame transformation does not change the form of the high-field Hamiltonian with the exception of an overall shift of the Larmor frequencies by $-\omega_{\text{rf}}$. In practice NMR experiments are carried out in a rotating detection frame, where the interactions are observed as offsets from the RF carrier frequency. Finally, we note that the applied RF fields will typically dominate the internal interactions in coupled spin-1/2 systems,

providing a great deal of control over the internal nuclear spin interactions. Multiple pulse sequences with variable amplitudes and phases are routinely used in modern multidimensional NMR experiments to manipulate the internal Hamiltonian by selectively decoupling or reintroducing various interaction terms at different periods of the experiment.

1.2.2 Nuclear Spin Dynamics

1.2.2.1 Time Evolution of the Density Operator

The time-evolution of the density operator $\rho(t)$, which represents the state of a system of nuclear spins at all times, is described by the Liouville-von Neumann equation:

$$\frac{d}{dt}\rho(t) = -i[H(t),\rho(t)] \quad (25)$$

The formal solution is:

$$\rho(t) = U(t)\rho(0)U(t)^{-1} \quad (26)$$

with the propagator $U(t)$ defined according to

$$U(t) = T \exp\left\{-i \int_0^t H(t') dt'\right\} \quad (27)$$

where T is the Dyson time-ordering operator, which describes the ordering of the exponential functions for a Hamiltonian that does not commute with itself at different times. The expectation value of an observable operator A at time t is calculated as follows:

$$\langle A \rangle = Tr\{A\rho(t)\} \quad (28)$$

It is readily seen from eq 25 that no time evolution occurs if the density matrix and the Hamiltonian commute. Furthermore, in the case of a self-commuting Hamiltonian the

time evolution can be described exactly in a straightforward fashion. However, in the context of most NMR experiments we will encounter situations where the time-dependent Hamiltonian does not commute with itself at different times. In such cases the time evolution can be evaluated numerically in very short time steps (during which the Hamiltonian is considered to be constant), or using average Hamiltonian theory (AHT) discussed in the next section.

1.2.2.2 Average Hamiltonian Theory

Magnus Expansion of the Propagator

Average Hamiltonian theory, initially introduced into NMR by Haeberlen and Waugh to describe the effects of multiple-pulse sequences for homonuclear spin decoupling,⁶⁴ attempts to describe the effective evolution of the spin system under a time-dependent Hamiltonian $H(t)$ over a given time interval t_c , by a time-independent average Hamiltonian \bar{H} :

$$U(t_c) = T \exp\left\{-i \int_0^{t_c} H(t) dt\right\} = \exp\{-i\bar{H}t_c\} \quad (29)$$

Provided that the Hamiltonian $H(t)$ is periodic with the period t_c , and the observation of the spin system is stroboscopic and synchronized with the period of the Hamiltonian, the average Hamiltonian also describes the time evolution over longer time periods:

$$U(nt_c) = U(t_c)^n = \exp\{-i\bar{H}nt_c\} \quad (30)$$

The time-independent effective Hamiltonian is given by the Magnus expansion:^{64,145}

$$\bar{H} = \bar{H}^{(1)} + \bar{H}^{(2)} + \bar{H}^{(3)} + \dots \quad (31)$$

with

$$\bar{H}^{(1)} = \frac{1}{t_c} \int_0^{t_c} dt_1 H(t_1) \quad (32)$$

$$\bar{H}^{(2)} = \frac{-i}{2t_c} \int_0^{t_c} dt_2 \int_0^{t_2} dt_1 [H(t_2), H(t_1)] \quad (33)$$

$$\bar{H}^{(3)} = \frac{-1}{6t_c} \int_0^{t_c} dt_3 \int_0^{t_3} dt_2 \int_0^{t_2} dt_1 \left\{ [H(t_3), [H(t_2), H(t_1)]] + [[H(t_3), H(t_2)], H(t_1)] \right\} \quad (34)$$

In the context of pulse sequences involving low- γ nuclei, such as those discussed in this thesis, the first few terms (or even the first-order term alone) are usually sufficient to provide a reasonable approximation for the effective Hamiltonian. Methods for the convenient calculation of higher order terms were presented recently by Hohwy and Nielsen.^{146,147}

Interaction Frames and AHT

In this section we present the essential result of average Hamiltonian theory using as an example a problem commonly encountered in multiple-pulse NMR experiments, namely the modification of the internal Hamiltonian (i.e., H_D , H_{CS} , etc.) by the introduction of time-dependent perturbations in the form of RF pulses. The propagator is expressed as (c.f. eq 27):

$$U(t) = T \exp \left\{ -i \int_0^t dt_1 (H_{int} + H_{RF}(t_1)) \right\} \quad (35)$$

When the effects of H_{RF} and H_{int} are separated as follows:⁶⁴

$$U(t) = U_{RF}(t) U_{int}(t) \quad (36)$$

the individual propagators take the forms

$$U_{RF}(t) = T \exp \left\{ -i \int_0^t dt_1 H_{RF}(t_1) \right\} \quad (37)$$

and

$$U_{int}(t) = T \exp \left\{ -i \int_0^t dt_1 \tilde{H}_{int}(t_1) \right\} \quad (38)$$

\tilde{H}_{int} , which is now time-dependent, is the Hamiltonian H_{int} in the interaction representation defined with respect to H_{RF} :

$$\tilde{H}_{int}(t) = U_{RF}^{-1}(t) H_{int} U_{RF}(t) \quad (39)$$

The most interesting situation arises for cyclic sequences of RF pulses, i.e.,:

$$U_{RF}(t_c) = 1 \quad (40)$$

In this case the pulses have no direct effect on the time evolution during the full cycle and the entire propagator (c.f. eq 35) is described entirely by the internal Hamiltonian in the RF interaction representation:

$$U(t_c) = U_{int}(t_c) = T \exp \left\{ -i \int_0^{t_c} dt_1 \tilde{H}_{int}(t_1) \right\} = \exp \left\{ -i \bar{\tilde{H}}_{int} t_c \right\} \quad (41)$$

where the Magnus expansion (c.f. eq 31) can be used to evaluate the effective internal Hamiltonian $\bar{\tilde{H}}_{int}$ to the desired order. In this thesis average Hamiltonian theory is used in Chapter 2 to describe the effects of finite RF pulses on the recoupled dipolar interaction in rotational-echo double resonance (REDOR) experiments.

1.3 Magic-Angle Spinning NMR

1.3.1 Powder Spectra

In the preceding section we have shown that the nuclear spin Hamiltonians corresponding to the chemical shielding and dipole-dipole interactions depend on the

orientation of the interaction tensors with respect to \mathbf{B}_0 . For polycrystalline (i.e., powder) samples, all possible orientations of the relevant molecular fragment are assumed to be present with equal probabilities. Therefore, a powder-average must be performed when evaluating the free-induction decay (FID) resulting from the evolution of the transverse magnetization (created from the equilibrium density operator $\rho(0) \sim I_z$ by an initial 90° y-pulse) under the internal Hamiltonian. For example for the chemical shielding interaction the FID is given by:

$$\langle I^+(t) \rangle \propto \int_0^{2\pi} d\phi \int_0^\pi d\theta \sin\theta \cdot \text{Tr}\{I^+ \exp(-iH_{CS}t) I_x \exp(iH_{CS}t)\} \exp(-\Gamma t) \quad (42)$$

where Γ describes the nuclear spin relaxation (e.g., due to insufficient proton decoupling). Figure 1-2 shows the simulated NMR spectra for the chemical shielding and heteronuclear dipolar interactions in a polycrystalline solid. The spectra display a strong orientational dependence and hence contain a great deal of information about molecular structure. However, due to this orientational dependence they cover a wide range of frequencies, which leads to severe overlap in systems containing more than a few isotopically labeled sites such as uniformly labeled biomolecules. For example, a single amide ^{15}N chemical shielding tensor spans approximately 150 ppm (see Figure 1-4), which corresponds to the entire range of ^{15}N chemical shifts encountered in typical peptides and proteins.

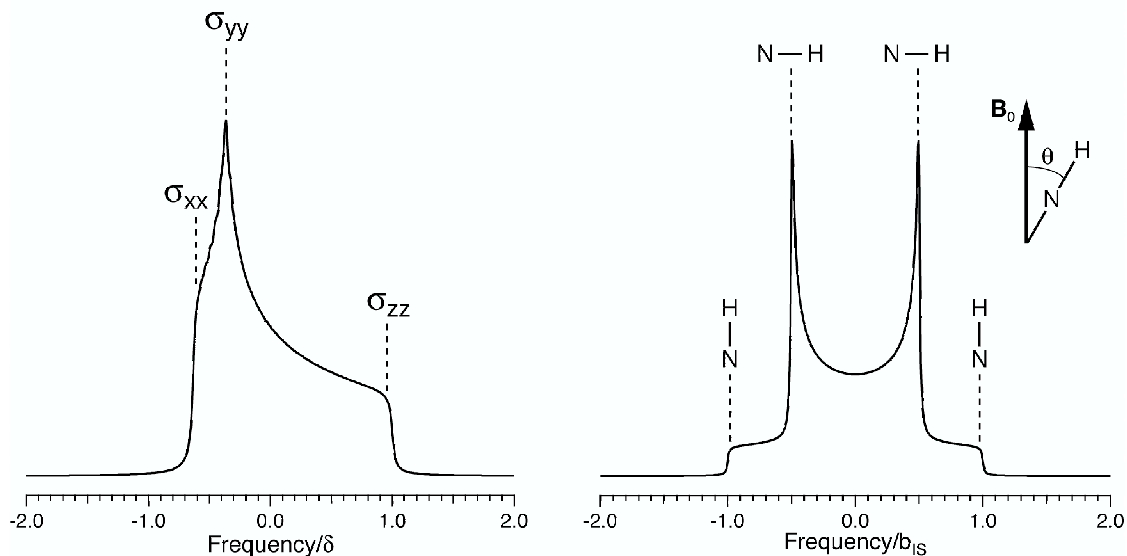


Figure 1-2. Simulated NMR spectra for the chemical shielding and heteronuclear dipolar interactions in a polycrystalline solid.

For the chemical shielding interaction (left) and the heteronuclear dipolar interaction (right) the NMR frequencies, displayed in the units of δ or b_{IS} , depend on the orientation of the molecular segment with respect to \mathbf{B}_0 . The dipolar interaction is axially symmetric ($\eta = 0$) with the unique z-axis of the PAS along the internuclear vector. Hence, the singularities observed in the spectra can be directly related to the orientation of the internuclear (e.g., ^{15}N - ^1H) vector with respect to \mathbf{B}_0 . Furthermore, for the heteronuclear dipolar coupling, the symmetric Pake pattern¹⁴⁸ is the result of the superposition of the two transitions in the coupled two-spin system. For the chemical shielding interaction, the singularities in the spectrum correspond to the alignment of the three principal components of the tensor parallel to \mathbf{B}_0 , and can be related to the orientation of the molecular segment in the field provided that the orientation of the chemical shielding tensor in the molecular frame (i.e., with respect to the various bond vectors) is known.

1.3.2 Internal Hamiltonians as Products of Spherical Tensors

The internal Hamiltonians which depend on the orientation of the molecular fragment with respect to the static field can be made time-dependent by the macroscopic rotation of the sample about an axis inclined at an angle θ_r with respect to \mathbf{B}_0 .^{52,53} Such spatial manipulations will in general lead to some averaging of the anisotropic

interaction. Below we will demonstrate that when the rotation axis is oriented at the “magic angle” θ_m with respect to \mathbf{B}_0 :

$$\theta_m = \cos^{-1}(1/\sqrt{3}) \approx 54.74^\circ \quad (43)$$

the anisotropic interactions that can be described by second rank tensors and are inhomogeneous in the sense of Maricq and Waugh⁶² (e.g., chemical shielding anisotropies and heteronuclear dipolar couplings among low- γ spins) are averaged to their isotropic values, provided that the rotation frequency exceeds the magnitude of the anisotropic interaction.

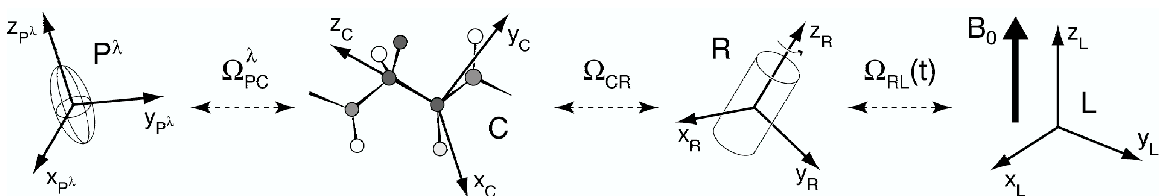


Figure 1-3. Reference frames for the description of NMR experiments in rotating solids.

The principal axis system (P^λ) for the interaction λ (e.g., chemical shielding anisotropy or dipolar coupling) is related to an arbitrarily chosen crystallite-fixed frame (C) through a set of Euler angles Ω_{PC}^λ . A polycrystalline (i.e., powder) sample contains a large number of crystallites with random orientations Ω_{CR} with respect to a rotor-fixed frame (R). Finally, the rotor-fixed frame can be transformed into the laboratory frame (L) using the set of angles $\Omega_{RL}(t)$, which is time-dependent for a rotating sample. The Euler angles are $\Omega_{AB} = \{\alpha_{AB}, \beta_{AB}, \gamma_{AB}\}$. For the dipolar interaction the z-axis of P^λ is parallel to the internuclear vector. Furthermore, the z-axis of R is defined to be the rotation axis, and the static magnetic field \mathbf{B}_0 lies along the z-axis of L.

The discussion of magic-angle spinning involves multiple rotations of second rank tensors between the various reference frames shown in Figure 1-3. To derive the internal Hamiltonians under MAS it is convenient to reformulate the bilinear Hamiltonians (c.f. eqs 7-10) in terms of spherical tensor operators as follows:^{142,143}

$$H_\lambda = \mathbf{V} \cdot \mathfrak{R}_\lambda \cdot \mathbf{U} = \sum_{l=0}^2 \sum_{m=-l}^l (-1)^m R_{l,-m}^\lambda T_{l,m}^\lambda \quad (44)$$

where $R_{l,m}$ and $T_{l,m}$ describe the interactions in ordinary and spin space, respectively. The spatial and spin terms can be affected independently by the reorientation of molecular segments (e.g., due to macroscopic sample rotation) and by radiofrequency pulses, respectively. The detailed derivation of the spin operators $T_{l,m}$ was summarized by Spiess.¹⁴³ Below we give the expressions for the $T_{0,0}$ and $T_{2,m}$ operators, which result from the coupling of two nuclear spin operators \mathbf{I} and \mathbf{S} and are particularly relevant for the analysis of NMR experiments in rotating solids:

$$T_{0,0} = \mathbf{I} \cdot \mathbf{S} \quad (45)$$

$$T_{2,0} = \frac{1}{\sqrt{6}} (3I_z S_z - \mathbf{I} \cdot \mathbf{S}) \quad (46)$$

$$T_{2,\pm 1} = \mp \frac{1}{2} (I^\pm S_z + I_z S^\pm) \quad (47)$$

$$T_{2,\pm 2} = \frac{1}{2} I^\pm S^\pm \quad (48)$$

where the raising and lowering operators for the I-spin are:

$$I^\pm = I_x \pm iI_y \quad (49)$$

Under the rotation from one coordinate system to a new coordinate system each spherical tensor element in the new system, $(T_{l,m})'$, can be expressed in terms of the elements in the old system, $T_{l,m}$, with the transformation involving only tensors of equal rank, i.e.,:

$$(T_{l,m})' = \sum_{m'=-l}^l T_{l,m'} D_{m',m}^{(l)}(\Omega) \quad (50)$$

The Wigner rotation matrices $D_{m',m}^{(l)}(\Omega)$,¹⁴⁹ which specify the coordinate transformation according to the Euler angles $\Omega = \{\alpha, \beta, \gamma\}$ (see Figure 1-3) can be expressed as:

$$D_{m',m}^{(l)}(\Omega) = e^{-im'\alpha} d_{m',m}^{(l)}(\beta) e^{-im\gamma} \quad (51)$$

The following relation between the Wigner matrices

$$D_{m',m}^{(l)}(\Omega_{AC}) = \sum_{m''=-l}^l D_{m',m''}^{(l)}(\Omega_{AB}) D_{m'',m}^{(l)}(\Omega_{BC}) \quad (52)$$

is used to describe successive rotations. Within this framework for each interaction λ , the general expression for the coefficients $R_{l,m}$ (c.f. eq 44) in the laboratory frame is:

$$R_{l,m}^\lambda = \sum_{m'=-l}^l \sum_{m''=-l}^l \sum_{m'''=-l}^l \rho_{l,m'}^\lambda D_{m',m''}^{(l)}(\Omega_{PC}) D_{m'',m'''}^{(l)}(\Omega_{CR}) D_{m''',m}^{(l)}(\Omega_{RL}) \quad (53)$$

where $\rho_{l,m'}^\lambda$ are the tensor elements in the principal axis system. In most applications of NMR only the $\rho_{0,0}$ and $\rho_{2,m}$ elements are relevant. For the chemical shielding interaction the tensor elements are given by:¹⁴³

$$\rho_{0,0}^{\text{CS}} = \gamma \sigma_{iso} \quad (54)$$

$$\rho_{2,0}^{\text{CS}} = \sqrt{\frac{3}{2}} \gamma \delta \quad (55)$$

$$\rho_{2,\pm 1}^{\text{CS}} = 0 \quad (56)$$

$$\rho_{2,\pm 2}^{\text{CS}} = -\frac{1}{2} \gamma \delta \eta \quad (57)$$

while for the dipolar coupling only the $\rho_{2,0}$ element is non-zero:

$$\rho_{2,0}^{\text{D}} = \sqrt{6} b_{IS} \quad (58)$$

where σ_{iso} , δ , η are the isotropic component, anisotropy, and asymmetry of the chemical shielding tensor, b_{IS} is the dipolar coupling constant, and γ is the gyromagnetic ratio. In the Zeeman interaction frame only the Hamiltonian terms proportional to $T_{l,0}$ (i.e., those

which commute with the I_z operator) are retained. Furthermore, only the $T_{0,0}$ and $T_{2,0}$ components, which describe the isotropic contributions and the angular dependence of NMR frequencies, respectively, are relevant in the context of most experiments,^{142,143} and the resulting expressions for the chemical shielding and dipolar interactions are:

$$H_{CS} = \left\{ \gamma B_0 \sigma_{iso} + \gamma B_0 \frac{1}{2} \delta \left[3 \cos^2 \beta_{PL} - 1 - \eta \sin^2 \beta_{PL} \cos(2\alpha_{PL}) \right] \right\} I_z \quad (59)$$

$$H_D = b_{IS} \frac{1}{2} (3 \cos^2 \beta_{PL} - 1) [3 I_z S_z - \mathbf{I} \cdot \mathbf{S}] \quad (60)$$

The reduced Wigner matrix elements used in the derivation of eqs 59 and 60 are:^{142,143}

$$d_{0,0}^{(2)}(\beta) = \frac{1}{2} (3 \cos^2 \beta - 1) \quad (61)$$

$$d_{\pm 2,0}^{(2)}(\beta) = \sqrt{\frac{3}{8}} \sin^2 \beta \quad (62)$$

Note that the expressions in eqs 59 and 60 are equivalent to the Hamiltonians in the Cartesian tensor notation (c.f., eqs 17 and 18), with $\beta_{PL} = \theta$ and $\alpha_{PL} = \phi$.

1.3.3 Internal Hamiltonians under MAS

For rotating samples the Hamiltonians for the chemical shielding and dipolar interactions are given by:

$$H_{CS} = \sum_k \omega_{CS}^k(t) I_{kz} \quad (63)$$

$$H_D = \sum_{k < l} \omega_D^{kl}(t) (3 I_{kz} I_{lz} - \mathbf{I}_k \cdot \mathbf{I}_l) \quad (64)$$

The orientation dependent coefficients $\omega_{\tilde{\lambda}}^{k,kl}(t)$ (where $\tilde{\lambda} = CS, D$) can be expressed as a Fourier series:⁸⁶

$$\omega_{\lambda}^{k,kl}(t) = \sum_{m=-2}^2 \omega_{\lambda}^{(m)} \exp(im\omega_r t) \quad (65)$$

with

$$\omega_{\lambda}^{(m)} = \omega_{\text{iso}}^{\lambda} \delta_{m,0} + \delta^{\lambda} \left\{ D_{0,-m}^{(2)}(\Omega_{\text{PR}}^{\lambda}) - \frac{\eta^{\lambda}}{\sqrt{6}} \left[D_{-2,-m}^{(2)}(\Omega_{\text{PR}}^{\lambda}) + D_{2,-m}^{(2)}(\Omega_{\text{PR}}^{\lambda}) \right] \right\} d_{-m,0}^{(2)}(\beta_{\text{RL}}) \quad (66)$$

where $\lambda = \text{CS}_k, D_{kl}$, $\omega_r/2\pi$ is the rotor frequency, $\delta_{m,0}$ is the Kronecker delta, and $\omega_{\text{iso}}^{\lambda}$, δ^{λ} and η^{λ} are the isotropic value, anisotropy and asymmetry parameter of interaction λ . In eq 66 we have assumed for simplicity that the principal axis frame coincides with the crystallite-fixed frame. For the dipolar interaction between spins k and l :

$$\omega_{\text{iso}}^{\text{D}_{kl}} = 0 \quad (67)$$

$$\delta^{\text{D}_{kl}} = b_{kl} \quad (68)$$

$$\eta^{\text{D}_{kl}} = 0 \quad (69)$$

and the expression in eq 66 becomes:

$$\omega_{D_{kl}}^{(m)} = b_{kl} D_{0,-m}^{(2)}(\Omega_{\text{PR}}^{\text{D}_{kl}}) d_{-m,0}^{(2)}(\beta_{\text{RL}}) \quad (70)$$

For macroscopic sample rotation exactly at the magic angle, $\beta_{\text{RL}} = \theta_m = \cos^{-1}(1/\sqrt{3})$, the

Fourier coefficients are given by:

$$\omega_{D_{kl}}^{(0)} = b_{kl} \frac{(3\cos^2 \beta_{\text{PR}}^{kl} - 1)}{2} \frac{(3\cos^2 \theta_m - 1)}{2} = 0 \quad (71)$$

$$\omega_{D_{kl}}^{(\pm 1)} = -\frac{1}{2\sqrt{2}} b_{kl} \sin(2\beta_{\text{PR}}^{kl}) \exp\{\pm i\gamma_{\text{PR}}^{kl}\} \quad (72)$$

$$\omega_{D_{kl}}^{(\pm 2)} = \frac{1}{4} b_{kl} \sin^2 \beta_{\text{PR}}^{kl} \exp\{\pm i2\gamma_{\text{PR}}^{kl}\} \quad (73)$$

Analogous, albeit somewhat more complicated, expressions can be written for the chemical shielding interaction. The above equations clearly demonstrate that the

macroscopic rotation of the sample at the magic-angle averages anisotropic interactions described by second rank tensors to their isotropic values.^{52,53,62} The time-independent coefficient $\omega_\lambda^{(0)}$ vanishes during MAS, and the coefficients oscillating at ω_r and $2\omega_r$ are averaged to zero with the period of one and one-half rotor cycle, respectively. When the rotation frequency greatly exceeds the anisotropy of the interaction, i.e., $\omega_r \gg |\delta^\lambda|$, the resulting NMR spectra are characterized primarily by resonances occurring at the isotropic chemical shifts and resemble solution-state NMR spectra. For relatively slow spinning frequencies (or very large anisotropies) rotational sidebands are observed,^{52,53,62} which carry information about the magnitudes and relative orientations of the various interaction tensors.^{62,63} Magic-angle spinning is illustrated in Figure 1-4 with the ^{15}N NMR spectrum of polycrystalline ^{15}N labeled N-acetyl-L-valine.

In conclusion we note that averaging by MAS is limited to nuclear spin interactions for which the Hamiltonian commutes with itself at all times, defined as inhomogeneous by Maricq and Waugh.⁶² These interactions include the chemical shielding anisotropy and heteronuclear dipolar couplings. In addition, in most cases the ^{13}C - ^{13}C dipolar interactions can also be considered inhomogeneous due to second averaging (see Section 1.2.1.2), provided that rotational resonance conditions are avoided.¹⁵⁰⁻¹⁵² On the other hand the homogeneous dipolar interactions between abundant protons in rigid solids cannot be fully averaged by MAS, even when the rotation frequency exceeds the magnitudes of the pairwise couplings. Finally, the high resolution and sensitivity afforded by MAS comes at the expense of structural information contained in the anisotropic interactions averaged by the sample rotation. Thus, it is necessary to “recouple” these interactions during indirect dimensions of

multidimensional NMR experiments, using radiofrequency pulse sequences specifically designed to interfere with the MAS averaging process. The design and applications of such pulse sequences are the main topic of this thesis.

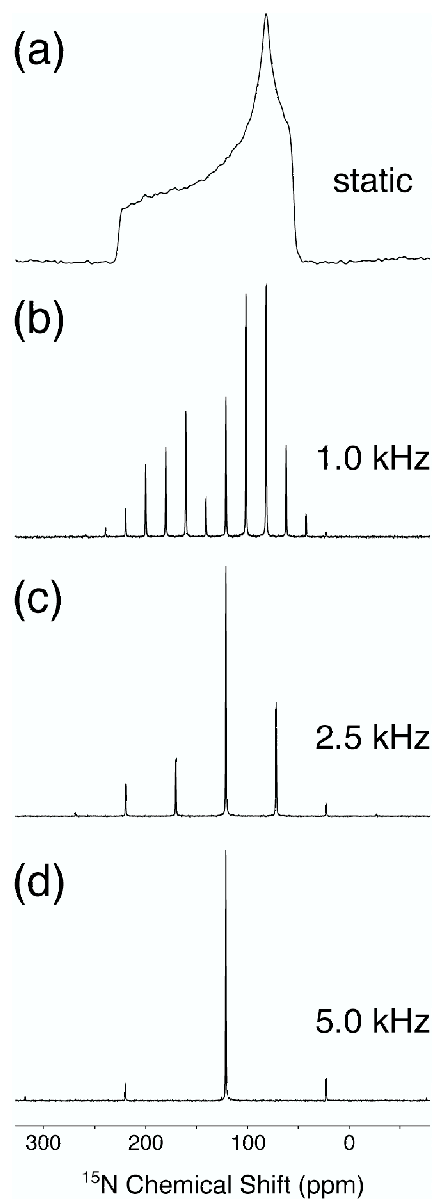


Figure 1-4. ^{15}N NMR spectra of polycrystalline ^{15}N labeled N-acetyl-L-valine.

In the static spectrum (a) the chemical shift anisotropy powder pattern characteristic of amide groups spans the region between approximately 50-200 ppm. Magic-angle spinning spectra obtained at spinning frequencies of $\omega_r/2\pi = 1.0, 2.5$ and 5.0 kHz are shown in (b)-(d), respectively. The MAS spectra are characterized by the centerband at the isotropic chemical shift regardless of the spinning frequency, and rotational sidebands at integer multiples of ω_r from the centerband. Spectra were acquired at 50.7 MHz ^{15}N frequency with using cross-polarization with proton decoupling. The static and MAS spectra are an average of 512 and 64 transients, respectively. Note that the spectral intensities are scaled to approximately the same height and the signal-to-noise ratio is highest in (d).

References

- (1) H. M. Berman, J. Westbrook, Z. Feng, G. Gilliland, T. N. Bhat, H. Weissig, I. N. Shindyalov and P. E. Bourne, "The Protein Data Bank," *Nucleic Acid Res.* **28**, 235-242 (2000).
- (2) M. M. Yusupov, G. Z. Yusupova, A. Baucom, K. Lieberman, T. N. Earnest, J. H. D. Cate and H. F. Noller, "Crystal Structure of the Ribosome at 5.5 Å Resolution," *Science* **292**, 883-896 (2001).
- (3) K. Wüthrich, "NMR of Proteins and Nucleic Acids," Wiley, New York, 1986.
- (4) J. Cavanagh, W. J. Fairbrother, A. G. Palmer and N. J. Skelton, "Protein NMR Spectroscopy: Principles and Practice," Academic Press, San Diego, 1996.
- (5) K. Pervushin, R. Riek, G. Wider and K. Wüthrich, "Attenuated T₂ relaxation by mutual cancellation of dipole-dipole coupling and chemical shift anisotropy indicates an avenue to NMR structures of very large biological macromolecules in solution," *Proc. Natl. Acad. Sci. USA* **94**, 12366-12371 (1997).
- (6) N. Tjandra and A. Bax, "Direct measurement of distances and angles in biomolecules by NMR in a dilute liquid crystalline medium," *Science* **278**, 1111-1114 (1997).
- (7) J. R. Tolman, J. M. Flanagan, M. A. Kennedy and J. H. Prestegard, "Nuclear magnetic dipole interactions in field-oriented proteins - Information for structure determination in solution," *Proc. Natl. Acad. Sci. USA* **92**, 9279-9283 (1995).
- (8) C. Fernandez, K. Adeishvili and K. Wuthrich, "Transverse relaxation-optimized NMR spectroscopy with the outer membrane protein OmpX in dihexanoyl phosphatidylcholine micelles," *Proc. Natl. Acad. Sci. USA* **98**, 2358-2363 (2001).

- (9) A. Arora, F. Abildgaard, J. Bushweller and L. K. Tamm, "Structure of outer membrane protein A transmembrane domain by NMR spectroscopy," *Nature Struct. Biol.* **8**, 334-338 (2001).
- (10) J. Fiaux, E. B. Bertelsen, A. L. Horwich and K. Wuthrich, "NMR analysis of a 900K GroEL-GroES complex," *Nature* **418**, 207-211 (2002).
- (11) V. Tugarinov, R. Muhandiram, A. Ayed and L. E. Kay, "Four-dimensional NMR spectroscopy of a 723-residue protein: Chemical shift assignments and secondary structure of malate synthase G," *J. Am. Chem. Soc.* **124**, 10025-10035 (2002).
- (12) D. P. Weliky, A. E. Bennett, A. Zvi, J. Anglister, P. J. Steinbach and R. Tycko, "Solid-state NMR evidence for an antibody-dependent conformation of the V3 loop of HIV-1 gp120," *Nature Struct. Biol.* **6**, 141-145 (1999).
- (13) A. E. McDermott, F. Creuzet, R. G. Griffin, L. E. Zawadzke, Q. Z. Ye and C. T. Walsh, "Rotational resonance determination of the structure of an enzyme-inhibitor complex: phosphorylation of an (amino alkyl) phosphonate inhibitor of D-alanyl-D-alanine ligase by ATP," *Biochemistry* **29**, 5767 (1990).
- (14) A. M. Christensen and J. Schaefer, "Solid-state NMR determination of intramolecular and intermolecular ^{31}P - ^{13}C distances for shikimate-3-phosphate and $[1\text{-}^{13}\text{C}]$ glyphosate bound to enolpyruvylshikimate-3-phosphate synthase," *Biochemistry* **32**, 2868-2873 (1993).
- (15) L. M. McDowell, C. A. Klug, D. D. Beusen and J. Schaefer, "Ligand geometry of the ternary complex of 5-enolpyruvylshikimate-3-phosphate synthase from rotational-echo double-resonance NMR," *Biochemistry* **35**, 5395-5403 (1996).

- (16) L. M. McDowell, M. S. Lee, R. A. McKay, K. S. Anderson and J. Schaefer, "Intersubunit communication in tryptophan synthase by ^{13}C and ^{19}F REDOR NMR," *Biochemistry* **35**, 3328-3334 (1996).
- (17) L. M. McDowell, A. Schmidt, E. R. Cohen, D. R. Studelska and J. Schaefer, "Structural constraints on the ternary complex of 5-enolpyruvylshikimate-3-phosphate synthase from rotational-echo double-resonance NMR," *J. Mol. Biol.* **256**, 160-171 (1996).
- (18) L. Kaustov, S. Kababya, S. C. Du, T. Baasov, S. Gropper, Y. Shoham and A. Schmidt, "Structural and mechanistic investigation of 3-deoxy-D-manno-octulosonate-8-phosphate synthase by solid-state REDOR NMR," *Biochemistry* **39**, 14865-14876 (2000).
- (19) L. Kaustov, S. Kababya, S. C. Du, T. Baasov, S. Gropper, Y. Shoham and A. Schmidt, "Direct identification of enzyme active site residues by solid-state REDOR NMR: Application to KDO8P synthase," *J. Am. Chem. Soc.* **122**, 2649-2650 (2000).
- (20) J. R. Long, N. Oyler, G. P. Drobny and P. S. Stayton, "Assembly of α -helical peptide coatings on hydrophobic surfaces," *J. Am. Chem. Soc.* **124**, 6297-6303 (2002).
- (21) J. R. Long, W. J. Shaw, P. S. Stayton and G. P. Drobny, "Structure and dynamics of hydrated statherin on hydroxyapatite as determined by solid-state NMR," *Biochemistry* **40**, 15451-15455 (2001).

- (22) W. J. Shaw, J. R. Long, A. A. Campbell, P. S. Stayton and G. P. Drobny, "A solid state NMR study of dynamics in a hydrated salivary peptide adsorbed to hydroxyapatite," *J. Am. Chem. Soc.* **122**, 7118-7119 (2000).
- (23) M. Gilbert, W. J. Shaw, J. R. Long, K. Nelson, G. P. Drobny, C. M. Giachelli and P. S. Stayton, "Chimeric peptides of statherin and osteopontin that bind hydroxyapatite and mediate cell adhesion," *J. Biol. Chem.* **275**, 16213-16218 (2000).
- (24) W. J. Shaw, J. R. Long, J. L. Dindot, A. A. Campbell, P. S. Stayton and G. P. Drobny, "Determination of statherin N-terminal peptide conformation on hydroxyapatite crystals," *J. Am. Chem. Soc.* **122**, 1709-1716 (2000).
- (25) K. V. Lakshmi, M. Auger, J. Raap, J. Lugtenburg, R. G. Griffin and J. Herzfeld, "Internuclear distance measurement in a reaction intermediate: solid-state ^{13}C NMR rotational resonance determination of the Schiff-base configuration in the M-photointermediate of bacteriorhodopsin," *J. Am. Chem. Soc.* **115**, 8515-8516 (1993).
- (26) J. M. Griffiths, A. E. Bennett, M. Engelhard, F. Siebert, J. Raap, J. Lugtenburg, J. Herzfeld and R. G. Griffin, "Structural investigation of the active site of bacteriorhodopsin: Geometric constraints on the roles of Asp-85 and Asp-212 in the proton pumping mechanism from solid-state NMR," *Biochemistry* **39**, 362-371 (2000).
- (27) Y. Li, R. J. Appleyard, W. A. Shuttleworth and J. N. S. Evans, "Time-resolved solid-state REDOR NMR measurements on 5-enolpyruvylshikimate-3-phosphate synthase," *J. Am. Chem. Soc.* **116**, 10799-10800 (1994).
- (28) J. C. Lansing, M. Hohwy, C. P. Jaroniec, A. F. L. Creemers, J. Lugtenburg, J. Herzfeld and R. G. Griffin, "Chromophore distortions in the bacteriorhodopsin

photocycle: Evolution of the H-C14-C15-H dihedral angle measured by solid-state NMR," *Biochemistry* **41**, 431-438 (2002).

- (29) A. T. Petkova, M. Hatanaka, C. P. Jaroniec, J. G. Hu, M. Belenky, M. Verhoeven, J. Lugtenburg, R. G. Griffin and J. Herzfeld, "Tryptophan interactions in bacteriorhodopsin: A heteronuclear solid-state NMR study," *Biochemistry* **41**, 2429-2437 (2002).
- (30) M. Sunde and C. C. F. Blake, "From the globular to the fibrous state: protein structure and structural conversion in amyloid formation," *Q. Rev. Biophys.* **31**, 1-39 (1998).
- (31) J. W. Kelly, "The alternative conformations of amyloidogenic proteins and their multi-step assembly pathways," *Curr. Opin. Struct. Biol.* **8**, 101-106 (1998).
- (32) R. G. S. Spencer, K. J. Halverson, M. Auger, A. E. McDermott, R. G. Griffin and P. T. Lansbury, "An unusual peptide conformation may precipitate amyloid formation in Alzheimer's disease: Application of solid-state NMR to the determination of protein secondary structure," *Biochemistry* **30**, 10382-10387 (1991).
- (33) P. T. Lansbury, P. R. Costa, J. M. Griffiths, E. J. Simon, M. Auger, K. J. Halverson, D. A. Kocisko, Z. S. Hendsch, T. T. Ashburn, R. G. S. Spencer, B. Tidor and R. G. Griffin, "Structural model for the β -amyloid fibril based on interstrand alignment of an antiparallel-sheet comprising a C-terminal peptide," *Nature Struct. Biol.* **2**, 990-998 (1995).
- (34) J. M. Griffiths, T. T. Ashburn, M. Auger, P. R. Costa, R. G. Griffin and P. T. Lansbury, "Rotational resonance solid-state NMR elucidates a structural model of pancreatic amyloid," *J. Am. Chem. Soc.* **117**, 3539-3546 (1995).

- (35) T. L. S. Benzinger, D. M. Gregory, T. S. Burkoth, H. Miller-Auer, D. G. Lynn, R. E. Botto and S. C. Meredith, "Propagating structure of Alzheimer's β -amyloid₍₁₀₋₃₅₎ is parallel β -sheet with residues in exact register," *Proc. Natl. Acad. Sci. USA* **95**, 13407-13412 (1998).
- (36) T. L. S. Benzinger, D. M. Gregory, T. S. Burkoth, H. Miller-Auer, D. G. Lynn, R. E. Botto and S. C. Meredith, "Two-dimensional structure of β -amyloid(10-35) fibrils," *Biochemistry* **39**, 3491-3499 (2000).
- (37) D. M. Gregory, T. L. S. Benzinger, T. S. Burkoth, H. Miller-Auer, D. G. Lynn, S. C. Meredith and R. E. Botto, "Dipolar recoupling NMR of biomolecular self-assemblies: determining inter- and intrastrand distances in fibrilized Alzheimer's β -amyloid peptide," *Solid State Nucl. Magn. Reson.* **13**, 149-166 (1998).
- (38) J. Heller, A. C. Kolbert, R. Larsen, M. Ernst, T. Bekker, M. Baldwin, S. B. Prusiner, A. Pines and D. E. Wemmer, "Solid-state NMR studies of the prion protein H1 fragment," *Protein Sci.* **5**, 1655-1661 (1996).
- (39) D. D. Laws, H. L. Bitter, K. Liu, H. L. Ball, K. Kaneko, H. Wille, F. E. Cohen, S. B. Prusiner, A. Pines and D. E. Wemmer, "Solid-state NMR studies of the secondary structure of a mutant prion protein fragment of 55 residues that induces neurodegeneration," *Proc. Natl. Acad. Sci. USA* **98**, 11686-11690 (2001).
- (40) O. N. Antzutkin, J. J. Balbach, R. D. Leapman, N. W. Rizzo, J. Reed and R. Tycko, "Multiple quantum solid-state NMR indicates a parallel, not antiparallel, organization of β -sheets in Alzheimer's β -amyloid fibrils," *Proc. Natl. Acad. Sci. USA* **97**, 13045-13050 (2000).

- (41) J. J. Balbach, Y. Ishii, O. N. Antzutkin, R. D. Leapman, N. W. Rizzo, F. Dyda, J. Reed and R. Tycko, "Amyloid fibril formation by A β 16-22, a seven-residue fragment of the Alzheimer's β -amyloid peptide, and structural characterization by solid state NMR," *Biochemistry* **39**, 13748-13759 (2000).
- (42) R. Tycko, "Solid-state NMR as a probe of amyloid fibril structure," *Curr. Opin. Chem. Biol.* **4**, 500-506 (2000).
- (43) R. Tycko, "Biomolecular solid state NMR: Advances in structural methodology and applications to peptide and protein fibrils," *Annu. Rev. Phys. Chem.* **52**, 575-606 (2001).
- (44) C. P. Jaroniec, C. E. MacPhee, N. S. Astrof, C. M. Dobson and R. G. Griffin, "Molecular conformation of a peptide fragment of transthyretin in an amyloid fibril," *Proc. Natl. Acad. Sci. USA*, in press (2002).
- (45) S. J. Opella, "NMR and membrane proteins," *Nature Struct. Biol.* **4**, 845-848 (1997).
- (46) S. J. Opella, C. Ma and F. M. Marassi, "Nuclear magnetic resonance of membrane-associated peptides and proteins," *Methods Enzymol.* **339**, 285-313 (2001).
- (47) R. Fu and T. A. Cross, "Solid-state nuclear magnetic resonance investigation of protein and polypeptide structure," *Annu. Rev. Biophys. Biomol. Struct.* **28**, 235-268 (1999).
- (48) F. Cruzet, A. McDermott, R. Gebhard, K. v. d. Hoef, M. B. Spijker-Assink, J. Herzfeld, J. Lugtenburg, M. H. Levitt and R. G. Griffin, "Determination of membrane protein structure by rotational resonance NMR: Bacteriorhodopsin," *Science* **251**, 783-786 (1991).

- (49) L. K. Thompson, A. E. McDermott, J. Raap, C. M. v. d. Wielen, J. Lugtenburg, J. Herzfeld and R. G. Griffin, "Rotational resonance NMR study of the active site structure in bacteriorhodopsin: Conformation of the Schiff base linkage," *Biochemistry* **31**, 7931-7938 (1992).
- (50) X. Feng, P. J. E. Verdegem, Y. K. Lee, D. Sandström, M. Edén, P. Bovee-Geurts, W. J. de Grip, J. Lugtenburg, H. J. M. de Groot and M. H. Levitt, "Direct determination of a molecular torsional angle in the membrane protein rhodopsin by solid-state NMR," *J. Am. Chem. Soc.* **119**, 6853-6857 (1997).
- (51) C. P. Jaroniec, J. C. Lansing, B. A. Tounge, M. Belenky, J. Herzfeld and R. G. Griffin, "Measurement of dipolar couplings in a uniformly ^{13}C , ^{15}N -labeled membrane protein: Distances between the Schiff base and aspartic acids in the active site of bacteriorhodopsin," *J. Am. Chem. Soc.* **123**, 12929-12930 (2001).
- (52) E. R. Andrew, A. Bradbury and R. G. Eades, "Nuclear magnetic resonance spectra from a crystal rotated at high speed," *Nature* **182**, 1659 (1958).
- (53) I. J. Lowe, "Free induction decay of rotating solids," *Phys. Rev. Lett.* **2**, 285 (1959).
- (54) A. Pines, M. G. Gibby and J. S. Waugh, "Proton-enhanced NMR of dilute spins in solids," *J. Chem. Phys.* **59**, 569-590 (1973).
- (55) J. Schaefer and E. O. Stejskal, " ^{13}C Nuclear Magnetic-Resonance of Polymers Spinning at Magic Angle," *J. Am. Chem. Soc.* **98**, 1031-1032 (1976).
- (56) E. O. Stejskal, J. Schaefer and J. S. Waugh, "Magic-Angle Spinning and Polarization Transfer in Proton- Enhanced Nmr," *J. Magn. Reson.* **28**, 105-112 (1977).

- (57) M. Mehring, A. Pines, W. K. Rhim and J. S. Waugh, "Spin-decoupling in the resolution of chemical shifts in solids by pulsed NMR," *J. Chem. Phys.* **54**, 3239-3240 (1971).
- (58) D. L. Vanderhart, W. L. Earl and A. N. Garroway, "Resolution in ^{13}C NMR of organic solids using high power proton decoupling and magic angle sample spinning," *J. Magn. Reson.* **44**, 361-401 (1981).
- (59) J. S. Waugh, "Theory of Broad-Band Spin Decoupling," *J. Magn. Reson.* **50**, 30-49 (1982).
- (60) J. S. Waugh, "Systematic Procedure for Constructing Broad-Band Decoupling Sequences," *J. Magn. Reson.* **49**, 517-521 (1982).
- (61) A. E. Bennett, C. M. Rienstra, M. Auger, K. V. Lakshmi and R. G. Griffin, "Heteronuclear decoupling in rotating solids," *J. Chem. Phys.* **103**, 6951-6957 (1995).
- (62) M. M. Maricq and J. S. Waugh, "NMR in rotating solids," *J. Chem. Phys.* **70**, 3300-3316 (1979).
- (63) J. Herzfeld and A. E. Berger, "Sideband intensities in NMR spectra of samples spinning at the magic angle," *J. Chem. Phys.* **73**, 6021-6030 (1980).
- (64) U. Haeberlen and J. S. Waugh, "Coherent averaging effects in magnetic resonance," *Phys. Rev.* **175**, 453-467 (1968).
- (65) U. Haeberlen, "High-Resolution NMR in Solids: Selective Averaging," Academic Press, New York, 1976.
- (66) J. H. Shirley, "Solution of the Schrödinger Equation with a Hamiltonian Periodic in Time," *Phys. Rev.* **138**, B979-B987 (1965).

- (67) S. Vega. in *Nuclear Magnetic Resonance Probes of Molecular Dynamics* (ed. R. Tycko) 155-222 (Kluwer Academic Publishers, Dordrecht, 1994).
- (68) J. S. Waugh, L. M. Huber and U. Haeberlen, "Approach to high-resolution NMR in solids," *Phys. Rev. Lett.* **20**, 180-182 (1968).
- (69) W. K. Rhim, D. D. Elleman and R. W. Vaughan, "Enhanced resolution for solid-state NMR," *J. Chem. Phys.* **58**, 1772-1773 (1973).
- (70) A. Bielecki, A. C. Kolbert and M. H. Levitt, "Frequency switched pulse sequences: Homonuclear decoupling and dilute spin NMR in solids," *Chem. Phys. Lett.* **155**, 341-346 (1989).
- (71) E. Vinogradov, P. K. Madhu and S. Vega, "Proton spectroscopy in solid state nuclear magnetic resonance with windowed phase modulated Lee-Goldburg decoupling sequences," *Chem. Phys. Lett.* **354**, 193-202 (2002).
- (72) E. Vinogradov, P. K. Madhu and S. Vega, "Phase modulated Lee-Goldburg magic angle spinning proton nuclear magnetic resonance experiments in the solid state: A bimodal Floquet theoretical treatment," *J. Chem. Phys.* **115**, 8983-9000 (2001).
- (73) E. Vinogradov, P. K. Madhu and S. Vega, "A bimodal Floquet analysis of phase modulated Lee-Goldburg high resolution proton magic angle spinning NMR experiments," *Chem. Phys. Lett.* **329**, 207-214 (2000).
- (74) E. Vinogradov, P. K. Madhu and S. Vega, "High-resolution proton solid-state NMR spectroscopy by phase-modulated Lee-Goldburg experiment," *Chem. Phys. Lett.* **314**, 443-450 (1999).
- (75) P. K. Madhu, X. Zhao and M. H. Levitt, "High-resolution ^1H NMR in the solid state using symmetry-based pulse sequences," *Chem. Phys. Lett.* **346**, 142-148 (2001).

- (76) M. Eden and M. H. Levitt, "Pulse sequence symmetries in the nuclear magnetic resonance of spinning solids: Application to heteronuclear decoupling," *J. Chem. Phys.* **111**, 1511-1519 (1999).
- (77) Y. Yarimagaev, P. N. Tutunjian and J. S. Waugh, "Sample Spinning at the Magic Angle with Rotation-Synchronized Rf Pulses," *J. Magn. Reson.* **47**, 51-60 (1982).
- (78) R. Tycko, G. Dabbagh and P. A. Mirau, "Determination of Chemical-Shift-Anisotropy Lineshapes in a Two- Dimensional Magic-Angle-Spinning Nmr Experiment," *J. Magn. Reson.* **85**, 265-274 (1989).
- (79) T. G. Oas, R. G. Griffin and M. H. Levitt, "Rotary resonance recoupling of dipolar interactions in solid-state nuclear magnetic resonance spectroscopy," *J. Chem. Phys.* **89**, 692-695 (1988).
- (80) M. H. Levitt, T. G. Oas and R. G. Griffin, "Rotary resonance recoupling in heteronuclear spin pair systems," *Isr. J. Chem.* **28**, 271-282 (1988).
- (81) T. Gullion and J. Schaefer, "Rotational-echo double-resonance NMR," *J. Magn. Reson.* **81**, 196-200 (1989).
- (82) R. Tycko and G. Dabbagh, "Measurement of Nuclear Magnetic Dipole-Dipole Couplings in Magic Angle Spinning Nmr," *Chem. Phys. Lett.* **173**, 461-465 (1990).
- (83) T. Gullion and S. Vega, "A simple magic angle spinning NMR experiment for the dephasing of rotational echoes of dipolar coupled homonuclear spin pairs," *Chem. Phys. Lett.* **194**, 423-428 (1992).
- (84) A. E. Bennett, J. H. Ok, R. G. Griffin and S. Vega, "Chemical shift correlation spectroscopy in rotating solids: Radio frequency driven dipolar recoupling and longitudinal exchange," *J. Chem. Phys.* **96**, 8624-8627 (1992).

- (85) J. M. Griffiths and R. G. Griffin, "Nuclear magnetic resonance methods for measuring dipolar couplings in rotating solids," *Anal. Chim. Acta* **283**, 1081-1101 (1993).
- (86) S. Dusold and A. Sebald, "Dipolar recoupling under magic-angle spinning conditions," *Annu. Rep. Nucl. Magn. Reson. Spectr.* **41**, 185-264 (2000).
- (87) M. H. Levitt. in *Encyclopedia of Nuclear Magnetic Resonance: Supplementary Volume* (eds. D. M. Grant and R. K. Harris) 165-196 (Wiley, Chichester, 2002).
- (88) R. K. Hester, J. L. Ackerman, B. L. Neff and J. S. Waugh, "Separated Local Field Spectra in Nmr - Determination of Structure of Solids," *Phys. Rev. Lett.* **36**, 1081-1083 (1976).
- (89) J. S. Waugh, "Uncoupling of Local Field Spectra in Nuclear Magnetic-Resonance - Determination of Atomic Positions in Solids," *Proc. Natl. Acad. Sci. USA* **73**, 1394-1397 (1976).
- (90) M. E. Stoll, A. J. Vega and R. W. Vaughan, "Heteronuclear Dipolar Modulated Chemical-Shift Spectra for Geometrical Information in Polycrystalline Solids," *J. Chem. Phys.* **65**, 4093-4098 (1976).
- (91) M. Linder, A. Hohener and R. R. Ernst, "Orientation of Tensorial Interactions Determined from 2- Dimensional Nmr Powder Spectra," *J. Chem. Phys.* **73**, 4959-4970 (1980).
- (92) M. G. Munowitz, R. G. Griffin, G. Bodenhausen and T. H. Huang, "Two-dimensional rotational spin-echo nuclear magnetic resonance in solids: Correlation of chemical shift and dipolar interactions," *J. Am. Chem. Soc.* **103**, 2529-2533 (1981).

- (93) M. G. Munowitz, W. P. Aue and R. G. Griffin, "Two-dimensional separation of dipolar and scaled isotropic chemical shift interactions in magic angle NMR spectra," *J. Chem. Phys.* **77**, 1686-1689 (1982).
- (94) M. G. Munowitz and R. G. Griffin, "Two-dimensional nuclear magnetic resonance in rotating solids: An analysis of line shapes in chemical shift-dipolar spectra," *J. Chem. Phys.* **76**, 2848-2858 (1982).
- (95) M. G. Munowitz and R. G. Griffin, "Two-dimensional nuclear magnetic resonance in rotating solids: Time reversal effects in chemical shift-dipolar spectra," *J. Chem. Phys.* **78**, 613-617 (1983).
- (96) L. M. McDowell and J. Schaefer, "High resolution NMR of biological solids," *Curr. Opin. Struct. Biol.* **6**, 624-629 (1996).
- (97) R. G. Griffin, "Dipolar recoupling in MAS spectra of biological solids," *Nature Struct. Biol.* **5**, 508-512 (1998).
- (98) A. E. Bennett, R. G. Griffin and S. Vega. in *Solid State NMR IV: Methods and Applications of Solid-State NMR* (ed. B. Blumich) 1-77 (Springer-Verlag, Berlin, 1994).
- (99) B. Q. Sun, P. R. Costa, D. Kocisko, P. T. Lansbury and R. G. Griffin, "Internuclear distance measurements in solid state nuclear magnetic resonance: Dipolar recoupling via rotor synchronized spin locking," *J. Chem. Phys.* **102**, 702-707 (1995).
- (100) B. Q. Sun, C. M. Rienstra, P. R. Costa, J. R. Williamson and R. G. Griffin, "3D ^{15}N - ^{13}C - ^{13}C chemical shift correlation spectroscopy in rotating solids," *J. Am. Chem. Soc.* **119**, 8540-8546 (1997).

- (101) S. K. Straus, T. Bremi and R. R. Ernst, "Experiments and strategies for the assignment of fully $^{13}\text{C}/^{15}\text{N}$ -labelled polypeptides by solid state NMR," *J. Biomol. NMR* **12**, 39-50 (1998).
- (102) M. Hohwy, H. J. Jakobsen, M. Edén, M. H. Levitt and N. C. Nielsen, "Broadband dipolar recoupling in the nuclear magnetic resonance of rotating solids: A compensated C7 pulse sequence," *J. Chem. Phys.* **108**, 2686-2694 (1998).
- (103) M. Hohwy, C. M. Rienstra, C. P. Jaroniec and R. G. Griffin, "Fivefold symmetric homonuclear dipolar recoupling in rotating solids: Application to double quantum spectroscopy," *J. Chem. Phys.* **110**, 7983-7992 (1999).
- (104) M. Hohwy, C. M. Rienstra and R. G. Griffin, "Band-selective homonuclear dipolar recoupling in rotating solids," *J. Chem. Phys.* **117**, 4973-4987 (2002).
- (105) C. M. Rienstra, M. E. Hatcher, L. J. Mueller, B. Q. Sun, S. W. Fesik and R. G. Griffin, "Efficient multispin homonuclear double-quantum recoupling for magic-angle spinning NMR: ^{13}C - ^{13}C correlation spectroscopy of U- ^{13}C -Erythromycin A," *J. Am. Chem. Soc.* **120**, 10602-10612 (1998).
- (106) C. M. Rienstra, M. Hohwy, M. Hong and R. G. Griffin, "2D and 3D ^{15}N - ^{13}C - ^{13}C NMR chemical shift correlation spectroscopy of solids: assignment of MAS spectra of peptides," *J. Am. Chem. Soc.* **122**, 10979-10990 (2000).
- (107) A. Detken, E. H. Hardy, M. Ernst, M. Kainosho, T. Kawakami, S. Aimoto and B. H. Meier, "Methods for sequential resonance assignment in solid, uniformly ^{13}C , ^{15}N labelled peptides: Quantification and application to antamanide," *J. Biomol. NMR* **20**, 203-221 (2001).

- (108) M. Hong, "Resonance assignment of $^{13}\text{C}/^{15}\text{N}$ labeled solid proteins by two- and three-dimensional magic-angle-spinning NMR," *J. Biomol. NMR* **15**, 1-14 (1999).
- (109) A. McDermott, T. Polenova, A. Bockmann, K. W. Zilm, E. K. Paulsen, R. W. Martin and G. T. Montelione, "Partial NMR assignments for uniformly ($^{13}\text{C},^{15}\text{N}$)-enriched BPTI in the solid state," *J. Biomol. NMR* **16**, 209-219 (2000).
- (110) M. Baldus, A. T. Petkova, J. Herzfeld and R. G. Griffin, "Cross polarization in the tilted frame: assignment and spectral simplification in heteronuclear spin systems," *Mol. Phys.* **95**, 1197-1207 (1998).
- (111) J. Pauli, M. Baldus, B. van Rossum, H. de Groot and H. Oschkinat, "Backbone and side-chain ^{13}C and ^{15}N signal assignments of the α -spectrin SH3 domain by magic angle spinning solid-state NMR at 17.6 Tesla," *ChemBiochem* **2**, 272-281 (2001).
- (112) B. J. van Rossum, F. Castellani, K. Rehbein, J. Pauli and H. Oschkinat, "Assignment of the nonexchanging protons of the alpha-spectrin SH3 domain by two- and three-dimensional $^1\text{H}-^{13}\text{C}$ solid-state magic-angle spinning NMR and comparison of solution and solid-state proton chemical shifts," *ChemBiochem* **2**, 906-914 (2001).
- (113) J. Pauli, B. van Rossum, H. Forster, H. J. M. de Groot and H. Oschkinat, "Sample optimization and identification of signal patterns of amino acid side chains in 2D RFDR spectra of the alpha-spectrin SH3 domain," *J. Magn. Reson.* **143**, 411-416 (2000).
- (114) T. A. Egorova-Zachernyuk, J. Hollander, N. Fraser, P. Gast, A. J. Hoff, R. Cogdell, H. J. M. de Groot and M. Baldus, "Heteronuclear 2D-correlations in a

- uniformly [^{13}C , ^{15}N] labeled membrane-protein complex at ultra-high magnetic fields," *J. Biomol. NMR* **19**, 243-253 (2001).
- (115) K. Takegoshi, K. Nomura and T. Terao, "Rotational resonance in the tilted rotating frame," *Chem. Phys. Lett.* **232**, 424-428 (1995).
- (116) K. Nomura, K. Takegoshi, T. Terao, K. Uchida and M. Kainosho, "Determination of the complete structure of a uniformly labeled molecule by rotational resonance solid-state NMR in the tilted rotating frame," *J. Am. Chem. Soc.* **121**, 4064-4065 (1999).
- (117) K. Nomura, K. Takegoshi, T. Terao, K. Uchida and M. Kainosho, "Three-dimensional structure determination of a uniformly labeled molecule by frequency-selective dipolar recoupling under magic-angle spinning," *J. Biomol. NMR* **17**, 111-123 (2000).
- (118) C. A. Michal and L. W. Jelinski, "REDOR 3D: Heteronuclear distance measurements in uniformly labeled and natural abundance solids," *J. Am. Chem. Soc.* **119**, 9059-9060 (1997).
- (119) C. P. Jaroniec, B. A. Tounge, C. M. Rienstra, J. Herzfeld and R. G. Griffin, "Measurement of ^{13}C - ^{15}N distances in uniformly ^{13}C labeled biomolecules: J-decoupled REDOR," *J. Am. Chem. Soc.* **121**, 10237-10238 (1999).
- (120) C. P. Jaroniec, B. A. Tounge, J. Herzfeld and R. G. Griffin, "Frequency selective heteronuclear dipolar recoupling in rotating solids: Accurate ^{13}C - ^{15}N distance measurements in uniformly ^{13}C , ^{15}N -labeled peptides," *J. Am. Chem. Soc.* **123**, 3507-3519 (2001).

- (121) C. P. Jaroniec, C. Filip and R. G. Griffin, "3D TEDOR NMR experiments for the simultaneous measurement of multiple carbon-nitrogen distances in uniformly ^{13}C , ^{15}N -Labeled Solids," *J. Am. Chem. Soc.* **124**, 10728-10742 (2002).
- (122) X. Feng, Y. K. Lee, D. Sandström, M. Eden, H. Maisel, A. Sebald and M. H. Levitt, "Direct determination of a molecular torsional angle by solid-state NMR," *Chem. Phys. Lett.* **257**, 314-320 (1996).
- (123) X. Feng, M. Eden, A. Brinkmann, H. Luthman, L. Eriksson, A. Gräslund, O. N. Antzutkin and M. H. Levitt, "Direct determination of a peptide torsional angle ψ by double-quantum solid-state NMR," *J. Am. Chem. Soc.* **119**, 12006-12007 (1997).
- (124) P. R. Costa, J. D. Gross, M. Hong and R. G. Griffin, "Solid-state NMR measurement of ψ in peptides: a NCCN 2Q-heteronuclear local field experiment," *Chem. Phys. Lett.* **280**, 95-103 (1997).
- (125) M. Hong, J. D. Gross and R. G. Griffin, "Site-resolved determination of peptide torsion angle ϕ from the relative orientations of backbone N-H and C-H bonds by solid-state NMR," *J. Phys. Chem. B* **101**, 5869-5874 (1997).
- (126) J. D. Gross, P. R. Costa and R. G. Griffin, "Tilted n-fold symmetric radio frequency pulse sequences: Applications to CSA and heteronuclear dipolar recoupling in homonuclear dipolar coupled spin networks," *J. Chem. Phys.* **108**, 7286-7293 (1998).
- (127) M. Hohwy, C. P. Jaroniec, B. Reif, C. M. Rienstra and R. G. Griffin, "Local structure and relaxation in solid-state NMR: Accurate measurement of amide N-H bond lengths and H-N-H bond angles," *J. Am. Chem. Soc.* **122**, 3218-3219 (2000).

- (128) B. Reif, M. Hohwy, C. P. Jaroniec, C. M. Rienstra and R. G. Griffin, "NH-NH vector correlation in peptides by solid state NMR," *J. Magn. Reson.* **145**, 132-141 (2000).
- (129) C. M. Rienstra, M. Hohwy, L. J. Mueller, C. P. Jaroniec, B. Reif and R. G. Griffin, "Determination of Multiple Torsion-Angle Constraints in U-¹³C, ¹⁵N-Labeled Peptides: 3D ¹H-¹⁵N-¹³C-¹H Dipolar Chemical Shift NMR Spectroscopy in Rotating Solids," *J. Am. Chem. Soc.* **124**, 11908-11922 (2002).
- (130) V. Ladizhansky, M. Veshtort and R. G. Griffin, "NMR determination of the torsion angle ψ in α -helical peptides and proteins: The HCCN dipolar correlation experiment," *J. Magn. Reson.* **154**, 317-324 (2002).
- (131) Y. Ishii, K. Hirao, T. Terao, T. Terauchi, M. Oba, K. Nishiyama and M. Kainosho, "Determination of peptide ϕ angles in solids by relayed anisotropy correlation NMR," *Solid State Nucl. Magn. Reson.* **11**, 169-175 (1998).
- (132) Y. Ishii, T. Terao and M. Kainosho, "Relayed anisotropy correlation NMR: determination of dihedral angles in solids," *Chem. Phys. Lett.* **256**, 133-140 (1996).
- (133) M. Hong, J. D. Gross, W. Hu and R. G. Griffin, "Determination of the peptide torsion angle ϕ by ¹⁵N chemical shift and ¹³C ^{α} -¹H ^{α} dipolar tensor correlation in solid-state MAS NMR," *J. Magn. Reson.* **135**, 169-177 (1998).
- (134) C. M. Rienstra, L. Tucker-Kellogg, C. P. Jaroniec, M. Hohwy, B. Reif, T. Lozano-Perez, B. Tidor and R. G. Griffin, "De novo determination of peptide structure with solid-state MAS NMR spectroscopy," *Proc. Natl. Acad. Sci. USA* **99**, 10260-10265 (2002).

- (135) F. Castellani, B. van Rossum, A. Diehl, M. Schubert, K. Rehbein and H. Oshkinat, "A first protein structure determined by solid-state magic-angle spinning NMR," *Nature*, in press (2002).
- (136) A. Abragam, "Principles of Nuclear Magnetism," Oxford University Press, New York, 1961.
- (137) C. P. Slichter, "Principles of Magnetic Resonance," Springer-Verlag, Berlin, 1990.
- (138) R. R. Ernst, G. Bodenhausen and A. Wokaun, "Principles of Nuclear Magnetic Resonance in One and Two Dimensions," Clarendon Press, Oxford, 1991.
- (139) M. Mehring, "Principles of High Resolution NMR in Solids," Springer-Verlag, Berlin, 1983.
- (140) B. C. Gerstein and C. R. Dybowski, "Transient Techniques in NMR of Solids," Academic Press, Orlando, 1985.
- (141) M. Munowitz, "Coherence and NMR," Wiley, New York, 1988.
- (142) K. Schmidt-Rohr and H. W. Spiess, "Multidimensional Solid-State NMR and Polymers," Academic Press, San Diego, 1994.
- (143) H. W. Spiess. in *Dynamic NMR Spectroscopy* (eds. P. Diehl, E. Fluck and R. Kosfeld) 55-214 (Springer-Verlag, Berlin, 1978).
- (144) M. E. Rose, "Elementary Theory of Angular Momentum," Wiley, New York, 1957.
- (145) W. Magnus, "On the exponential solution of differential equations for a linear operator," *Pure Appl. Math.* **7**, 649 (1954).

- (146) M. Hohwy and N. C. Nielsen, "Elimination of high order terms in multiple pulse nuclear magnetic resonance spectroscopy: Application to homonuclear decoupling in solids," *J. Chem. Phys.* **106**, 7571-7586 (1997).
- (147) M. Hohwy and N. C. Nielsen, "Systematic design and evaluation of multiple-pulse experiments in nuclear magnetic resonance spectroscopy using a semi-continuous Baker-Campbell-Hausdorff expansion," *J. Chem. Phys.* **1998**, 3780-3791 (1998).
- (148) G. E. Pake, "NMR in hydrated crystals: Fine structure of the ^1H line," *J. Chem. Phys.* **16**, 327 (1948).
- (149) J. J. Sakurai, "Modern Quantum Mechanics," Addison-Wesley, Redwood City, 1985.
- (150) B. H. Meier and W. L. Earl, "A double quantum filter for rotating solids," *J. Am. Chem. Soc.* **109**, 7937-7942 (1987).
- (151) D. P. Raleigh, M. H. Levitt and R. G. Griffin, "Rotational resonance in solid state NMR," *Chem. Phys. Lett.* **146**, 71-76 (1988).
- (152) M. H. Levitt, D. P. Raleigh, F. Cruzet and R. G. Griffin, "Theory and simulations of homonuclear spin pair systems in rotating solids," *J. Chem. Phys.* **92**, 6347-6364 (1990).

CHAPTER 2. REDOR NMR AT HIGH MAS FREQUENCIES

Note: Reproduced with permission from C. P. Jaroniec, B. A. Tounge, C. M. Rienstra, J. Herzfeld and R. G. Griffin, "Recoupling of heteronuclear dipolar interactions with rotational-echo double-resonance at high magic-angle spinning frequencies," *J. Magn. Reson.* 146 (2000) 132-139. Copyright 2000 Academic Press.

ABSTRACT

Heteronuclear dipolar recoupling with rotational-echo double-resonance (REDOR) is investigated in the rapid magic-angle spinning regime, where radiofrequency irradiation occupies a significant fraction of the rotor period (10–60%). We demonstrate, in two model ^{13}C - ^{15}N spin systems, $[1\text{-}^{13}\text{C}, ^{15}\text{N}]$ and $[2\text{-}^{13}\text{C}, ^{15}\text{N}]$ glycine, that REDOR $\Delta S/S_0$ curves acquired at high MAS rates and relatively low recoupling fields are nearly identical to the $\Delta S/S_0$ curve expected for REDOR with ideal δ -function pulses. The only noticeable effect of the finite π pulse length on the recoupling is a minor scaling of the dipolar oscillation frequency. Experimental results are explained using both numerical calculations and average Hamiltonian theory, which is used to derive analytical expressions for evolution under REDOR recoupling sequences with different π pulse phasing schemes. For xy -4 and extensions thereof, finite pulses scale only the dipolar oscillation frequency by a well-defined factor. For other phasing schemes (e.g., xx -4 and $x\bar{x}$ -4) both the frequency and amplitude of the oscillation are expected to change.

2.1 Introduction

Distance and dihedral angle constraints are powerful means for characterizing the three-dimensional structure of biomolecules. In solution-state NMR, the use of the nuclear Overhauser effect to establish through-space connectivities between ^1H nuclei is the foundation of structural studies of proteins and nucleic acids.¹ In addition, recently developed experiments^{2,3} can be used to correlate anisotropic interactions and provide direct information about dihedral angles. In magic-angle spinning (MAS) solid-state NMR, homo- and heteronuclear dipolar recoupling techniques⁴⁻⁸ are employed to measure internuclear distances and relative orientations of dipolar tensors.

The rotational-echo double resonance (REDOR) pulse sequence^{9,10} is frequently used to recouple heteronuclear dipolar interactions in isolated pairs of spin-1/2 nuclei, usually at relatively low magic-angle spinning frequencies ($\omega/2\pi \sim 2-8$ kHz). REDOR is well-compensated for pulse imperfections and resonance offsets¹¹ when recoupling π pulses are phased according to schemes based on $xy-4$,¹² and the technique has been successfully applied to many systems of biological interest.¹³⁻¹⁷

REDOR experiments in spin systems involving multiple low- γ nuclei¹⁸⁻²¹ and/or strong ^1H couplings²² can potentially benefit from spinning frequencies in the regime $\omega/2\pi \sim 10-30$ kHz. However, a concern about the performance of REDOR at high MAS frequencies is the effect of the finite π pulse length on the recoupling.^{23,24} The major aim of the work presented here is to investigate the REDOR recoupling dynamics under conditions where a significant fraction of the rotor period is occupied by rf pulses.

2.2 Theory

The effect of finite pulses on the REDOR (Figure 2-1) dipolar dephasing curve has been considered previously using Floquet theory^{25,26} and average Hamiltonian theory (AHT).²³ Here we derive analytical expressions for the first-order average Hamiltonians²⁷ for REDOR sequences with finite pulse lengths and different π pulse phasing schemes. Calculations were performed for the following phasing schemes: (i) $xyxy$ (REDOR xy -4), (ii) $xxxx$ (REDOR xx -4), and (iii) $x\bar{x}x\bar{x}$ (REDOR $x\bar{x}$ -4). Considering only the heteronuclear dipolar coupling and finite pulse lengths (i.e., neglecting resonance offsets, CSAs and pulse imperfections such as rf inhomogeneity and phase transients), all phasing schemes derived from the xy -4 scheme¹² have the same first-order average Hamiltonian (in our experiments we have used the xy -16 scheme). REDOR xx -4 and REDOR $x\bar{x}$ -4 simulations are included for comparison, although we have not performed experiments with these phasing schemes. In addition, for comparison with the analytical AHT results, we have carried out simulations for the different REDOR sequences by the stepwise numerical propagation of the density operator for a two-spin system.

The high-field truncated Hamiltonian for the heteronuclear dipolar coupling between spins I and S under magic-angle spinning can be expressed as²⁸

$$H_{IS}(t) = -\frac{1}{2}b_{IS}\left\{\sin^2(\beta)\cos[2(\gamma + \omega_r t)] - \sqrt{2}\sin(2\beta)\cos(\gamma + \omega_r t)\right\}2I_z S_z, \quad (1)$$

where

$$b_{IS} = -\left(\frac{\mu_0}{4\pi}\right)\frac{\gamma_I\gamma_S\hbar}{r_{IS}^3} \quad (2)$$

is the dipolar coupling constant, which depends on the I-S distance, r_{IS} , and gyromagnetic ratios characteristic of the I and S spins, γ_I and γ_S , respectively. The Euler angles, β and γ ,

relate the I-S dipole vector to the rotor-fixed reference frame.

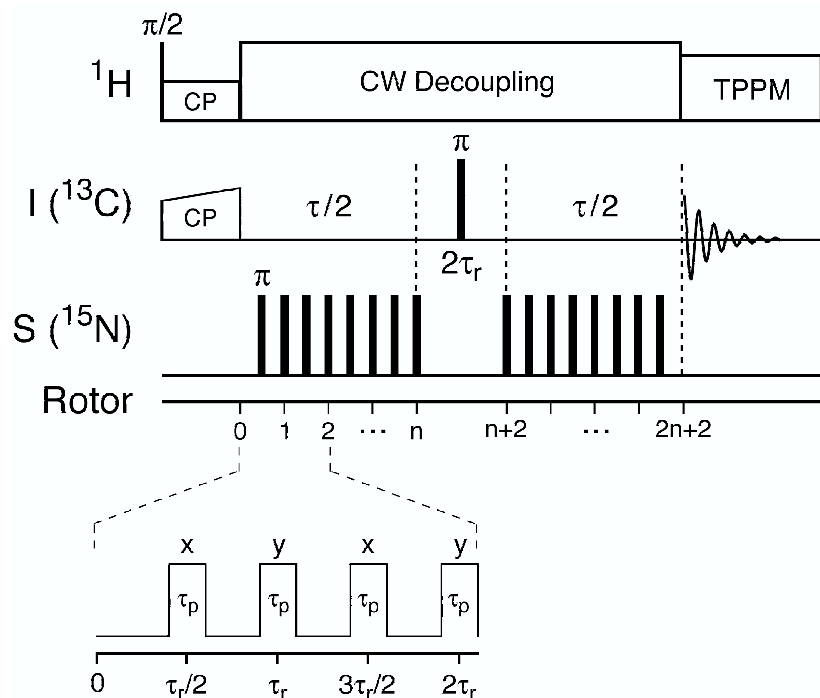


Figure 2-1. REDOR pulse sequence.

Following ramped ^1H - ^{13}C cross-polarization,⁴³ the ^{13}C signal is observed as a spin-echo. The intensity of the echo is modulated due to the ^{13}C - ^{15}N dipole interactions, recoupled by applying rotor-synchronized π pulses to ^{15}N spins. Timing of ^{15}N pulses within the rotor period is shown in the inset and the basic xy -4 phase cycle is indicated. The experiments shown used the xy -16 scheme.¹² Reference (S_0) experiments were performed in the absence of ^{15}N pulses.

In the interaction representation defined by the rf field, the Hamiltonian for the I-S dipolar coupling acquires an additional time-dependence according to

$$\tilde{H}_{IS}(t) = U_{rf}^{-1}(t, t_0) H_{IS}(t) U_{rf}(t, t_0), \quad (3)$$

where the propagator due to the rf pulse on the S spin along the x axis of the rotating frame is defined as

$$U_{rf}(t_2, t_1) = \exp\{-i\omega_{rf} S_x(t_2 - t_1)\}. \quad (4)$$

For the different REDOR sequences considered here, the rf pulses applied to the S spin

impart a time-dependence to the S_z operator and the interaction frame Hamiltonian can be written^{25,26}

$$\tilde{H}_{IS}(t) = \omega_{IS}(t)\{f(t)2I_zS_z + g(t)2I_zS_x + h(t)2I_zS_y\}, \quad (5)$$

where $\omega_{IS}(t)$ is the crystallite-dependent dipolar oscillation frequency (c.f. eq 1), and the coefficients $f(t)$, $g(t)$ and $h(t)$ are as shown in Figure 2-2. $f(t)$ is identical for all π pulse phasing schemes and toggles between ± 1 during subsequent delays between pulses. $g(t)$ and $h(t)$ are a direct consequence of the finite pulses: they can be non-zero only during the pulses and are different for the various phasing schemes.²⁶

The first-order average Hamiltonian is calculated as the average of the interaction frame Hamiltonian over the cycle time, t_c , of the pulse sequence:²⁷

$$\bar{H}_{IS}^{(1)} = \frac{1}{t_c} \int_{t_0}^{t_0+t_c} \tilde{H}_{IS}(t) dt. \quad (6)$$

Explicit calculation of the first-order average Hamiltonian for the I-S dipolar coupling for REDOR xy -4 with finite pulses yields

$$\bar{H}_{IS}^{(1)} = -\frac{\sqrt{2}}{\pi} b_{IS} \frac{\cos(\frac{\pi}{2}\varphi)}{1-\varphi^2} \sin(2\beta) \sin(\gamma) 2I_zS_z, \quad (7)$$

where

$$\varphi = \frac{2\tau_p}{\tau_r} \quad (8)$$

is the fraction of the rotor period occupied by rf pulses, defined in the range $0 \leq \varphi \leq 1$.

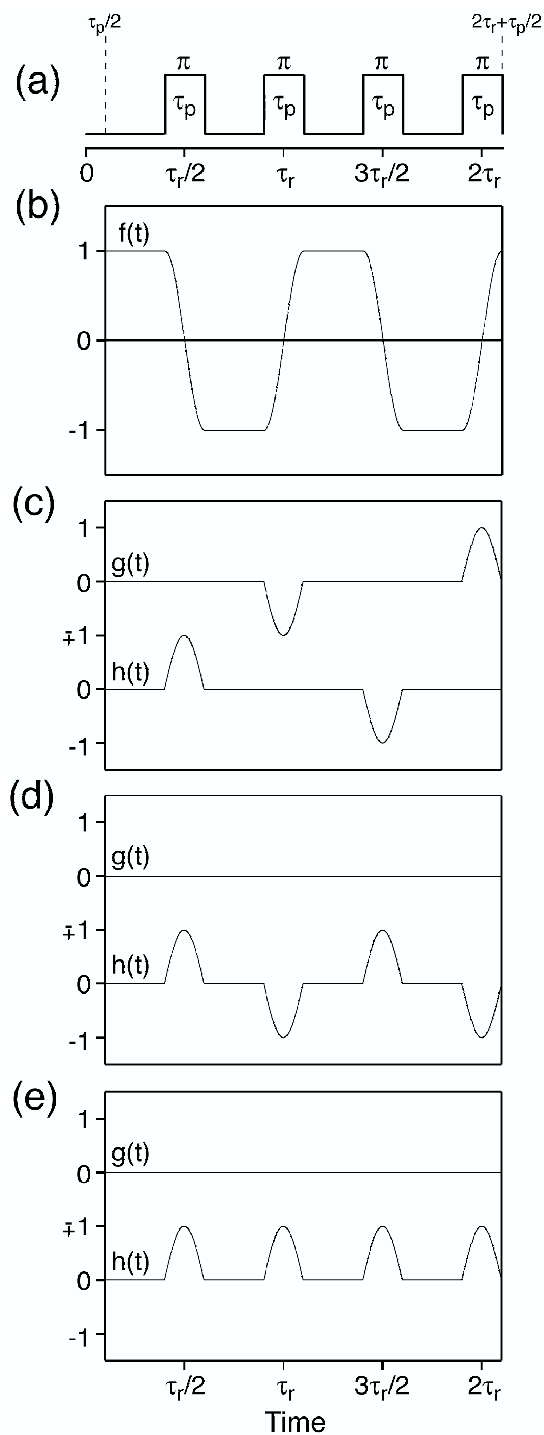


Figure 2-2. Coefficients in the interaction frame Hamiltonian for REDOR.

Details of the REDOR pulse sequence (a). $f(t)$, $g(t)$ and $h(t)$ coefficients in the interaction frame Hamiltonian (c.f. eq 5) for REDOR sequences with different phasing schemes (b)-(e). The $f(t)$ coefficient (b) is identical for all phasing schemes and the $g(t)$ and $h(t)$ coefficients shown for: (c) REDOR $xy-4$, (d) REDOR $xx-4$, (e) and REDOR $x\bar{x}-4$, are different for the various phasing schemes.

With the initial density operator $\rho(0) = I_x$, the evolution under the average Hamiltonian in eq 7 results in the observable signal for individual crystallites:

$$S(\tau) = \cos(\omega\tau), \quad (9)$$

with

$$\omega = -\frac{\sqrt{2}}{\pi} b_{IS} \frac{\cos\left(\frac{\pi}{2}\varphi\right)}{1-\varphi^2} \sin(2\beta) \sin(\gamma). \quad (10)$$

We note that the effective dipolar coupling constant, b_{IS}^{eff} , for REDOR xy -4 with finite pulses, differs from the dipolar coupling constant for the sequence with ideal δ -function pulses (i.e., $\varphi = 0$) only by the factor:

$$\kappa \equiv \frac{b_{IS}^{eff}}{b_{IS}} = \frac{\cos\left(\frac{\pi}{2}\varphi\right)}{1-\varphi^2}. \quad (11)$$

In the limit of windowless rf irradiation we obtain $\lim_{\varphi \rightarrow 1} \kappa = \frac{\pi}{4}$. However, for relatively large values of φ which are of practical interest, κ remains close to unity. For $\varphi = 0.6$ (e.g., $\omega_r/2\pi = 30$ kHz and $\omega_{rf}/2\pi = 50$ kHz) the effective dipolar coupling is expected to be only $\sim 8\%$ lower than the coupling in the $\varphi = 0$ limit.

Similar derivations of the first-order average Hamiltonian for REDOR xx -4 and REDOR $x\bar{x}$ -4 yield

$$\bar{H}_{IS}^{(1)} = -\frac{\sqrt{2}}{\pi} b_{IS} \frac{\cos\left(\frac{\pi}{2}\varphi\right)}{1-\varphi^2} \sin(2\beta) \left[\sin(\gamma) 2I_z S_z + \varphi \cos(\gamma) 2I_z S_y \right] \quad (12)$$

and

$$\bar{H}_{IS}^{(1)} = -\frac{1}{\pi} b_{IS} \left[\sqrt{2} \frac{\cos\left(\frac{\pi}{2}\varphi\right)}{1-\varphi^2} \sin(2\beta) \sin(\gamma) 2I_z S_z + \frac{\varphi \cos(\pi\varphi)}{1-4\varphi^2} \sin^2(\beta) \cos(2\gamma) 2I_z S_y \right], \quad (13)$$

respectively.

For both sequences the observable signal for individual crystallites is given by

$$S(\tau) = \cos\left(\sqrt{\Omega^2 + \Phi^2} \tau\right), \quad (14)$$

with

$$\Omega_{xx} = \Omega_{x\bar{x}} = -\frac{\sqrt{2}}{\pi} b_{IS} \frac{\cos\left(\frac{\pi}{2} \varphi\right)}{1 - \varphi^2} \sin(2\beta) \sin(\gamma), \quad (15a)$$

$$\Phi_{xx} = -\frac{\sqrt{2}}{\pi} b_{IS} \frac{\varphi \cos\left(\frac{\pi}{2} \varphi\right)}{1 - \varphi^2} \sin(2\beta) \cos(\gamma), \quad (15b)$$

$$\Phi_{x\bar{x}} = -\frac{1}{\pi} b_{IS} \frac{\varphi \cos(\pi\varphi)}{1 - 4\varphi^2} \sin^2(\beta) \cos(2\gamma). \quad (15c)$$

Note that for REDOR xx -4, in the special case of windowless rf irradiation of constant phase ($\varphi = 1$ in eq 15a–15b), the observable signal reduces to the expression independent of the Euler angle γ , expected for $n = \pm 1$ rotary resonance recoupling:²⁹

$$S(\tau) = \cos(\tilde{\omega}\tau), \quad (16)$$

with

$$\tilde{\omega} = -\frac{1}{2\sqrt{2}} b_{IS} \sin(2\beta). \quad (17)$$

In Figure 2-3 we compare the analytical finite pulse AHT expressions (c.f. eq 9-10 and 14-15) with numerical simulations. The REDOR $(S_0 - S)/S_0 = \Delta S/S_0$ curves (S_0 and S represent the reference and dipolar dephasing experiments, respectively) were calculated for $b_{IS}/2\pi = 190$ Hz (corresponding to a C–N distance of 2.53 Å) and $\varphi = 0.1$ – 0.66 . Excellent agreement is obtained between the first-order average Hamiltonian analysis and the numerical simulations for all phasing schemes considered. For REDOR xy -4 (Figure 2-3a), the dipolar coupling is scaled from that expected for the ideal δ -function pulse sequence by a well-defined factor (c.f. eq 11). However, the amplitude of

the oscillation remains unchanged. The effect of finite pulses on the dipolar coupling for REDOR xx -4 (Figure 2-3b) and REDOR $x\bar{x}$ -4 (Figure 2-3c) is more complicated; for these sequences both the dipolar oscillation frequency and amplitude are expected to change under conditions where the recoupling pulses occupy a significant fraction of the rotor period.

2.3 Experimental

NMR experiments were performed on custom-designed spectrometers (courtesy of Dr. D. J. Ruben) operating at ^1H Larmor frequencies of 500.1 and 750.0 MHz. Custom-designed quadruple- (500.1 MHz) and triple-resonance (750.0 MHz) transmission line MAS probes were used, equipped with Chemagnetics (Fort Collins, CO) spinner modules (4 and 3.2 mm for the 500.1 and 750.0 MHz probes, respectively). Samples were centerpacked in rotors and the spinning frequencies in the range $\omega_r/2\pi \sim 5$ –17 kHz (see text for details) were controlled to ± 5 Hz using spin rate controllers from Doty Scientific (Columbia, SC) and Bruker (Karlsruhe, Germany). This spinning frequency stability was adequate for performing all experiments described, and active synchronization of rf pulses within the rotor cycle was not required.

The REDOR pulse sequence employed in the experiments is shown in Figure 2-1. Ramped cross-polarization⁴³ was used to create the initial ^{13}C transverse magnetization. In the experiments carried out on the 500.1 MHz spectrometer, the ^{13}C refocusing pulse was 10 μs , and ^{15}N pulses were 10–20 μs and phased according to the xy -16 scheme.¹² We have investigated the performance of xy -4, xy -8 and xy -16 on $[1\text{-}^{13}\text{C}, ^{15}\text{N}]\text{glycine}$ (data not

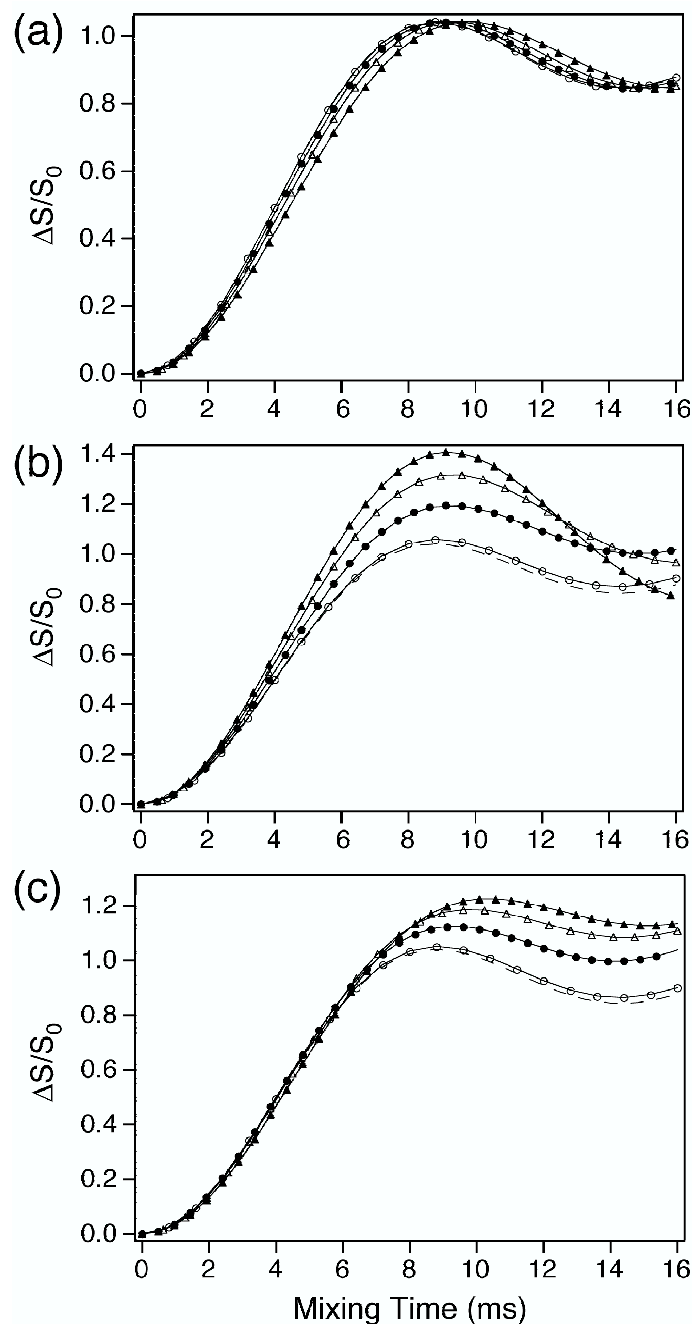


Figure 2-3. Comparison of average Hamiltonian and numerical simulations for REDOR.

REDOR $\Delta S/S_0$ curves were calculated numerically and using the average Hamiltonian expressions (see text) for $b_{IS}/2\pi = 190$ Hz and different values of φ for: (a) REDOR xy -4, (b) REDOR xx -4, and (c) REDOR $x\bar{x}$ -4. Average Hamiltonian calculations are shown as discrete points for $\varphi = 0.1$ (\circ), 0.33 (\bullet), 0.5 (\triangle), and 0.66 (\blacktriangle). Numerical simulations for the corresponding combination of φ and phasing scheme are shown as solid lines (—). For reference we also show the $\Delta S/S_0$ curve calculated for the ideal δ -function pulse sequence (---).

shown) and observed identical dipolar dephasing curves for all phasing schemes. CW ^1H decoupling ($\omega_{rf}/2\pi = 83\text{--}100$ kHz) was applied during the REDOR period and 83 kHz TPPM ^1H decoupling³⁴ (phase difference $\phi = 12^\circ$, $\tau = 5.3$ μs) was used during the acquisition of the FID. The experiments on the 750.0 MHz spectrometer (c.f. Figure 2-6) were carried out with 125 kHz CW or TPPM ^1H decoupling during the indirect dimension and 125 kHz TPPM ^1H decoupling (phase difference $\phi = 10\text{--}18^\circ$, $\tau = 3.6\text{--}3.7$ μs) during signal acquisition. In all experiments the recycle delay was 3.0 s and 16 transients were acquired per time point. The experiments were repeated at least three times (with good reproducibility) and subsequently averaged.

2.4 Results and Discussion

In Figures 4a and 4b we show experimental REDOR $\Delta S/S_0$ curves and simulations for $[1\text{-}^{13}\text{C},^{15}\text{N}]\text{glycine}$ ($b_{IS}/2\pi \sim 200$ Hz) and $[2\text{-}^{13}\text{C},^{15}\text{N}]\text{glycine}$ ($b_{IS}/2\pi \sim 900$ Hz), respectively, recorded at spinning frequencies $\omega_r/2\pi = 5\text{--}15$ kHz and recoupling rf fields $\omega_{rf}/2\pi = 25\text{--}50$ kHz (i.e., $0.1 \leq \varphi \leq 0.606$). The lower fields were used to create experimental conditions, where rf pulses occupy a significant fraction of the rotor period. For clarity, only a few representative $\Delta S/S_0$ curves are shown in Figure 2-4. According to the simulations for REDOR *xy-4* (c.f. Figure 2-3a), the finite π pulses are expected to scale the dipolar coupling by the factor κ given in eq 11. As already noted, for most experimental conditions of practical interest we anticipate only a minor (i.e., $< 10\%$) decrease in b_{IS} . The scaling of the dipolar coupling can be observed experimentally in

both model compounds considered here. In Figure 2-4 we show that an increase in φ from 0.1 to 0.6 results in a relatively small decrease in the dipolar oscillation frequency.

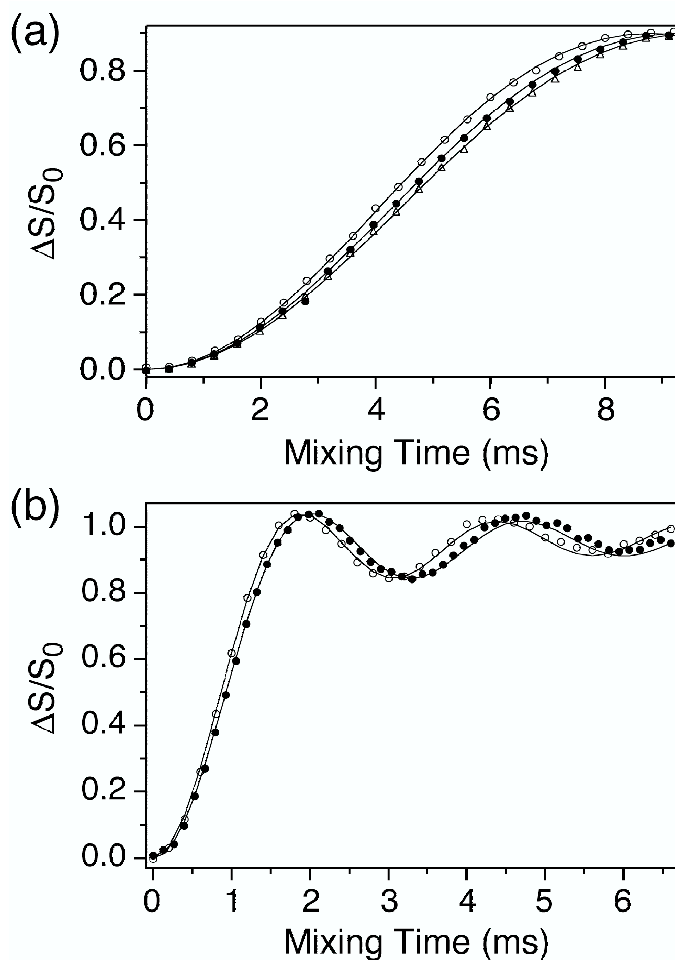


Figure 2-4. Experimental REDOR $\Delta S/S_0$ curves for $[1-^{13}\text{C}, ^{15}\text{N}]$ glycine and $[2-^{13}\text{C}, ^{15}\text{N}]$ glycine.

$\Delta S/S_0$ curves for $[1-^{13}\text{C}, ^{15}\text{N}]$ glycine (a) are shown for $\varphi = 0.1$ (○), 0.455 (●), and 0.606 (△), and $\Delta S/S_0$ curves for $[2-^{13}\text{C}, ^{15}\text{N}]$ glycine (b) are shown for $\varphi = 0.2$ (○) and 0.606 (●). $\Delta S/S_0$ curves simulated according to eq 18 (see text) are also shown (—). All experiments were performed at 500.1 MHz ^1H frequency, $\omega_r/2\pi = 5\text{--}15$ kHz, and $\omega_{rf}^{15\text{N}}/2\pi = 25\text{--}50$ kHz. During REDOR, CW ^1H decoupling was applied at 100 kHz (a) and 83 kHz (b). In all experiments 83 kHz TPPM ^1H decoupling³⁴ (phase difference $\phi = 12^\circ$, $\tau = 5.3$ μsec) was used during detection. For $[1-^{13}\text{C}, ^{15}\text{N}]$ glycine, the REDOR period was incremented in steps of 0.4 ms ($\varphi = 0.1, 0.2$), and 0.396 ms ($\varphi = 0.303, 0.455, 0.606$). For $[2-^{13}\text{C}, ^{15}\text{N}]$ glycine, the increments were 0.4 ms ($\varphi = 0.1$), 0.2 ms ($\varphi = 0.2$), and 0.132 ms ($\varphi = 0.303, 0.455, 0.606$).

For a more quantitative comparison of the average Hamiltonian result of eq 11 and experimental measurements of b_{IS}^{eff} , we fit the REDOR $\Delta S/S_0$ curves with the analytical expression:

$$\langle \Delta S/S_0 \rangle(\tau) = \lambda \left[1 - \int_0^\pi d\beta \sin(\beta) \int_0^{2\pi} d\gamma \cos \left\{ -\frac{\sqrt{2}}{\pi} b_{IS}^{eff} \sin(2\beta) \sin(\gamma) \tau \right\} \right]. \quad (18)$$

Here, the scaling factor λ accounts for the contribution to the S_0 curve from ^{13}C spins without a neighboring ^{15}N (a result of dilution in natural abundance material and/or imperfect isotopic labeling). The incorporation of ^{13}C and ^{15}N labels in $[1-^{13}\text{C}, ^{15}\text{N}]$ and $[2-^{13}\text{C}, ^{15}\text{N}]$ glycine (Cambridge Isotope Laboratories, Andover, MA) was $\sim 98\text{--}99\%$. The $[2-^{13}\text{C}, ^{15}\text{N}]$ glycine sample was not diluted in natural abundance glycine and experimental data were best fit with $\lambda = 1.0$. $[1-^{13}\text{C}, ^{15}\text{N}]$ glycine was diluted in the ratio of $\sim 1:10$ in natural abundance glycine. With $\pm 1\%$ uncertainties in the dilution and ^{13}C and ^{15}N labeling we expect $\lambda \sim 0.85\text{--}0.90$. For the REDOR experiment with $\varphi = 0.1$ the best fit was obtained for $\lambda = 0.865$, which was fixed at this value for all subsequent simulations.

For each experiment the effective dipolar coupling, b_{IS}^{eff} , was determined by minimizing the reduced χ^2 :³⁰

$$\chi_v^2 = \frac{1}{\nu} \sum_{i=1}^n \frac{1}{\sigma_i^2} [s_{\text{exp}}^i - s_{\text{sim}}^i]^2, \quad (19)$$

where s_{exp}^i and s_{sim}^i are the intensities of the i th experimental and simulated points, respectively, σ_i^2 is the variance of the i th experimental point, and ν is the number of degrees of freedom defined as the difference between the number of experimental points in the $\Delta S/S_0$ curve, n , and the number of adjustable parameters used in the fit. In our simulations b_{IS}^{eff} was the only adjustable parameter (i.e., $\nu = n - 1$), and for each φ , σ_i^2

were obtained according to

$$\sigma_i^2 = \frac{1}{N-1} \sum_{j=1}^N \left\{ \left[s_{\text{exp}}^i \right]_j - \overline{s_{\text{exp}}^i} \right\}^2. \quad (20)$$

Here, N is the number of independently recorded $\Delta S/S_0$ curves ($N = 3-9$ in our experiments), $\left[s_{\text{exp}}^i \right]_j$ is the intensity of the i th experimental point, s_{exp}^i , in the j th $\Delta S/S_0$ curve, and $\overline{s_{\text{exp}}^i}$ is the average of N determinations of s_{exp}^i .

Table 2-1. Experimental C'-N and C^α-N Dipolar Couplings in Glycine

τ_p (μs)	τ_r (μs)	φ	$b_{C'N}^{\text{eff}}/2\pi$ (Hz)	$b_{C^\alpha N}^{\text{eff}}/2\pi$ (Hz)
10	200	0.100	189 ± 2^a	869 ± 35^a
10	100	0.200	188 ± 2	886 ± 10
10	66	0.303	178 ± 5	875 ± 11
15	66	0.455	179 ± 2	854 ± 12
20	66	0.606	173 ± 2	826 ± 20

^aUncertainties in b_{IS}^{eff} (reported at 95% confidence level) were obtained following standard procedures described in ref 30.

The resulting values of the effective dipolar coupling constants for [$1\text{-}^{13}\text{C}, ^{15}\text{N}$] and [$2\text{-}^{13}\text{C}, ^{15}\text{N}$]glycine are listed in Table 2-1. The b_{IS}^{eff} values were fit with the analytical AHT expression, describing the scaling of the dipolar coupling due to the finite pulses:

$$b_{IS}^{\text{eff}} = b_{IS} \frac{\cos\left(\frac{\pi}{2}\varphi\right)}{1-\varphi^2}. \quad (21)$$

The fitting was performed by minimizing χ_V^2 (c.f. eq 19), where the single fit parameter was b_{IS} , the dipolar coupling in the limit of ideal δ -function pulses. For both model compounds all experimentally determined effective dipolar couplings are within 10% of the coupling in the $\varphi=0$ limit, and the agreement between AHT calculations and experimental results shown in Figure 2-5 is good. Therefore, for REDOR experiments

where rf pulses occupy a significant fraction of the rotor period, the dipolar coupling constant, b_{IS} , can be calculated from the experimentally determined effective coupling as

$$b_{IS} = b_{IS}^{eff} (1 - \varphi^2) / \cos(\frac{\pi}{2} \varphi).$$

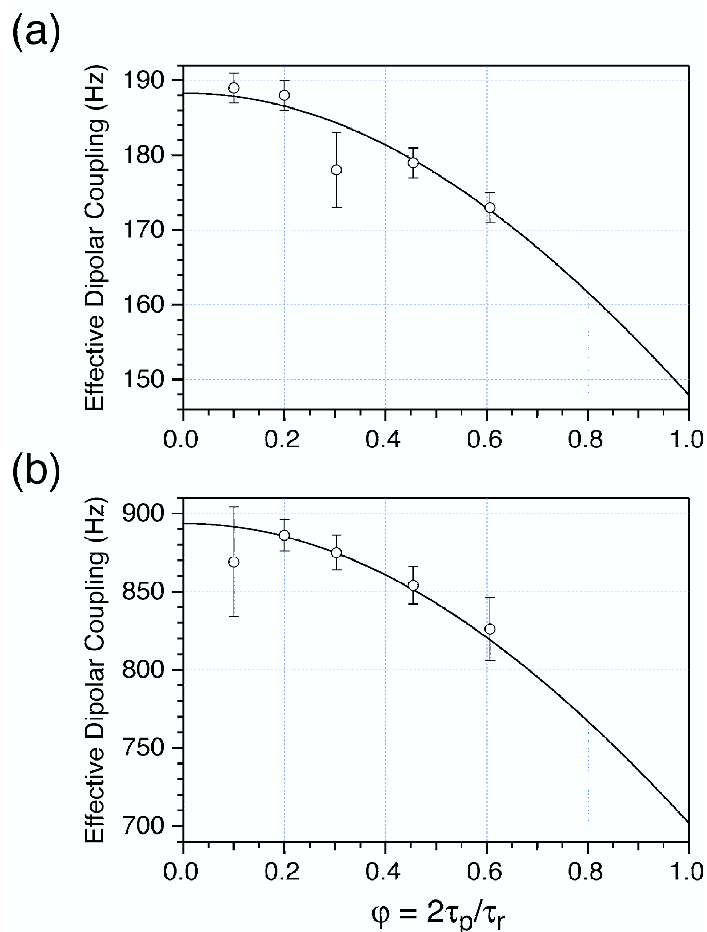


Figure 2-5. Comparison of experimental and predicted dipolar couplings in glycine. Experimentally determined effective dipolar couplings (\circ) and the best-fit theoretical b_{IS}^{eff} vs. φ curves ($—$) calculated using eq 21 are shown for: $[1-^{13}\text{C}, ^{15}\text{N}]$ glycine with $b_{IS}/2\pi = 188$ Hz (a) and $[2-^{13}\text{C}, ^{15}\text{N}]$ glycine with $b_{IS}/2\pi = 894$ Hz (b).

For the strong $^{13}\text{C}-^{15}\text{N}$ coupling in $[2-^{13}\text{C}, ^{15}\text{N}]$ glycine only the $\varphi = 0.1$ experiment ($\omega_r/2\pi = 5.0$ kHz, $\omega_p/2\pi = 50$ kHz) deviates slightly from theory. However, for $\omega_r/2\pi \leq 5.0$ kHz we expect the accuracy and precision of the fit for the strong dipolar coupling to be somewhat compromised, due to the limitation in the number of points that can be

acquired on the $\Delta S/S_0$ curve. In our experiments, the minimum increment for the REDOR period is $2\tau_r$ (i.e., only 18 data points could be acquired for 6.8 ms of dipolar evolution at $\omega_r/2\pi = 5.0$ kHz).

For the weaker ^{13}C – ^{15}N coupling in $[1\text{-}^{13}\text{C},^{15}\text{N}]$ glycine all experimental points, except $\varphi = 0.303$, agree well with theory. The effective C'–N dipolar coupling for $\varphi = 0.303$ was determined to be $b_{IS}^{\text{eff}}/2\pi = 178 \pm 5$ Hz (note that the uncertainty in the value of $b_{IS}^{\text{eff}}/2\pi$ for this φ is significantly higher than uncertainties for other φ given in Table 1). Careful inspection of the experimental data (not shown), revealed that points between ~ 7 – 9 ms of the $\varphi = 0.303$ $\Delta S/S_0$ curve, reproducibly had ~ 2 – 3% lower intensity than expected for the simple model of C–N dipolar evolution described by eq 18, resulting in a worse fit (9 $\Delta S/S_0$ curves were recorded for these experimental conditions and all exhibited the same feature). We also note that for identical $\omega_r/2\pi$ and $\omega_{rf}^H/2\pi$, but different $\omega_{rf}^{15N}/2\pi$ (i.e., $\varphi = 0.455$ and 0.606 experiments), $\Delta S/S_0$ curves could be fit very well to eq 18. Therefore, the somewhat anomalous appearance of the $\varphi = 0.303$ $\Delta S/S_0$ curve, may be related to a particularly unfavorable mismatch between the ^{15}N recoupling and ^1H decoupling rf fields under these experimental conditions.³¹⁻³³

As an example of the potential impact of higher spinning frequencies on REDOR experiments, in Figure 2-6 we compare REDOR reference (S_0) curves for the C^α resonance in $[1,2\text{-}^{13}\text{C},^{15}\text{N}]$ glycine recorded at $\omega_r/2\pi = 7.576$ – 16.667 kHz, where the coherent evolution under the C'– C^α J coupling was removed as described previously.²¹ It is clear that for the CH_2 group in glycine the combination of fast MAS and two-pulse phase modulated (TPPM) ^1H decoupling³⁴ significantly attenuates the dephasing of the

^{13}C spin-echo; the echo intensity at 20 ms of evolution increases from approximately 0.25 to 0.6 as the spinning frequency is increased from 7.576 to 16.667 kHz. In principle, the $\Delta S/S_0$ analysis should account for the rapid dephasing of the spin-echo. However, points on the $\Delta S/S_0$ curve will be defined with a higher signal-to-noise ratio when the echo-decay is attenuated, and this is of particular importance for REDOR data acquired for long evolution times (20-30 ms). In systems for which no complications are introduced by rapid spinning, there do not appear to be any fundamental disadvantages to performing REDOR experiments at $\omega_r/2\pi \sim 10\text{--}30$ kHz. The spin-echo intensity can be significantly higher under these conditions, while the recoupling performance is not appreciably affected (c.f. Figures 2-4 and 2-5).

The ^{13}C spin-echo intensity observed in the rapid spinning regime depends strongly on decoupling conditions, due to the ^1H reservoir becoming partially inhomogeneous.³⁵ Specifically, at $\omega_r/2\pi \geq \sim 10$ kHz CW ^1H decoupling deteriorates, while high power TPPM decoupling effectively restores the echo intensity. In analogy to the line broadening observed in spectra of well-isolated spin pairs,³⁶⁻³⁹ the signal loss associated with CW decoupling can be described by the magnitude of the second-order cross-term between the ^1H chemical shielding and $^{13}\text{C}\text{-}^1\text{H}$ dipolar coupling tensors relative to the $^1\text{H}\text{-}^1\text{H}$ spin diffusion rate constant.^{38,39} A particularly unfavorable situation for CW-decoupled spin systems can arise from the combination of high static magnetic fields, where the ^1H CSA magnitude increases, and very high MAS frequencies, for which the proton spin diffusion rate decreases and the tightly coupled spin system approaches an ensemble of isolated spin pairs.³⁹ Under TPPM ^1H decoupling ($\tau_{-\phi/2} \tau_{+\phi/2}$)_n the magnitude of the second-order cross-term can be scaled down significantly

by a proper choice of the phase difference, ϕ , leading to a decrease in the residual dipolar line width.³⁸ In addition, Ernst et al. have recently shown that the performance of high power TPPM ^1H decoupling does not deteriorate at high static magnetic fields for spinning frequencies up to 30 kHz.³⁹ Similar indications that the ^1H reservoir displays partially inhomogeneous behavior in CH_2 groups for spinning frequencies in the $\omega_r/2\pi \sim 15$ kHz regime have been observed recently in rotating frame experiments.⁴⁰

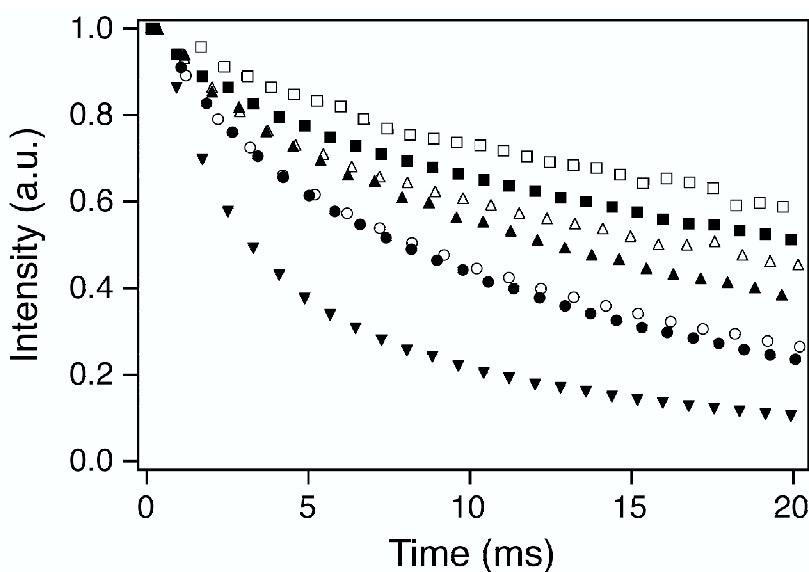


Figure 2-6. Experimental REDOR S_0 curves for the C^α resonance in $[\text{U-}^{13}\text{C}, ^{15}\text{N}]$ glycine.

S_0 curves were recorded at 750.0 MHz ^1H frequency by replacing the non-selective ^{13}C refocusing π pulse with a rotor-synchronized frequency-selective Gaussian π pulse, to remove coherent evolution under $\text{C}'\text{-C}^\alpha$ J coupling.²¹ The Gaussian pulses were $\sim 200\text{--}300$ μs (the exact pulse length was adjusted to occupy an even number of rotor periods) and 125 kHz CW ^1H decoupling was applied for the duration of the Gaussian pulse. During the indirect dimension and signal acquisition, 125 kHz TPPM ^1H decoupling (phase difference $\phi = 10\text{--}18^\circ$, $\tau = 3.6\text{--}3.7$ μs) was used at spinning frequencies of 7.576 (\bullet), 10.0 (\circ), 11.905 (\blacktriangle), 13.889 (\triangle), 15.152 (\blacksquare), and 16.667 kHz (\square). TPPM decoupling was optimized for each spinning frequency by minimizing the C^α line width in the direct dimension. For comparison we also show the S_0 curve at 15.152 kHz MAS and 125 kHz CW ^1H decoupling (\blacktriangledown).

The use of higher MAS frequencies for REDOR experiments on multiply ^{13}C labeled systems at high magnetic fields also offers some advantages. First, rapid spinning effectively attenuates residual ^{13}C - ^{13}C dipolar couplings, which also contribute to the dephasing of the spin-echo.²⁰ In addition, high rotation frequencies are required to avoid rotational resonance conditions,⁴¹ which can lead to severe line broadening in uniformly ^{13}C labeled samples. Finally, for ^{13}C spins with large CSA (e.g., carbonyl groups), fast spinning will result in an increased signal-to-noise ratio in the direct dimension, as the intensity of rotational sidebands is reduced.^{35,42}

2.5 Conclusions

We have investigated the performance of the REDOR recoupling sequence in model ^{13}C - ^{15}N spin systems under conditions where a significant fraction of the rotor period (10–60%) is occupied by rf pulses. Experimental results were explained using numerical simulations and average Hamiltonian calculations. For *xy-4* and related phasing schemes, the finite pulses were shown to have a minor effect on the dipolar scaling factor expected for REDOR with ideal δ -function pulses. Under most experimental conditions of practical interest, the dipolar scaling factor is reduced by only 1-5%; at relatively high spinning frequencies and weak rf fields the effect may be slightly larger (~5-10%). The changes in the dipolar scaling factor can be quantitatively described using the analytical expressions presented here, allowing for the accurate determination of the dipolar coupling. Therefore, we conclude that there appear to be no fundamental disadvantages to using REDOR recoupling at spinning frequencies in the $\omega_r/2\pi \sim 10$ –30 kHz regime. However, we would also like to note that since the primary aim of this work

was to investigate the effect of finite rf pulses on the heteronuclear dipolar coupling, the model compounds selected represent favorable spin systems, with relatively weak ^{15}N - ^1H dipolar couplings and negligible ^{15}N chemical-shielding anisotropy. In general, these interactions will be non-negligible and can potentially influence REDOR dipolar dephasing curves.

Acknowledgments

We thank M. Hohwy for the FORTRAN subroutines used in the numerical simulations and acknowledge many helpful discussions with B. Reif and M. Hohwy. C.P.J. thanks the NSF for a Predoctoral Fellowship, B.A.T. thanks the American Cancer Society for a Postdoctoral Fellowship (PF-99-260-01-GMC), and C.M.R. thanks the Howard Hughes Medical Institute for a Predoctoral Fellowship. This research was also supported by NIH grants GM-23289, GM-36810 and RR-00995.

References

- (1) K. Wüthrich, "NMR of Proteins and Nucleic Acids," Wiley, New York (1986).
- (2) B. Reif, M. Hennig, and C. Griesinger, "Direct measurement of angles between bond vectors in high-resolution NMR," *Science* **276**, 1230-1233 (1997).
- (3) D. Yang, R. Konrat, and L. E. Kay, "A multidimensional NMR experiment for measurement of the protein dihedral angle ψ based on cross-correlated relaxation between $^1\text{H}^\alpha$ - $^{13}\text{C}^\alpha$ dipolar and $^{13}\text{C}'$ (carbonyl) chemical shift anisotropy mechanisms," *J. Am. Chem. Soc.* **119**, 11938-11940 (1997).
- (4) J. M. Griffiths and R. G. Griffin, "Nuclear magnetic resonance methods for measuring dipolar couplings in rotating solids," *Anal. Chim. Acta* **283**, 1081-1101 (1993).
- (5) A. E. Bennett, R. G. Griffin, and S. Vega, "Recoupling of homo- and heteronuclear dipolar interactions in rotating solids," in "Solid State NMR IV: Methods and Applications of Solid-State NMR" (B. Blumich, Ed.), pp. 1-77, Springer-Verlag, Berlin (1994).
- (6) L. M. McDowell and J. Schaefer, "High resolution NMR of biological solids," *Curr. Opin. Struct. Biol.* **6**, 624-629 (1996).
- (7) R. G. Griffin, "Dipolar recoupling in MAS spectra of biological solids," *Nature Struct. Biol.* **5**, 508-512 (1998).
- (8) R. Fu and T. A. Cross, "Solid-state nuclear magnetic resonance investigation of protein and polypeptide structure," *Annu. Rev. Biophys. Biomol. Struct.* **28**, 235-268 (1999).

- (9) T. Gullion and J. Schaefer, "Rotational-echo double-resonance NMR," *J. Magn. Reson.* **81**, 196-200 (1989).
- (10) T. Gullion and J. Schaefer, "Detection of weak heteronuclear dipolar coupling by rotational-echo double-resonance nuclear magnetic resonance," *Adv. Magn. Reson.* **13**, 57-83 (1989).
- (11) T. Gullion and J. Schaefer, "Elimination of resonance offset effects in rotational-echo, double-resonance NMR," *J. Magn. Reson.* **92**, 439-442 (1991).
- (12) T. Gullion, D. B. Baker, and M. S. Conradi, "New, compensated Carr-Purcell sequences," *J. Magn. Reson.* **89**, 479-484 (1990).
- (13) Y. Li, R. J. Appleyard, W. A. Shuttleworth, and J. N. S. Evans, "Time-resolved solid-state REDOR NMR measurements on 5-enolpyruvylshikimate-3-phosphate synthase," *J. Am. Chem. Soc.* **116**, 10799-10800 (1994).
- (14) L. M. McDowell, A. Schmidt, E. R. Cohen, D. R. Studelska, and J. Schaefer, "Structural constraints on the ternary complex of 5-enolpyruvylshikimate-3-phosphate synthase from rotational-echo double-resonance NMR," *J. Mol. Biol.* **256**, 160-171 (1996).
- (15) K. Nishimura, A. Naito, S. Tuzi, H. Saito, C. Hashimoto, and M. Aida, "Determination of the three-dimensional structure of crystalline Leu-enkephalin based on six sets of accurately determined interatomic distances from ^{13}C -REDOR NMR and the conformation-dependent ^{13}C chemical shifts," *J. Phys. Chem. B* **102**, 7476-7483 (1998).

- (16) C. A. Michal and L. W. Jelinski, "Rotational-echo double-resonance in complex biopolymers: a study of *Nephila clavipes* dragline silk," *J. Biomol. NMR* **12**, 231-241 (1998).
- (17) M. E. Merritt, S. Th. Sigurdsson, and G. P. Drobny, "Long-range distance measurements to the phosphodiester backbone of solid nucleic acids using ^{31}P - ^{19}F REDOR NMR," *J. Am. Chem. Soc.* **121**, 6070-6071 (1999).
- (18) C. A. Michal and L. W. Jelinski, "REDOR 3D: Heteronuclear distance measurements in uniformly labeled and natural abundance solids," *J. Am. Chem. Soc.* **119**, 9059-9060 (1997).
- (19) T. Gullion and C. H. Pennington, " θ -REDOR: an MAS NMR method to simplify multiple coupled heteronuclear spin systems," *Chem. Phys. Lett.* **290**, 88-93 (1998).
- (20) J. Schaefer, "REDOR-determined distances from heterospins to clusters of ^{13}C labels," *J. Magn. Reson.* **137**, 272-275 (1999).
- (21) C. P. Jaroniec, B. A. Tounge, C. M. Rienstra, J. Herzfeld, and R. G. Griffin, "Measurement of ^{13}C - ^{15}N distances in uniformly ^{13}C labeled biomolecules: J-decoupled REDOR," *J. Am. Chem. Soc.* **121**, 10237-10238 (1999).
- (22) K. Saalwächter, R. Graf, and H. W. Spiess, "Recoupled polarization transfer ^1H - ^{13}C multiple-quantum correlation in solids under ultra-fast MAS," *J. Magn. Reson.* **140**, 471-476 (1999).
- (23) A. Naito, K. Nishimura, S. Kimura, S. Tuzi, M. Aida, N. Yasuoka, and H. Saito, "Determination of the three-dimensional structure of a new crystalline form of N-acetyl-Pro-Gly-Phe as revealed by ^{13}C REDOR, X-ray diffraction, and molecular dynamics simulation," *J. Phys. Chem.* **100**, 14995-15004 (1996); A. Naito, S. Tuzi,

- and H. Saito, "Dipolar interactions and interatomic distances," in "Solid State NMR of Polymers" (I. Ando and T. Asakura, Eds.), pp. 23-49, Elsevier, Amsterdam (1998).
- (24) R. Fu, S. A. Smith, and G. Bodenhausen, "Recoupling of heteronuclear dipolar interactions in solid state magic-angle spinning NMR by simultaneous frequency and amplitude modulation," *Chem. Phys. Lett.* **272**, 361-369 (1997).
- (25) A. Schmidt and S. Vega, "The transition amplitudes of centerband and sidebands in NMR spectra of rotating solids," *Isr. J. Chem.* **32**, 215-230 (1992).
- (26) O. Weintraub and S. Vega, "Floquet density matrices and effective Hamiltonians in magic-angle-spinning NMR spectroscopy," *J. Magn. Reson. A* **105**, 245-267 (1993).
- (27) U. Haeberlen and J. S. Waugh, "Coherent averaging effects in magnetic resonance," *Phys. Rev.* **175**, 453-467 (1968).
- (28) M. Mehring, "Principles of High Resolution NMR in Solids," Springer-Verlag, Berlin (1983).
- (29) T. G. Oas, R. G. Griffin, and M. H. Levitt, "Rotary resonance recoupling of dipolar interactions in solid-state nuclear magnetic resonance spectroscopy," *J. Chem. Phys.* **89**, 692-695 (1988).
- (30) D. P. Shoemaker, C. W. Garland, and J. W. Nibler, "Experiments in Physical Chemistry," McGraw-Hill, New York (1989), and references therein.
- (31) Y. Ishii, J. Ashida, and T. Terao, " ^{13}C - ^1H dipolar recoupling dynamics in ^{13}C multiple-pulse solid-state NMR," *Chem. Phys. Lett.* **246**, 439-445 (1995).

- (32) A. E. Bennett, "Dipolar Recoupling and Decoupling in Solid State Nuclear Magnetic Resonance Spectroscopy," Ph.D. Thesis, Massachusetts Institute of Technology (1995).
- (33) A. E. Bennett, C. M. Rienstra, J. M. Griffiths, W. Zhen, P. T. Lansbury, Jr., and R. G. Griffin, "Homonuclear radio frequency-driven recoupling in rotating solids," *J. Chem. Phys.* **108**, 9463-9479 (1998).
- (34) A. E. Bennett, C. M. Rienstra, M. Auger, K. V. Lakshmi, and R. G. Griffin, "Heteronuclear decoupling in rotating solids," *J. Chem. Phys.* **103**, 6951-6957 (1995).
- (35) M. M. Maricq and J. S. Waugh, "NMR in rotating solids," *J. Chem. Phys.* **70**, 3300-3316 (1979).
- (36) I. J. Shannon, K. D. M. Harris, and S. Arumugam, "High-resolution solid-state ^{13}C NMR studies of ferrocene as a function of magic angle sample spinning frequency," *Chem. Phys. Lett.* **196**, 588-594 (1992).
- (37) P. Tekely, P. Palmas, and D. Canet, "Effect of proton spin exchange on the residual ^{13}C MAS NMR linewidths. Phase-modulated irradiation for efficient heteronuclear decoupling in rapidly rotating solids," *J. Magn. Reson. A* **107**, 129-133 (1994).
- (38) M. Ernst, S. Bush, A. C. Kolbert, and A. Pines, "Second-order recoupling of chemical-shielding and dipolar-coupling tensors under spin decoupling in solid-state NMR," *J. Chem. Phys.* **105**, 3387-3397 (1996).
- (39) M. Ernst, H. Zimmermann, and B. H. Meier, "A simple model for heteronuclear spin decoupling in solid-state NMR," *Chem. Phys. Lett.* **317**, 581-588 (2000).

- (40) M. Hohwy, C. M. Rienstra, C. P. Jaroniec, and R. G. Griffin, "Fivefold symmetric homonuclear dipolar recoupling in rotating solids: Application to double quantum spectroscopy," *J. Chem. Phys.* **110**, 7983-7992 (1999).
- (41) D. P. Raleigh, M. H. Levitt, and R. G. Griffin, "Rotational resonance in solid state NMR," *Chem. Phys. Lett.* **146**, 71-76 (1988).
- (42) J. Herzfeld and A. E. Berger, "Sideband intensities in NMR spectra of samples spinning at the magic angle," *J. Chem. Phys.* **73**, 6021-6030 (1980).
- (43) G. Metz, X. Wu, and S. O. Smith, "Ramped-amplitude cross-polarization in magic-angle-spinning NMR," *J. Magn. Reson. A* **110**, 219-227 (1994).

CHAPTER 3. J-DECOUPLED REDOR: CARBON-NITROGEN DISTANCE MEASUREMENTS IN U-¹³C LABELED SOLIDS

Note: Reproduced with permission from C. P. Jaroniec, B. A. Tounge, C. M. Rienstra, J. Herzfeld and R. G. Griffin, "Measurement of ¹³C-¹⁵N distances in uniformly ¹³C labeled biomolecules: J-decoupled REDOR," J. Am. Chem. Soc. 121 (1999) 10237-10238. Copyright 1999 American Chemical Society.

ABSTRACT

We describe a solid-state MAS NMR experiment (J-decoupled REDOR) for distance measurements between a single ¹⁵N nucleus and individual ¹³C nuclei within a tightly coupled cluster. The experiment builds upon the REDOR pulse sequence, which uses rotor-synchronized π pulses to recouple heteronuclear dipolar interactions. The coherent evolution under ¹³C-¹³C dipolar couplings is attenuated using relatively fast MAS. Scalar ¹³C-¹³C (J-coupling) interactions are refocused by applying a rotor-synchronized, frequency selective Gaussian π pulse on resonance with a single ¹³C spin. The dipolar interaction between this ¹³C and the ¹⁵N spin is recoupled, while the J-couplings to other ¹³C nuclei are refocused. Failure to refocus the J-couplings among the ¹³C spins compromises the accurate measurement of ¹³C-¹⁵N dipole interactions, which are often of similar magnitude (ca. 30-60 Hz). $\Delta S/S_0$ curves obtained in multiply ¹³C labeled systems with J-decoupled REDOR match those obtained with conventional REDOR for isolated ¹³C-¹⁵N spin pairs. We demonstrate the technique in uniformly ¹³C, ¹⁵N labeled amino acids glycine and L-threonine.

3.1 Introduction

Measurement of distances between pairs of heteronuclei (e.g., ^{13}C - ^{15}N , ^{13}C - ^{31}P and ^{13}C - ^{19}F) is important for constraining the conformation of biomolecules in the solid-state. In particular, rotational-echo double-resonance (REDOR),^{1,2} which recouples heteronuclear dipolar interactions during magic angle spinning (MAS), has been extensively applied to problems of biological interest.³⁻⁷ Most of these experiments have been performed on isolated spin pairs, where the interpretation of experimental results is relatively straightforward. Nevertheless, it is of considerable interest to perform such measurements in multiple spin systems, because of the possibility of measuring several distances in a single sample. However, in REDOR experiments on multiply ^{13}C labeled samples the dephasing profiles are complicated by additional interactions. While placing all REDOR dephasing pulses on the ^{15}N channel avoids the recoupling of ^{13}C spins by the π -pulse train,⁸ the homonuclear ^{13}C - ^{13}C dipolar and scalar (J-coupling) interactions can still contribute to the dephasing of ^{13}C coherences. Here we discuss an approach to ^{13}C observe REDOR, which relies on the selective excitation of the ^{13}C spectrum that removes the coherent evolution of the spin system under homonuclear ^{13}C - ^{13}C J-couplings.

Several recently proposed techniques address the problem of heteronuclear distance measurements in spin systems consisting of multiple ^{13}C and ^{15}N nuclei.⁹⁻¹¹ In particular, the multiple pulse decoupled REDOR sequence¹¹ was designed to attenuate the effects of residual homonuclear ^{13}C - ^{13}C dipolar couplings on the dephasing of ^{13}C coherences. However, this experiment does not explicitly account for ^{13}C - ^{13}C J-couplings, which compromise the accurate measurement of weak heteronuclear dipolar couplings. In

peptides, J-couplings between directly bonded ^{13}C nuclei are ca. 30-60 Hz, and the most informative ^{13}C - ^{15}N dipolar couplings are often of similar magnitude (e.g., 25 Hz for a 5.0 Å distance).

3.2 Results and Discussion

For a spin system consisting of n ^{13}C nuclei and a single ^{15}N spin, the effective Hamiltonian for the REDOR pulse sequence (Figure 3-1a) in the rapid spinning regime is given by the sum of Hamiltonians H_D and H_J describing the ^{13}C - ^{15}N dipolar and ^{13}C - ^{13}C scalar interactions, respectively:²

$$H = H_D + H_J = \sum_{i=1}^n \omega_i 2C_{iz} N_z + \sum_{i < j} \pi J_{ij} 2C_{iz} C_{jz}, \quad (1)$$

with

$$\omega = -\frac{\sqrt{2}}{\pi} \kappa b_{IS} \sin(2\beta) \sin(\gamma). \quad (2)$$

In eq 1 J_{ij} is the C_i - C_j scalar coupling constant (in hertz) and ω is the effective C_i - N dipolar coupling (defined in detail in Chapter 2). The dipolar coupling constant, b_{IS} , is proportional to the inverse cube of the internuclear distance, r_{IS} , and the Euler angles β and γ relate the principal axis system of the interaction to the rotor-fixed reference frame. Equation 1 assumes that: (i) J couplings can be treated in the weak coupling limit,¹² and (ii) coherent evolution of ^{13}C signals under ~ 2 kHz dipolar couplings between directly bonded ^{13}C nuclei is refocused by rapid spinning ($\omega_r/2\pi \sim 10$ kHz) for integer multiples of the rotor period.

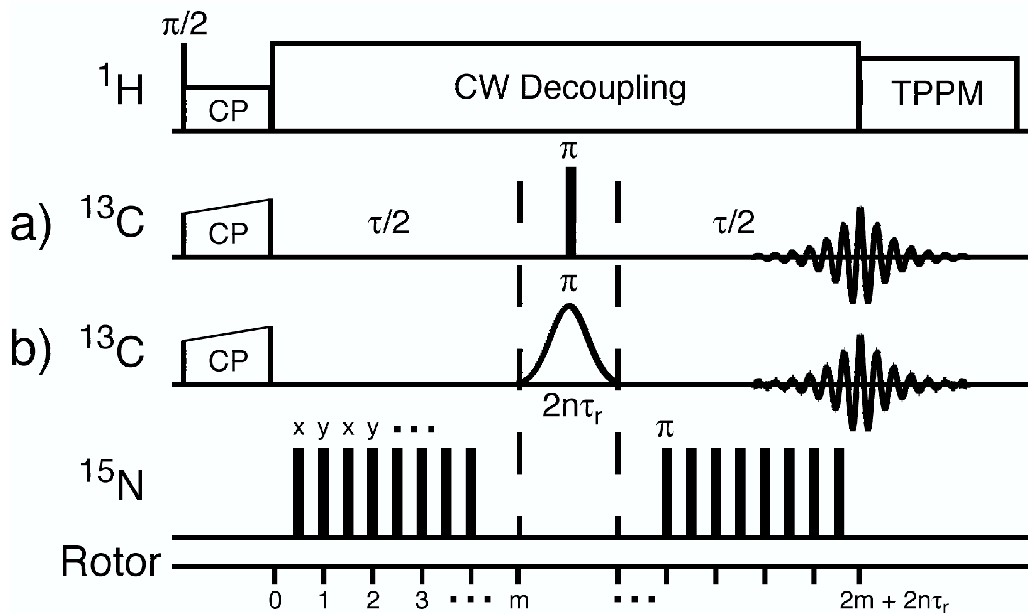


Figure 3-1. REDOR and J-decoupled REDOR pulse sequences.

Pulse sequences for conventional REDOR (a) and J-decoupled REDOR (b). The ^{15}N π pulse length was $10\ \mu\text{s}$ and the pulses were phased according to the xy -16 scheme.¹³ For the sequence in (a) the ^{13}C π pulse length was $10\ \mu\text{s}$, and for experiments on uniformly ^{13}C labeled samples, the coherence filter: $(\pi/2) - z$ -filter $- (\pi/2)$ was inserted prior to signal acquisition. For J-decoupled REDOR (b) the Gaussian π pulse parameters were: $\tau_{\text{Gauss}} = 0.6\ \text{ms}$, 64 increments, and 5% truncation. CW ^1H decoupling at $100\ \text{kHz}$ was applied during the evolution period, and $83\ \text{kHz}$ TPPM¹⁴ was used during acquisition. The phase cycle used: $\phi_{\text{Gauss}} = xy\bar{x}\bar{y}$, $\phi_{\text{rec'r}} = x\bar{x}x\bar{x}$, ensures that the only ^{13}C spins contributing to the observable signal are those inverted by the selective pulse.

For a coupled three-spin system (C_1 - C_2 - N) the initial density operator following cross-polarization is given by:

$$\rho(0) = C_{1x} + C_{2x}. \quad (3)$$

The evolution under the effective Hamiltonian in eq 1 generates both in-phase ($\sim C_{1x}$ and C_{2x}) and anti-phase ($\sim C_{1y}C_{2z}$ and $C_{1z}C_{2y}$) coherences as follows:

$$\begin{aligned} \rho(\tau) &= \exp\{-iH\tau\}\rho(0)\exp\{iH\tau\} \\ &= C_{1x}c_1c_J + C_{2x}c_2c_J + 2C_{1y}C_{2z}c_Js_J + 2C_{1z}C_{2y}c_2s_J \\ &\quad + 2C_{1y}N_zs_1c_J + 2C_{2y}N_zs_2c_J - 4C_{1x}C_{2z}N_zs_1s_J - 4C_{1z}C_{2x}N_zs_2s_J \end{aligned} \quad (4)$$

with

$$\begin{aligned}
c_i &= \cos(\omega_i \tau) \\
s_i &= \sin(\omega_i \tau) \\
c_J &= \cos(\pi J_{12} \tau) \\
s_J &= \sin(\pi J_{12} \tau)
\end{aligned}
\tag{5}$$

The antiphase coherences $\sim C_{1y}C_{2z}$ and $C_{1z}C_{2y}$ can evolve into observable magnetization under J_{12} during the detection period, leading to phase-twisted spectra (Figure 3-2a). This problem can be overcome by filtering the coherence prior to detection (see Figure 3-1 caption). Figure 3-2a shows slices from spin-echo experiments for [U- ^{13}C , ^{15}N]glycine for 8.4 ms of evolution under the ^{13}C - ^{13}C J-coupling acquired with and without the coherence filter. The spectrum obtained with a simple spin-echo experiment displays phase-twisted lineshapes. In contrast, the spin-echo experiment followed by the coherence filter results in purely absorptive signals.

The problem of coherent evolution under ^{13}C - ^{13}C J-couplings during dipolar dephasing (S) and reference (S_0) experiments is addressed by replacing the hard π pulse with a rotor-synchronized, frequency selective Gaussian π pulse applied to one ^{13}C spin (Figure 3-1b). For all evolution times the dipole interaction between this ^{13}C and the ^{15}N spin is retained as in conventional REDOR, while the J-couplings to the remaining ^{13}C nuclei are refocused (the signs of all spin terms having the form $2C_{iz}C_{jz}$; $j = 1, 2, \dots, n - i$, are reversed following the selective inversion of the C_i spin). This type of homonuclear J-decoupling was used previously to enhance resolution in two-dimensional solution¹⁵ and solid-state¹⁶ spectra. With the assumption that the selective pulse on C_i can be treated as an ideal pulse, the effective Hamiltonian for the pulse sequence in Figure 3-1b is given by the two-spin REDOR Hamiltonian

$$H = \omega_i 2C_{iz}N_z
\tag{6}$$

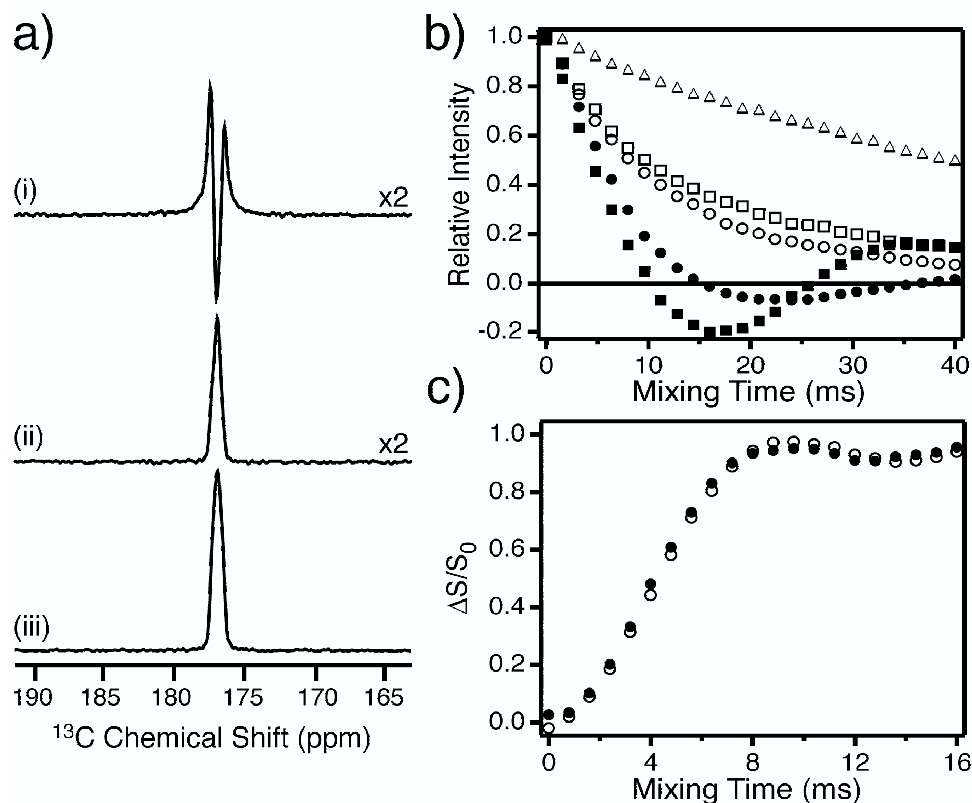


Figure 3-2. REDOR and J-decoupled REDOR experiments in glycine.

Comparison of conventional and J-decoupled REDOR for glycine samples with one and two ^{13}C labels. (a) slices through S_0 curves acquired for $[\text{U-}^{13}\text{C},^{15}\text{N}]$ glycine (only C' resonance is shown) with the following pulse sequences on ^{13}C : (i) $\text{CP} - \tau/2 - \pi - \tau/2 - \text{acquire}$; (ii) $\text{CP} - \tau/2 - \pi - \tau/2 - \text{coherence filter} - \text{acquire}$; (iii) $\text{CP} - \tau/2 - \pi (\text{Gauss}) - \tau/2 - \text{acquire}$; $\tau = 8.4$ ms; (b) S_0 curves for the C' resonance in $[\text{U-}^{13}\text{C},^{15}\text{N}]$ glycine ($\blacksquare =$ conventional REDOR; $\square =$ J-decoupled REDOR) and the C' resonance in $[\text{U-}^{13}\text{C},^{15}\text{N}]$ threonine ($\bullet =$ conventional REDOR; $\circ =$ J-decoupled REDOR). Also shown is the S_0 curve for $[\text{1-}^{13}\text{C},^{15}\text{N}]$ glycine (\triangle); (c) $\Delta S/S_0$ curves obtained with conventional REDOR for C' resonance in $[\text{1-}^{13}\text{C},^{15}\text{N}]$ glycine (\circ) and J-decoupled REDOR in $[\text{U-}^{13}\text{C},^{15}\text{N}]$ glycine (\bullet). Experimental data were scaled to account for the 10 and 20% dilution of singly and doubly ^{13}C labeled glycine samples, respectively, in natural abundance glycine. All experiments were performed at 500 MHz ^1H frequency and $\omega_r/2\pi = 10.0$ kHz (± 5 Hz). Other experimental parameters are given in the Figure 3-1 caption.

and the observable signal averaged over the crystallite ensemble is²

$$S(\tau) = \iint d\beta \sin(\beta) dy \cos(\omega_i \tau). \quad (7)$$

Since the selective pulse removes all ^{13}C - ^{13}C J-couplings to the spin of interest, the coherence filter is not necessary to obtain in-phase spectra (Figure 3-2a). Although the experimental Gaussian pulse is not ideal, it is a *constant-time* element present in all S and S_0 experiments and any effects due to the pulse can be taken into account by calculating $(S_0 - S)/S_0 = \Delta S/S_0$ curves.² For $[1\text{-}^{13}\text{C},^{15}\text{N}]$ glycine at $\omega_r/2\pi = 10.0$ kHz and 500 MHz ^1H frequency (data not shown), S and S_0 curves experience only an overall scaling ($\sim 25\%$ loss in signal intensity) for a 0.6 ms Gaussian π pulse relative to a hard π pulse.

Figure 3-2b compares S_0 curves for $[U\text{-}^{13}\text{C},^{15}\text{N}]$ glycine and $[U\text{-}^{13}\text{C},^{15}\text{N}]$ threonine obtained with conventional and J-decoupled REDOR. The selective pulse applied to the C' and C^γ spins in glycine and threonine, respectively, removes the coherent evolution due to ~ 50 Hz $\text{C}'\text{-C}^\alpha$, and ~ 30 Hz $\text{C}^\beta\text{-C}^\gamma$ J couplings, resulting in S_0 curves of positive intensity for all evolution times. For comparison with a spin-pair sample, the S_0 curve for $[1\text{-}^{13}\text{C},^{15}\text{N}]$ glycine is also included. Although the selective pulse refocuses the ^{13}C - ^{13}C J-couplings, residual ^{13}C - ^{13}C dipole interactions may still be present at 10 kHz spinning, and the 100 kHz ^1H CW decoupling used here is not sufficient to provide identical dephasing profiles for the isolated C' spin and the C' with residual dipole coupling to the C^α spin.¹⁷ Besides using a higher amplitude CW field, the dephasing problem can be alleviated by employing higher MAS frequencies to attenuate residual ^{13}C - ^{13}C dipole couplings,¹¹ and implementing two-pulse phase-modulated (TPPM) decoupling¹⁴ instead of CW in the S and S_0 experiments. Figure 3-2c shows that nearly identical $\Delta S/S_0$ curves are obtained for the $\text{C}'\text{-N}$ coupling in $[1\text{-}^{13}\text{C},^{15}\text{N}]$ and $[U\text{-}^{13}\text{C},^{15}\text{N}]$ glycine with conventional and J-decoupled REDOR sequences, respectively.

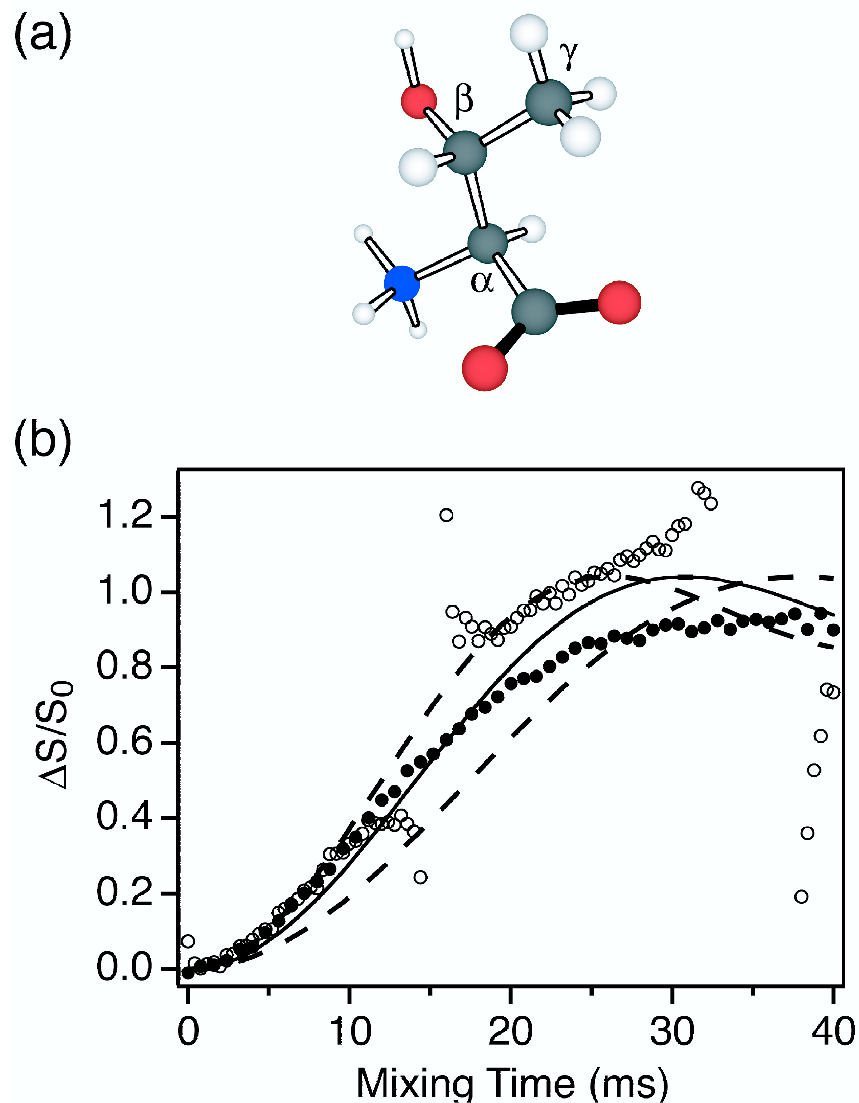


Figure 3-3. REDOR and J-decoupled REDOR experiments in [U- ^{13}C , ^{15}N]threonine. (a) Neutron diffraction structure of threonine¹⁸ and (b) $\Delta S/S_0$ curves for the C^γ resonance in [U- ^{13}C , ^{15}N]threonine obtained with conventional REDOR (\circ) and J-decoupled REDOR (\bullet). $\Delta S/S_0$ curve (—) simulated according to eq 7 for the C^γ -N coupling of 54 Hz obtained from the neutron diffraction structure and curves (---) for 44 and 64 Hz couplings are shown for comparison. Experimental parameters are given in the captions of Figures 3-1 and 3-2.

In principle, the $\Delta S/S_0$ analysis for conventional REDOR accounts for the evolution under ^{13}C - ^{13}C J-couplings. However, for multiply ^{13}C labeled systems the quality of experimental data is compromised due to multiple zero-crossings and low signal

intensities in S and S_0 curves. This is demonstrated in Figure 3-3 for the case of ~ 50 Hz C^γ -N dipole coupling in $[U\text{-}^{13}\text{C},^{15}\text{N}]$ threonine, where $\Delta S/S_0$ curves obtained with conventional and J-decoupled REDOR are compared. Accurate determination of weak couplings requires evolution times on the order of 30 ms.¹¹ However in the presence of homonuclear J-couplings, conventional REDOR $\Delta S/S_0$ curves can account for J-coupling effects only up to ~ 10 ms (depending on the exact value of J). On the other hand, J-decoupled REDOR has the ability to provide useful experimental data for the entire evolution period because the S_0 curve has a simple exponential decay profile. As the result, the quality of the data appears to be mainly limited by residual ^{13}C - ^{13}C dipole couplings, insufficient ^1H decoupling and ^{15}N pulse imperfections. The simulated $\Delta S/S_0$ curve for the neutron diffraction¹⁸ C^γ -N coupling of 54 Hz and curves for 44 and 64 Hz dipole couplings are included for comparison. Reasonably good agreement between the 54 Hz simulation and experiment is obtained up to ~ 20 ms, and it is evident that experimental data in the 10-20 ms range are important for the accurate determination of weak dipole couplings. For longer evolution times the observed dipolar dephasing is less than that predicted by the simulation, possibly due to the problems noted above. We note here that dipolar couplings involving ^{13}CO , $^{13}\text{C}^\alpha$ and $^{13}\text{C}^\beta$ in $[U\text{-}^{13}\text{C},^{15}\text{N}]$ threonine were also measured using J-decoupled REDOR. The individual $\Delta S/S_0$ curves are not shown, however Figure 3-4 illustrates the feasibility of selectively inverting all ^{13}C resonances in $[U\text{-}^{13}\text{C},^{15}\text{N}]$ threonine using frequency selective Gaussian pulses.

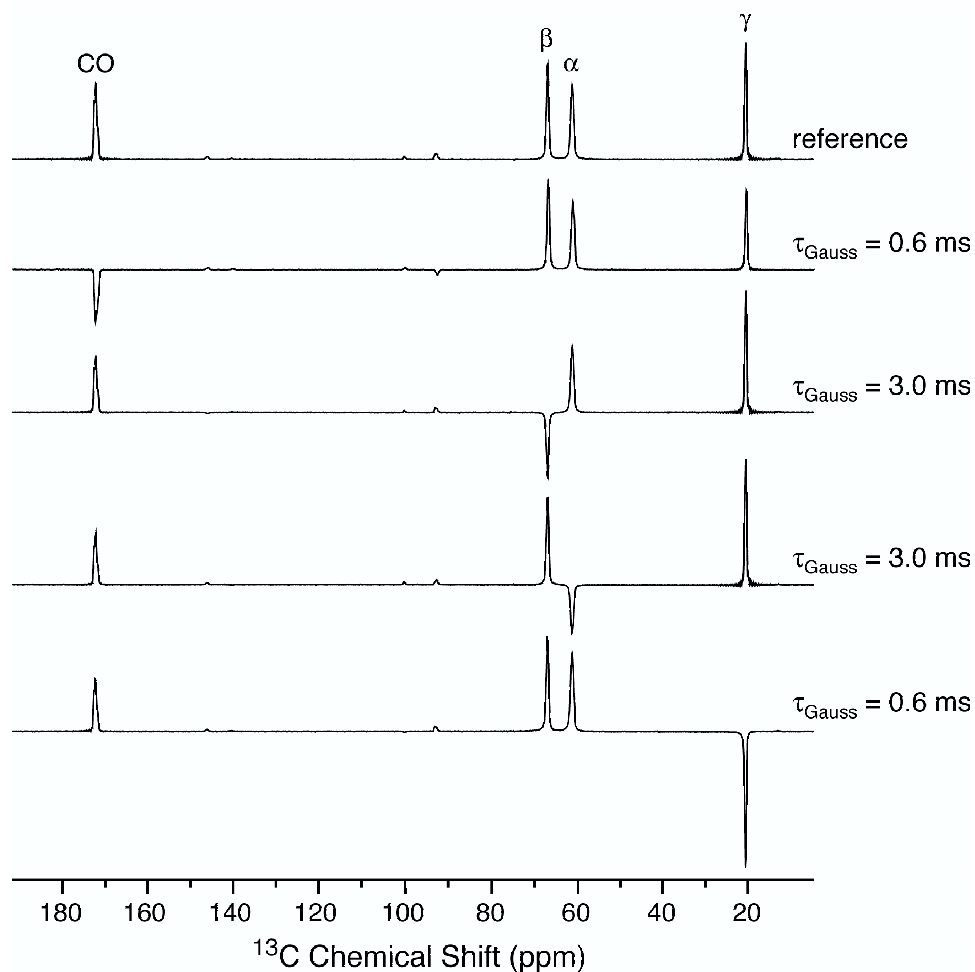


Figure 3-4. Selective inversion of ^{13}C resonances in $[\text{U-}^{13}\text{C}, ^{15}\text{N}]$ threonine.

The ^{13}C signals were inverted using the pulse sequence: $\text{CP} - (\pi/2) - z\text{-filter} - \pi(\text{Gauss}) - z\text{-filter} - (\pi/2) - \text{acquire}$. Frequency selective Gaussian pulses of 0.6-3.0 ms were used. Spectra were recorded at 500 MHz ^1H Larmor frequency and $\omega_r/2\pi = 10$ kHz.

3.3 Conclusions

We have described a REDOR experiment, which refocuses ^{13}C - ^{13}C J-couplings and enables accurate distance measurements in spin systems consisting of a heteronucleus interacting with a tightly coupled cluster of ^{13}C spins. The technique is expected to be particularly useful for measurements of weak ^{13}C - ^{15}N dipolar couplings, because in the presence of ^{13}C - ^{13}C J-couplings the REDOR experiment designed for spin

pairs does not provide reliable data for evolution times greater than ~10 ms. Extensions of the technique to selective carbon-nitrogen distance measurements in uniformly ^{13}C and ^{15}N labeled systems are currently being pursued in our laboratory.

Acknowledgments

Stimulating discussions with M. Hohwy, B. Reif, D.J. Ruben, and C.J. Turner and the careful reading of the manuscript by M. Hohwy and B. Reif are gratefully acknowledged. C.P.J. would like to thank NSF for a Predoctoral Fellowship, B.A.T. is an American Cancer Society Postdoctoral Fellow (PF-99-260-01-GMC), and C.M.R. was a Howard Hughes Medical Institute Predoctoral Fellow. This research was supported by the NIH grants GM-23289, GM-36810 and RR-00995.

References

- (1) T. Gullion and J. Schaefer, "Rotational-echo double-resonance NMR," *J. Magn. Reson.* **81**, 196-200 (1989).
- (2) T. Gullion and J. Schaefer, "Detection of weak heteronuclear dipolar coupling by rotational-echo double-resonance nuclear magnetic resonance," *Adv. Magn. Reson.* **13**, 57-83 (1989).
- (3) L. M. McDowell and J. Schaefer, "High resolution NMR of biological solids," *Curr. Opin. Struct. Biol.* **6**, 624-629 (1996).
- (4) A. M. Christensen and J. Schaefer, "Solid-state NMR determination of intramolecular and intermolecular ^{31}P - ^{13}C distances for shikimate-3-phosphate and $[1\text{-}^{13}\text{C}]$ glyphosate bound to enolpyruvylshikimate-3-phosphate synthase," *Biochemistry* **32**, 2868-2873 (1993).
- (5) Y. Li, R. J. Appleyard, W. A. Shuttleworth and J. N. S. Evans, "Time-resolved solid-state REDOR NMR measurements on 5-enolpyruvylshikimate-3-phosphate synthase," *J. Am. Chem. Soc.* **116**, 10799-10800 (1994).
- (6) C. A. Michal and L. W. Jelinski, "Rotational-echo double-resonance in complex biopolymers: a study of *Nephila clavipes* dragline silk," *J. Biomol. NMR* **12**, 231-241 (1998).
- (7) K. Nishimura, A. Naito, S. Tuzi, H. Saito, C. Hashimoto and M. Aida, "Determination of the three-dimensional structure of crystalline Leu-enkephalin based on six sets of accurately determined interatomic distances from ^{13}C -REDOR NMR and the conformation-dependent ^{13}C chemical shifts," *J. Phys. Chem. B* **102**, 7476-7483 (1998).

- (8) T. Gullion and S. Vega, "A simple magic angle spinning NMR experiment for the dephasing of rotational echoes of dipolar coupled homonuclear spin pairs," *Chem. Phys. Lett.* **194**, 423-428 (1992).
- (9) C. A. Michal and L. W. Jelinski, "REDOR 3D: Heteronuclear distance measurements in uniformly labeled and natural abundance solids," *J. Am. Chem. Soc.* **119**, 9059-9060 (1997).
- (10) T. Gullion and C. H. Pennington, " θ -REDOR: an MAS NMR method to simplify multiple coupled heteronuclear spin systems," *Chem. Phys. Lett.* **290**, 88-93 (1998).
- (11) J. Schaefer, "REDOR-determined distances from heterospins to clusters of ^{13}C labels," *J. Magn. Reson.* **137**, 272-275 (1999).
- (12) R. R. Ernst, G. Bodenhausen and A. Wokaun, "Principles of Nuclear Magnetic Resonance in One and Two Dimensions," Clarendon Press, Oxford (1991).
- (13) T. Gullion, D. B. Baker and M. S. Conradi, "New, compensated Carr-Purcell sequences," *J. Magn. Reson.* **89**, 479-484 (1990).
- (14) A. E. Bennett, C. M. Rienstra, M. Auger, K. V. Lakshmi and R. G. Griffin, "Heteronuclear decoupling in rotating solids," *J. Chem. Phys.* **103**, 6951-6957 (1995).
- (15) R. Brüschweiler, C. Griesinger, O. W. Sørensen and R. R. Ernst, "Combined use of hard and soft pulses for ω_1 decoupling in two-dimensional NMR spectroscopy," *J. Magn. Reson.* **78**, 178-185 (1988).
- (16) S. K. Straus, T. Bremi and R. R. Ernst, "Resolution enhancement by homonuclear J decoupling in solid-state MAS NMR," *Chem. Phys. Lett.* **262**, 709-715 (1996).

- (17) D. L. VanderHart and G. C. Campbell, "Off-resonance proton decoupling on-resonance and near-resonance," *J. Magn. Reson.* **134**, 88-112 (1998).
- (18) M. Ramanadham, S. K. Sikka and R. Chidambaram, "Structure determination of L_S-threonine by neutron diffraction," *Pramana* **1**, 247-259 (1973).

CHAPTER 4. FREQUENCY SELECTIVE REDOR: ACCURATE CARBON-NITROGEN DISTANCE MEASUREMENTS IN U-¹³C, ¹⁵N-LABELED PEPTIDES

Note: Reproduced with permission from C. P. Jaroniec, B. A. Tounge, J. Herzfeld and R. G. Griffin, "Frequency selective heteronuclear dipolar recoupling in rotating solids: Accurate ¹³C-¹⁵N distance measurements in uniformly ¹³C, ¹⁵N-labeled peptides," J. Am. Chem. Soc. 123 (2001) 3507-3519. Copyright 2001 American Chemical Society.

ABSTRACT

We describe a magic-angle spinning NMR experiment for selective ¹³C-¹⁵N distance measurements in uniformly ¹³C, ¹⁵N-labeled solids, where multiple ¹³C-¹⁵N and ¹³C-¹³C interactions complicate the accurate measurement of structurally-interesting, weak ¹³C-¹⁵N dipolar couplings. The new experiment, termed FSR (*frequency selective REDOR*), combines the REDOR pulse sequence with a frequency selective spin-echo to recouple a single ¹³C-¹⁵N dipolar interaction in a multiple spin system. Concurrently the remaining ¹³C-¹⁵N dipolar couplings and all ¹³C-¹³C scalar couplings to the selected ¹³C are suppressed. The ¹³C-¹⁵N coupling of interest is extracted by a least-squares fit of the experimentally observed modulation of the ¹³C spin-echo intensity to the analytical expression describing the dipolar dephasing in an isolated heteronuclear spin pair under conventional REDOR. The experiment is demonstrated in three uniformly-¹³C, ¹⁵N-labeled model systems: asparagine, N-acetyl-L-Val-L-Leu and N-formyl-L-Met-L-Leu-L-Phe; in N-formyl-[U-¹³C, ¹⁵N]L-Met-L-Leu-L-Phe we have determined a total of 16 internuclear distances in the 2.5–6 Å range.

4.1 Introduction

Solid-state nuclear magnetic resonance (SSNMR) experiments designed to measure dipolar couplings are very important in structural investigations of biological systems,¹⁻³ which are not amenable to X-ray diffraction or solution-state NMR methods.⁴⁻⁶ Such systems include membrane proteins,^{1,3,7-11} large enzyme-inhibitor complexes,^{12,13} chemical and photochemical reaction intermediates,^{9,11,14} peptide-protein complexes,¹⁵ and peptide aggregates.¹⁶⁻²² In particular, the accurate measurement of ^{13}C - ^{13}C and ^{13}C - ^{15}N dipolar couplings corresponding to internuclear distances in the 3–6 Å range can provide detailed information about the three-dimensional structure of biological solids.

The resolution and sensitivity of SSNMR experiments are optimized by the combination of high static magnetic fields ($B_0 \geq \sim 11.7$ T) with (i) macroscopic orientation of the sample with respect to the external field³ or (ii) rapid rotation of the sample about an axis tilted away from B_0 by the 'magic-angle,' $\theta = \tan^{-1} \sqrt{2}$. In the case of magic-angle spinning (MAS),^{23,24} the high resolution is achieved at the expense of structural information, as MAS effectively attenuates the dipolar couplings between low- γ nuclei, such as ^{13}C and ^{15}N . However, the fact that spin components of the dipolar Hamiltonian can be manipulated using radiofrequency (rf) pulses allows dipolar couplings to be reintroduced into the spin dynamics using pulse sequences designed to interfere in a controlled fashion with the spatial modulation of the dipolar interaction due to MAS.

Various homonuclear and heteronuclear dipolar recoupling techniques have been developed and applied to distance measurements in pairs of spin- $\frac{1}{2}$ nuclei, determination of relative orientations of dipole vectors, and polarization transfer in chemical shift

correlation experiments. Most of the existing recoupling experiments including a number of applications have been reviewed in detail.^{1,25,26} Here we focus our attention on accurate ^{13}C - ^{15}N distance measurements in uniformly- ^{13}C , ^{15}N -labeled biomolecules.

The recoupling of isolated low- γ heteronuclear spin pairs can be accomplished using windowless techniques such as cross-polarization (CP)²⁷ or rotary resonance recoupling (R^3)^{28,29} and related experiments,³⁰ as well as pulsed methods based on rotational-echo double-resonance (REDOR).^{31,32} Typically, REDOR experiments employ phase-alternated π pulse schemes (e.g., xy -4, xy -8, etc.)³³ to compensate for pulse imperfections and resonance offsets,³⁴ and can provide ^{13}C - ^{15}N distances up to $\sim 6 \text{ \AA}$.^{2,26} Furthermore, for sequences based on xy -4, finite pulse effects are relatively minor³⁵ making REDOR compatible with the high MAS frequencies ($\omega_r/2\pi \approx 10$ – 20 kHz) required for high field studies of U- ^{13}C , ^{15}N -labeled systems with strong ^1H couplings.

Although experiments which probe heteronuclear distances in isolated spin pairs continue to provide valuable structural information, there is a compelling motivation for developing SSNMR techniques for distance measurements in larger spin systems, where multiple internuclear distances can be determined. In particular, such techniques provide a means to circumvent time-consuming and laborious preparation of multiple specifically labeled samples. Instead, a single multiply labeled sample will suffice. However, the application of methods developed for spin pairs to distance measurements in U- ^{13}C , ^{15}N -labeled systems is generally not straightforward, due to the presence of multiple homonuclear and heteronuclear spin-spin interactions. This is particularly exacerbated for weak heteronuclear couplings, which provide the most useful information about the three-dimensional arrangement of nuclei in the system. For example, it is well-known

that REDOR dipolar dephasing of a single S spin by multiple I spins in an I_nS spin system depends on the magnitudes and relative orientations of all dipolar couplings.³⁶⁻³⁹ (The situation is analogous for heteronuclear I–S correlation experiments^{40,41} based on transferred-echo double-resonance (TEDOR),⁴² where cross-peak intensities depend on multiple couplings.) In the simplest multispin system of this type (I_2S), the dephasing profile is most sensitive to changes in spin topology when the two I–S interactions have similar magnitude and the I_1 –S– I_2 angle, θ_{12} , is close to 0° or 180° .³⁶ (Similar observations have also been made in a number of dipole vector correlation experiments designed to measure bond and dihedral angles.^{30,43-47}) However, in general, when the size and approximate geometry of the spin system are completely unknown, the accurate measurement of weak couplings in the presence of stronger ones becomes problematic.³⁶

Several modified versions of REDOR have been developed to overcome the dependence of dipolar dephasing curves in coupled spin clusters on multiple couplings and their relative orientations. θ -REDOR⁴⁸ encodes the information about all I–S couplings into the observable S spin signal in an I_nS system, while eliminating the dependence on the relative orientation of the interactions. Although θ -REDOR is very useful for reporting simultaneously on all dipolar couplings present in the multiple spin system, the extension of this method to the accurate measurement of weak couplings in uniformly- ^{13}C , ^{15}N -labeled peptides is not straightforward. For this particular task, frequency selective methods appear to be more generally applicable. An example of this approach is frequency selective dipolar recoupling (FDR),^{49,50} where rotor-synchronized π pulses (one per rotor period) are applied to the observed S (^{13}C) nuclei, and $\pi/2$ pulses⁴⁹ or a combination of $\pi/2$ and π pulses⁵⁰ are applied to the I (^{15}N) spins. The FDR pulse

sequence generates a dipolar Hamiltonian similar to REDOR, but with an important modification: the I-spin resonance offset, δ_I , is explicitly encoded into the spin dynamics. For on-resonance I nuclei ($\delta_I = 0$) the Hamiltonian is purely dipolar, and when $\delta_I \gg b_{IS}$ (where b_{IS} is the I-S dipolar coupling constant), the dipolar dephasing is quenched. The FDR method was demonstrated in several model multispin systems including [1,4- ^{13}C , 1,2- ^{15}N]Gly-Gly·HCl,⁵⁰ where the four ^{13}C - ^{15}N dipolar couplings were measured (in particular the 20 Hz C_4 - N_1 coupling corresponding to $\sim 5.4 \text{ \AA}$ distance could be observed in the presence of the $\sim 200 \text{ Hz}$ C_4 - N_2 coupling).

Complications can arise when applying FDR (and other REDOR experiments) to U- ^{13}C , ^{15}N -labeled systems. The π -pulse train on the ^{13}C channel would recouple the ^{13}C nuclei,^{51,52} create unwanted coherences and therefore fail to simply and cleanly recouple ^{13}C - ^{15}N pairs. The irradiation of the ^{15}N nuclei, however, does not suffer from such an effect since in peptides the dipolar coupling strengths go in the order ^{13}C - ^{13}C (2 kHz) \gg ^{15}N - ^{15}N (50 Hz), and amide ^{15}N resonances exhibit a relatively small chemical dispersion. The accurate measurement of weak ^{13}C - ^{15}N couplings ($b_{CN} \approx 20$ – 100 Hz) corresponding to distances in the 3–6 Å range is further complicated by ^{13}C - ^{13}C scalar couplings since the dipolar evolution time is limited to approximately $(2J_{CC})^{-1}$ (~ 10 – 15 ms in peptides, where one-bond ^{13}C - ^{13}C J couplings are in the 30–60 Hz range⁵³).

We have recently described a J-decoupled REDOR experiment,⁵⁴ which suppresses ^{13}C - ^{13}C scalar couplings and enables the measurement of weak dipolar couplings between a single ^{15}N nucleus and individual ^{13}C nuclei within a coupled cluster. In that experiment the homonuclear J couplings, assumed to be in the weak-coupling limit ($H_J = 2\pi J_{12} S_{1z} S_{2z}$),⁵⁵ are refocused by a frequency selective spin-echo,⁵⁶ realized in

practice by applying a frequency selective π pulse to a single ^{13}C spin. (Homocoupling of this type has also been used for resolution enhancement in two-dimensional correlation spectroscopy.^{57,58}) The basic principle of using frequency selective spin-echoes to retain certain interactions while refocusing others can be extended to include heteronuclear dipolar couplings. Here we describe a selective recoupling experiment based on this idea and termed FSR (*f*requency selective REDOR), which combines REDOR with a frequency selective spin-echo generated by a pair of frequency selective π pulses applied to a ^{13}C - ^{15}N spin pair in the multispin system. We note that although in our implementation we use REDOR ($H_D \propto I_z S_z$) to achieve broadband recoupling, in principle, other sequences, which generate an analogous effective dipolar Hamiltonian (e.g., SPI-R³)³⁰ could also be used. For multiple ^{13}C , ^{15}N spin systems with sufficient ^{13}C and ^{15}N chemical shift dispersion, the application of the FSR pulse sequence generates an observable ^{13}C signal, which depends on a single ^{13}C - ^{15}N dipolar coupling; the remaining ^{13}C - ^{15}N interactions and all ^{13}C - ^{13}C scalar couplings involving the selected ^{13}C are suppressed. The dipolar coupling of interest is extracted by fitting the modulation of the ^{13}C spin-echo to the analytical expression describing dipolar dephasing in an isolated heteronuclear spin pair under conventional REDOR.³² We demonstrate the utility of the FSR experiment by measuring a number of structurally-interesting internuclear distances in U- ^{13}C , ^{15}N -labeled peptides, N-acetyl-L-Val-L-Leu and N-formyl-L-Met-L-Leu-L-Phe; for the latter peptide a total of 16 distances in the 2.5–6 Å regime were determined, with a precision in the range 0.1–0.3 Å.

4.2 Experimental

4.2.1 NMR Experiments

NMR spectra were recorded at 11.7 T (500.1 MHz ^1H , 125.8 MHz ^{13}C , 50.7 MHz ^{15}N) using a custom-designed spectrometer (courtesy of Dr. David J. Ruben) with a custom-designed quadruple-resonance MAS probe and a Chemagnetics (Fort Collins, CO) triple-resonance MAS probe. The probes were equipped with 4.0 mm Chemagnetics spinning modules. Spinning frequencies of 10.0 or 12.5 kHz were used in all experiments and regulated to ± 5 Hz with a Doty Scientific (Columbia, SC) spinning frequency controller. Samples were centerpacked in the rotors to minimize the effects of rf inhomogeneity (measured to be $\sim 5\text{--}10\%$ FWHM using the standard nutation method⁵⁹).

The FSR pulse sequence is presented in Figure 1. Ramped cross-polarization^{27,60} from ^1H creates the initial ^{13}C magnetization. Subsequently, a REDOR pulse sequence^{31,32} is initiated for time $\tau/2 = n\tau_r$ to recouple the $^{13}\text{C}\text{--}^{15}\text{N}$ dipolar interactions in a non-selective fashion. All rotor-synchronized π pulses (timing shown in inset) are applied on the ^{15}N channel to avoid the recoupling of ^{13}C spins,^{51,52} and phased according to the $xy\text{-}4$ scheme³³ to compensate for pulse imperfections and resonance offsets.

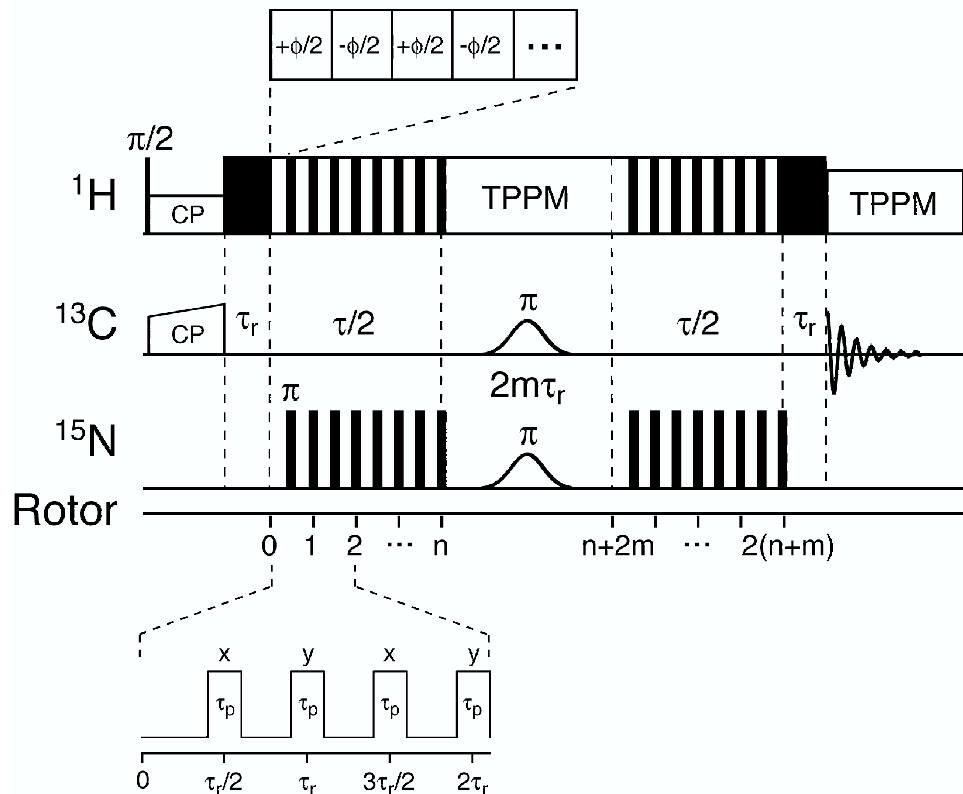


Figure 4-1. Frequency selective REDOR (FSR) pulse sequence.

Following ramped cross-polarization^{27,60} from ^1H to ^{13}C the ^{13}C - ^{15}N dipolar couplings are reintroduced via a REDOR^{31,32} sequence. The frequency selective recoupling of ^{13}C - ^{15}N spin pairs is achieved by the generation of a ^{13}C spin-echo using a pair of rotor-synchronized frequency selective π pulses applied simultaneously on the ^{13}C and ^{15}N channels (the frequency of the ^{15}N selective pulse is independent of the REDOR π pulses). Couplings to protons during the ^{13}C - ^{15}N dipolar recoupling period are attenuated using a combination of CW and TPPM⁶¹ decoupling, represented by filled and hollow rectangles, respectively. To account for the relaxation of spin coherences, a reference (S_0) experiment is recorded for each dipolar dephasing (S) experiment, by acquiring the ^{13}C spin-echo in the absence of the selective ^{15}N pulse, which results in the refocusing of all ^{15}N dipolar couplings to the selected ^{13}C .

The frequency selective spin-echo is generated by the application of simultaneous rotor-synchronized selective π pulses on the ^{13}C and ^{15}N channels, where the frequency of the ^{15}N pulse can be varied independently of the REDOR π pulses. Selective irradiation accomplishes the following: (i) signals originating from ^{13}C nuclei not affected by the ^{13}C selective pulse are eliminated by phase cycling ($\phi_{\text{Gauss}} = xy\bar{x}\bar{y}$, $\phi_{\text{rec}'} = x\bar{x}x\bar{x}$), (ii) all

^{13}C – ^{13}C scalar couplings to the selected ^{13}C are suppressed,⁵⁴ and (iii) the ^{13}C spin-echo intensity is modulated by ^{13}C – ^{15}N dipolar couplings only to the ^{15}N nuclei irradiated by the selective pulse, while the dipolar couplings to the non-irradiated ^{15}N are refocused. In our implementation, we use Gaussian pulses on both channels, timed such that their maxima coincide with the midpoint of the selective irradiation period occupying an even number of rotor cycles ($2m\tau_r$). Selective pulses were calibrated using the pulse sequence: $\text{CP}_x - (\pi/2)_y - z\text{-filter} - \tau_{\text{Gauss}} - z\text{-filter} - (\pi/2) - \text{acquire}$, where τ_{Gauss} was fixed at a constant value while the amplitude of the pulse was increased resulting in the nutation of the observable magnetization (a π pulse corresponds to maximum inversion).

Following the selective irradiation period, a REDOR pulse sequence, identical to that applied prior to the selective pulses, is initiated for time $\tau/2 = n\tau_r$. During this period, dipolar couplings involving the selected ^{13}C – ^{15}N spin pairs are retained, while ^{13}C – ^{13}C scalar couplings and remaining ^{13}C – ^{15}N dipolar couplings are refocused. Additional delays of τ_r , during which no dipolar evolution occurs, are inserted following CP and immediately before signal acquisition. The purpose of the second delay is to avoid the acquisition of the ^{13}C FID during ^{15}N rf irradiation; the delay following CP preserves the symmetry of the sequence and ensures that ^{13}C isotropic chemical shift and ^{13}C – ^{13}C scalar couplings are completely refocused. The influence of proton couplings during the ^{13}C – ^{15}N recoupling period is attenuated by a combination of resonant continuous-wave (CW) and two-pulse phase modulation (TPPM)⁶¹ decoupling (see Results and Discussion Section for details). TPPM decoupling was used during acquisition.

Unless otherwise indicated, the ^{15}N REDOR π pulse length was 18 μs ($\omega_{rf}/2\pi \approx 28$ kHz), the TPPM ^1H decoupling was ~ 120 kHz ($\phi = 15^\circ$, $\tau = 4.0$ μs), the CW decoupling

was 125 kHz, and the ^{13}C and ^{15}N Gaussian pulses were 1.0–5.0 ms and 1.0–10.0 ms, respectively. Each selective pulse was divided into 64–512 increments, and the Gaussian profile was truncated at 1% of the maximum amplitude.

4.2.2 Internuclear Distance Measurements

During the FSR pulse sequence the information about a single ^{13}C – ^{15}N dipolar coupling is encoded into the observable signal intensity. Therefore, the dipolar coupling constant of interest can be extracted by fitting the experimentally observed modulation of the ^{13}C spin-echo intensity to the analytical expression describing the dipolar dephasing in an isolated heteronuclear spin pair under conventional REDOR:³²

$$\Delta S/S_0(\tau) = \lambda \left[1 - \langle \cos(\omega_{CN}\tau) \rangle \right]. \quad (1)$$

$\Delta S/S_0 = 1 - S/S_0$, where S_0 and S represent the reference and dipolar dephasing experiments, respectively (*c.f.* Figure 4-1). The dipolar coupling, ω_{CN} , is a function of the ^{13}C – ^{15}N dipolar coupling constant, b_{CN} , and $\langle \dots \rangle$ represents the average over random orientations of the dipole vector in the powder sample (see Theoretical Background Section for details). The scaling factor, λ , accounts for the contribution to S_0 from ^{13}C spins without a neighboring ^{15}N , which is the result of imperfect isotopic labeling and/or dilution of the labeled compound with natural abundance material.

In the FSR experiment, λ also accounts for a small scaling of the dipolar dephasing amplitude resulting from the imperfect inversion of ^{15}N spin coherences by the ^{15}N selective pulse and/or decay of coherences due to insufficient ^1H decoupling during the selective pulse. The amplitude scaling was found to be negligible for 1–10 ms ^{15}N

selective pulses when recoupling ^{15}N with small chemical shielding anisotropy (CSA) and small effective ^{15}N – ^1H coupling (e.g., NH_3^+ groups under the experimental conditions employed in this work) (data not shown). For ^{15}N nuclei with larger CSA and ^{15}N – ^1H coupling (e.g., amide groups) the scaling was also negligible for short (~ 1 ms) ^{15}N selective pulses. However, for pulses in the 6–10 ms range the dephasing amplitude had to be scaled down by ~ 5 – 10 % in order to accurately simulate experimental data. For most systems internal references are available, in the form of strong ^{13}C – ^{15}N dipolar couplings which exhibit several oscillations during typical mixing times, and λ can be easily calibrated. For example, in U- ^{13}C , ^{15}N -labeled peptides investigated in this work, which were not diluted in natural abundance material, we expect $\lambda \approx 1.0$ for conventional REDOR. However, we find that FSR experiments for ~ 200 Hz ^{13}C – ^{15}N couplings (e.g., Val(C^β)–Val(N) in N-acetyl-L-Val-L-Leu), which employed 10 ms ^{15}N selective pulses, are best-fit with $\lambda \approx 0.90$ – 0.95 .

For each experiment designed to measure a single ^{13}C – ^{15}N distance the reduced χ^2 , $\chi_v^2 \propto \sum_i w_i (s_{exp}^i - s_{sim}^i)^2$,⁶² was minimized by adjusting the dipolar coupling constant, b_{CN} , and amplitude scaling factor, λ , where b_{CN} was varied freely and λ was allowed to vary only within a narrow range (determined from the data for strong ^{13}C – ^{15}N couplings). The uncertainties in b_{CN} (reported at 95% confidence level) were obtained according to the procedure described in ref 62. First, the best-fit dipolar coupling, b_{CN}^* , is determined with $\chi_{v,\min}^2$. Subsequently, several trial b_{CN} values are selected around b_{CN}^* , and experimental data are re-fit by optimizing λ within the previously defined range. The b_{CN} values, for which the condition $\chi_{v,\max}^2 = F(v)\chi_{v,\min}^2$ is satisfied ($F(v)$ is a constant, which depends on the number of degrees of freedom, v , and the desired confidence level),

represent the uncertainties in the best-fit dipolar coupling constant. The internuclear C–N distances, r_{CN} , are related to the dipolar coupling constants via eq 6 below (see Theoretical Background Section for details).

4.2.3 ^{13}C , ^{15}N -Labeled Model Systems

The model compounds used in the experiments were: [$1\text{-}^{13}\text{C}$, ^{15}N]glycine, [acetyl- $1,2\text{-}^{13}\text{C}$, ^{15}N]N-acetylvaline (NAV), [^{13}C , ^{15}N]asparagine, [^{13}C , ^{15}N]N-acetyl-L-Val-L-Leu (VL) and N-formyl- ^{13}C , ^{15}N]L-Met-L-Leu-L-Phe (MLF). All ^{13}C , ^{15}N -labeled amino acids and [$1,2\text{-}^{13}\text{C}$]acetic anhydride were purchased from Cambridge Isotope Laboratories (Andover, MA). VL and MLF were synthesized by Synpep (Dublin, CA) and American Peptide (Sunnyvale, CA), respectively, using standard solid phase methods and purified by HPLC. Prior to the NMR experiments glycine, asparagine and NAV were diluted to $\sim 10\%$ in respective natural abundance compounds and recrystallized by slow evaporation of aqueous solutions. VL was crystallized from a 1:1 (v/v) H_2O :acetone solution⁶³ and we confirmed using X-ray crystallography (courtesy of W. Davis) that the crystal structure is in good agreement with the published structure.⁶⁴ The recrystallization of N-formyl-L-Met-L-Leu-L-Phe from 2-propanol results in microcrystals, which are not of sufficiently high quality for X-ray crystallography. However, an X-ray structure has been reported for the methyl ester analogue of MLF, N-formyl-L-Met-L-Leu-L-Phe-O-methyl (MLF-OMe).⁶⁵ The inspection of VL and MLF-OMe crystal structures indicates that intermolecular ^{13}C – ^{15}N couplings are expected to have a relatively minor effect on the structurally-interesting sidechain-to-backbone ^{13}C – ^{15}N distances in the 3–4 Å range in these peptides (see Supporting Information). Therefore, initial FSR experiments were

performed on peptides not diluted in natural abundance compounds. However, for measurements of intramolecular distances in the 4–6 Å regime a MLF sample was prepared by diluting N-formyl-[U-¹³C,¹⁵N]L-Met-L-Leu-L-Phe to ~ 10% in the natural abundance peptide followed by recrystallization from 2-propanol.

4.3 Theory

4.3.1 Broadband Recoupling in Multispin Systems

We consider a coupled multiple spin system consisting of n ¹³C spins and m ¹⁵N spins. In the rapid spinning regime the first-order effective Hamiltonian^{66,67} describing the spin-spin couplings during the REDOR π -pulse train (Figure 4-1) can be written:³²

$$H = \sum_{i=1}^n \sum_{j=1}^m \omega_{C_i N_j} 2C_{iz} N_{jz} + \sum_{i < j} \pi J_{C_i C_j} 2C_{iz} C_{jz}. \quad (2)$$

The C and N operators represent ¹³C and ¹⁵N spins, respectively, and $J_{C_i C_j}$ is the C_i – C_j scalar coupling constant. For ¹⁵N π pulses of finite length and phase-alternated according to xy -4 (or extensions thereof),³³ the dipolar coupling coefficients have the form:³⁵

$$\omega_{C_i N_j} = -\frac{4}{\pi} \frac{\cos\left(\frac{\pi}{2}\varphi\right)}{1-\varphi^2} \text{Im}\left\{\omega_{C_i N_j}^{(1)}\left(\Omega_{PR}^{ij}\right)\right\}, \quad (3)$$

where the fraction of the rotor period, τ_r , occupied by pulses of length τ_p is defined as

$$\varphi = \frac{2\tau_p}{\tau_r}. \quad (4)$$

The Fourier component rotating at ω_r in the MAS Hamiltonian for the dipolar coupling is given by:⁶⁸

$$\omega_{C_i N_j}^{(1)}(\Omega_{PR}^{ij}) = -b_{C_i N_j} \left\{ \sum_{m=-2}^2 D_{0,m}^{(2)}(\Omega_{PC}^{ij}) D_{m,-1}^{(2)}(\Omega_{CR}) \right\} d_{-1,0}^{(2)}(\beta_{RL}), \quad (5)$$

where the C_i-N_j dipolar coupling constant:

$$b_{C_i N_j} = -\frac{\mu_0}{4\pi} \frac{\gamma_C \gamma_N \hbar}{r_{C_i N_j}^3} \quad (6)$$

is a function of the gyromagnetic ratios, γ_C and γ_N , of the coupled spins and the C_i-N_j internuclear distance, $r_{C_i N_j}$. The Wigner rotation matrices, $D_{0,m}^{(2)}(\Omega_{PC}^{ij})$, $\Omega_{PC}^{ij} = \{0, \beta_{PC}^{ij}, \gamma_{PC}^{ij}\}$, describe the transformations of individual C_i-N_j dipole vectors from their principal axis systems (P^{ij}) to a common crystallite-fixed frame (C). The subsequent transformation of all crystallites in the powder sample into the rotor-fixed frame (R) is described by $D_{m,-1}^{(2)}(\Omega_{CR})$, and the reduced rotation matrix, $d_{-1,0}^{(2)}(\beta_{RL})$, transforms the rotor-fixed frame into the laboratory frame (L) via a rotation by the magic-angle, $\beta_{RL} = \tan^{-1} \sqrt{2}$. In the case of a single C-N dipolar coupling, for which the principal axis system coincides with the crystallite-fixed frame (i.e., $\Omega_{PC} = \{0,0,0\}$), eq 5 becomes:

$$\omega_{CN}^{(1)}(\Omega_{PR}) = \frac{b_{CN}}{2\sqrt{2}} \sin(2\beta_{PR}) e^{i\gamma_{PR}}, \quad (7)$$

and the expression for ω_{CN} (c.f. eqs 2 and 3) simplifies to:

$$\omega_{CN} = -\frac{\sqrt{2}}{\pi} \frac{\cos(\frac{\pi}{2}\varphi)}{1-\varphi^2} b_{CN} \sin(2\beta_{PR}) \sin(\gamma_{PR}). \quad (8)$$

Eq 8 differs from the expression for ideal δ -pulse REDOR³² only by the factor $\cos(\frac{\pi}{2}\varphi)/(1-\varphi^2)$, which describes the finite pulse effects.³⁵

The initial transverse ¹³C density matrix created by cross-polarization²⁷ from ¹H can be written:

$$\rho(\tau_0) = \sum_i p_i C_{ix}, \quad (9)$$

where p_i represents the starting polarization on the i^{th} ^{13}C spin. In the absence of relaxation, the density matrix for individual crystallites evolves under the effective Hamiltonian in eq 2 according to:⁵⁵

$$\rho(\tau) = U(\tau)\rho(\tau_0)U(\tau)^{-1}, \quad (10)$$

with

$$U(\tau) = \prod_{i,j} \exp\{-i\omega_{C_i N_j} \tau 2C_{iz} N_{jz}\} \prod_{i < j} \exp\{-i\pi J_{C_i C_j} \tau 2C_{iz} C_{jz}\}. \quad (11)$$

Explicit calculation yields

$$\rho(\tau) = \sum_i \left\{ p_i C_{ix} \prod_j \cos(\omega_{C_i N_j} \tau) \prod_{j \neq i} \cos(\pi J_{C_i C_j} \tau) \right\} + \dots, \quad (12)$$

where only the part of $\rho(\tau)$ corresponding to observable coherences is given. The resulting ^{13}C spin-echo intensity is:

$$S(\tau) = \left\langle \text{tr} \left\{ \left(\sum_i C_i^+ \right) \rho(\tau) \right\} \right\rangle = \left\langle \sum_i \left\{ \tilde{p}_i \prod_j \cos(\omega_{C_i N_j} \tau) \prod_{j \neq i} \cos(\pi J_{C_i C_j} \tau) \right\} \right\rangle, \quad (13)$$

where coefficients \tilde{p}_i include the appropriate normalization constants and $\langle \dots \rangle$ denotes the average the Euler angles, $\Omega_{CR} = \{\alpha_{CR}, \beta_{CR}, \gamma_{CR}\}$, which define random crystallites in the powder sample. Eq 13 provides the basic result:³⁶⁻³⁹ for Hamiltonians of the form given in eq 2, the observable coherences evolve simultaneously as products of cosine terms describing all spin-spin couplings in the multispin system, and the dependence of the observable signal on the relative orientations of all dipole vectors is encoded in the frequencies, $\omega_{C_i N_j}$. As a result of the dependence on multiple couplings and their relative

orientations, the accurate measurement of weak heteronuclear dipolar couplings in multispin systems of unknown topology is very difficult.³⁶

4.3.2 Selective Recoupling in Multispin Systems

The effective spin-spin coupling Hamiltonian of eq 2 is a sum of commuting bilinear terms, which, in principle, can be refocused by spin-echo⁵⁶ techniques. Consider the pulse sequence of the type shown in Figure 4-1, where simultaneous rf irradiation on ¹³C and ¹⁵N channels is bracketed by two identical dipolar evolution periods of duration $\tau/2$. Assuming that a pair of ideal π pulses is applied in a frequency selective fashion to spins C_k and N_l in the multispin cluster the propagator for the entire pulse sequence can be written:

$$U(\tau) = \exp\{-iH(\tau/2)\} \exp\{-i\pi C_{kx}\} \exp\{-i\pi N_{lx}\} \exp\{-iH(\tau/2)\}. \quad (14)$$

H can be expressed as a sum of three terms:

$$H = H_0 + H_1 + H_2, \quad (15)$$

where H_0 , H_1 and H_2 contain the two-spin operators affected by neither, one and both pulses, respectively:

$$H_0 = \sum_i \sum_{j \neq i} \omega_{C_i N_j} 2C_{iz} N_{jz} + \sum_{i < j} \pi J_{C_i C_j} 2C_{iz} C_{jz}, \quad (16a)$$

$$H_1 = \sum_{i \neq l} \omega_{C_k N_i} 2C_{kz} N_{iz} + \sum_{i \neq k} \omega_{C_i N_l} 2C_{iz} N_{lz} + \sum_{i \neq k} \pi J_{C_k C_i} 2C_{kz} C_{iz}, \quad (16b)$$

$$H_2 = \omega_{C_k N_l} 2C_{kz} N_{lz}. \quad (16c)$$

The sign of H_1 is inverted by the selective ^{13}C and ^{15}N π pulses, which leads to the refocusing of those interactions during the FSR pulse sequence. H_0 and H_2 are unaffected by the π pulses and eq 14 can be simplified to:

$$U(\tau) = \exp\{-iH_0\tau\} \exp\{-iH_2\tau\} \exp\{-i\pi C_{kx}\} \exp\{-i\pi N_{lx}\}. \quad (17)$$

Furthermore, in the FSR experiment we are only interested in the dipolar dephasing of the transverse magnetization on the ^{13}C spin, C_k , irradiated by the ^{13}C selective pulse, and therefore the initial density matrix is:

$$\rho(\tau_0) = p_k C_{kx}. \quad (18)$$

Since in eq 17 the exponential operators containing H_0 , C_{kx} and N_{lx} commute with the initial density matrix they have no effect on the time evolution (*c.f.* eq 10) and can be neglected. The resulting propagator for the complete FSR pulse sequence is given by:

$$U(\tau) = \exp\{-i\omega_{C_k N_l} \tau 2C_{kz} N_{lz}\}. \quad (19)$$

Therefore, spin C_k evolves only under the dipolar coupling to the selected N_l spin in the multispin system, while the remaining ^{13}C - ^{15}N dipolar couplings and ^{13}C - ^{13}C scalar couplings, which would complicate the evolution, are suppressed. The ^{13}C spin-echo intensity averaged over the crystallite ensemble is equivalent to that expected for an isolated spin pair under conventional REDOR:³²

$$S(\tau) = \langle \tilde{p}_k \cos(\omega_{C_k N_l} \tau) \rangle. \quad (20)$$

Experimentally, the frequency selective ^{13}C and ^{15}N pulses do not correspond to instantaneous π rotations, and in our implementation selective excitation of resonances is achieved with weak Gaussian-shaped pulses⁶⁹ (e.g., $\sim \pm 500$ Hz ^{15}N excitation bandwidth requires a 4 ms pulse). Nevertheless, in practice we find that the selective pulses act in nearly ideal fashion; the effects due to their application appear to be relatively minor and

are compensated by recording reference experiments. We also note here that it is *essential* that rotor-synchronization is maintained throughout the entire experiment, since for efficient refocusing of the dipolar interactions the phase of the REDOR sequence^{25,70} must remain unchanged. We used a standard spinning frequency controller (see Experimental Section), and the resulting ± 5 Hz stability in the MAS rate was adequate for maintaining the required rotor-synchronization.

4.4 Results and Discussion

4.4.1 Selective Recoupling in [U-¹³C, ¹⁵N]Asparagine

Asparagine (Figure 4-2a) represents a favorable model system for demonstrating frequency selective ¹³C–¹⁵N recoupling experiments in uniformly-¹³C,¹⁵N-labeled compounds. The difference in C^α and C^β isotropic chemical shifts is ~ 16 ppm and the N' and N^{δ2} resonances are separated by ~ 75 ppm (Figures 4-2b and 4-2c), which enables straightforward frequency selective irradiation of ¹³C–¹⁵N spin pairs. Furthermore, the four ¹³C–¹⁵N dipolar couplings to be measured (Figure 4-2a) cover a relatively wide range of internuclear distances (~ 1.5 – 4 Å).

Prior to quantitative C–N distance determination we qualitatively investigate the selective recoupling of C^β–N' and C^β–N^{δ2} interactions using the FSR pulse sequence. The C^β resonance is selectively irradiated with a 1.0 ms Gaussian pulse and ¹⁵N Gaussian pulses are applied at different frequencies in the ¹⁵N spectrum. ¹⁵N REDOR π pulses are approximately centered between the N' and N^{δ2} resonances ($\delta \sim 75$ ppm in Figure 4-2c), so that the effective field during REDOR is identical for both ¹⁵N, and the dipolar

evolution time (see Figure 4-1) is set to $\tau = 8.0$ ms. Figure 4-3 demonstrates the selective recoupling of $C^\beta-N'$ and $C^\beta-N^{\delta 2}$ interactions using a frequency selective spin-echo generated by the simultaneous ^{13}C and ^{15}N selective pulses; the C^β signal is dephased only by the ^{15}N nuclei on-resonance with the Gaussian pulse, while the couplings to off-resonance ^{15}N are refocused. The selectivity of the FSR experiment can be tuned by adjusting the duration of the ^{15}N Gaussian pulse, where the recoupling conditions become increasingly narrow for long, weak pulses. The recoupling bandwidths obtained with 1–10 ms pulses are in the ± 2000 – ± 200 Hz range.

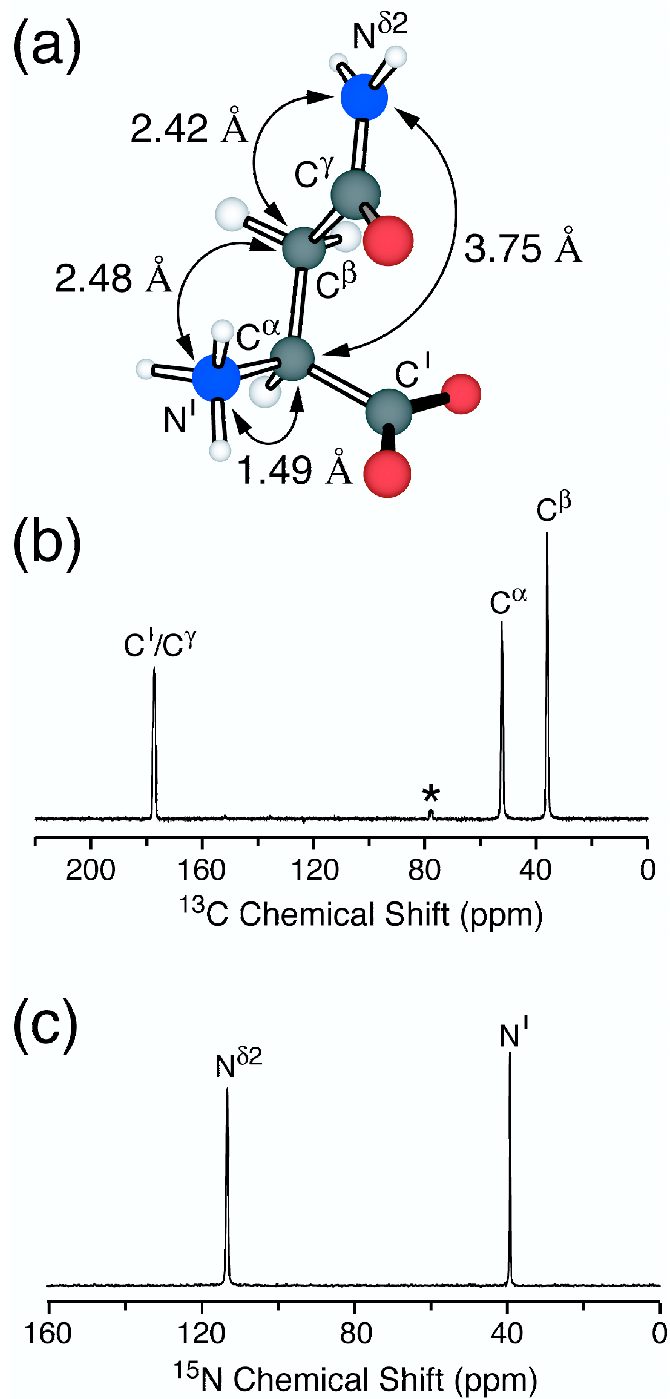


Figure 4-2. Asparagine neutron diffraction structure and ^{13}C and ^{15}N MAS spectra. (a) Neutron diffraction structure of asparagine.⁷¹ The internuclear distances of interest in this work are indicated. ^{13}C (b) and ^{15}N (c) MAS spectra of [U- ^{13}C , ^{15}N]asparagine recorded at $\omega/2\pi = 12.5$ kHz. Rotational sidebands are denoted by an asterisk.

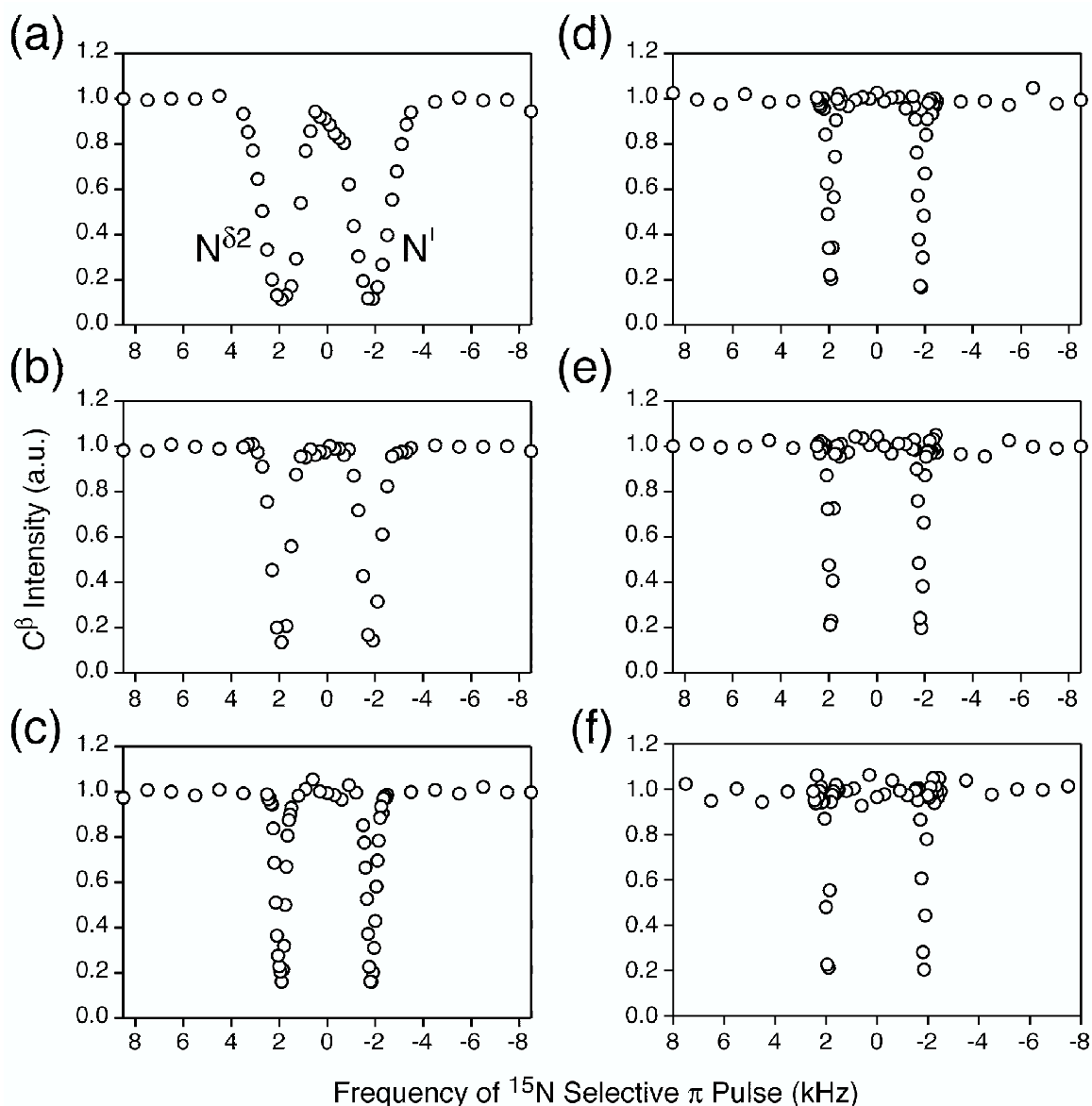


Figure 4-3. Selective recoupling of $C^\beta-N'$ and $C^\beta-N^{\delta 2}$ dipolar interactions in $[U-^{13}C, ^{15}N]$ asparagine.

The pulse sequence in Figure 4-1 was used with the total dipolar evolution time, $\tau = 8.0$ ms. Experiments were performed at $\omega/2\pi = 10.0$ kHz \pm 5 Hz with a 1.0 ms Gaussian pulse applied to the C^β resonance. We show the results of ‘frequency sweep’ experiments for ^{15}N Gaussian pulses of: (a) 1.0, (b) 2.0, (c) 4.0, (d) 6.0, (e) 8.0, and (f) 10.0 ms. Each experimental point (\circ) is the ratio of the intensity of the C^β resonance in the presence and absence of the ^{15}N selective pulse. The ^{15}N selective pulse bandwidths, outside of which negligible recoupling takes place, were found to be approximately: (a) ± 2000 , (b) 1000, (c) 500, (d) 300, (e) 250, and (f) 200 Hz.

Having demonstrated the feasibility of pairwise recoupling of selected heteronuclear interactions in a multiple spin system, we apply the FSR experiment to the quantitative measurement of several internuclear distances in [U- ^{13}C , ^{15}N]asparagine. In Figures 4-4a and 4-4b we determine the $\text{C}^\beta\text{-N}'$ and $\text{C}^\beta\text{-N}^{\delta 2}$ distances, respectively, where a 1.0 ms ^{13}C selective pulse is applied to the C^β resonance, a 1.0 ms ^{15}N selective pulse is applied on-resonance with the ^{15}N to be recoupled, and the dipolar evolution time, τ , is incremented. The simulation of experimental data to the two-spin model (see Experimental Section for details) results in best-fit $\text{C}^\beta\text{-N}'$ and $\text{C}^\beta\text{-N}^{\delta 2}$ distances of $2.49 \pm 0.02 \text{ \AA}$ and $2.44 \pm 0.02 \text{ \AA}$, respectively; these distances are in good agreement with the neutron diffraction values of 2.48 \AA for $\text{C}^\beta\text{-N}'$ and 2.42 \AA for $\text{C}^\beta\text{-N}^{\delta 2}$.⁷¹

For comparison with the individual distance measurements, Figure 4-4c shows the dipolar dephasing in a coupled pseudo three-spin ($\text{N}^{\delta 2}\text{-C}^\beta\text{-N}'$) system, where simultaneous recoupling of both $^{13}\text{C}\text{-}^{15}\text{N}$ interactions significantly alters the evolution relative to the ‘spin-pair’ cases. The data were simulated using the $\text{C}^\beta\text{-N}'$ and $\text{C}^\beta\text{-N}^{\delta 2}$ couplings determined from FSR experiments (Figures 4-4a and 4-4b) with the relative orientation, $\theta_{12} = 123^\circ$, obtained from the neutron diffraction structure,⁷¹ and the agreement between experiment and simulation is good. In this favorable case of two $^{13}\text{C}\text{-}^{15}\text{N}$ couplings of approximately equal magnitude, we can obtain information about both couplings from the non-selective experiment. However as noted previously, in general the accurate extraction of weak dipolar couplings from dipolar dephasing data in multiple spin systems of unknown topology is very difficult.³⁶

In Figure 4-5 we show the measurement of $\text{C}^\alpha\text{-N}'$ and $\text{C}^\alpha\text{-N}^{\delta 2}$ distances in [U- ^{13}C , ^{15}N]asparagine. It is clear that the rapid dipolar oscillation due to the one-bond $\text{C}^\alpha\text{-N}'$

coupling is suppressed when the ^{15}N selective pulse is applied off-resonance with N' and selective dephasing of the C^α signal by $\text{N}^{\delta 2}$ can be accomplished (Figure 4-5a). We note that for experiments where one-bond ^{13}C - ^{15}N couplings are refocused the reference and dephasing curves for evolution times greater than ~ 10 – 12 ms can appear somewhat ‘noisy’ relative to experiments involving the refocusing of weaker (e.g., two-bond) couplings. This may be the result of short-term fluctuations in the spinning frequency, the effects of which are expected to be most pronounced at long evolution times when attempting to refocus strong couplings. (In such cases we found that averaging several experiments acquired at different times significantly reduces the scatter in the data.) The experimental data were simulated (Figures 4-5b and 4-5c) and the resulting distances are 1.50 ± 0.02 Å for C^α - N' and 3.58 ± 0.20 Å for C^α - $\text{N}^{\delta 2}$. These compare well with the respective neutron diffraction distances of 1.49 and 3.75 Å.⁷¹ A summary of all distance measurements in $[\text{U-}^{13}\text{C}, ^{15}\text{N}]\text{asparagine}$ is provided in Table 4-1.

Table 4-1. Internuclear Distances in Asparagine

atoms ^a		$r_{\text{C-N}}$ (Å)	
		NMR ^b	neutron ^c
N'	C^α	1.50 ± 0.02	1.49
	C^β	2.49 ± 0.02	2.48
$\text{N}^{\delta 2}$	C^α	3.58 ± 0.20	3.75
	C^β	2.44 ± 0.02	2.42

^aNomenclature given in Figure 4-2a. ^bNMR distances (with uncertainties at 95% confidence level) were determined using frequency selective REDOR as described in the text. ^cRef 71.

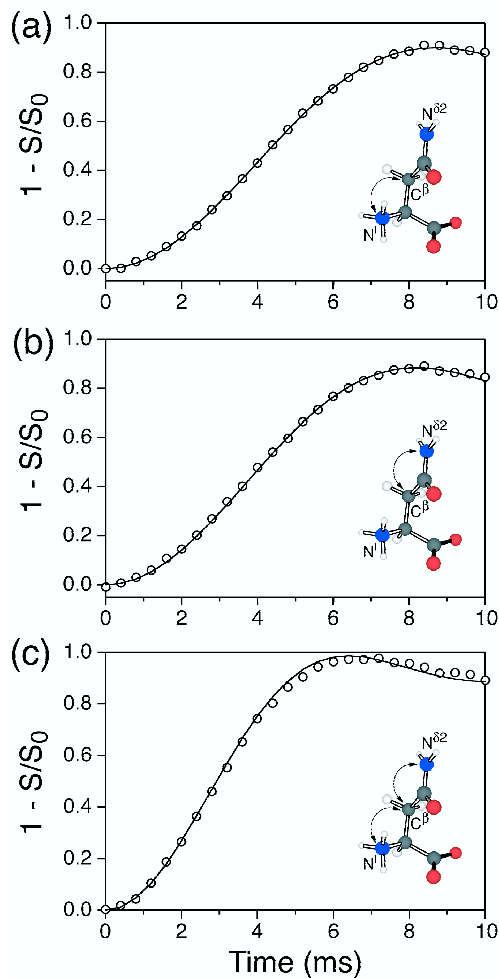


Figure 4-4. Internuclear distance measurements for C^β in $[U-^{13}C, ^{15}N]$ asparagine.

Pairwise frequency selective recoupling of C^β - N' (a) and C^β - $N^{\delta 2}$ (b) interactions. Experiments were performed at $\omega/2\pi = 10.0 \text{ kHz} \pm 5 \text{ Hz}$ and 8 scans were averaged for each time point. A 1.0 ms Gaussian pulse was applied to the C^β resonance and a 1.0 ms Gaussian pulse was applied on resonance with N' (a) or $N^{\delta 2}$ (b). The simulations (—) in (a) and (b) are least-squares fits of the experimental data (\circ) to the analytical expression describing the dipolar evolution in an isolated heteronuclear spin pair under conventional REDOR, where finite pulse effects have been taken into account. The best-fit values for the dipolar coupling constants are $b_{CN}(C^\beta-N') = 198 \pm 3 \text{ Hz}$ and $b_{CN}(C^\beta-N^{\delta 2}) = 210 \pm 3 \text{ Hz}$, corresponding to C^β - N' and C^β - $N^{\delta 2}$ distances of $2.49 \pm 0.02 \text{ \AA}$ and $2.44 \pm 0.02 \text{ \AA}$, respectively (*c.f.* Table 4-1). In (c) we show experimental data (\circ) and simulation (—) for the J-decoupled REDOR experiment,⁵⁴ in which C^β - N' and C^β - $N^{\delta 2}$ interactions are simultaneously recoupled and the dipolar dephasing of the C^β spin depends on both ^{13}C - ^{15}N couplings and their relative orientation (see text for details). The input parameters for the simulation are the C^β - N' and C^β - $N^{\delta 2}$ dipolar couplings (determined to be 198 and 210 Hz from the FSR experiments in (a) and (b)) and the projection angle between the C^β - N' and C^β - $N^{\delta 2}$ dipole vectors (determined to be $\theta_{12} = 123^\circ$ from the asparagine neutron diffraction structure⁷¹).

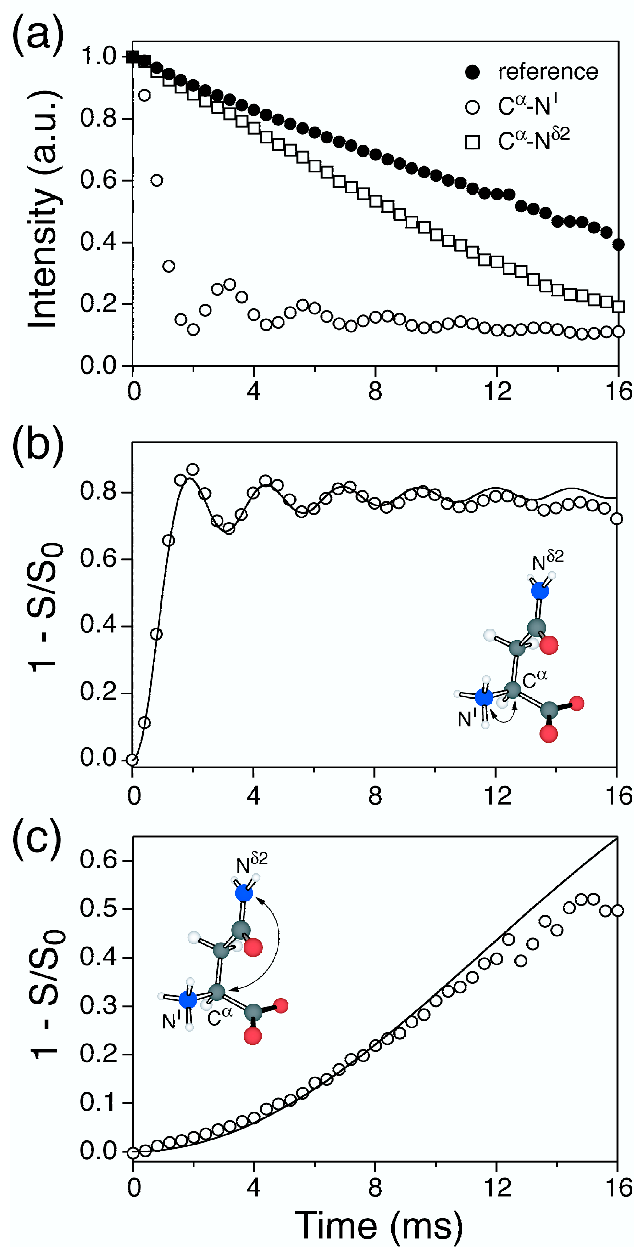


Figure 4-5. Internuclear distance measurements for C^α in [U-¹³C, ¹⁵N]asparagine. (a) Reference (S_0) curve (●) and dipolar dephasing (S) curves for C^α-N' (○) and C^α-N^{δ2} (□) couplings. Experimental $\Delta S/S_0$ curves (○) and analytical simulations (—) for C^α-N' (b) and C^α-N^{δ2} (c) couplings. The best-fit values for the dipolar coupling constants are $b_{CN}(\text{C}^\alpha\text{-N}') = 907 \pm 35$ Hz and $b_{CN}(\text{C}^\alpha\text{-N}^{\delta 2}) = 67 \pm 8$ Hz, corresponding to C^α-N' and C^α-N^{δ2} distances of 1.50 ± 0.02 Å and 3.58 ± 0.20 Å, respectively (*c.f.* Table 4-1). Spectra were recorded at $\omega_r/2\pi = 10.0$ kHz \pm 5 Hz, and 6 experiments (8 scans per experiment) were averaged for each time point. A 1.0 ms Gaussian pulse was applied to the C^α resonance and a 1.0 ms Gaussian pulse was applied on resonance with N' (b) and N^{δ2} (c).

4.4.2 Internuclear Distance Measurements in U-¹³C,¹⁵N-Labeled Peptides

In the following we present accurate ¹³C–¹⁵N distance measurements in model peptides, [U-¹³C,¹⁵N]N-acetyl-L-Val-L-Leu (VL) and N-formyl-[U-¹³C,¹⁵N]L-Met-L-Leu-L-Phe (MLF). Frequency selective recoupling in these peptides is more challenging compared to asparagine, since the amide ¹⁵N resonances have very similar frequencies. However, we found that 6–10 ms ¹⁵N Gaussian pulses, having $\sim\pm 300\text{--}\pm 200$ Hz bandwidths (*c.f.* Figure 4-3), were sufficient to selectively recouple the individual amide ¹⁵N in VL and MLF.

Figure 4-6 shows the X-ray structure of N-acetyl-L-Val-L-Leu⁶⁴ as well as one-dimensional ¹³C and ¹⁵N MAS spectra of the U-¹³C,¹⁵N-labeled peptide. The ¹³C and ¹⁵N chemical shift assignments were obtained from two-dimensional ¹³C–¹³C and ¹³C–¹⁵N correlation experiments (see Supporting Information). The ¹³C–¹³C correlation spectra do not provide unambiguous assignments for the Val and Leu methyl resonances. The assignment of the Leu(C^δ) resonances remains ambiguous since we did not attempt to perform ¹³C–¹⁵N distance measurements involving those ¹³C. However, using the FSR experiments for both Val(C^γ) we were able to assign the downfield resonance (denoted C^{γ1}) to the CH₃ approximately *syn* to Val(N) and the upfield resonance (denoted C^{γ2}) to the CH₃ approximately *anti* to Val(N) (*c.f.* Figure 4-6a).

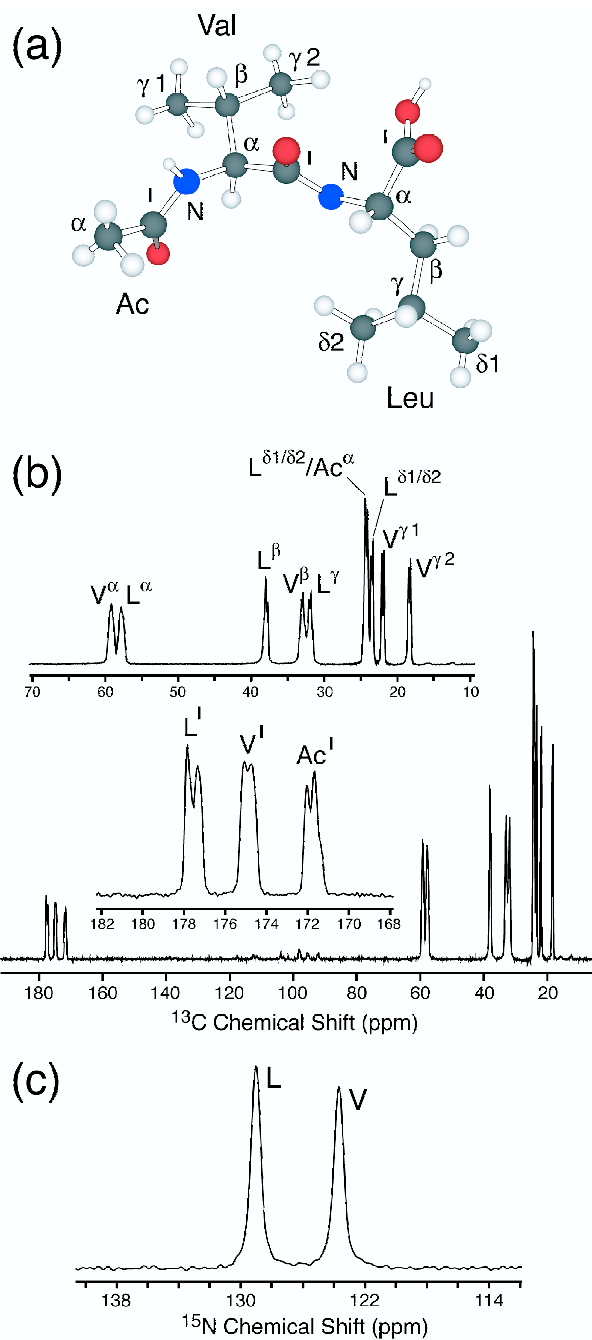


Figure 4-6. N-acetyl-L-Val-L-Leu crystal structure and ^{13}C and ^{15}N MAS spectra.

(a) X-ray diffraction structure of N-acetyl-L-Val-L-Leu.⁶⁴ ^{13}C (b) and ^{15}N (c) MAS spectra of $[\text{U-}^{13}\text{C},^{15}\text{N}]$ N-acetyl-L-Val-L-Leu recorded at $\omega_r/2\pi = 10.0$ kHz. Most ^{13}C resonances exhibit resolved splittings due to $\sim 30\text{--}60$ Hz $^{13}\text{C}\text{--}^{13}\text{C}$ J couplings. ^{13}C and ^{15}N chemical shift assignments were obtained from two-dimensional $^{13}\text{C}\text{--}^{13}\text{C}$ and $^{13}\text{C}\text{--}^{15}\text{N}$ correlation spectra (see Supporting Information). Val($\text{C}^{\gamma 1}$) and Val($\text{C}^{\gamma 2}$) resonances were assigned based on the FSR experiments presented in this work. Assignment of Leu($\text{C}^{\delta 1}$) and Leu($\text{C}^{\delta 2}$) resonances remains ambiguous, since distance measurements involving those nuclei were not performed here.

Representative FSR experiments in $[U-^{13}C,^{15}N]$ N-acetyl-L-Val-L-Leu are presented in Figure 4-7 and all distances measured in the peptide are summarized in Table 4-2. The frequency selective experiments enable the measurement of internuclear distances, which provide indispensable information about the three-dimensional structure of the peptide, but are not easily accessible via non-selective methods. For example, Val(C^β) can be recoupled to Val(N) and Leu(N) in separate experiments. While the two-bond Val(C^β)–Val(N) dipolar coupling (Figure 4-7a), which would dominate the non-selective experiment, provides no useful structural data, the Val(C^β)–Leu(N) coupling (Figure 4-7b) provides valuable information about the backbone torsion angle ψ_1 . Since $[U-^{13}C,^{15}N]$ VL was not diluted in the natural abundance compound, the distances reported are limited to the sidechain-to-backbone distances in the 2.5–3.5 Å range, for which the dipolar dephasing depends primarily on a single intramolecular coupling (see Supporting Information). (Accurate measurements of longer distances are demonstrated below for MLF.) Overall the experimental data are reproduced very well with the analytical two-spin model (*c.f.* eq 1) and most measured distances agree closely (within ~ 0.1 Å) with those determined by X-ray crystallography (see Table 4-2).

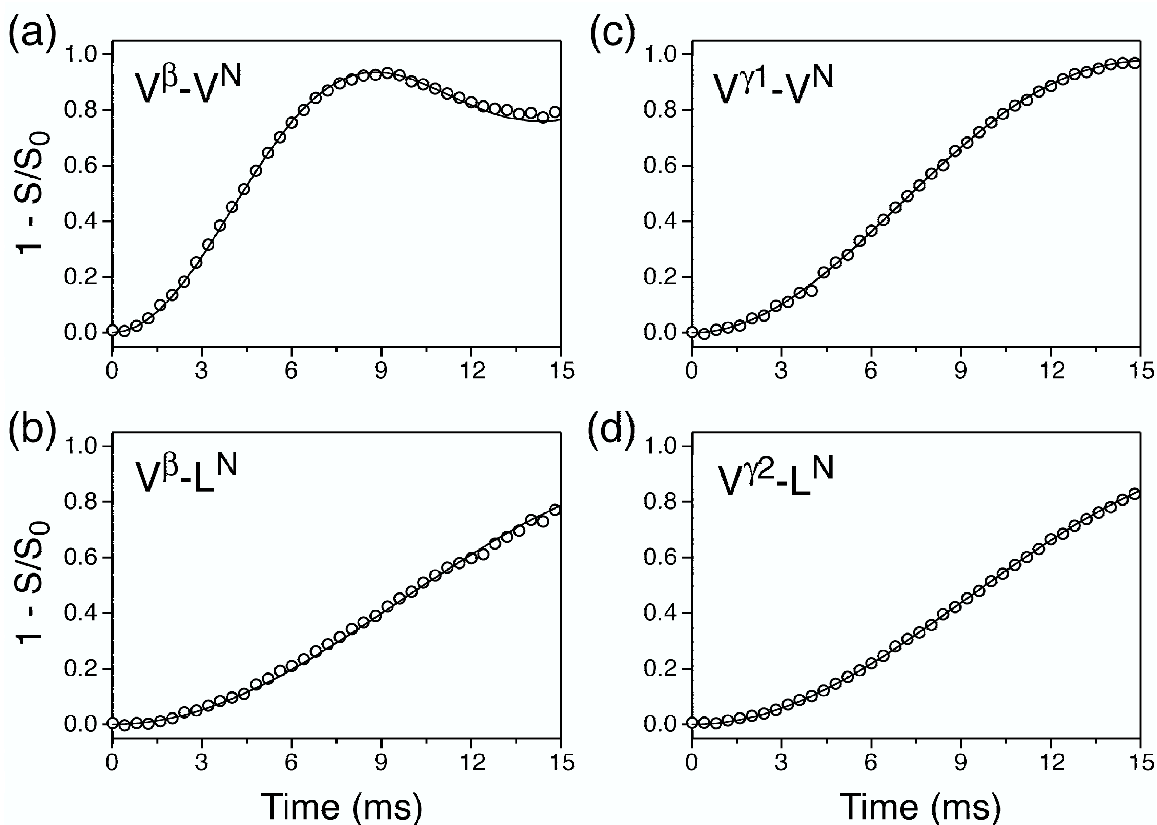


Figure 4-7. Representative internuclear distance measurements in [U- ^{13}C , ^{15}N]N-acetyl-L-Val-L-Leu.

Experimental $\Delta S/S_0$ curves (\circ) and analytical simulations (—) are shown for the selective pairwise recoupling of (a) Val(C^β)–Val(N), (b) Val(C^β)–Leu(N), (c) Val($\text{C}^{\gamma 1}$)–Val(N), and (d) Val($\text{C}^{\gamma 2}$)–Leu(N). The internuclear distances measured in [U- ^{13}C , ^{15}N]N-acetyl-L-Val-L-Leu are summarized in Table 4-2. Experiments were performed at $\omega_r/2\pi = 10.0 \text{ kHz} \pm 5 \text{ Hz}$, and 32 scans were averaged for each time point. The ^{13}C Gaussian pulse was 3.0 ms for experiments involving Val($\text{C}^{\gamma 1}$) and Val($\text{C}^{\gamma 2}$), and 5.0 ms for Val(C^β), Leu(C^β) and Leu(C^γ). The (i) Val($\text{C}^{\gamma 1}$)/Val($\text{C}^{\gamma 2}$) and (ii) Val(C^β)/Leu(C^γ) distance measurements were performed simultaneously since the chemical shifts are similar for these nuclei, and Val($\text{C}^{\gamma 1}$)–Val($\text{C}^{\gamma 2}$) and Val(C^β)–Leu(C^γ) ^{13}C – ^{13}C J couplings are negligible relative to the ^{13}C – ^{15}N dipolar couplings of interest. The ^{15}N Gaussian pulse was 10.0 ms, applied on resonance with the Val(N) or Leu(N) resonances.

Table 4-2. Internuclear Distances in N-acetyl-L-Val-L-Leu

atoms ^a		r_{C-N} (Å)	
		NMR ^b	X-ray ^c
Val(N)	Val(C ^β)	2.50±0.02	2.48
	Val(C ^{γ1})	3.01±0.02	2.97
	Val(C ^{γ2})	3.58±0.08 ^d	3.81
Leu(N)	Val(C ^β)	3.35±0.06	3.46
	Val(C ^{γ2})	3.31±0.03	3.40
	Leu(C ^β)	2.51±0.02	2.49
	Leu(C ^γ)	3.28±0.06	3.29

^aNomenclature given in Figure 4-6a. ^bNMR distances (with uncertainties at 95% confidence level) were determined using frequency selective REDOR as described in the text. ^cCourtesy of W. Davis (MIT). All distances agree to 0.02 Å or better with those determined in ref 64. ^dThe magnitude of intermolecular Val(C^{γ2})–Val(N) couplings (see Supporting Information) is non-negligible relative to the intramolecular Val(C^{γ2})–Val(N) coupling.

Representative FSR experiments in [U-¹³C,¹⁵N]N-acetyl-L-Val-L-Leu are presented in Figure 4-7 and all distances measured in the peptide are summarized in Table 4-2. The frequency selective experiments enable the measurement of internuclear distances, which provide indispensable information about the three-dimensional structure of the peptide, but are not easily accessible via non-selective methods. For example, Val(C^β) can be recoupled to Val(N) and Leu(N) in separate experiments. While the two-bond Val(C^β)–Val(N) dipolar coupling (Figure 4-7a), which would dominate the non-selective experiment, provides no useful structural data, the Val(C^β)–Leu(N) coupling (Figure 4-7b) provides valuable information about the backbone torsion angle ψ_1 . Since [U-¹³C,¹⁵N]VL was not diluted in the natural abundance compound, the distances reported are limited to the sidechain-to-backbone distances in the 2.5–3.5 Å range, for which the dipolar dephasing depends primarily on a single intramolecular coupling (see Supporting Information). (Accurate measurements of longer distances are demonstrated below for MLF.) Overall the experimental data are reproduced very well with the analytical two-

spin model (*c.f.* eq 1) and most measured distances agree closely (within $\sim 0.1 \text{ \AA}$) with those determined by X-ray crystallography (see Table 4-2).

The X-ray structure of N-formyl-L-Met-L-Leu-L-Phe-OMe,⁶⁵ which is closely related to the MLF peptide investigated in this work, is shown in Figure 4-8a. Figures 4-8b and 4-8c show one-dimensional ^{13}C and ^{15}N MAS spectra, respectively, of N-formyl-[U- ^{13}C , ^{15}N]L-Met-L-Leu-L-Phe. The ^{13}C and ^{15}N chemical shift assignments were reported previously in ref 72. The FSR experiments presented here were used to assign the Leu methyl resonances. ^{13}C - ^{15}N distance measurements were not performed for the downfield resonance (denoted $\text{C}^{\delta 1}$) due to spectral overlap with Leu(C^{γ}) (the Leu(C^{γ})-Leu(C^{δ}) J coupling is $\sim 30 \text{ Hz}$). The MLF-OMe X-ray structure⁶⁵ indicates that only one Leu(C^{δ}) is in close proximity to Leu(N). For the upfield resonance (denoted $\text{C}^{\delta 2}$) the dipolar coupling to Leu(N) was found to be relatively strong; assuming similar structures for MLF and MLF-OMe we have tentatively assigned the upfield resonance to the CH_3 closer to Leu(N) (*c.f.* Figure 4-8a).

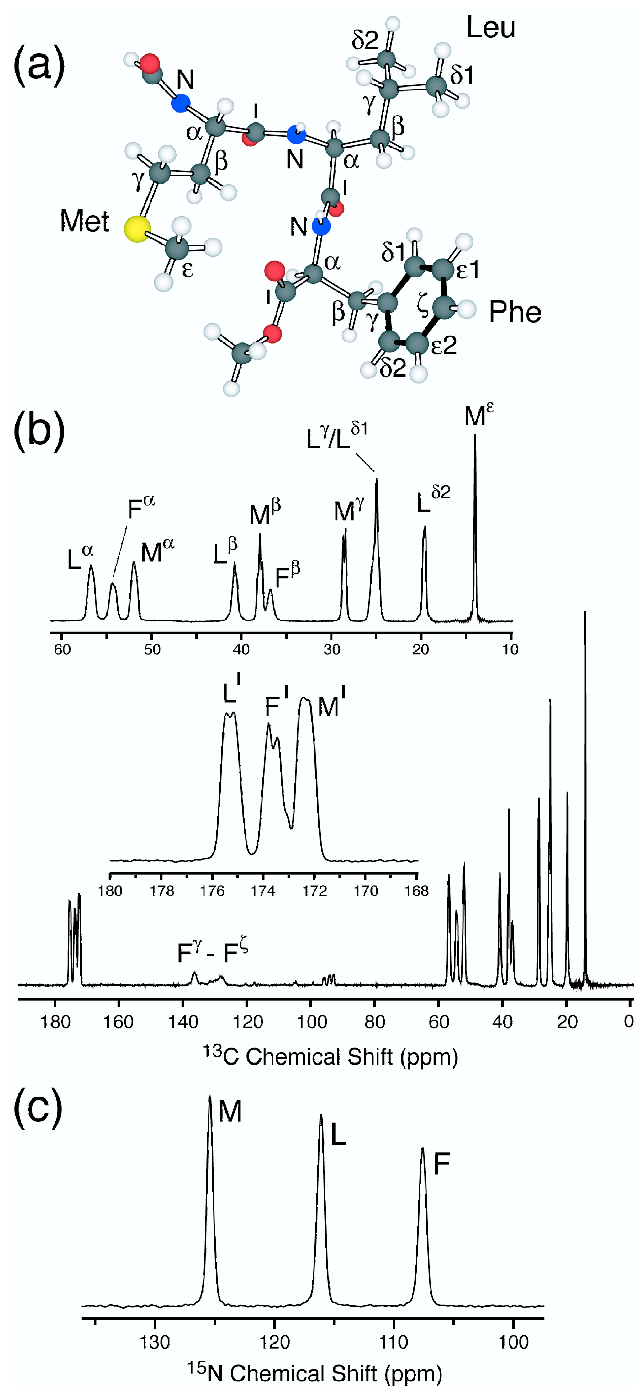


Figure 4-8. N-formyl-L-Met-L-Leu-L-Phe-OMe crystal structure and N-formyl-L-Met-L-Leu-L-Phe ^{13}C and ^{15}N MAS spectra.

(a) X-ray diffraction structure of N-formyl-L-Met-L-Leu-L-Phe-OMe.⁶⁵ ^{13}C (b) and ^{15}N (c) MAS spectra of N-formyl-[U- ^{13}C , ^{15}N]L-Met-L-Leu-L-Phe recorded at $\omega/2\pi = 10.0$ kHz. ^{13}C and ^{15}N chemical shift assignments have been reported previously,⁷² and the assignment of Leu($\text{C}^{\delta 1}$) and Leu($\text{C}^{\delta 2}$) resonances is based on FSR experiments presented in this work.

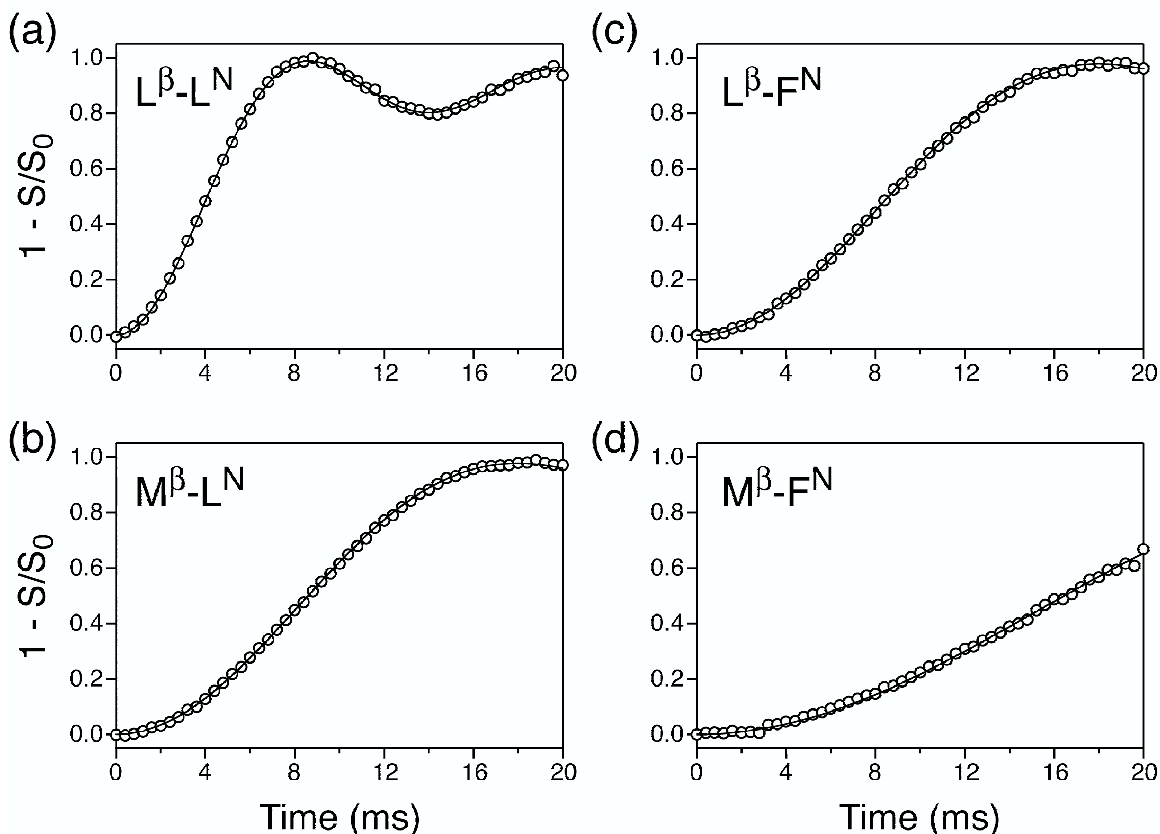


Figure 4-9. Representative internuclear distance measurements in N-formyl-[U-¹³C,¹⁵N]L-Met-L-Leu-L-Phe.

Experimental $\Delta S/S_0$ curves (\circ) and analytical simulations (—) are shown for the selective pairwise recoupling of (a) Leu(C^β)–Leu(N), (b) Met(C^β)–Leu(N), (c) Leu(C^β)–Phe(N), and (d) Met(C^β)–Phe(N). The experiments shown have been performed on [U-¹³C,¹⁵N]MLF undiluted in natural abundance material, but are not appreciably affected by intermolecular couplings (see Supporting Information). Experiments were performed at $\omega_r/2\pi = 10.0 \text{ kHz} \pm 5 \text{ Hz}$, and 32 scans were averaged for each time point. The ¹³C Gaussian pulse was 2.0 ms for experiments involving Met(C^β) and Leu(C^β), and 4.0 ms for Met(C^γ) and Leu($C^{\delta 2}$). The Met(C^β)/Leu(C^β) distance measurements were performed simultaneously. The ¹⁵N Gaussian pulse was 10.0 ms, applied on resonance with Met(N), Leu(N) or Phe(N). The summary of all distance measurements in N-formyl-[U-¹³C,¹⁵N]L-Met-L-Leu-L-Phe is given in Table 4-3.

Representative FSR experiments in N-formyl-[U-¹³C,¹⁵N]L-Met-L-Leu-L-Phe (undiluted in natural abundance MLF) are shown in Figure 4-9. For example, the Met(C^β)–Phe(N) dipolar coupling can be observed in the presence of the stronger Met(C^β)–Met(N) and Met(C^β)–Leu(N) couplings (Figure 4-9d); the measured

Met(C^β)–Phe(N) distance (short relative to that expected for an extended β-sheet type structure) identifies the turn in the MLF backbone (see Figure 4-10). Table 4-3 provides the summary of all internuclear distances determined in [U-¹³C,¹⁵N]MLF diluted to ~10% in the natural abundance peptide. (Figure 4-10 shows the X-ray structure of N-formyl-L-Met-L-Leu-L-Phe-OMe with several structure-constraining distances determined in MLF superimposed.) Accurate determinations of internuclear distances up to ~6 Å could be performed, and of the total 16 measured distances, 14 are in the 3–6 Å range and provide valuable structural constraints. Most measured distances in MLF are in relatively good agreement with the corresponding distances in the X-ray structure of MLF-OMe.⁶⁵ This indicates that while the three-dimensional structures of MLF and MLF-OMe are not identical, there appears to be a high degree of similarity between them.

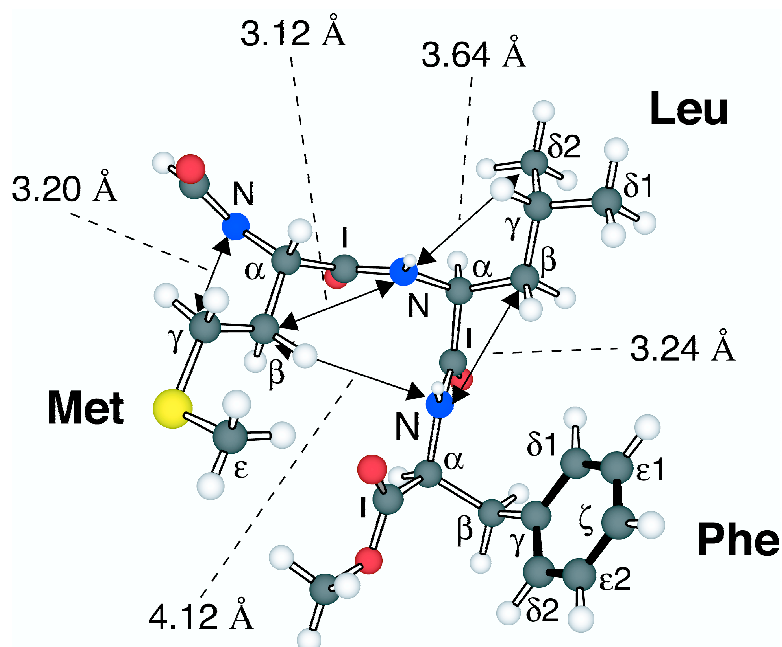


Figure 4-10. Representative distances measured in N-formyl-L-Met-L-Leu-L-Phe. X-ray structure of N-formyl-L-Met-L-Leu-L-Phe-OMe with several structure-constraining distances determined in 10% diluted N-formyl-[U-¹³C,¹⁵N]L-Met-L-Leu-L-Phe superimposed (*c.f.* Table 4-3).

Table 4-3. Internuclear Distances in N-formyl-L-Met-L-Leu-L-Phe

atoms ^a		r_{C-N} (Å)	
		NMR ^b	X-ray ^c
Met(N)	Met(C ^β)	2.52±0.02	2.50
	Met(C ^γ)	3.20±0.03	3.04
	Met(C ^ε)	5.4±0.3	5.71
	Leu(C ^β)	5.7±0.7	6.03
	Leu(C ^{δ2})	5.5±0.3	6.28
Leu(N)	Met(C ^β)	3.12±0.03	3.20
	Met(C ^γ)	4.17±0.10	4.56
	Met(C ^ε)	5.5±0.3	5.93
	Leu(C ^β)	2.46±0.02	2.50
	Leu(C ^{δ2})	3.64±0.09	3.63
Phe(N)	Met(C ^γ)	3.4±0.2	3.41
	Met(C ^β)	4.12±0.15	4.06
	Met(C ^γ)	4.8±0.2	5.43
	Met(C ^ε)	5.2±0.3	5.62
	Leu(C ^β)	3.24±0.12	3.12
	Leu(C ^{δ2})	5.4±0.3	5.38

N-formyl-[U-¹³C,¹⁵N]L-Met-L-Leu-L-Phe was diluted to ~ 10% in the natural abundance peptide to attenuate intermolecular ¹³C–¹⁵N contacts. ^aNomenclature given in Figure 4-8a. ^bNMR distances (with uncertainties at 95% confidence level) were determined using frequency selective REDOR as described in the text. ^cFor comparison with the NMR results, distances are given for the methyl ester analogue, N-formyl-L-Met-L-Leu-L-Phe-OMe (ref 65).

4.4.3 Effect of ¹H Decoupling on REDOR Experiments

Although insufficient proton decoupling during REDOR does not prohibit the measurement of relatively accurate ¹³C–¹⁵N dipolar couplings,⁷³ the quality of the experimental data does depend on the efficient attenuation of the dipolar contacts between the low- γ nuclei and protons. We find that for REDOR sequences of the type shown in Figure 4-1 (where all recoupling π pulses are applied to the non-observed spins) reference experiments can be used to compensate for insufficient proton decoupling during the delays between the pulses; however, insufficient decoupling during the π pulses can result in a significant scaling of the dipolar dephasing amplitude.

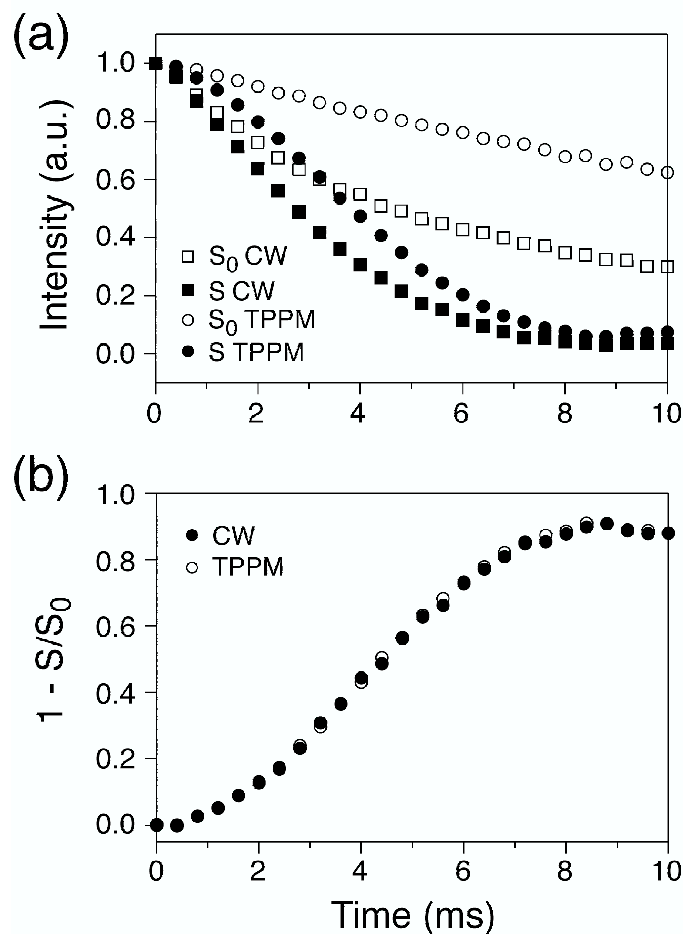


Figure 4-11. Effect of ^1H decoupling on REDOR experiments.

Comparison of ^1H decoupling schemes during the dipolar evolution period of FSR experiments in $[\text{U-}^{13}\text{C}, ^{15}\text{N}]$ asparagine. Results for the selective recoupling of $\text{C}^\beta\text{-N}'$ are shown. (Identical results were obtained for $\text{C}^\beta\text{-N}^{\delta 2}$.) Experiments were performed at $\omega_r/2\pi = 10.0 \text{ kHz} \pm 5 \text{ Hz}$, and 8 scans were averaged for each time point. ^{15}N π pulses were $18 \mu\text{s}$ and 1.0 ms Gaussian pulses were applied to C^β and N' . For all experiments ^1H decoupling was 125 kHz CW during ^{15}N π pulses and 120 kHz TPPM ($\phi = 15^\circ$, $\tau = 4.0 \mu\text{s}$) during the selective irradiation period. (a) Reference (S_0) (\square, \circ) and dipolar dephasing (S) (\blacksquare, \bullet) experiments recorded in the presence of 120 kHz CW (\square, \blacksquare) and TPPM (\circ, \bullet) ^1H decoupling during the free-evolution periods corresponding to delays between ^{15}N π pulses. (b) $\Delta S/S_0$ curves calculated using data in (a) for CW (\bullet) and TPPM (\circ) ^1H decoupling.

Figure 4-11 shows a comparison of ^1H decoupling schemes during the dipolar evolution period of FSR experiments in $[\text{U-}^{13}\text{C}, ^{15}\text{N}]$ asparagine. The ^{15}N rf field was $\sim 28 \text{ kHz}$ and ^1H decoupling field during the ^{15}N π pulses was 125 kHz CW in all experiments,

ensuring a sufficiently high $\omega_{rf}(^1\text{H}) : \omega_{rf}(^{15}\text{N})$ mismatch.⁷⁴⁻⁷⁶ During the delays between the pulses 120 kHz continuous wave (CW) or two pulse phase modulation (TPPM)⁶¹ decoupling was used, and we observe a significant improvement in the ^{13}C spin-echo intensity with TPPM decoupling (Figure 4-11a). This effect is of practical importance for systems yielding spectra with low signal-to-noise ratios. However, inefficient ^1H decoupling during the free-evolution periods is effectively compensated by the $\Delta S/S_0$ analysis, as nearly identical $\Delta S/S_0$ curves are obtained for both decoupling schemes (Figure 4-11b).

The effects of insufficient ^1H decoupling during the ^{15}N rf pulses cannot be compensated with reference experiments. In Figure 4-12 we investigate these effects in spin systems with different ^{15}N - ^1H dipolar couplings by acquiring a series of dipolar dephasing curves in the presence of CW decoupling held constant at ~ 85 kHz and ^{15}N rf fields of ~ 25 , 35 and 50 kHz. For $[1\text{-}^{13}\text{C}, ^{15}\text{N}]\text{glycine}$ (Figures 4-12a and 4-12b), where the strong ^{15}N - ^1H interactions are attenuated by the rapid hopping of the NH_3^+ group under the experimental conditions employed here,⁷⁷ the effects of ^{15}N - ^1H recoupling due to the insufficient mismatch of ^1H and ^{15}N rf fields⁷⁴⁻⁷⁶ appear to be minimal (Figure 4-12a) and the $\Delta S/S_0$ curves recorded for different ^{15}N fields are nearly identical (Figure 4-12b). The situation is quite different in the case of the relatively rigid amide group in $[\text{acetyl-1,2-}^{13}\text{C}, ^{15}\text{N}]\text{N-acetylvaline}$, for which the ^{15}N - ^1H coupling is strong (~ 10 kHz). Here, both reference and dipolar dephasing curves for the (acetyl- CH_3)- N' coupling (Figure 4-12c) show significant deviations from ideal behavior for $\omega_{rf}(^1\text{H}) : \omega_{rf}(^{15}\text{N})$ less than 3:1.⁷⁴⁻⁷⁶ The resulting $\Delta S/S_0$ curves (Figure 4-12d) display a significant amplitude scaling ($\sim 15\%$) as $\omega_{rf}(^1\text{H}) : \omega_{rf}(^{15}\text{N})$ changes from ~ 3.5 to 1.5. However, regardless of the

rf field mismatch, the $\Delta S/S_0$ curves in NAV could be simulated (not shown) with approximately the same dipolar coupling constant ($b_{CN} = 211 \pm 2$ Hz), but different amplitude scaling factors.

As shown by others⁷³ and suggested by the experiments presented here, in many cases reasonably accurate distances can be obtained using REDOR even in the presence of relatively low power CW ^1H decoupling. However, significant scaling of the dipolar dephasing amplitude may potentially become problematic for weak coupling measurements, where $\Delta S/S_0$ buildup is slow. The efficient attenuation of proton couplings significantly improves the ^{13}C spin-echo intensity and avoids the scaling of the dipolar dephasing amplitude in spin systems with strong ^{15}N - ^1H couplings. Efficient proton decoupling does not necessarily imply the use of very high power levels. When only moderate ^1H rf fields (e.g., ~ 80 kHz) are available due to probe limitations, TPPM decoupling during delays between ^{15}N pulses (see Figure 4-1) effectively restores the spin-echo intensity and the use of slightly longer ^{15}N π pulses provides a sufficiently high $\omega_{rf}(^1\text{H}) : \omega_{rf}(^{15}\text{N})$ ratio required to minimize the ^{15}N - ^1H interactions.

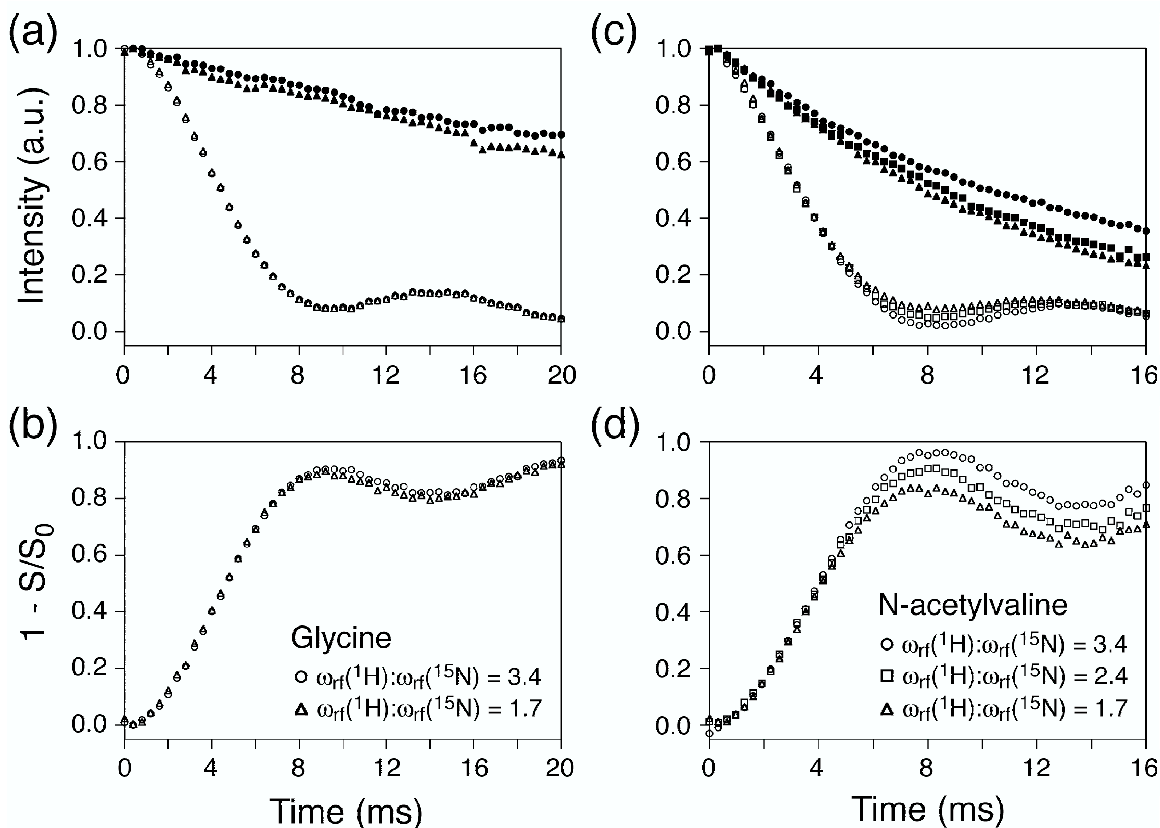


Figure 4-12. Effect of ^1H decoupling on REDOR experiments.

Effect of ^1H decoupling during periods corresponding to ^{15}N pulses in spin systems with ^{15}N - ^1H dipolar couplings of different magnitude. Dipolar recoupling data are presented for $[1\text{-}^{13}\text{C}, ^{15}\text{N}]$ glycine (a)–(b), for which the ^{15}N - ^1H couplings are effectively attenuated by rapid hopping of the NH_3^+ group under the experimental conditions employed in this work,⁷⁷ and for $[\text{acetyl-}1,2\text{-}^{13}\text{C}, ^{15}\text{N}]$ N-acetylvaline (NAV) (c)–(d), where the relatively rigid amide group displays a strong (~ 10 kHz) ^{15}N - ^1H dipolar coupling. Experiments were performed at $\omega/2\pi = 12.5$ kHz \pm 5 Hz, and 16 scans were averaged for each time point. In (a) and (c) we show S_0 (filled symbols) and S (hollow symbols) curves for the ~ 200 Hz ^{13}C - ^{15}N dipolar couplings in both compounds ($\text{C}'\text{-N}'$ in glycine and (acetyl- CH_3)- N' in NAV). All S_0 experiments were acquired in the presence of ^{15}N π pulses. ^1H decoupling was fixed at ~ 85 kHz CW for all experiments and the ^{15}N π pulse lengths were 20 μs (\bullet, \circ), 14 μs (\blacksquare, \square) and 10 μs ($\blacktriangle, \triangle$), corresponding to ^{15}N rf fields of 25 kHz ($\omega_{\text{rf}}(^1\text{H}):\omega_{\text{rf}}(^{15}\text{N}) \approx 3.4$), 35.7 kHz ($\omega_{\text{rf}}(^1\text{H}):\omega_{\text{rf}}(^{15}\text{N}) \approx 2.4$), and 50 kHz ($\omega_{\text{rf}}(^1\text{H}):\omega_{\text{rf}}(^{15}\text{N}) \approx 1.7$), respectively. The ^{13}C spin-echo reference curves acquired with no ^{15}N irradiation (data not shown) were identical within experimental error to the S_0 experiments acquired in the presence of 20 μs ^{15}N π pulses. $\Delta S/S_0$ curves calculated using S_0 and S experiments in (a) and (c) are shown for glycine (b) and NAV (d) for ^{15}N π pulses of 20 μs (\circ), 14 μs (\square) and 10 μs (\triangle). In (a) and (b) the glycine data for 14 μs ^{15}N π pulses have been omitted for clarity.

4.4.4 Effect of ^{15}N CSA on REDOR Experiments

In Figure 4-13 we present experimental data and numerical simulations showing the effect of the chemical shielding anisotropy (CSA) of the irradiated spins (^{15}N in our case) on REDOR dipolar dephasing curves acquired with several commonly used compensated π pulse phasing schemes (xy -4, xy -8 and xy -16).³³ [1 - ^{13}C , ^{15}N]Glycine, with a negligible ^{15}N CSA ($\delta \approx 5$ ppm, $\eta = 0$),⁷⁷ is used as a reference, and as expected $\Delta S/S_0$ curves recorded with xy -4, xy -8 and xy -16 (Figure 4-13a) are nearly identical. The situation is quite different for a larger ^{15}N CSA ($\delta = 106$ ppm, $\eta = 0.27$)⁷⁸ in [acetyl-1,2- ^{13}C , ^{15}N]NAV, where significant effects are observed in the presence of xy -16 phase cycling relative to xy -4 and xy -8 (Figure 4-13b). The experimental observations are compared to numerical simulations (performed with the SIMPSON simulation software⁷⁹) (Figure 4-13c). For the ‘two-spin’ ((acetyl- CH_3)– N') system (see Figure 4-13 caption for details) the $\Delta S/S_0$ curves simulated for the xy -4 and xy -8 schemes are nearly identical and closely follow the result for finite pulse REDOR in the absence of ^{15}N CSA. However, an amplitude scaling is observed in the xy -16 simulation, which reproduces the experimental result shown in Figure 4-13b. The experiments and simulations presented here suggest that xy -4 and xy -8 are equally well-compensated for ^{15}N CSA effects. However, additional simulations (not shown) indicate that for increasing CSA the dephasing curves for all phasing schemes can display some scaling of amplitude and frequency of the oscillation; in general, xy -4 simulations appear to most closely approach the ideal dipolar dephasing curve.

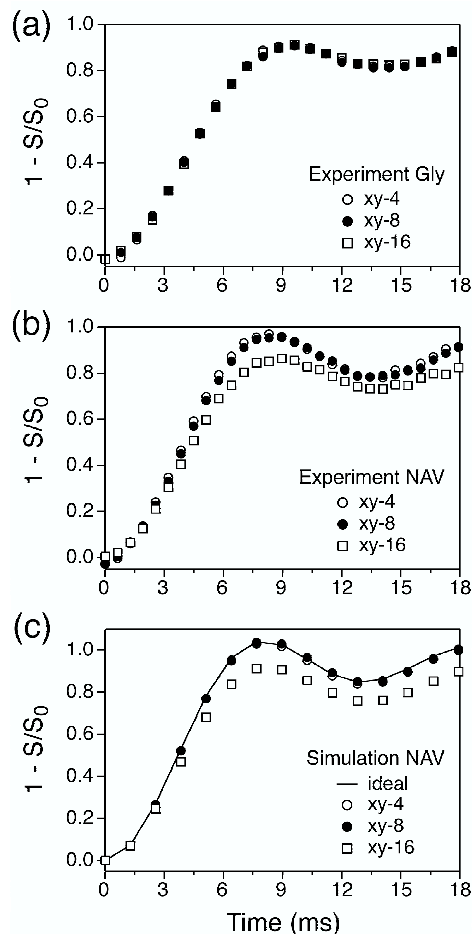


Figure 4-13. Effect of ^{15}N chemical shielding anisotropy on ^{13}C -observe REDOR experiments.

Three common ^{15}N π pulse phase cycling schemes³³ (xy-4 (○), xy-8 (●), and xy-16 (□)), designed to compensate for pulse errors and resonance offsets, are compared in (a) and (b). We show REDOR experiments for C'–N' coupling in [$1\text{-}^{13}\text{C}, ^{15}\text{N}$]glycine (^{15}N CSA: $\delta \approx 5$ ppm, $\eta = 0$)⁷⁷ (a) and (acetyl- CH_3)–N' coupling in [acetyl-1,2- $^{13}\text{C}, ^{15}\text{N}$]N-acetylvaline (^{15}N CSA: $\delta = 106$ ppm, $\eta = 0.27$)⁷⁸ (b). Spectra were recorded at $\omega_r/2\pi = 12.5$ kHz \pm 5 Hz, and 4 experiments (16 scans per experiment) were averaged for each time point. (c) Simulated REDOR $\Delta S/S_0$ curves assuming the (acetyl- CH_3)–N' dipolar coupling constant ($b_{CN} = 220$ Hz) obtained from the NAV X-ray structure⁶⁴ and finite ^{15}N π pulses for: no ^{15}N CSA ($\delta = \eta = 0$) (—), and ^{15}N CSA parameters of NAV⁷⁸ at $B_0 = 11.7$ T ($\delta = 5.37$ kHz, $\eta = 0.27$) with xy-4 (○), xy-8 (●), and xy-16 (□) phase-alternation of ^{15}N π pulses. The spinning frequency of 12.5 kHz was used in the simulations and the orientation of the amide ^{15}N CSA tensor in the molecular frame given in ref 80 was assumed (σ_{22} perpendicular to the peptide plane and σ_{33} in the peptide plane with $\sigma_{33}/\text{N-H}$ projection angle of 20°). With these assumptions the approximate orientation of the (acetyl- CH_3)–N' dipole vector in the ^{15}N CSA principal axis system is given by the Euler angles $\Omega = \{0, -64^\circ, -180^\circ\}$. All numerical simulations in (c) were performed using the SIMPSON simulation software.⁷⁹

The influence of ^{15}N CSA on REDOR dipolar dephasing with several simple phasing schemes (xx -4, $x\bar{x}$ -4 and xy -4) has been discussed previously using Floquet theory.⁸¹ According to average Hamiltonian theory,^{66,67} for ^{13}C -observe REDOR with ^{15}N π pulses of finite length phased according to xy -4 or extensions thereof (see Figure 4-1), the ^{15}N CSA is not expected to contribute to the spin dynamics to first-order. In the rf interaction frame the ^{15}N pulses transform only the N_z operator and the first-order effective Hamiltonian for the ^{15}N CSA is analogous to that calculated for the heteronuclear dipolar coupling (*c.f.* eqs 2 and 3):

$$H_{\text{CSA}}^{(1)} \propto \text{Im}\{\omega_{\text{CSA}}^{(1)}(\Omega_{PR})\}N_z, \quad (21)$$

where $\omega_{\text{CSA}}^{(1)}$ describes the transformation of the ^{15}N CSA tensor from its principal axis system to the rotor-fixed frame.⁶⁸ Since the experiments are designed to follow the time evolution of ^{13}C coherences, and the first-order effective ^{13}C - ^{15}N dipolar coupling and ^{15}N CSA Hamiltonians commute, to this order of approximation the ^{15}N CSA has no effect on the dipolar dephasing.³⁰ Therefore, the deviations from ideal behavior observed for the different xy -type phasing schemes with increasing ^{15}N CSA must be due to higher order terms in the effective Hamiltonian expansion.^{66,67}

4.5 Conclusions

We have described a magic-angle spinning NMR experiment, which enables accurate internuclear ^{13}C - ^{15}N distance measurements in uniformly- ^{13}C , ^{15}N -labeled solids. In multispin systems, the extraction of weak ^{13}C - ^{15}N dipolar couplings using non-selective recoupling experiments is complicated by multiple ^{13}C - ^{15}N and ^{13}C - ^{13}C spin-

spin interactions. The frequency selective REDOR technique presented here is based on a simple principle: a ^{13}C spin-echo is generated in a frequency selective fashion by a pair of selective π pulses applied to a ^{13}C - ^{15}N spin pair in the center of the dipolar evolution period. The intensity of the ^{13}C spin-echo is modulated only by the dipolar coupling to the selected ^{15}N ; the remaining ^{13}C - ^{15}N dipolar couplings and ^{13}C - ^{13}C scalar couplings involving the selected ^{13}C are refocused. With efficient proton decoupling and the use of well-compensated π pulse phasing schemes, the spin dynamics can be described by the analytical expression for dipolar dephasing in an isolated heteronuclear spin pair under conventional REDOR, and the extraction of the ^{13}C - ^{15}N dipolar coupling of interest is straightforward. We have demonstrated the utility of the experiment for accurate internuclear distance measurements in several U- ^{13}C , ^{15}N -labeled systems; in the model tripeptide, N-formyl-L-Met-L-Leu-L-Phe, a total of 16 ^{13}C - ^{15}N intramolecular distances in the 2.5–6 Å range were determined with ~ 0.1 – 0.3 Å precision.

The selective recoupling in FSR relies on ^{13}C and ^{15}N chemical shift resolution, and the technique is expected to greatly benefit from high static magnetic fields and high MAS frequencies. However, even under optimal conditions the measurements of multiple ^{13}C - ^{15}N distances involving most backbone ^{15}N in U- ^{13}C , ^{15}N -labeled biological macromolecules, where spectral overlap can be quite severe, are expected to be challenging. Nevertheless, some potentially promising applications of the technique to systems of biological interest include ^{13}C - ^{15}N distance measurements in the active site of multiply labeled proteins and structural investigations of peptide aggregates and molecules present at interfaces (e.g., U- ^{13}C , ^{15}N -labeled peptide bound to a protein).

Acknowledgments

The authors thank Chad Rienstra, Bernd Reif, Morten Hohwy and David Ruben for stimulating discussions, and William Davis for his assistance in obtaining the X-ray structure of N-acetyl-L-Val-L-Leu. C.P.J. thanks the NSF for a Predoctoral Fellowship, and B.A.T. thanks the American Cancer Society for a Postdoctoral Fellowship (PF-99-260-01-GMC). This research was supported by NIH grants GM-23289, GM-36810, and RR-00995.

Supporting Information

Table 4-S1. Selected Intermolecular C–N Distances up to 6 Å in N-acetyl-L-Val-L-Leu

atoms ^a	$r_{\text{C-N}} (\text{Å})^b$
Val(C ^β)–Val(N)	5.31
Val(C ^{γ1})–Val(N)	5.13
Val(C ^{γ2})–Val(N)	4.87
Val(C ^{γ2})–Val(N)	5.46
Leu(C ^β)–Leu(N)	5.16
Leu(C ^γ)–Leu(N)	5.28
Leu(C ^γ)–Leu(N)	5.77

^aNomenclature given in Figure 4-6a. Tabulated distances (up to 6 Å) are limited to those corresponding to the intramolecular sidechain-to-backbone C–N distances measured in this work. ^bRef 64.

Table 4-S2. Selected Intermolecular C–N Distances up to 6 Å in N-formyl-L-Met-L-Leu-L-Phe-OMe

atoms ^a	$r_{\text{C-N}} (\text{Å})^b$
Met(C ^β)–Met(N)	5.09
Met(C ^γ)–Met(N)	4.36
Met(C ^β)–Leu(N)	5.44
Leu(C ^β)–Leu(N)	5.38
Leu(C ^{δ2})–Leu(N)	4.05
Leu(C ^{δ2})–Leu(N)	4.79
Leu(C ^{δ2})–Leu(N)	5.74
Met(C ^β)–Phe(N)	5.13
Leu(C ^β)–Phe(N)	5.49

^aNomenclature given in Figure 4-8a. Tabulated distances (up to 6 Å) are limited to those corresponding to the intramolecular sidechain-to-backbone C–N distances measured in this work. ^bRef 65.

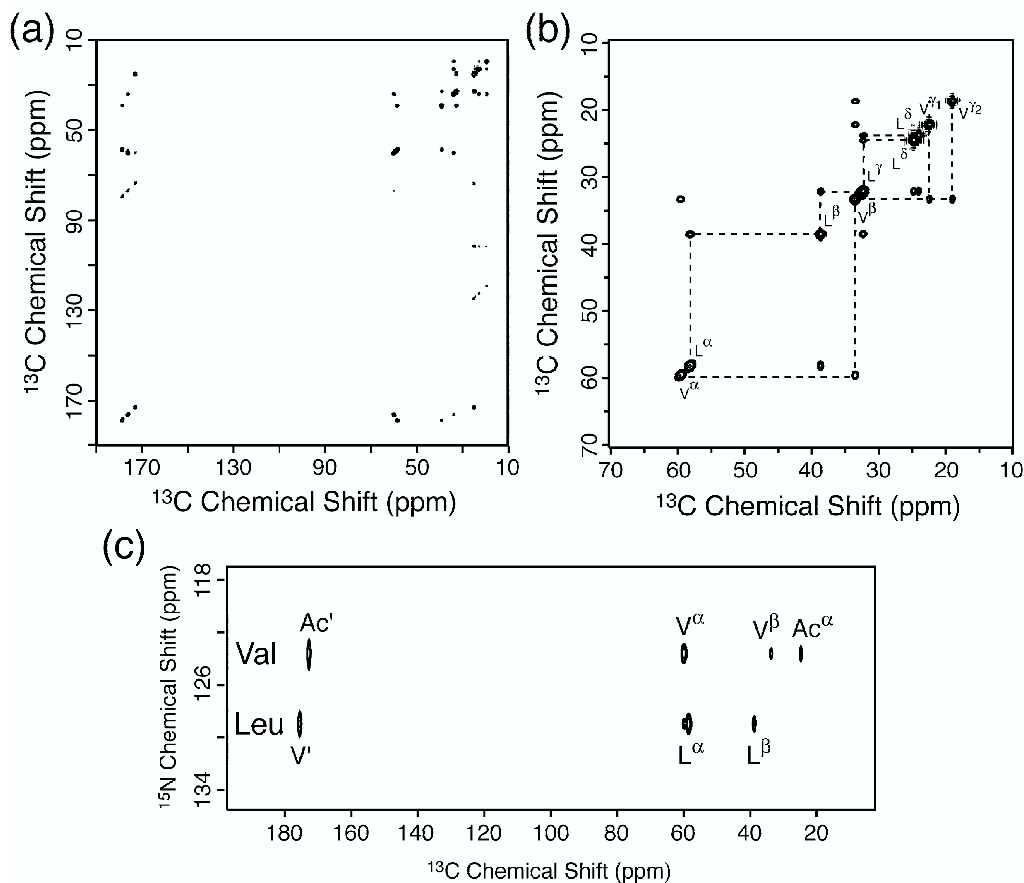


Figure 4-S1. Resonance assignments for [U-¹³C, ¹⁵N]N-acetyl-L-Val-L-Leu.

¹³C-¹³C (a)-(b) and ¹³C-¹⁵N (c) 2D chemical shift correlation spectra for [U-¹³C, ¹⁵N]N-acetyl-L-Val-L-Leu. Essential ¹³C and ¹⁵N resonance assignments are indicated. For the ¹³C-¹³C correlation experiment we show the full spectrum (a) and close-up of the aliphatic region (b). The ¹³C-¹³C correlation experiment was performed at $\omega_r/2\pi = 12.5$ kHz with RFDR⁵² as the mixing sequence ($\tau_{mix} = 1.28$ ms). The ¹³C-¹⁵N correlation experiment was performed at $\omega_r/2\pi = 8.3$ kHz, where the ¹⁵N-¹³C polarization transfer was accomplished via ramped CP. All experiments were recorded at 500 MHz ¹H frequency.

References

- (1) R. G. Griffin, "Dipolar recoupling in MAS spectra of biological solids," *Nature Struct. Biol.* **5**, 508-512 (1998).
- (2) L. M. McDowell and J. Schaefer, "High resolution NMR of biological solids," *Curr. Opin. Struct. Biol.* **6**, 624-629 (1996).
- (3) S. J. Opella, "NMR and membrane proteins," *Nature Struct. Biol.* **4**, 845-848 (1997).
- (4) D. E. McRee, "Practical Protein Crystallography," Academic Press, San Diego (1993).
- (5) W. Saenger, "Principles of Nucleic Acid Structure," Springer-Verlag, New York (1984).
- (6) K. Wüthrich, "NMR of Proteins and Nucleic Acids," Wiley, New York (1986).
- (7) F. Cruzet, A. McDermott, R. Gebhard, K. van der Hoef, M. B. Spijker-Assink, J. Herzfeld, J. Lugtenburg, M. H. Levitt and R. G. Griffin, "Determination of membrane protein structure by rotational resonance NMR: Bacteriorhodopsin," *Science* **251**, 783-786 (1991).
- (8) L. K. Thompson, A. E. McDermott, J. Raap, C. M. van der Wielen, J. Lugtenburg, J. Herzfeld and R. G. Griffin, "Rotational resonance NMR study of the active site structure in bacteriorhodopsin: Conformation of the Schiff base linkage," *Biochemistry* **31**, 7931-7938 (1992).
- (9) K. V. Lakshmi, M. Auger, J. Raap, J. Lugtenburg, R. G. Griffin and J. Herzfeld, "Internuclear distance measurement in a reaction intermediate: solid-state ^{13}C NMR

- rotational resonance determination of the Schiff-base configuration in the M-photointermediate of bacteriorhodopsin," *J. Am. Chem. Soc.* **115**, 8515-8516 (1993).
- (10) X. Feng, P. J. E. Verdegem, Y. K. Lee, D. Sandström, M. Edén, P. Bovee-Geurts, W. J. de Grip, J. Lugtenburg, H. J. M. de Groot and M. H. Levitt, "Direct determination of a molecular torsional angle in the membrane protein rhodopsin by solid-state NMR," *J. Am. Chem. Soc.* **119**, 6853-6857 (1997).
- (11) J. M. Griffiths, A. E. Bennett, M. Engelhard, F. Siebert, J. Raap, J. Lugtenburg, J. Herzfeld and R. G. Griffin, "Structural investigation of the active site of bacteriorhodopsin: Geometric constraints on the roles of Asp-85 and Asp-212 in the proton pumping mechanism from solid-state NMR," *Biochemistry* **39**, 362-371 (2000).
- (12) A. E. McDermott, F. Creuzet, R. G. Griffin, L. E. Zawadzke, Q. Z. Ye and C. T. Walsh, "Rotational resonance determination of the structure of an enzyme-inhibitor complex: phosphorylation of an (amino alkyl) phosphonate inhibitor of D-alanyl-D-alanine ligase by ATP," *Biochemistry* **29**, 5767 (1990).
- (13) L. M. McDowell, A. Schmidt, E. R. Cohen, D. R. Studelska and J. Schaefer, "Structural constraints on the ternary complex of 5-enolpyruvylshikimate-3-phosphate synthase from rotational-echo double-resonance NMR," *J. Mol. Biol.* **256**, 160-171 (1996).
- (14) Y. Li, R. J. Appleyard, W. A. Shuttleworth and J. N. S. Evans, "Time-resolved solid-state REDOR NMR measurements on 5-enolpyruvylshikimate-3-phosphate synthase," *J. Am. Chem. Soc.* **116**, 10799-10800 (1994).

- (15) D. P. Weliky, A. E. Bennett, A. Zvi, J. Anglister, P. J. Steinbach and R. Tycko, "Solid-state NMR evidence for an antibody-dependent conformation of the V3 loop of HIV-1 gp120," *Nature Struct. Biol.* **6**, 141-145 (1999).
- (16) R. G. S. Spencer, K. J. Halverson, M. Auger, A. E. McDermott, R. G. Griffin and P. T. Lansbury, "An unusual peptide conformation may precipitate amyloid formation in Alzheimer's disease: Application of solid-state NMR to the determination of protein secondary structure," *Biochemistry* **30**, 10382-10387 (1991).
- (17) J. M. Griffiths, T. T. Ashburn, M. Auger, P. R. Costa, R. G. Griffin and P. T. Lansbury, "Rotational resonance solid-state NMR elucidates a structural model of pancreatic amyloid," *J. Am. Chem. Soc.* **117**, 3539-3546 (1995).
- (18) P. T. Lansbury, P. R. Costa, J. M. Griffiths, E. J. Simon, M. Auger, K. J. Halverson, D. A. Kocisko, Z. S. Hendsch, T. T. Ashburn, R. G. S. Spencer, B. Tidor and R. G. Griffin, "Structural model for the β -amyloid fibril based on interstrand alignment of an antiparallel-sheet comprising a C-terminal peptide," *Nature Struct. Biol.* **2**, 990-998 (1995).
- (19) T. L. S. Benzinger, D. M. Gregory, T. S. Burkoth, H. Miller-Auer, D. G. Lynn, R. E. Botto and S. C. Meredith, "Propagating structure of Alzheimer's β -amyloid₍₁₀₋₃₅₎ is parallel β -sheet with residues in exact register," *Proc. Natl. Acad. Sci. USA* **95**, 13407-13412 (1998).
- (20) D. M. Gregory, T. L. S. Benzinger, T. S. Burkoth, H. Miller-Auer, D. G. Lynn, S. C. Meredith and R. E. Botto, "Dipolar recoupling NMR of biomolecular self-assemblies: determining inter- and intrastrand distances in fibrilized Alzheimer's β -amyloid peptide," *Solid State Nucl. Magn. Reson.* **13**, 149-166 (1998).

- (21) T. L. S. Benzinger, D. M. Gregory, T. S. Burkoth, H. Miller-Auer, D. G. Lynn, R. E. Botto and S. C. Meredith, "Two-dimensional structure of β -amyloid(10-35) fibrils," *Biochemistry* **39**, 3491-3499 (2000).
- (22) R. Tycko, O. Antzutkin, J. Balbach, Y. Ishii, F. Blanco and J. Reed. in *41st Experimental Nuclear Magnetic Resonance Conference* (Asilomar, CA, 2000).
- (23) E. R. Andrew, A. Bradbury and R. G. Eades, "Nuclear magnetic resonance spectra from a crystal rotated at high speed," *Nature* **182**, 1659 (1958).
- (24) I. J. Lowe, "Free induction decay of rotating solids," *Phys. Rev. Lett.* **2**, 285 (1959).
- (25) A. E. Bennett, R. G. Griffin and S. Vega. in *Solid State NMR IV: Methods and Applications of Solid-State NMR* (ed. B. Blumich) 1-77 (Springer-Verlag, Berlin, 1994).
- (26) S. Dusold and A. Sebald, "Dipolar recoupling under magic-angle spinning conditions," *Annu. Rep. Nucl. Magn. Reson. Spectr.* **41**, 185-264 (2000).
- (27) A. Pines, M. G. Gibby and J. S. Waugh, "Proton-enhanced NMR of dilute spins in solids," *J. Chem. Phys.* **59**, 569-590 (1973).
- (28) T. G. Oas, R. G. Griffin and M. H. Levitt, "Rotary resonance recoupling of dipolar interactions in solid-state nuclear magnetic resonance spectroscopy," *J. Chem. Phys.* **89**, 692-695 (1988).
- (29) M. H. Levitt, T. G. Oas and R. G. Griffin, "Rotary resonance recoupling in heteronuclear spin pair systems," *Isr. J. Chem.* **28**, 271-282 (1988).
- (30) P. R. Costa, J. D. Gross, M. Hong and R. G. Griffin, "Solid-state NMR measurement of ψ in peptides: a NCCN 2Q-heteronuclear local field experiment," *Chem. Phys. Lett.* **280**, 95-103 (1997).

- (31) T. Gullion and J. Schaefer, "Rotational-echo double-resonance NMR," *J. Magn. Reson.* **81**, 196-200 (1989).
- (32) T. Gullion and J. Schaefer, "Detection of weak heteronuclear dipolar coupling by rotational-echo double-resonance nuclear magnetic resonance," *Adv. Magn. Reson.* **13**, 57-83 (1989).
- (33) T. Gullion, D. B. Baker and M. S. Conradi, "New, compensated Carr-Purcell sequences," *J. Magn. Reson.* **89**, 479-484 (1990).
- (34) T. Gullion and J. Schaefer, "Elimination of resonance offset effects in rotational-echo, double-resonance NMR," *J. Magn. Reson.* **92**, 439-442 (1991).
- (35) C. P. Jaroniec, B. A. Tounge, C. M. Rienstra, J. Herzfeld and R. G. Griffin, "Recoupling of heteronuclear dipolar interactions with rotational-echo double-resonance at high magic-angle spinning frequencies," *J. Magn. Reson.* **146**, 132-139 (2000).
- (36) C. A. Fyfe and A. R. Lewis, "Investigation of the viability of solid-state NMR distance determinations in multiple spin systems of unknown structure," *J. Phys. Chem. B* **104**, 48-55 (2000).
- (37) J. M. Goetz and J. Schaefer, "REDOR dephasing by multiple spins in the presence of molecular motion," *J. Magn. Reson.* **127**, 147-154 (1997).
- (38) K. Nishimura, A. Naito, S. Tuzi and H. Saito, "Analysis of dipolar dephasing pattern in I-S_n multispin system for obtaining the information of molecular packing and its application to crystalline N-acetyl-Pro-Gly-Phe by REDOR solid state NMR," *J. Phys. Chem. B* **103**, 8398-8404 (1999).

- (39) C. A. Fyfe, A. R. Lewis, J. M. Chézeau and H. Grondey, " $^{19}\text{F}/^{29}\text{Si}$ distance determinations in fluoride-containing octadecasil from solid-state NMR measurements," *J. Am. Chem. Soc.* **119**, 12210-12222 (1997).
- (40) E. R. H. van Eck and W. S. Veeman, "A solid-state NMR 3D heteronuclear dipolar-correlation experiment. The correlation of $\delta(^{13}\text{C})$, $\delta(^{15}\text{N})$, and $D_{(\text{C-N})}$," *J. Magn. Reson. A* **109**, 250-252 (1994).
- (41) C. A. Michal and L. W. Jelinski, "REDOR 3D: Heteronuclear distance measurements in uniformly labeled and natural abundance solids," *J. Am. Chem. Soc.* **119**, 9059-9060 (1997).
- (42) A. W. Hing, S. Vega and J. Schaefer, "Transferred-echo double-resonance NMR," *J. Magn. Reson.* **96**, 205-209 (1992).
- (43) X. Feng, M. Eden, A. Brinkmann, H. Luthman, L. Eriksson, A. Gräslund, O. N. Antzutkin and M. H. Levitt, "Direct determination of a peptide torsional angle ψ by double-quantum solid-state NMR," *J. Am. Chem. Soc.* **119**, 12006-12007 (1997).
- (44) X. Feng, Y. K. Lee, D. Sandström, M. Eden, H. Maisel, A. Sebald and M. H. Levitt, "Direct determination of a molecular torsional angle by solid-state NMR," *Chem. Phys. Lett.* **257**, 314-320 (1996).
- (45) M. Hong, J. D. Gross and R. G. Griffin, "Site-resolved determination of peptide torsion angle ϕ from the relative orientations of backbone N-H and C-H bonds by solid-state NMR," *J. Phys. Chem. B* **101**, 5869-5874 (1997).
- (46) M. Hohwy, C. P. Jaroniec, B. Reif, C. M. Rienstra and R. G. Griffin, "Local structure and relaxation in solid-state NMR: Accurate measurement of amide N-H bond lengths and H-N-H bond angles," *J. Am. Chem. Soc.* **122**, 3218-3219 (2000).

- (47) B. Reif, M. Hohwy, C. P. Jaroniec, C. M. Rienstra and R. G. Griffin, "NH-NH vector correlation in peptides by solid state NMR," *J. Magn. Reson.* **145**, 132-141 (2000).
- (48) T. Gullion and C. H. Pennington, " θ -REDOR: an MAS NMR method to simplify multiple coupled heteronuclear spin systems," *Chem. Phys. Lett.* **290**, 88-93 (1998).
- (49) A. E. Bennett, L. R. Becerra and R. G. Griffin, "Frequency-selective heteronuclear recoupling in rotating solids," *J. Chem. Phys.* **100**, 812-814 (1994).
- (50) A. E. Bennett, C. M. Rienstra, P. T. Lansbury and R. G. Griffin, "Frequency-selective heteronuclear dephasing by dipole couplings in spinning and static solids," *J. Chem. Phys.* **105**, 10289-10299 (1996).
- (51) T. Gullion and S. Vega, "A simple magic angle spinning NMR experiment for the dephasing of rotational echoes of dipolar coupled homonuclear spin pairs," *Chem. Phys. Lett.* **194**, 423-428 (1992).
- (52) A. E. Bennett, J. H. Ok, R. G. Griffin and S. Vega, "Chemical shift correlation spectroscopy in rotating solids: Radio frequency driven dipolar recoupling and longitudinal exchange," *J. Chem. Phys.* **96**, 8624-8627 (1992).
- (53) J. Cavanagh, W. J. Fairbrother, A. G. Palmer and N. J. Skelton, "Protein NMR Spectroscopy: Principles and Practice," Academic Press, San Diego (1996).
- (54) C. P. Jaroniec, B. A. Tounge, C. M. Rienstra, J. Herzfeld and R. G. Griffin, "Measurement of ^{13}C - ^{15}N distances in uniformly ^{13}C labeled biomolecules: J-decoupled REDOR," *J. Am. Chem. Soc.* **121**, 10237-10238 (1999).
- (55) R. R. Ernst, G. Bodenhausen and A. Wokaun, "Principles of Nuclear Magnetic Resonance in One and Two Dimensions," Clarendon Press, Oxford (1991).

- (56) E. L. Hahn, "Spin Echoes," *Phys. Rev.* **80**, 580 (1950).
- (57) S. K. Straus, T. Bremi and R. R. Ernst, "Resolution enhancement by homonuclear J decoupling in solid-state MAS NMR," *Chem. Phys. Lett.* **262**, 709-715 (1996).
- (58) R. Brüschweiler, C. Griesinger, O. W. Sørensen and R. R. Ernst, "Combined use of hard and soft pulses for ω_1 decoupling in two-dimensional NMR spectroscopy," *J. Magn. Reson.* **78**, 178-185 (1988).
- (59) A. Bax, "Two-Dimensional Nuclear Magnetic Resonance in Liquids," Delft University Press, Dordrecht (1982).
- (60) G. Metz, X. Wu and S. O. Smith, "Ramped-amplitude cross-polarization in magic-angle-spinning NMR," *J. Magn. Reson. A* **110**, 219-227 (1994).
- (61) A. E. Bennett, C. M. Rienstra, M. Auger, K. V. Lakshmi and R. G. Griffin, "Heteronuclear decoupling in rotating solids," *J. Chem. Phys.* **103**, 6951-6957 (1995).
- (62) D. P. Shoemaker, C. W. Garland and J. W. Nibler, "Experiments in Physical Chemistry," McGraw-Hill, New York (1989).
- (63) P. L. Stewart, R. Tycko and S. J. Opella, "Peptide backbone conformation by solid-state nuclear magnetic resonance spectroscopy," *J. Chem. Soc. Faraday Trans. I* **84**, 3803-3819 (1988).
- (64) P. J. Carroll, P. L. Stewart and S. J. Opella, "Structures of two model peptides: N-Acetyl-D,L-valine and N-Acetyl-L-valyl-L-leucine," *Acta Cryst.* **C46**, 243-246 (1990).

- (65) E. Gavuzzo, F. Mazza, G. Pochetti and A. Scatturin, "Crystal structure, conformation, and potential energy calculations of the chemotactic peptide N-formyl-L-Met-L-Leu-L-Phe-OMe," *Int. J. Peptide Protein Res.* **34**, 409-415 (1989).
- (66) U. Haeberlen and J. S. Waugh, "Coherent averaging effects in magnetic resonance," *Phys. Rev.* **175**, 453-467 (1968).
- (67) U. Haeberlen, "High-Resolution NMR in Solids: Selective Averaging," Academic Press, New York (1976).
- (68) M. Mehring, "Principles of High Resolution NMR in Solids," Springer-Verlag, Berlin (1983).
- (69) R. Freeman, "Spin Choreography: Basic Steps in High Resolution NMR," Spektrum, Oxford (1997).
- (70) T. Gullion and M. S. Conradi, "Time symmetries in rotating sample NMR," *J. Magn. Reson.* **86**, 39-45 (1990).
- (71) J. J. Verbist, M. S. Lehmann, T. F. Koetzle and W. C. Hamilton, "Precision Neutron Diffraction Structure Determination of Protein and Nuclei Acid Components. VI. The crystal and molecular structure of the amino acid L-asparagine monohydrate.," *Acta Crystallogr.* **B28**, 3006 (1972).
- (72) M. Hong and R. G. Griffin, "Resonance assignments for solid peptides by dipolar-mediated $^{13}\text{C}/^{15}\text{N}$ correlation solid-state NMR," *J. Am. Chem. Soc.* **120**, 7113-7114 (1998).
- (73) A. K. Mehta, D. J. Hirsh, N. Oyler, G. P. Drobny and J. Schaefer, "Carbon-proton dipolar decoupling in REDOR," *J. Magn. Reson.* **145**, 156-158 (2000).

- (74) Y. Ishii, J. Ashida and T. Terao, " ^{13}C - ^1H dipolar recoupling dynamics in ^{13}C multiple-pulse solid-state NMR," *Chem. Phys. Lett.* **246**, 439-445 (1995).
- (75) A. E. Bennett, Ph. D. Thesis, Massachusetts Institute of Technology, 1995.
- (76) A. E. Bennett, C. M. Rienstra, J. M. Griffiths, W. Zhen, P. T. Lansbury and R. G. Griffin, "Homonuclear radio frequency-driven recoupling in rotating solids," *J. Chem. Phys.* **108**, 9463-9479 (1998).
- (77) J. R. Long, B. Q. Sun, A. Bowen and R. G. Griffin, "Molecular dynamics and magic angle spinning NMR," *J. Am. Chem. Soc.* **116**, 11950-11956 (1994).
- (78) M. Hong, J. D. Gross, W. Hu and R. G. Griffin, "Determination of the peptide torsion angle ϕ by ^{15}N chemical shift and $^{13}\text{C}^\alpha$ - $^1\text{H}^\alpha$ dipolar tensor correlation in solid-state MAS NMR," *J. Magn. Reson.* **135**, 169-177 (1998).
- (79) M. Bak, J. T. Rasmussen and N. C. Nielsen, "SIMPSON: A general simulation program for solid-state NMR spectroscopy," *J. Magn. Reson.* **147**, 296-330 (2000).
- (80) T. G. Oas, C. J. Hartzell, F. W. Dahlquist and G. P. Drobny, "The amide ^{15}N chemical shift tensors of four peptides determined from ^{13}C dipole-coupled chemical shift powder patterns," *J. Am. Chem. Soc.* **109**, 5962-5966 (1987).
- (81) O. Weintraub and S. Vega, "Floquet density matrices and effective Hamiltonians in magic-angle-spinning NMR spectroscopy," *J. Magn. Reson. A* **105**, 245-267 (1993).

CHAPTER 5. FREQUENCY SELECTIVE REDOR DISTANCE MEASUREMENTS IN THE ACTIVE SITE OF BACTERIORHODOPSIN

Note: Reproduced with permission from C. P. Jaroniec, J. C. Lansing, B. A. Tounge, M. Belenky, J. Herzfeld and R. G. Griffin, "Measurement of dipolar couplings in a uniformly ^{13}C , ^{15}N -labeled membrane protein: Distances between the Schiff base and aspartic acids in the active site of bacteriorhodopsin," J. Am. Chem. Soc. 123 (2001) 12929-12930. Copyright 2001 American Chemical Society.

ABSTRACT

Frequency selective REDOR is used to measure ^{13}C - ^{15}N dipolar couplings in the active site of a 248-residue uniformly ^{13}C , ^{15}N -labeled membrane protein, light-adapted bacteriorhodopsin in its native purple membrane. The distances from the retinal Schiff base nitrogen to the Asp-85 and Asp-212 sidechain carboxyl carbons were found to be 4.7 ± 0.3 Å and 4.9 ± 0.5 Å, respectively. The Asp-85 distance agrees with the 4.3-5.0 Å distances in recent diffraction structures of light-adapted bacteriorhodopsin, while the Asp-212 distance appears to be somewhat longer in the NMR measurement than the 4.0-4.4 Å diffraction values.

5.1 Introduction

In recent years a number of magic-angle spinning (MAS) solid-state nuclear magnetic resonance (SSNMR) methods have been developed^{1,2} for ^{13}C and ^{15}N resonance assignments in uniformly ^{13}C , ^{15}N labeled peptides and proteins.³⁻⁸ The ^{13}CO , $^{13}\text{C}\alpha$, $^{13}\text{C}\beta$ and amide ^{15}N chemical shifts can be used to estimate the backbone torsion angles ϕ and ψ .⁹⁻¹² Additional constraints on the local structure in U- ^{13}C , ^{15}N labeled systems can be obtained from measurements of the relative orientations of dipolar tensors.¹³ Long-range dipolar couplings in peptides and proteins can provide valuable information about tertiary structure. However, the accurate determination of weak dipolar interactions in U- ^{13}C , ^{15}N labeled molecules is complicated by the presence of strong couplings.¹⁴⁻¹⁸ This problem can be circumvented by controlled “dilution” of the multiple spin system¹⁹ or by the use of spectrally selective dipolar recoupling techniques.²⁰⁻²² To date selective recoupling techniques have been applied to accurate measurements of multiple long-range ^{13}C - ^{13}C ^{23,24} and ^{13}C - ^{15}N ²² distances in small U- ^{13}C , ^{15}N labeled peptides. In this communication we demonstrate the application of frequency selective REDOR (FSR)²² to the measurement of two ^{13}C - ^{15}N dipolar couplings in the active site of light-adapted [U- ^{13}C , ^{15}N]bacteriorhodopsin (bR) in its native purple membrane. The measured distances are in reasonable agreement with ones reported in recent diffraction structures of light-adapted bR, and the NMR methods described are directly applicable to bR photocycle intermediates, for which high-resolution diffraction structures are more difficult to obtain. The experiments presented here are the first example of long-range MAS NMR distance measurements in a U- ^{13}C , ^{15}N -labeled macromolecule.

5.2 Experimental

5.2.1 Preparation of Light-Adapted [U-¹³C, ¹⁵N]Bacteriorhodopsin

Uniformly ¹³C, ¹⁵N-labeled peptone for the culture medium of *Halobacterium salinarum*^{25,26} was obtained from the anaerobic acid hydrolysis of *Methylophilus methylotrophus* grown on ¹³C-labeled methanol and ¹⁵N-labeled ammonium sulfate.²⁷ The purple membranes were isolated using the method of Oesterhelt and Stoeckenius.²⁸ Prior to the NMR experiments the purple membrane sample (~40 mg) was washed 3 times with a 0.1 M NaCl solution at pH 10.0. Following each wash the sample was centrifuged for 1 h at ~43000g. After the final spin the bacteriorhodopsin (bR) pellet was packed into a transparent single-crystal sapphire rotor (5 mm o.d.) and sealed.

The rotor was placed in the NMR probe and the light-adapted (LA) state (bR₅₆₈) was prepared *in situ* via overnight irradiation with white-light at 0 °C (the light from a 1000 W xenon lamp was filtered through water and heat absorbing filter and delivered to the sample via a glass optic fiber bundle). Subsequently, the sample temperature was decreased to ca. -30 °C. The presence of pure bR₅₆₈ was confirmed prior to and following the distance measurements by monitoring the characteristic chemical shift of the retinal Schiff base nitrogen in a 1D ¹⁵N CPMAS spectrum (Figure 5-2).²⁹

5.2.2 NMR Spectroscopy

NMR spectra were recorded at 7.4 and 11.7 T using custom-designed spectrometers (courtesy of Dr. David J. Ruben). For the experiments at 7.4 T a custom-designed triple-resonance MAS probe equipped with a 5.0 mm Chemagnetics (Fort

Collins, CO) spinning module was used, and for the experiments at 11.7 T a 4.0 mm Chemagnetics T3 triple-resonance MAS probe was used. Spinning frequencies were regulated to ± 5 Hz using Doty Scientific (Columbia, SC) and Bruker (Karlsruhe, Germany) spinning frequency controllers. Further details regarding NMR pulse sequences and experimental conditions are provided in the figure captions.

5.2.3 Numerical Simulations and Distance Measurements

Numerical simulations of the FSR experiment²² were performed using the SIMPSON NMR simulation software.³⁰ The simulations included the exact profiles of the Gaussian pulses. In the FSR experiment on bR, the dephasing of the Asp-85 and Asp-212 C γ signals is primarily a function of the dipolar coupling to the retinal Schiff base nitrogen; the couplings from C γ to other ¹⁵N, as well as Asp C γ -C β , etc. J-couplings are suppressed.²² The dephasing is also affected by the non-negligible magnitudes of the ¹³C and ¹⁵N anisotropic chemical shielding (CSA) interactions, and to a minor extent their relative orientations.³¹ Therefore, ¹⁵N and ¹³C CSAs were included in the simulations (previously reported bR₅₆₈ ¹⁵N and ¹³C CSA principal values were used^{29,32}). Relative orientations of the dipolar and CSA tensors are not known for bR, and simulations were performed for 1024 sets of different relative tensor orientations. Subsequently, the average dephasing curves expected for different distances in the 4.0-5.5 Å regime were calculated, and used to extract the internuclear distances using standard reduced χ^2 analysis.³³ We found that for each value of the dipolar coupling the simulations for different relative tensor orientations are clustered very closely around the average dephasing curve, with the largest deviation observed when the principal axis systems of

the three tensors are aligned. The systematic errors in the estimated dipolar coupling introduced by the choice of an incorrect relative tensor orientation could be ignored, since they were significantly smaller ($< 0.1 \text{ \AA}$) than the random errors in the measured distances (ca. $0.3\text{-}0.5 \text{ \AA}$).

5.3 Results and Discussion

Bacteriorhodopsin (bR) is a 26 kDa integral membrane protein produced by *Halobacterium salinarum*. The single polypeptide chain forms a bundle of seven transmembrane helices enveloping a chromophore formed by a Schiff base (SB) between retinal and Lys-216 (see Figure 5-1). Dark-adapted bR comprises two species: bR₅₅₅ and bR₅₆₈, with different retinal conformations. Light adaptation of bR, by irradiation with white light, converts bR₅₅₅ to bR₅₆₈, which is the starting point of the proton pumping photocycle (see ref 34 for a review on bR).

In the one-dimensional MAS spectrum of bR₅₆₈ (Figure 5-2) the Schiff base nitrogen resonates ~ 135 ppm downfield from the $\zeta\text{-NH}_3^+$ groups of Lys residues and ~ 50 ppm downfield from the amide backbone peak.²⁹ This enables the selective inversion of the SB nitrogen and FSR distance measurements²² to ^{13}C nuclei in the active site. Recent diffraction structures of bR₅₆₈ (from 1.55 to 2.9 \AA resolution)³⁵⁻³⁷ report distances to the SB nitrogen in the $4.3\text{-}5.0 \text{ \AA}$ range for Asp-85 C γ and in the $4.0\text{-}4.4 \text{ \AA}$ range for Asp-212 C γ (Table 5-1).

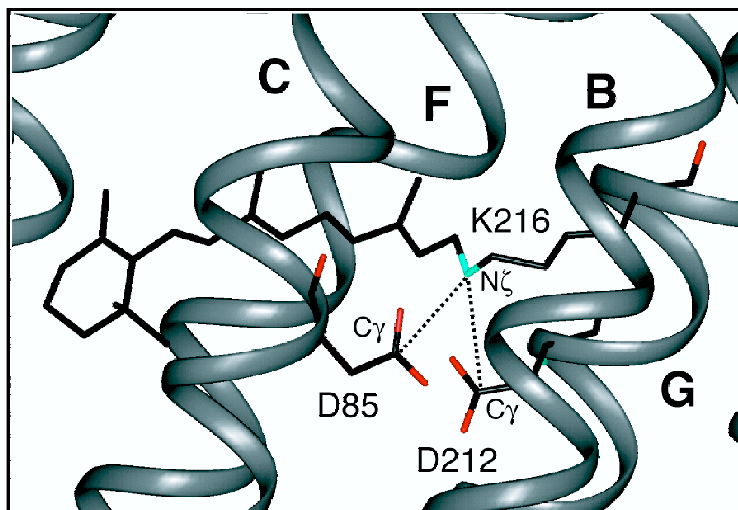


Figure 5-1. The active site of bacteriorhodopsin.

Shown are the B, C, F and G α -helices, the chromophore (comprising retinal with its Schiff base linkage to Lys216), and the Asp 85 and Asp 212 sidechains. The distances between the Schiff base nitrogen and Asp C γ , measured in this work, are indicated by dotted lines.

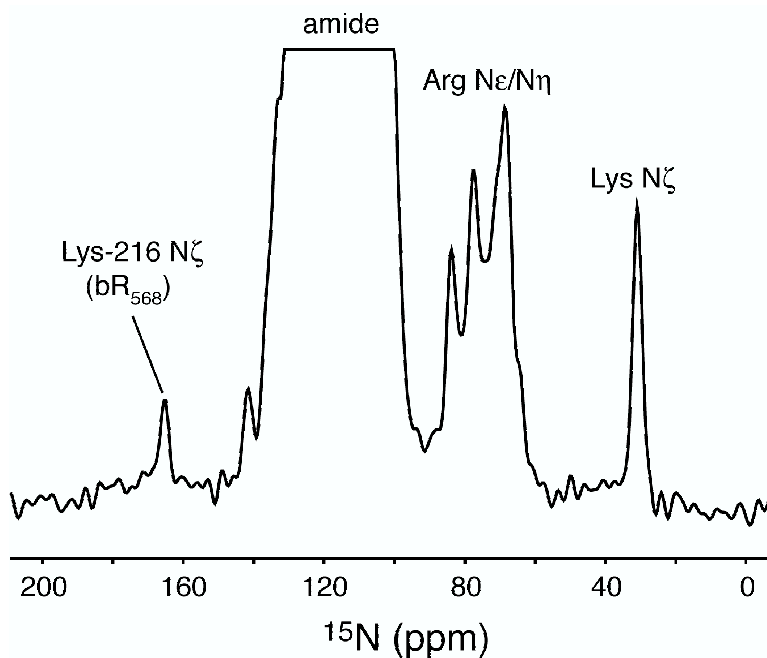


Figure 5-2. One-dimensional ^{15}N MAS spectrum of light-adapted bacteriorhodopsin. The spectrum was recorded at 317 MHz ^1H frequency, $\omega_r/2\pi = 6.5$ kHz and -30 $^\circ\text{C}$. Approximately 5000 transients were averaged. The LA state of bR (bR $_{568}$) was prepared as described in the experimental section.

Table 5-1. Diffraction Distances from the Retinal Schiff Base Nitrogen in bR₅₆₈

PDB	Resolution (Å)	to Asp85 C γ (Å)	to Asp212 C γ (Å)
1BRR ^a	2.9	5.06	4.14
		5.01	4.13
		4.96	3.98
1QHJ ^b	1.9	4.28	4.41
1C3W ^c	1.55	4.45	4.12

^aRef 35. ^bRef 36. ^cRef 37.

Figure 5-3a shows a region of a 2D RFDR³⁸ ¹³C-¹³C chemical shift correlation spectrum of dark-adapted [U-¹³C,¹⁵N]bR displaying Asp and Glu sidechain methylene to carboxyl cross-peaks. The resonance assignments are based on previous studies of selectively [4-¹³C]Asp labeled bR.^{32,39} Asp85 and Asp212 C β -C γ cross-peaks are well-resolved and, in principle, the distances to the SB can be measured via a 3D FSR experiment (where the decay rate of cross-peaks in the FSR dimension is determined by the dipolar coupling to the SB ¹⁵N). However, with the current technology a 3D experiment for a membrane protein, such as bR, is subject to signal-to-noise and time limitations. Therefore, we have reduced the experiment to a 2D (see Figure 5-4) by implementing a filter prior to FSR, designed to retain only Asp C γ resonances in the CO spectral region, while eliminating all other signals (although in practice some residual Glu C δ intensity remains). The filter consists of a selective storage pulse applied to Asp C β , followed by coherence transfer to C γ and C α via RFDR. The subsequent REDOR filter eliminates signals in the CO spectral region, which originate from nuclei directly bonded to a ¹⁵N nucleus (Asn C γ , Gln C δ and C'). We have confirmed that the resulting 1D spectrum is equivalent to a weighted projection through the Asp C β -C γ and Glu C γ -C δ region in the 2D correlation spectrum (Figure 5-3b).

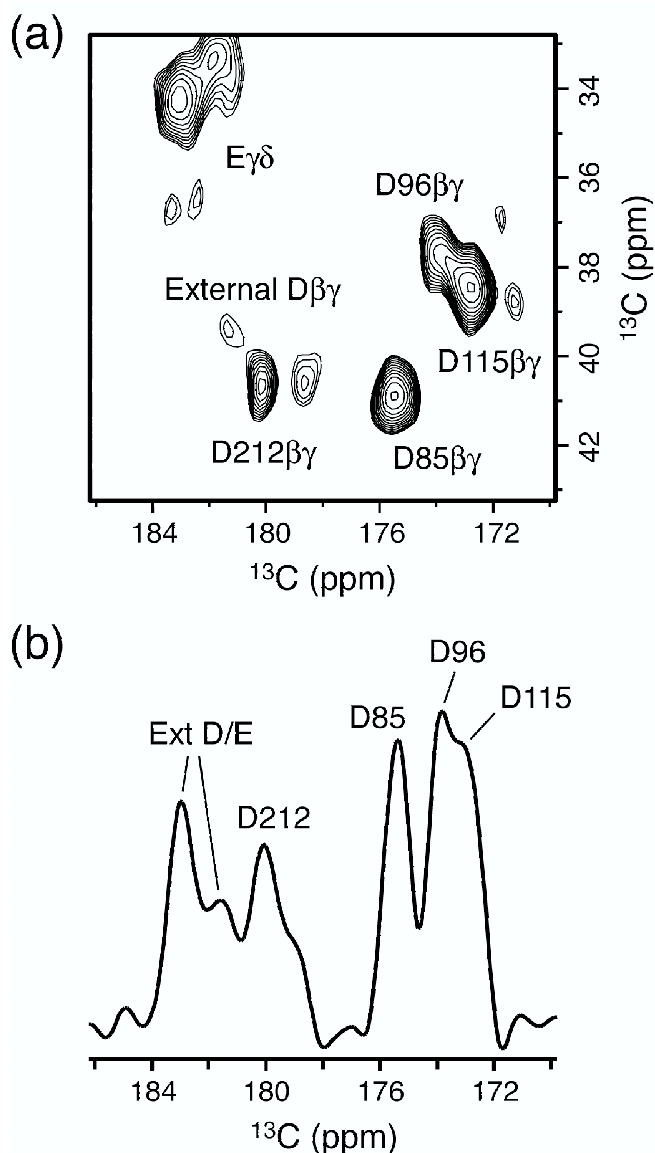


Figure 5-3. Two-dimensional RFDR ^{13}C - ^{13}C chemical shift correlation and filtered one-dimensional ^{13}C MAS spectra of dark-adapted $[\text{U-}^{13}\text{C}, ^{15}\text{N}]$ bacteriorhodopsin.

Spectra were recorded at 11.7 T (500 MHz ^1H frequency), 12.5 kHz MAS and $-80\text{ }^\circ\text{C}$. The 2D correlation spectrum shown in (a) displays only Asp $\text{C}\beta$ - $\text{C}\gamma$ and Glu $\text{C}\gamma$ - $\text{C}\delta$ cross-peaks. To eliminate Asn $\text{C}\gamma$ and Gln $\text{C}\delta$ signals in t_2 the conventional 2D RFDR sequence³⁸ was followed by a REDOR⁴⁰ ^{13}C - ^{15}N dipolar filter: $\text{CP}-t_1-(\pi/2)_\psi$ -RFDR $-(\pi/2)$ -REDOR filter- t_2 . RFDR and REDOR filter lengths were 0.96 ms and 1.44 ms, respectively. The data were acquired by shifting phase ψ according to Ruben and co-workers⁴¹ as (16, 512) complex points with dwell times (320, 20) μs . Each FID was 512 scans, with a 4.0-s recycle delay, resulting in a total measurement time of ~ 18 h. ^{13}C chemical shifts are indirectly referenced to the methyl ^1H resonance of DSS.⁴² The filtered spectrum in (b) was recorded using the pulse sequence in Figure 5-4 with the FSR period omitted. A total of 16384 scans were averaged, with a 4.0-s recycle delay, yielding a total measurement time of ~ 18 h.

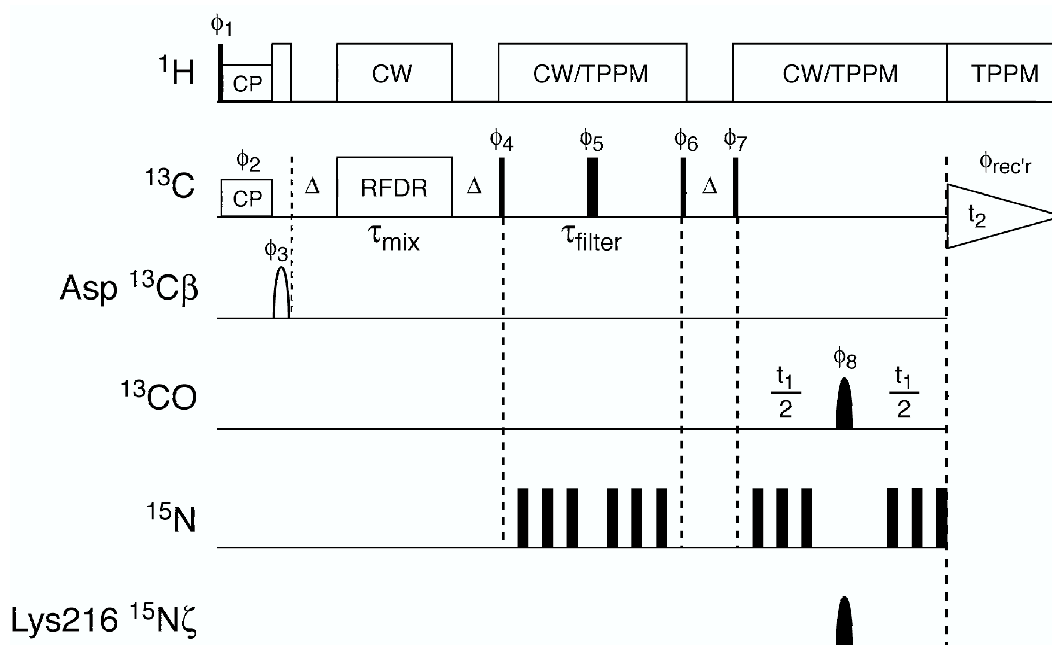


Figure 5-4. Two-dimensional experiment for the measurement of dipolar couplings between the retinal SB nitrogen and Asp C γ in [U- ^{13}C , ^{15}N]bR.

Spectra were recorded at 7.4 T, 6494 Hz MAS, and $-30\text{ }^{\circ}\text{C}$. Light-adapted bR was prepared as described in the experimental section. Narrow and wide rectangles represent $\pi/2$ and π pulses, respectively. The ^{13}C Gaussian $3\pi/2$ pulse applied in the Asp C β spectral region following CP was 1.232 ms long. RFDR and REDOR filter times were both 1.232 ms. REDOR and FSR ^{15}N π pulse lengths were 13 μs (xy -4 phase cycling). During FSR (t_1) Gaussian π pulse lengths were 0.308 ms and 4.004 ms for Asp ^{13}CO and Lys216 $^{15}\text{N}\zeta$, respectively. Gaussian pulses were divided into 64 steps and truncated at 1%. The z-filters were $\Delta=50\text{ }\mu\text{s}$. Proton decoupling was 125 and 100 kHz during mixing and acquisition, respectively (see ref 22). Phase cycle: $\phi_1=1$, $\phi_2=1$, $\phi_3=24$, $\phi_4=1$, $\phi_5=2$, $\phi_6=11111111\ 11111111\ 11111111\ 11111111\ 33333333\ 33333333\ 33333333\ 33333333$, $\phi_7=11111111\ 22222222\ 33333333\ 44444444$, $\phi_8=11223344$, $\phi_{\text{rec'r}}=42244224\ 31133113\ 24422442\ 13311331\ 24422442\ 13311331\ 42244224\ 31133113$, where 1= x , 2= y , 3= $-x$, 4= $-y$.

FSR distance measurements from Lys216 N ζ to Asp85 C γ and Asp212 C γ in light-adapted bR are presented in Figure 5-5. Spectra in Figures 5-5a and 5-5b clearly show that Asp85 and Asp212 C γ are selectively dephased by the retinal SB ^{15}N , while the other Asp signals remain unchanged. FSR dephasing curves for several ^{13}C - ^{15}N distances

in the 4.0-5.5 Å range were calculated using the SIMPSON NMR simulation software³⁰ (see experimental section). Experimental S/S_0 curves for Asp85 and Asp212 are compared with 4.0, 4.5, 5.0 and 5.5 Å simulations in Figures 5-5c and 5-5d. Asp85 and Asp212 distances were found to be 4.7 ± 0.3 Å and 4.9 ± 0.5 Å, respectively. The Asp85 distance is in agreement with recent diffraction distances (4.3-5.0 Å), and the Asp212 distance appears to be somewhat longer than the diffraction values (4.0-4.4 Å).³⁵⁻³⁷

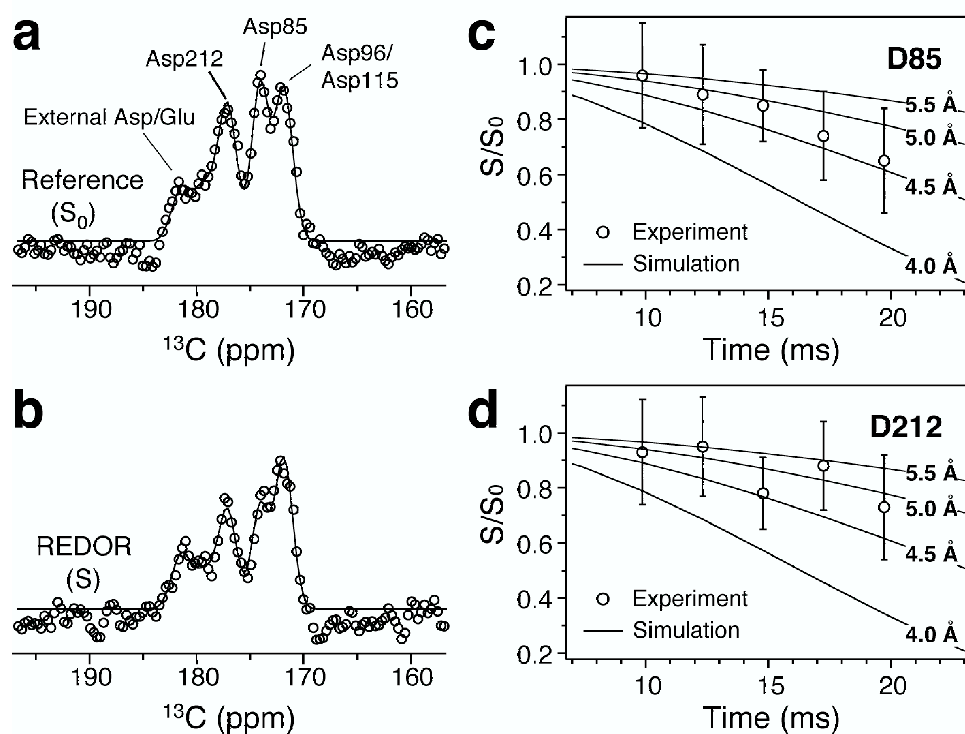


Figure 5-5. Distance measurements from the Schiff base Lys216 N ζ to Asp85 C γ and Asp212 C γ in light-adapted [U- ^{13}C , ^{15}N]bR.

(a) Reference (S_0) and (b) REDOR (S) spectra recorded using the pulse sequence in Figure 2 with $t_1=19.712$ ms. Experimental spectra (\circ) and fits with Gaussian lineshapes (lines) are juxtaposed. (c) Asp85 C γ and (d) Asp212 C γ REDOR S/S_0 curves. Experimental data (\circ) were obtained with 32768 and 65536 transients for $t_1 < 15$ ms and $t_1 > 15$ ms, respectively (interleaving S_0 and S spectra for each t_1 point in blocks of 256 transients). The error bars in the experimental S/S_0 points were calculated from the uncertainties in the Gaussian lineshape fits. Using a 2.0 s-recycle delay, the total duration of the experiment was ~ 10 days. Simulations (lines) for 4.0, 4.5, 5.0 and 5.5 Å carbon-nitrogen distances were generated using SIMPSON.³⁰ The best-fit distances are 4.7 ± 0.3 Å for Asp85 and 4.9 ± 0.5 Å for Asp212.

5.4 Conclusions

We have applied frequency selective REDOR to distance measurements between the Schiff base and aspartic acids in the active site of uniformly ^{13}C , ^{15}N labeled bacteriorhodopsin. The measured distances are in reasonable agreement with recent diffraction studies, and complement previous structural investigations of the bR active site by SSNMR.⁴³ The methods described can be applied to the characterization of bR photocycle intermediates.

Acknowledgments

This research was supported by NIH Grants GM-23289, GM-36810 and RR-00995. C.P.J. thanks the NSF for a Predoctoral Fellowship, and B.A.T. thanks the American Cancer Society for a Postdoctoral Fellowship (PF-99-260-01-GMC).

References

- (1) R. G. Griffin, "Dipolar recoupling in MAS spectra of biological solids," *Nature Struct. Biol.* **5**, 508-512 (1998).
- (2) S. Dusold and A. Sebald, "Dipolar recoupling under magic-angle spinning conditions," *Annu. Rep. Nucl. Magn. Reson. Spectr.* **41**, 185-264 (2000).
- (3) C. M. Rienstra, M. Hohwy, M. Hong and R. G. Griffin, "2D and 3D ^{15}N - ^{13}C - ^{13}C NMR chemical shift correlation spectroscopy of solids: assignment of MAS spectra of peptides," *J. Am. Chem. Soc.* **122**, 10979-10990 (2000).
- (4) J. J. Balbach, Y. Ishii, O. N. Antzutkin, R. D. Leapman, N. W. Rizzo, F. Dyda, J. Reed and R. Tycko, "Amyloid fibril formation by A β 16-22, a seven-residue fragment of the Alzheimer's β -amyloid peptide, and structural characterization by solid state NMR," *Biochemistry* **39**, 13748-13759 (2000).
- (5) A. Detken, E. H. Hardy, M. Ernst, M. Kainosho, T. Kawakami, S. Aimoto and B. H. Meier, "Methods for sequential resonance assignment in solid, uniformly ^{13}C , ^{15}N labelled peptides: Quantification and application to antamanide," *J. Biomol. NMR* **20**, 203-221 (2001).
- (6) A. Detken, M. Ernst and B. H. Meier, "Towards biomolecular structure determination by high-resolution solid-state NMR: Assignment of solid peptides," *Chimia* **55**, 844-851 (2001).
- (7) A. McDermott, T. Polenova, A. Bockmann, K. W. Zilm, E. K. Paulsen, R. W. Martin and G. T. Montelione, "Partial NMR assignments for uniformly (^{13}C , ^{15}N)-enriched BPTI in the solid state," *J. Biomol. NMR* **16**, 209-219 (2000).

- (8) J. Pauli, M. Baldus, B. van Rossum, H. de Groot and H. Oschkinat, "Backbone and side-chain ^{13}C and ^{15}N signal assignments of the α -spectrin SH3 domain by magic angle spinning solid-state NMR at 17.6 Tesla," *ChemBiochem* **2**, 272-281 (2001).
- (9) S. Spera and A. Bax, "Empirical correlation between protein backbone conformation and $\text{C}\alpha$ and $\text{C}\beta$ ^{13}C nuclear magnetic resonance chemical shifts," *J. Am. Chem. Soc.* **113**, 5490-5492 (1991).
- (10) G. Cornilescu, F. Delaglio and A. Bax, "Protein backbone angle restraints from searching a database for chemical shift and sequence homology," *J. Biomol. NMR* **13**, 289-302 (1999).
- (11) D. S. Wishart and B. D. Sykes, "Chemical shifts as a tool for structure determination," *Methods Enzymol.* **239**, 363-392 (1994).
- (12) D. S. Wishart and D. A. Case, "Use of chemical shifts in macromolecular structure determination," *Methods Enzymol.* **338**, 3-34 (2001).
- (13) X. Feng, Y. K. Lee, D. Sandström, M. Eden, H. Maisel, A. Sebald and M. H. Levitt, "Direct determination of a molecular torsional angle by solid-state NMR," *Chem. Phys. Lett.* **257**, 314-320 (1996).
- (14) C. A. Fyfe and A. R. Lewis, "Investigation of the viability of solid-state NMR distance determinations in multiple spin systems of unknown structure," *J. Phys. Chem. B* **104**, 48-55 (2000).
- (15) P. Hodgkinson and L. Emsley, "The accuracy of distance measurements in solid-state NMR," *J. Magn. Reson.* **139**, 46-59 (1999).
- (16) P. R. Costa, Ph. D. Thesis, Massachusetts Institute of Technology, 1996.

- (17) M. Hohwy, C. M. Rienstra, C. P. Jaroniec and R. G. Griffin, "Fivefold symmetric homonuclear dipolar recoupling in rotating solids: Application to double quantum spectroscopy," *J. Chem. Phys.* **110**, 7983-7992 (1999).
- (18) V. Ladizhansky and S. Vega, "Polarization transfer dynamics in Lee-Goldburg cross polarization nuclear magnetic resonance experiments on rotating solids," *J. Chem. Phys.* **112**, 7158-7168 (2000).
- (19) B. Reif, C. P. Jaroniec, C. M. Rienstra, M. Hohwy and R. G. Griffin, "¹H-¹H MAS correlation spectroscopy and distance measurements in a deuterated peptide," *J. Magn. Reson.* **151**, 320-327 (2001).
- (20) D. P. Raleigh, M. H. Levitt and R. G. Griffin, "Rotational resonance in solid state NMR," *Chem. Phys. Lett.* **146**, 71-76 (1988).
- (21) K. Takegoshi, K. Nomura and T. Terao, "Rotational resonance in the tilted rotating frame," *Chem. Phys. Lett.* **232**, 424-428 (1995).
- (22) C. P. Jaroniec, B. A. Tounge, J. Herzfeld and R. G. Griffin, "Frequency selective heteronuclear dipolar recoupling in rotating solids: Accurate ¹³C-¹⁵N distance measurements in uniformly ¹³C,¹⁵N-labeled peptides," *J. Am. Chem. Soc.* **123**, 3507-3519 (2001).
- (23) K. Nomura, K. Takegoshi, T. Terao, K. Uchida and M. Kainosho, "Determination of the complete structure of a uniformly labeled molecule by rotational resonance solid-state NMR in the tilted rotating frame," *J. Am. Chem. Soc.* **121**, 4064-4065 (1999).
- (24) K. Nomura, K. Takegoshi, T. Terao, K. Uchida and M. Kainosho, "Three-dimensional structure determination of a uniformly labeled molecule by frequency-

- selective dipolar recoupling under magic-angle spinning," *J. Biomol. NMR* **17**, 111-123 (2000).
- (25) R. T. Batey, M. Inada, E. Kujawinski, J. D. Puglisi and J. R. Williamson, "Preparation of isotopically labeled ribonucleotides for multidimensional NMR spectroscopy of RNA," *Nucleic Acid Res.* **20**, 4515-4523 (1992).
- (26) R. T. Batey, J. L. Battiste and J. R. Williamson, "Preparation of isotopically enriched RNAs for heteronuclear NMR," *Methods Enzymol.* **261**, 300-322 (1995).
- (27) M. B. Gochnauer and D. J. Kushner, "Growth and nutrition of extremely halophilic bacteria," *Can. J. Microbiol.* **15**, 1157-1165 (1969).
- (28) D. Oesterhelt and W. Stoeckenius, "Isolation of the cell membrane of *Halobacterium halobium* and its fractionation into red and purple membrane," *Methods Enzymol.* **31**, 667-678 (1974).
- (29) H. J. M. de Groot, G. S. Harbison, J. Herzfeld and R. G. Griffin, "Nuclear magnetic resonance study of the Schiff base in bacteriorhodopsin: Counterion effects on the ^{15}N shift anisotropy," *Biochemistry* **28**, 3346-3353 (1989).
- (30) M. Bak, J. T. Rasmussen and N. C. Nielsen, "SIMPSON: A general simulation program for solid-state NMR spectroscopy," *J. Magn. Reson.* **147**, 296-330 (2000).
- (31) Additional simulations indicate that CSA dependence is significantly reduced when higher MAS frequencies ($\omega_r \gg |\omega_{\text{CSA}}|$) are employed. In this work the maximum spinning frequencies were limited to ~ 6.5 kHz, since we have used the low-temperature NMR probe equipped with a 5-mm stator, capable of trapping and characterizing bR photocycle intermediates in situ.

- (32) G. Metz, F. Siebert and M. Engelhard, "High-resolution solid state ^{13}C NMR of bacteriorhodopsin: Characterization of $[4\text{-}^{13}\text{C}]\text{Asp}$ resonances," *Biochemistry* **31**, 455-462 (1992).
- (33) D. P. Shoemaker, C. W. Garland and J. W. Nibler, "Experiments in Physical Chemistry," McGraw-Hill, New York (1989).
- (34) U. Haupts, J. Tittor and D. Oesterhelt, "Closing in on bacteriorhodopsin: Progress in understanding the molecule," *Annu. Rev. Biophys. Biomol. Struct.* **28**, 367-399 (1999).
- (35) L. O. Essen, R. Siegert, W. D. Lehmann and D. Oesterhelt, "Lipid patches in membrane protein oligomers: Crystal structure of the bacteriorhodopsin-lipid complex," *Proc. Natl. Acad. Sci. USA* **95**, 11673-11678 (1998).
- (36) H. Belrhali, P. Nollert, A. Royant, C. Menzel, J. P. Rosenbusch, E. M. Landau and E. Pebay-Peyroula, "Protein, lipid and water organization in bacteriorhodopsin crystals: a molecular view of the purple membrane at 1.9 Å resolution," *Structure* **7**, 909-917 (1999).
- (37) H. Luecke, B. Schobert, H. T. Richter, J. Cartailier and J. K. Lanyi, "Structure of bacteriorhodopsin at 1.55 Å resolution," *J. Mol. Biol.* **291**, 899-911 (1999).
- (38) A. E. Bennett, J. H. Ok, R. G. Griffin and S. Vega, "Chemical shift correlation spectroscopy in rotating solids: Radio frequency driven dipolar recoupling and longitudinal exchange," *J. Chem. Phys.* **96**, 8624-8627 (1992).
- (39) G. Metz, F. Siebert and M. Engelhard, "Asp85 is the only internal aspartic acid that gets protonated in the M-intermediate and the purple-to-blue transition of

bacteriorhodopsin - A solid-state ^{13}C CPMAS NMR investigation," *FEBS Lett.* **303**, 237-241 (1992).

- (40) T. Gullion and J. Schaefer, "Rotational-echo double-resonance NMR," *J. Magn. Reson.* **81**, 196-200 (1989).
- (41) D. J. States, R. A. Haberkorn and D. J. Ruben, "A two-dimensional nuclear Overhauser experiment with pure absorption phase in four quadrants," *J. Magn. Reson.* **48**, 286-292 (1982).
- (42) D. S. Wishart, C. G. Bigam, J. Yao, F. Abildgaard, H. J. Dyson, E. Oldfield, J. L. Markley and B. D. Sykes, " ^1H , ^{13}C and ^{15}N chemical shift referencing in biomolecular NMR," *J. Biomol. NMR* **6**, 135-140 (1995).
- (43) J. M. Griffiths, A. E. Bennett, M. Engelhard, F. Siebert, J. Raap, J. Lugtenburg, J. Herzfeld and R. G. Griffin, "Structural investigation of the active site of bacteriorhodopsin: Geometric constraints on the roles of Asp-85 and Asp-212 in the proton pumping mechanism from solid-state NMR," *Biochemistry* **39**, 362-371 (2000).

CHAPTER 6. 3D TEDOR NMR EXPERIMENTS FOR THE SIMULTANEOUS MEASUREMENT OF MULTIPLE CARBON-NITROGEN DISTANCES IN U-¹³C, ¹⁵N-LABELED SOLIDS

Note: Reproduced with permission from C. P. Jaroniec, C. Filip and R. G. Griffin, “3D TEDOR NMR experiments for the simultaneous measurement of multiple carbon-nitrogen distances in uniformly ¹³C, ¹⁵N-labeled solids,” J. Am. Chem. Soc. 124 (2002) 10728-10742. Copyright 2002 American Chemical Society.

ABSTRACT

We describe three-dimensional magic-angle-spinning NMR experiments for the simultaneous measurement of multiple carbon-nitrogen distances in uniformly ¹³C, ¹⁵N labeled solids. The approaches employ transferred echo double resonance (TEDOR) for ¹³C-¹⁵N coherence transfer and ¹⁵N and ¹³C frequency labeling for site-specific resolution, and build on several previous 3D TEDOR techniques. The novel feature of the 3D TEDOR pulse sequences presented here is that they are specifically designed to circumvent the detrimental effects of homonuclear ¹³C-¹³C J-couplings on the measurement of weak ¹³C-¹⁵N dipolar couplings. In particular, homonuclear J-couplings lead to two undesirable effects: (i) they generate anti-phase and multiple-quantum (MQ) spin coherences, which lead to spurious cross-peaks and phase-twisted lines in the 2D ¹⁵N-¹³C correlation spectra, and thus degrade the spectral resolution and prohibit the extraction of reliable cross-peak intensities, and (ii) they significantly reduce cross-peak intensities for strongly J-coupled ¹³C sites (e.g., CO and C^α). The first experiment employs z-filter periods to suppress the anti-phase and MQ coherences and generates 2D spectra with purely absorptive peaks for all TEDOR mixing times. The second approach

uses band-selective ^{13}C pulses to refocus J-couplings between ^{13}C spins within the selective pulse bandwidth and ^{13}C spins outside the bandwidth. The internuclear distances are extracted using a simple analytical model, which accounts explicitly for multiple spin-spin couplings contributing to cross-peak buildup. The experiments are demonstrated in two U- ^{13}C , ^{15}N labeled peptides, N-acetyl-L-Val-L-Leu (N-ac-VL) and N-formyl-L-Met-L-Leu-L-Phe (N-f-MLF), where 20 and 26 ^{13}C - ^{15}N distances up to $\sim 5\text{-}6$ Å were measured, respectively. Of the measured distances, 10 in N-ac-VL and 13 in N-f-MLF are greater than 3 Å and provide valuable structural constraints.

6.1 Introduction

Recent advances in magic-angle-spinning (MAS) solid-state nuclear magnetic resonance (SSNMR) instrumentation and methodology¹⁻³ have greatly extended the applicability of SSNMR from selectively to multiply ¹³C, ¹⁵N labeled peptides and proteins. At moderate magnetic field strengths of 7-14 Tesla (¹H Larmor frequencies of 300-600 MHz), complete sequence specific ¹³C and ¹⁵N resonance assignments have been obtained for several uniformly ¹³C, ¹⁵N labeled micro-crystalline peptides^{4,5} and peptides that self-assemble to form amyloid fibrils,⁶⁻⁸ and partial resonance assignments were determined for the 76-residue human ubiquitin.^{9,10} At magnetic fields of 17.5-19 Tesla (¹H Larmor frequencies of 750-800 MHz), resonance assignments for several uniformly ¹³C, ¹⁵N labeled proteins have been recently presented.¹¹⁻¹⁴ Specifically, partial assignments have been obtained for the 58-residue bovine pancreatic trypsin inhibitor (BPTI)¹¹ and the 150 kDa LH2 light-harvesting membrane-protein complex,¹² and nearly complete sequence specific ¹³C and ¹⁵N¹³ and non-exchangeable ¹H¹⁴ assignments have been reported for the 62-residue α -spectrin SH3 domain.

Site-specific resonance assignments are a source of valuable structural information in biomolecular solution- and solid-state NMR because the difference between the experimentally observed isotropic chemical shifts and the corresponding random coil values can be used to predict the conformation of the protein backbone.¹⁵⁻²¹ Additional information about secondary and tertiary structure in solid-phase peptides and proteins can be obtained from direct measurements of homo- and heteronuclear dipolar couplings, reintroduced during MAS using dipolar recoupling techniques.¹⁻³ The experiments used for sequential resonance assignments generally exploit the strongest

spin-spin interactions and are relatively straightforward to implement in uniformly ^{13}C , ^{15}N labeled systems. On the other hand, long-range distance measurements in these systems are more complicated. The nuclei form a tightly coupled network via through-space (dipolar coupling) and through-bond (J-coupling) spin-spin interactions; consequently, the strongest couplings can interfere with the accurate determination of the weaker ones.²²⁻²⁶ In the following we will focus our attention on the problem of heteronuclear ^{13}C - ^{15}N recoupling in multiple spin systems, with the ultimate goal of measuring multiple carbon-nitrogen distances simultaneously in uniformly ^{13}C , ^{15}N labeled peptides and proteins.

A number of experiments have been developed to reintroduce the dipolar coupling between a pair of low- γ spin $I=1/2$ nuclei (e.g., ^{13}C , ^{15}N , ^{31}P) during MAS.¹⁻³ Some of the most robust and versatile heteronuclear recoupling experiments are derived from rotational echo double resonance (REDOR)^{27,28} and the closely related transferred echo double resonance (TEDOR).^{29,30} (Applications of these methods to systems of importance in biology and materials science have been summarized in several recent reviews.^{1-3,31}) During REDOR,^{27,28} the I - S dipolar coupling is reintroduced by a train of rotor-synchronized 180° pulses applied to the S -spins. This results in the dephasing of the I -spin echo with a modulation frequency proportional to the magnitude of the dipolar coupling. TEDOR^{29,30} (the basic pulse sequence consists of two REDOR periods bracketing a pair of 90° pulses on I and S spins) acts to transfer magnetization between dipolar coupled I and S nuclei, where the buildup of the S -spin magnetization is proportional to the magnitude of the I - S dipolar coupling. TEDOR coherence transfer dynamics are analogous to the well-known solution-state INEPT experiment,³² which

uses the heteronuclear J-coupling to achieve coherence transfer, and solid-state INEPT experiments,³³ for which coherence transfer is accomplished via heteronuclear dipolar couplings. While REDOR and TEDOR are both well-established for selectively ^{13}C , ^{15}N labeled samples, their application to multiply labeled systems is less straightforward. Depending on the details of the particular experiment the recoupling dynamics can depend on multiple spin-spin couplings and their relative orientations, which potentially complicates accurate measurements of weak ^{13}C - ^{15}N dipolar couplings.²⁵

Various experiments based on REDOR and TEDOR have been proposed to circumvent the problems associated with multiple spin systems.³⁴⁻⁴⁷ Most recently we described a frequency selective REDOR (FSR)⁴⁴ experiment and demonstrated its applications to uniformly ^{13}C , ^{15}N labeled peptides and proteins.^{44,48} The experiment was specifically developed to perform accurate site-specific measurements of weak ^{13}C - ^{15}N dipolar couplings in U- ^{13}C , ^{15}N labeled samples. Accordingly, for a tripeptide N-formyl-L-Met-L-Leu-L-Phe (N-f-MLF), 16 ^{13}C - ^{15}N distances up to ~ 6 Å were measured using FSR with ~ 0.1 - 0.3 Å precision⁴⁴ and used in combination with multiple dihedral angle constraints⁴⁹ to calculate the three-dimensional high-resolution structure of N-f-MLF.⁵⁰ In the special case of a biological macromolecule exhibiting sufficient ^{13}C and ^{15}N chemical shift resolution, frequency selective REDOR was applied to a 248-residue membrane protein, bacteriorhodopsin, to determine two distances between the retinal Schiff base nitrogen and carboxyl groups of aspartate residues, D85 and D212, across the active site.⁴⁸

In the following we discuss three-dimensional heteronuclear correlation (HETCOR) experiments, which are designed to *simultaneously* measure multiple long-

range carbon-nitrogen distances in uniformly ^{13}C , ^{15}N labeled samples. During a 3D HETCOR experiment a series of 2D I - S chemical shift correlation spectra are recorded as a function of the duration of the I - S coherence transfer period (also referred to as the mixing time); for distance measurements the coherence transfer proceeds via I - S dipolar couplings. Cross-peaks located at $(\Omega_{Sj}, \Omega_{Ii})$ in the 2D spectra, where Ω_{Ii} and Ω_{Sj} are the isotropic chemical shifts of the i^{th} I -spin and the j^{th} S -spin, respectively, are observed only for I - S spin pairs having a sufficiently strong dipolar coupling, and the buildup of cross-peak intensities as a function of the mixing time provides information about I - S distances in a site-specific fashion. The experiments discussed here employ TEDOR for ^{13}C - ^{15}N coherence transfer and build on 3D TEDOR techniques described previously by Fyfe and co-workers,³⁴ van Eck and Veeman,³⁵ and Michal and Jelinski.³⁶ We note that a 3D HETCOR experiment of this type based on band-selective ^{13}C - ^{15}N cross-polarization^{4,51} has also been discussed.⁵²

The previous 3D TEDOR pulse sequences,^{34,35} where the initial S -spin magnetization is frequency labeled and transferred using TEDOR to the I -spins for detection, are not directly applicable to uniformly ^{13}C , ^{15}N labeled systems, because ^{13}C - ^{13}C dipolar and/or ^{13}C and ^{15}N chemical shift anisotropy (CSA) interactions are active during the mixing period and interfere with the ^{13}C - ^{15}N coherence transfer process. These 3D TEDOR experiments were recently extended to multiple ^{13}C , ^{15}N spin systems by Michal and Jelinski,³⁶ who described an approach where the initial ^{13}C magnetization is transferred to ^{15}N for frequency labeling and subsequently transferred back to ^{13}C for detection; the resulting experiment is relatively insensitive to strong ^{13}C - ^{13}C dipolar couplings and significant ^{13}C and ^{15}N CSA interactions. While this modified 3D TEDOR

experiment³⁶ addresses many of the problems associated with uniformly ¹³C,¹⁵N labeled samples it is not explicitly compensated for homonuclear ¹³C-¹³C J-couplings ($J = 30\text{-}60$ Hz in peptides⁵³), which interfere with the measurement of weak ¹³C-¹⁵N dipolar couplings. These homonuclear J-couplings generate anti-phase and multiple-quantum (MQ) spin coherences during the mixing period, which lead to spurious cross-peaks and phase-twisted lines in the 2D spectra, and prohibit the extraction of reliable cross-peak intensities. These problems become particularly severe for mixing times on the order of $t_{mix} \approx \frac{1}{2J}$. Furthermore, the cross-peaks are modulated by the J-evolution, which leads to significantly reduced intensities for strongly J-coupled ¹³C sites (e.g., CO and C α).

In this paper we describe two modified 3D TEDOR experiments specifically designed to address the problems associated with the homonuclear J-couplings. The first approach employs z -filter periods to suppress the anti-phase and MQ coherences, generates 2D ¹⁵N-¹³C correlation spectra with pure absorption mode peaks for all TEDOR mixing times, and provides information about all carbon-nitrogen distances simultaneously. The second approach uses band-selective ¹³C pulses to refocus J-couplings between ¹³C spins within the selective pulse bandwidth and ¹³C spins outside the bandwidth and is particularly applicable to distance measurements involving strongly J-coupled ¹³C sites (homonuclear J-decoupling of this type has been used previously in solution- and solid-state NMR experiments^{43,44,54,55}). The ¹³C-¹⁵N distances are extracted using a simple analytical model, which accounts explicitly for multiple spin-spin interactions contributing to cross-peak buildup. The methods are demonstrated in model U-¹³C,¹⁵N labeled peptides, N-acetyl-L-Val-L-Leu and N-formyl-L-Met-L-Leu-L-Phe, where 20 and 26 ¹³C-¹⁵N distances up to $\sim 5\text{-}6$ Å were measured, respectively.

6.2 Experimental

6.2.1 NMR Experiments

NMR spectra were recorded at 11.7 T (500.1 MHz ^1H , 125.8 MHz ^{13}C , 50.7 MHz ^{15}N) using a custom-designed spectrometer (courtesy of Dr. David J. Ruben) with a Chemagnetics (Fort Collins, CO) triple-resonance MAS probe. The probe was equipped with a 4.0 mm Chemagnetics spinning module. The spinning frequency of 10.0 kHz was used in the experiments and regulated to ± 5 Hz with a Doty Scientific (Columbia, SC) spinning frequency controller. Samples were centerpacked in the rotors to minimize the effects of rf inhomogeneity. The 3D TEDOR pulse sequences are shown in Figure 6-1 and described in detail in the Theoretical Background section below. Unless otherwise indicated, the ^{15}N REDOR π pulse length was 10 μs , the ^{13}C and ^{15}N $\pi/2$ pulses were 5 μs , the TPPM decoupling was ~ 100 kHz (total phase difference = 12° , TPPM pulse length = 5.0 μs) during mixing and ~ 83 kHz (total phase difference = 12° , TPPM pulse length = 6.0 μs) during t_1 and t_2 , the CW decoupling was 100 kHz, and the ^{13}C band-selective Gaussian pulse (Figure 6-1b) was 0.4 ms, divided into 64 increments, and truncated at 1% of the maximum amplitude.

6.2.2 U- ^{13}C , ^{15}N -Labeled Peptides

The peptides used in the experiments were: [U- ^{13}C , ^{15}N]N-acetyl-L-Val-L-Leu (N-ac-VL) and N-formyl-[U- ^{13}C , ^{15}N]L-Met-L-Leu-L-Phe (N-f-MLF). The U- ^{13}C , ^{15}N labeled amino acids and [1,2- ^{13}C]acetic anhydride used in the peptide synthesis were purchased from Cambridge Isotope Laboratories (Andover, MA). N-ac-VL and N-f-MLF were

synthesized by Synpep (Dublin, CA) and American Peptide (Sunnyvale, CA), respectively, using standard solid phase methods and purified by HPLC. To minimize the effects of intermolecular couplings on the measured distances, the U-¹³C,¹⁵N labeled peptides were diluted in the respective natural abundance peptides followed by recrystallization from appropriate solvents: N-ac-VL was diluted to ~20% and crystallized from a 1:1 (v/v) H₂O:acetone solution⁵⁶ and N-f-MLF was diluted to ~10% and crystallized from 2-propanol.^{4,44}

6.3 Theory

6.3.1 3D TEDOR Pulse Sequences

The 3D TEDOR experiments are presented in Figure 6-1. The 3D *z*-filtered TEDOR sequence (Figure 6-1a) (also denoted in the following as 3D ZF TEDOR) provides information about all ¹³C-¹⁵N dipolar couplings simultaneously. The 3D band-selective TEDOR sequence (3D BASE TEDOR) shown in Figure 6-1b probes dipolar couplings for ¹³C spins within the selective pulse bandwidth and is particularly applicable to distance measurements involving sites with strong ¹³C-¹³C J-couplings (e.g., CO and C^α).

The desired TEDOR coherence transfer pathway for a heteronuclear *I-S* spin pair (*I* and *S* represent ¹³C and ¹⁵N, respectively) with the effective dipolar coupling, ω , is:

$$\begin{aligned}
 I_x &\xrightarrow{REDOR} 2I_y S_z \sin(\omega t_{mix} / 2) \xrightarrow{90_x(I), 90_x(S)} -2I_z S_y \sin(\omega t_{mix} / 2) \xrightarrow{t_1} \\
 &-2I_z S_y \sin(\omega t_{mix} / 2) e^{i\Omega_S t_1} \xrightarrow{90_{-x}(I), 90_{xy}(S)} -2I_y S_z \sin(\omega t_{mix} / 2) e^{i\Omega_S t_1} \\
 &\xrightarrow{REDOR} I_x \sin^2(\omega t_{mix} / 2) e^{i\Omega_S t_1} \xrightarrow{t_2} I_x \sin^2(\omega t_{mix} / 2) e^{i\Omega_S t_1} e^{i\Omega_I t_2}
 \end{aligned}$$

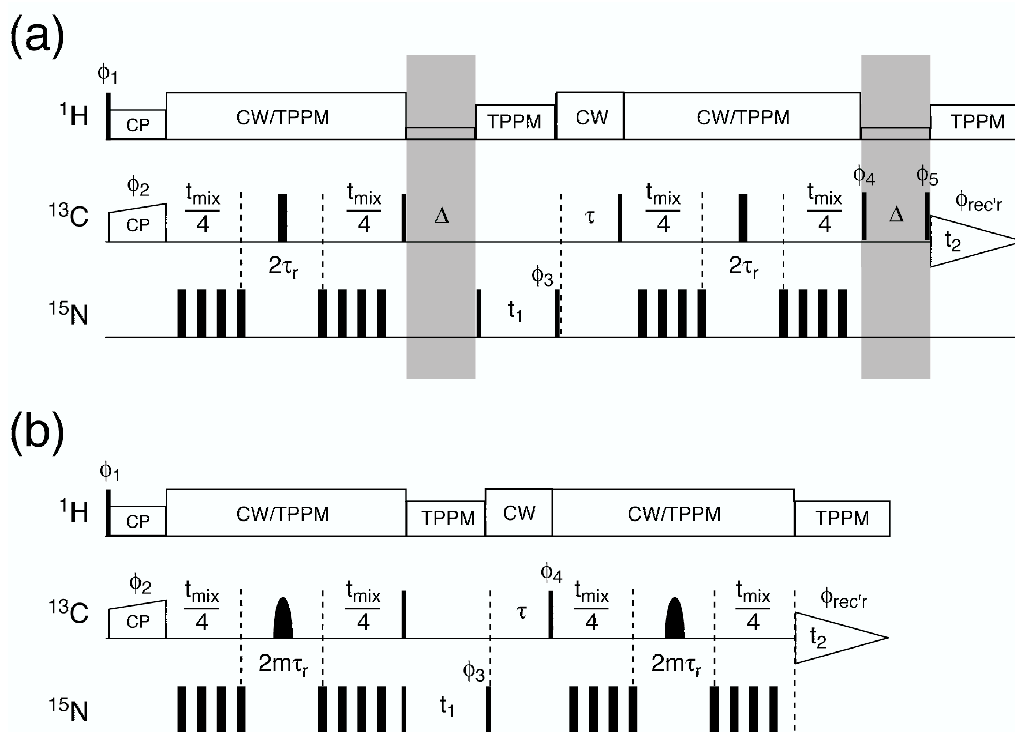


Figure 6-1. 3D TEDOR pulse sequences.

3D z -filtered TEDOR (a) and 3D band-selective TEDOR (b) pulse sequences. Narrow and wide solid rectangles represent $\pi/2$ and π pulses, respectively. During REDOR two π pulses per rotor period are applied on the ^{15}N channel and phase cycled according to the xy -4 scheme.⁵⁷ The short delay, τ , ensures that the total delay between the REDOR mixing periods is equal to an integer number of rotor cycles and is required for efficient reconversion of anti-phase coherences into observable ^{13}C magnetization. In (a) the modifications to the recently described 3D TEDOR experiment³⁶ are highlighted by gray rectangles. The modifications consist of two z -filter periods, Δ , which eliminate multiple quantum and anti-phase spin coherences generated by ^{13}C - ^{13}C J-evolution (see text for details). During the z -filters a weak proton rf field, $\omega_{\text{rf}} \approx \omega_r$, was applied⁵⁸ to facilitate the rapid dephasing of transverse ^{13}C spin coherences via the contact with the abundant proton bath. In (b) band-selective ^{13}C Gaussian π pulses refocus ^{13}C - ^{13}C J-couplings to nuclei outside the π pulse bandwidth. The phase cycles were: (a) $\phi_1 = 16 \times (1) 16 \times (3)$, $\phi_2 = 1$, $\phi_3 = 13$, $\phi_4 = 2244$, $\phi_{\text{rec}'r} = 11112222 33334444$, $\phi_{\text{rec}'r} = 42241331 24423113 24423113 42241331$; (b) $\phi_1 = 8 \times (1) 8 \times (3)$, $\phi_2 = 1$, $\phi_3 = 13$, $\phi_4 = 11223344$, $\phi_{\text{rec}'r} = 31241342 13423124$, where $1 = x$, $2 = y$, $3 = -x$, $4 = -y$. All remaining pulses (except ^{15}N π pulses during REDOR which were phase cycled xy -4 and ^1H spin-lock which had phase y) have phase x . Hypercomplex data were acquired by shifting ϕ_3 according to Ruben and co-workers.⁵⁹

The transverse I -spin (^{13}C) magnetization is created using ramped cross-polarization from protons.⁶⁰ Subsequently, a REDOR sequence,^{27,28} initiated for a time $t_{\text{mix}}/2$, reintroduces the I - S dipolar coupling and generates I -spin coherence in anti-phase with respect to the S -spin ($\sim I_y S_z$). The first pair of 90° pulses on the I and S spins results in coherence transfer to the S -spin ($\sim I_z S_y$). This coherence is frequency labeled in t_1 with the S -spin chemical shift, Ω_S . The second pair of 90° pulses on the I and S spins transfer the coherence back to the I -spin ($\sim I_y S_z$). The resulting anti-phase coherence is reconverted into observable I -spin magnetization ($\sim I_x$) during the second REDOR period and frequency labeled with the I -spin chemical shift, Ω_I , during the acquisition of the FID in t_2 . Assuming quadrature detection in t_1 and t_2 ,^{53,61} a Fourier transformation of the time-domain data results in a 2D spectrum with a cross-peak at the frequency (Ω_S, Ω_I) . For each crystallite in the powder sample the cross-peak intensity is modulated as a function of the mixing time, t_{mix} , according to $\sin^2(\omega t_{\text{mix}}/2)$.

In our implementation of 3D TEDOR experiments for uniformly $^{13}\text{C},^{15}\text{N}$ labeled samples, all REDOR pulses are applied on the ^{15}N channel to avoid the recoupling of ^{13}C spins,^{62,63} and phased according to the xy -4 scheme⁵⁷ to compensate for pulse imperfections and resonance offset effects (pulse timings have been described in detail elsewhere⁴⁴). The MQ and anti-phase terms in the density matrix created by homonuclear J-evolution are suppressed using two z -filter periods, Δ , highlighted by gray rectangles. For 3D BASE TEDOR the band-selective ^{13}C pulse, centered in the period occupying an even number of rotor cycles ($2m\tau_r$), refocuses homonuclear J-couplings. The influence of proton couplings during the ^{13}C - ^{15}N recoupling periods is attenuated by a combination of continuous-wave (CW) and two-pulse phase modulation (TPPM)⁶⁴ decoupling as

described in detail previously.⁴⁴ TPPM decoupling was used during t_1 and t_2 . The delay, τ , following t_1 evolution ensures that the total delay between the REDOR mixing periods is equal to an integral number of rotor cycles and is crucial to the efficient reconversion of anti-phase coherences to observable ^{13}C magnetization.

6.3.2 Spin Dynamics in U- ^{13}C , ^{15}N Labeled Systems

We consider a uniformly ^{13}C , ^{15}N labeled sample spinning rapidly about the magic angle ($\theta_m = \tan^{-1}\sqrt{2}$) at a frequency far from rotational resonance conditions.⁶⁵ For the 3D TEDOR pulse sequence shown in Figure 6-1a, the spin system can be considered to evolve under isotropic chemical shifts and homonuclear J-couplings during the free evolution periods, t_1 and t_2 :

$$H = \sum_k \Omega_{I_k} I_{kz} + \sum_k \Omega_{S_k} S_{kz} + \sum_{j < k} \pi J_{jk} 2I_{jz} I_{kz}, \quad (1)$$

and under the recoupled heteronuclear dipolar interactions and homonuclear J-couplings during the two REDOR mixing periods, t_{mix} :

$$H = \sum_{j,k} \omega_{jk} 2I_{jz} S_{kz} + \sum_{j < k} \pi J_{jk} 2I_{jz} I_{kz}. \quad (2)$$

In the above expressions I and S angular momentum operators represent the ^{13}C and ^{15}N spins, respectively, Ω_I and Ω_S are the ^{13}C and ^{15}N isotropic chemical shifts, and J is the ^{13}C - ^{13}C J-coupling constant (in hertz). ω is the orientation-dependent effective ^{13}C - ^{15}N dipolar coupling reintroduced by the REDOR sequence (a detailed expression for ω can be found in ref 44 and references therein), which is a function of the dipolar coupling constant, D (in hertz), and hence the internuclear distance, r :

$$D = -\left(\frac{\mu_0}{4\pi}\right) \frac{\gamma_I \gamma_S \hbar}{2\pi r^3}. \quad (3)$$

Since all terms in eqs 1 and 2 commute with each other, the time-evolution of spin coherences can be derived using straightforward product-operator calculations.⁶⁶ A detailed analysis of the spin dynamics for a simple multiple spin system (I_2 - S) was performed explicitly. Complete results are presented in the Appendix and the most important points are summarized below. The main conclusion of the analysis is that the presence of a network of multiple J-coupled ^{13}C spins causes serious limitations for measuring weak ^{13}C - ^{15}N dipolar couplings in uniformly ^{13}C , ^{15}N labeled systems using 3D TEDOR schemes, which are not explicitly compensated for homonuclear J-couplings.

To derive the basic spin dynamics for 3D TEDOR experiments it is sufficient to monitor the evolution of the transverse magnetization for only one of ^{13}C nuclei in the I_2 - S system, for instance I_{1x} . During the REDOR mixing period the initial density operator evolves under the Hamiltonian in eq 2 according to:

$$I_{1x} \xrightarrow{\text{REDOR}} I_{1x} c_{\omega_1} c_J + 2I_{1y} I_{2z} c_{\omega_1} s_J + 2I_{1y} S_z s_{\omega_1} c_J - 4I_{1x} I_{2z} S_z s_{\omega_1} s_J, \quad (4)$$

where

$$\begin{aligned} s_{\omega_1} &= \sin(\omega_1 t_{\text{mix}} / 2) \\ c_{\omega_1} &= \cos(\omega_1 t_{\text{mix}} / 2) \\ s_J &= \sin(\pi J t_{\text{mix}} / 2) \\ c_J &= \cos(\pi J t_{\text{mix}} / 2) \end{aligned} \quad (5)$$

and ω_1 and J represent the I_1 - S dipolar coupling and the I_1 - I_2 J-coupling, respectively.

Equation 4 highlights the fundamental problems associated with the presence of homonuclear J-couplings during REDOR mixing. The initial transverse ^{13}C magnetization evolves not only into ^{13}C - ^{15}N anti-phase spin coherences ($\sim I_y S_z$), which

generate the desired cross-peaks at (Ω_s, Ω_I) in the 2D correlation spectra and give useful information about ^{13}C - ^{15}N distances, but also into multiple spin coherences that depend on ^{13}C - ^{13}C correlations. These are represented by zero-quantum (ZQ) and double-quantum (DQ) coherences with respect to the ^{13}C spin operators ($\sim I_{1x}I_{2y}S_y$) at the end of the first REDOR (excitation) period followed by 90° pulses on the I and S channels, and by anti-phase coherences ($\sim I_{1y}I_{2z}$) at the end of the second REDOR (reconversion) period. Evolution of these spurious coherences during t_1 and t_2 leads to severe distortions in the resulting 2D spectra. As shown in detail in the Appendix, additional cross-peaks occur in the indirect dimension and phase-twisted lineshapes develop along both spectral dimensions with increasing mixing time. These artifacts, which are not related to I - S dipolar couplings, degrade the spectral resolution and prohibit the extraction of reliable cross-peak intensities.

Two improved 3D TEDOR schemes are proposed to compensate for the detrimental effects of homonuclear J-couplings. In the 3D ZF TEDOR pulse sequence (Figure 6-1a), the spurious cross-peaks and phase-twisted lineshapes are suppressed by inserting two z -filters (highlighted by gray rectangles) prior to t_1 and t_2 free evolution periods. During the filtering periods the spin coherences, which give purely absorptive lines are stored longitudinally, while those responsible for the occurrence of anti-phase signals remain in the transverse plane and are rapidly dephased through the interaction with the abundant proton bath. The resulting 2D spectra contain a purely absorptive cross-peak located at $(\Omega_{N_j}, \Omega_{C_i})$ for each dipolar coupled carbon-nitrogen spin-pair, C_i - N_j . The cross-peak intensity is given by:

$$V_{ij}(t_{mix}) = V_i(0) \left\langle \sin^2(\omega_{ij} t_{mix} / 2) \prod_{k=1}^{N_i} \cos^2(\omega_{ik} t_{mix} / 2) \right\rangle \prod_{l=1}^{m_i} \cos^2(\pi J_{il} t_{mix} / 2). \quad (6)$$

Here $V_i(0)$ is the reference intensity for the i^{th} ^{13}C spin in the one-dimensional cross-polarization experiment, ω_{ij} is the active ^{13}C - ^{15}N dipolar coupling which generates the cross-peak located at $(\Omega_{N_j}, \Omega_{C_i})$, N_i is the number of ^{15}N spins simultaneously coupled to the i^{th} ^{13}C nucleus, the summation index k runs over n_i passive dipolar couplings, ω_{ik} , where $n_i = N_i - 1$, $\langle \dots \rangle$ represents the average over different crystallites in the powder, and the summation index l runs over m_i ^{13}C spins J-coupled to the i^{th} ^{13}C spin. We note that for an isolated I - S spin pair with no I -spin J-coupling partners and in the absence of relaxation, the maximum achievable cross-peak intensity is approximately 52% of the reference cross-polarization intensity.³⁰ In a model spin-pair, [2 - ^{13}C , ^{15}N]glycine with $D \approx 900$ Hz, we have achieved a TEDOR coherence transfer efficiency of $\sim 45\%$ of the cross-polarization signal, which compares well with the theoretical maximum of 52% (data not shown).

3D ZF TEDOR allows all carbon-nitrogen distances to be measured simultaneously in a single 3D experiment. For the i^{th} ^{13}C resonance located at frequency Ω_{C_i} in the direct dimension, a pattern of N_i cross-peaks emerges in the indirect dimension with increasing mixing time. Qualitatively, each $(\Omega_{N_j}, \Omega_{C_i})$ cross-peak builds up at a rate which directly reflects the strength of the corresponding active dipolar coupling, ω_{ij} , and N_i provides information about the effective size of the ^{13}C - ^{15}N spin cluster (i.e., number of ^{15}N spins simultaneously coupled to the i^{th} ^{13}C spin, for which the ^{13}C - ^{15}N couplings are sufficiently strong for the cross-peaks to be detectable experimentally). For most accurate distance measurements, however, the dependencies on all interaction parameters included in eq 6, as well as the influence of relaxation and experimental imperfections, must be

rigorously taken into account (see Internuclear Distance Measurements section below for details).

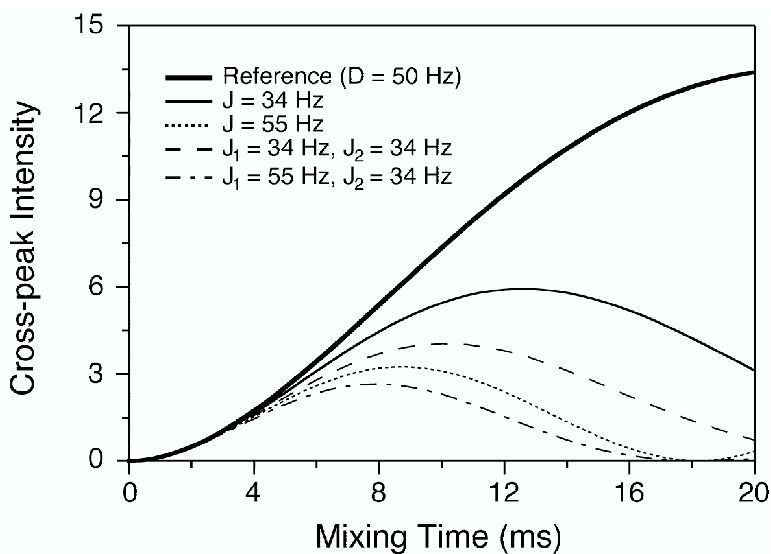


Figure 6-2. TEDOR cross-peak simulations.

TEDOR cross-peak buildup curves simulated using eq 6 for a ^{13}C - ^{15}N spin-pair with the dipolar coupling $D = 50$ Hz ($r = 4$ Å). The ^{13}C - ^{15}N spin-pair is considered to be either isolated (thick solid line) or in the presence of one- or two additional J-coupled ^{13}C nuclei. For each coupling topology, the strengths of the ^{13}C - ^{13}C J-couplings are given in the inset (values typical for U- ^{13}C labeled peptides were used), and the buildup curves were multiplied by $\exp(-\Gamma t_{\text{mix}})$, with $\Gamma = 50$ s $^{-1}$, to model relaxation effects. For these and all other TEDOR buildup curves shown in this paper the cross-peak intensities are given as a percentage of the ^{13}C signal in a reference one-dimensional cross-polarization experiment (i.e., $V(0) = 100$ in eq 6).

Although the 3D ZF TEDOR pulse sequence suppresses ^{13}C coherences responsible for artifacts in the 2D spectra, the distribution of the initial magnetization among multiple coherences reduces the amount of the available spin order that is stored in ^{13}C - ^{15}N dipolar correlations. Quantitatively, this is described in eq 6 by the J-modulation of cross-peak intensities (contained in the $\cos^2(\pi J t_{\text{mix}}/2)$ terms), where the extent of the modulation for a particular ^{13}C site depends on the exact coupling topology (i.e., number of J-coupled ^{13}C spins and the corresponding coupling strengths). In Figure

6-2 we present a series of simulated TEDOR cross-peak buildup curves for a 50 Hz dipolar coupling (corresponding to a ^{13}C - ^{15}N distance of 4 Å) and several J-coupling topologies typical for U- ^{13}C labeled peptides. The cross-peak intensities in the presence of J-couplings are found to be reduced approximately 2- to 5-fold for the various topologies investigated. As expected, the effects are the smallest for weakly J-coupled ^{13}C sites (e.g., sidechain CH_3 groups) and most severe for strongly coupled sites (e.g., CO and C^α); this limits the range of ^{13}C - ^{15}N dipolar couplings observable experimentally for strongly J-coupled ^{13}C nuclei using 3D ZF TEDOR.

Homonuclear J-couplings can be suppressed in solid-state NMR experiments using band-selective refocusing pulses as demonstrated previously,^{43,44,55} and here we have adapted this J-decoupling strategy in the context of 3D TEDOR experiments. The resulting band-selective experiment (3D BASE TEDOR) shown in Figure 6-1b refocuses homonuclear J-couplings between ^{13}C spins within the selective pulse bandwidth and ^{13}C spins outside the bandwidth, and extends the range of ^{13}C - ^{15}N distances that can be measured for strongly J-coupled ^{13}C sites. Assuming that ^{13}C - ^{13}C J-couplings between nuclei within the selective pulse bandwidth are negligible, the REDOR mixing Hamiltonian is purely dipolar:

$$H = \sum_{j,k} \omega_{jk} 2I_{jz} S_{kz}, \quad (7)$$

where the summation index j runs over ^{13}C spins inverted by the selective pulse. The cross-peak intensities are given by:

$$V_{ij}(t_{mix}) = V_i(0) \left\langle \sin^2(\omega_{ij} t_{mix} / 2) \prod_{k=1}^{N_i} \cos^2(\omega_{ik} t_{mix} / 2) \right\rangle, \quad (8)$$

where all terms have been defined in eq 6. We note that homonuclear J-decoupling is achieved at the expense of distance measurements being limited to those ^{13}C spins having resonance frequencies within the selective pulse bandwidth, which requires the acquisition of multiple 3D NMR spectra to cover the full ^{13}C spectral window.

6.3.3 Internuclear Distance Measurements

In principle, internuclear distances from the N_i ^{15}N nuclei dipolar coupled to the i^{th} ^{13}C spin can be determined from the 3D ZF TEDOR experiment by fitting the buildup of cross-peaks located at $(\Omega_{Nk}, \Omega_{Ci})$ in the 2D spectra, where $k = 1, 2, \dots, N_i$, with a set of N_i equations of the form given in eq 6, which depend on N_i dipolar couplings and m_i J-couplings. For 3D BASE TEDOR the J-couplings can be neglected (see eq 8). In addition, parameters describing relaxation and experimental imperfections must be included in the simulations. The major difficulty associated with this approach is that the cross-peak buildup exhibits a formal dependence on the relative orientation of the N_i dipolar couplings. This would require the use of Euler angles describing the orientations of all dipolar tensors as additional fit parameters, which is impractical.

Instead, we use a simple analytical model to fit the cross-peak intensities and extract carbon-nitrogen distances. The approach is based on Bessel function expansions of dipolar-dephasing NMR signals derived by Mueller⁶⁷ and it provides an approximate description of the TEDOR spin dynamics, which depends on dipolar coupling magnitudes alone and is free of geometric parameters. Below we summarize the main features of the model and evaluate its utility for distance measurements by comparison with “exact” TEDOR cross-peak buildup simulations for an I - S_2 spin system.

As shown in detail by Mueller⁶⁷ the cosine modulated REDOR dipolar dephasing signal for individual crystallites in a powder sample can be written:

$$S_{REDOR}(t) = \cos(\omega t) = \left[J_0(\sqrt{2}Dt) \right]^2 + f\left(J_k(\sqrt{2}Dt), \beta, \gamma \right). \quad (9)$$

Here ω is the orientation-dependent effective ^{13}C - ^{15}N dipolar coupling reintroduced by the REDOR sequence (c.f. eq 2), t is a generalized time variable, D is the dipolar coupling constant (c.f. eq 3), $J_0(x)$ is a Bessel function of zeroth order, and $f\left(J_k(x), \beta, \gamma \right)$ is a complicated expression which depends on infinite series of Bessel functions, $J_k(x)$, and Euler angles, β and γ , describing the orientation of the dipolar tensor in the rotor-fixed reference frame. The first few terms of the Bessel function expansion provide an excellent description of the powder averaged REDOR dephasing signal;⁶⁷ in fact the $J_0(x)$ term alone gives a reasonable approximation. These observations are equally valid for TEDOR experiments.⁶⁷

Utilizing such a zeroth order approximation we proceed to describe the 3D TEDOR experiments by neglecting all orientation dependent terms in eq 9. The resulting simulation model consists of a set of N_i equations, which are used to simultaneously fit the buildup of N_i cross-peaks corresponding to the i^{th} ^{13}C nucleus:

$$\begin{aligned} V_{i1}(t_{mix}) &= \Lambda_i \left(1 - \left[J_0(\sqrt{2}D_{i1}t_{mix}) \right]^2 \right) \prod_{k=2}^{N_i} \left(1 + \left[J_0(\sqrt{2}D_{ik}t_{mix}) \right]^2 \right) \\ V_{i2}(t_{mix}) &= \Lambda_i \left(1 - \left[J_0(\sqrt{2}D_{i2}t_{mix}) \right]^2 \right) \prod_{k=1,2}^{N_i} \left(1 + \left[J_0(\sqrt{2}D_{ik}t_{mix}) \right]^2 \right) \\ &\vdots \\ V_{iN_i}(t_{mix}) &= \Lambda_i \left(1 - \left[J_0(\sqrt{2}D_{iN_i}t_{mix}) \right]^2 \right) \prod_{k=1}^{N_i-1} \left(1 + \left[J_0(\sqrt{2}D_{ik}t_{mix}) \right]^2 \right) \end{aligned} \quad (10)$$

For 3D ZF TEDOR the expression for Λ_i is given by

$$\Lambda_i = \frac{1}{2^{N_i}} V_i(0) \lambda_i \exp(-\Gamma_i t_{mix}) \prod_{l=1}^{m_i} \cos^2(\pi J_{il} t_{mix} / 2), \quad (11)$$

whereas for the band-selective experiment the J-coupling terms can be neglected:

$$\Lambda_i = \frac{1}{2^{N_i}} V_i(0) \lambda_i \exp(-\Gamma_i t_{mix}). \quad (12)$$

Most terms in eqs 10-12 have been defined in eqs 6 and 9. The relaxation of spin coherences due to insufficient proton decoupling is modeled as a single exponential with the relaxation rate, Γ_i . The constant, λ_i , describes the amplitude scaling of cross-peaks, which can arise from experimental imperfections, higher order CSA and ^{13}C - ^{13}C , ^1H - ^{13}C and ^1H - ^{15}N dipolar coupling effects, and possible systematic deviations associated with the description of experimental data using the approximate model (see discussion below). For the peptides investigated here amplitude scaling factors were in the $\lambda = 0.5$ -1.0 range, and typical relaxation rates were $\Gamma = 50$ -150 s^{-1} . The use of single λ_i and Γ_i parameters to fit all cross-peaks corresponding to the i^{th} ^{13}C spin reduces the number of required fit parameters and is justified because the experimental and internal molecular parameters contributing to relaxation and amplitude scaling for each of the $(\Omega_{Nk}, \Omega_{Ci})$ cross-peaks do not depend on whether a given ^{13}C - ^{15}N coupling is active or passive (c.f. eq 6). We note here that we have attempted to use separate two-dimensional spin-echo experiments with ^{13}C - ^{13}C J-decoupling⁴³ to independently determine the ^{13}C relaxation rate, Γ . For the majority of ^{13}C sites in N-ac-VL the spin-echo relaxation rates were found to be somewhat smaller than the values of Γ giving the best fits to cross-peaks observed in the 3D TEDOR experiments, and can therefore be used to provide a lower bound for Γ .

In summary, the main features of the simulation model are: (i) for the i^{th} ^{13}C nucleus coupled to N_i ^{15}N spins all N_i ^{13}C - ^{15}N distances are determined by simultaneously

fitting the experimentally observed buildup of cross-peaks located at $(\Omega_{Nk}, \Omega_{Ci})$, $k = 1, 2, \dots, N_i$, using eqs 10-12 with $N_i + 2$ fit parameters (N_i dipolar coupling constants, D_{ik} , a relaxation rate, Γ_i , and an amplitude scaling factor, λ_i), (ii) no knowledge of dipolar tensor orientations and no powder averaging are required, and (iii) the cross-peak intensities at long mixing times are inversely proportional to the number of ^{15}N spins, N_i , simultaneously coupled to the ^{13}C nucleus, $V_{ik}(t_{mix}) \propto (2^{N_i})^{-1}$, which places a practical limit on the magnitude of the weakest ^{13}C - ^{15}N couplings that can be determined using 3D TEDOR methods (for the di- and tripeptides investigated in this work ^{13}C - ^{15}N dipolar couplings corresponding to distances in the 4-6 Å regime could be determined). We note that for 3D ZF TEDOR the buildup of cross-peaks for the i^{th} ^{13}C nucleus also depends on the coupling topology of the m_i J-coupled ^{13}C nuclei (c.f. eq 11). These parameters are held constant in the simulations since ^{13}C - ^{13}C J-couplings in peptides do not vary significantly for different types of couplings (i.e., CO- C^α , C^α - C^β , etc.).⁵³ We measured the ^{13}C - ^{13}C J-couplings (see Table 6-1) in N-acetyl-L-Val-L-Leu and found them to be clustered closely around the reported average values.⁵³ For N-acetyl-L-Val-L-Leu cross-peak simulations the experimentally determined J-couplings were used. For N-formyl-L-Met-L-Leu-L-Phe the J-coupling constants were not explicitly determined and in simulations we used the values: $^1J_{\text{CO}-\text{C}^\alpha} = 55$ Hz and $^1J_{\text{C}^\alpha-\text{C}^\beta} = ^1J_{\text{C}^\beta-\text{C}^\gamma} = ^1J_{\text{C}^\gamma-\text{C}^\delta} = 34$ Hz.

6.3.4 Uncertainties in the Measured Distances

In the following section, we discuss the uncertainties in distances determined using 3D TEDOR experiments. Specifically, we have investigated the errors due to: (i) random noise, (ii) use of incorrect values of ^{13}C - ^{13}C J-coupling constants in 3D ZF TEDOR simulations, and (iii) use of approximate analytical expressions in eqs 10-12 to model the cross-peak buildup. For the model peptides investigated here we have found that carbon-nitrogen distances could be measured with the relative precision of approximately ± 10 - 20% , where the uncertainty is mainly attributed to the use of the approximate simulation model.

Table 6-1. Carbon-Carbon J-Coupling Constants in N-acetyl-L-Val-L-Leu

atoms		$^1J_{CC}$ (Hz)
Ac(CO)	Ac(C $^\alpha$)	51
Val(CO)	Val(C $^\alpha$)	52
Leu(CO)	Leu(C $^\alpha$)	61
Val(C $^\alpha$)	Val(C $^\beta$)	35
Leu(C $^\alpha$)	Leu(C $^\beta$)	34
Val(C $^\beta$)	Val(C $^\gamma^1$)	35
Val(C $^\beta$)	Val(C $^\gamma^2$)	32
Leu(C $^\beta$)	Leu(C $^\gamma$)	37
Leu(C $^\gamma$)	Leu(C $^{\delta^1}$)	35
Leu(C $^\gamma$)	Leu(C $^{\delta^2}$)	28

Coupling constants were measured using a two-dimensional spin-echo sequence described elsewhere.⁴³ In fitting the experimental J-dephasing curves we assumed the contributions from $^2J_{CC}$ and weaker couplings to be negligible.

The effects of random noise were evaluated using a Monte Carlo approach.⁶⁸ For each set of N_i experimental cross-peak buildup curves corresponding to the i^{th} ^{13}C spin, a large number of sets of buildup curves ($N \geq 1000$) were generated by adding to each mixing time point a random amount of noise with a Gaussian probability distribution (the width of the distribution was determined by the experimental signal-to-noise ratio

measured from the 2D spectra). Each set of generated curves was subsequently fit using a grid of simulated cross-peak buildup curves, where each curve in the grid was calculated as a function of the internuclear distances, relaxation rate and scaling factor. The fitting was performed for the N random noise trials and best-fit parameters for each trial were stored. The best-fit results for each trial were subsequently used to generate probability distribution plots for the different fit parameters; the final best-fit distances were extracted from the average of the distribution, and the width of the distribution provided a measure of the random error in the measured distances. The signal-to-noise ratio for the model peptides investigated here was relatively high and for the majority of ^{13}C sites the errors in the measured distances due to random noise were found to be less than $\pm 0.1 \text{ \AA}$.

For 3D ZF TEDOR the effect of using incorrect ^{13}C - ^{13}C J-coupling constants (c.f. eq 11) on the ^{13}C - ^{15}N distance measurements was also investigated. For N-acetyl-L-Val-L-Leu, where the exact values of the J-couplings are known (see Table 6-1), we found that the best-fit distances were not appreciably affected when incorrect J-couplings (which differed by as much as $\pm 25\%$ from the actual values) were used in the simulations. Quantitatively, the differences in the best-fit ^{13}C - ^{15}N distances were less than $\pm 0.1 \text{ \AA}$ for distances in the 4 \AA regime.

As noted above, the approximate model used to describe the buildup of cross-peaks in the 2D spectra is the main source of uncertainty in the ^{13}C - ^{15}N distances measured using 3D TEDOR experiments. In order to quantify these systematic errors we have compared the approximate model described in eq 10 with “exact” powder averaged simulations based on average Hamiltonian theory (AHT)⁶⁹ (see eq 8) for a model I - S_2 spin system. A grid of exact simulations was generated using eq 8 for pairs of dipolar

couplings with varying magnitudes and relative orientations. Specifically, the buildup curves were calculated for mixing times $t_{mix} = 0-20$ ms. Distances between 1.2 and 5.0 Å were used with a 0.1 Å increment, and for each pair of couplings the angle, θ , between the dipolar vectors was varied between 0° and 90° in 10° increments (the amplitude scaling factor and relaxation rate were set to $\lambda = 0.5$ and $\Gamma = 50$ s⁻¹, respectively, for the exact simulations). Subsequently, each exact simulation in the grid was fit using a grid of approximate simulations generated using eq 10 for distances in the 1.0-7.0 Å range, where the parameters λ and Γ were allowed to vary freely during the fit.

The results of fitting the exact AHT simulations using the approximate analytical model are presented in Figure 6-3. Overall, the analytical model provides a good description of the spin dynamics in the $I-S_2$ system for the various coupling topologies (perfect agreement is indicated by the solid line of slope 1.0). For a given exact simulation input distance corresponding to the active dipolar coupling, the majority of best-fit distances obtained from the approximate simulations, which span a wide range of passive couplings and relative orientations, are well within $\pm 10\%$ of the input distance (indicated by the dashed lines) and virtually all best-fit distances are within $\pm 20\%$ of the input distance (indicated by the dotted lines). A closer examination of the results indicates that the approximate best-fit distances, which differ by more than 10% from the input distance used for the AHT simulation, correspond to a small subset of coupling topologies for which the two dipolar couplings are of similar magnitude and the angle between the dipolar vectors is in the $\theta = 0-20^\circ$ range. This is consistent with previous observations.^{25,36} The uncertainties of $\pm 10-20\%$ in the 3D TEDOR distance measurements are reasonable, and the utility of the simple analytical simulation model is further

supported by good correspondence between the NMR and X-ray distances determined for the di- and tripeptides investigated here (see Results and Discussion section).

Finally, we note that the uncertainties in the distances measured using 3D TEDOR experiments are somewhat larger than those obtained for frequency selective REDOR measurements. For example, the error in a ^{13}C - ^{15}N distance measured as 4.0 Å using 3D TEDOR can be assumed to be in the ± 0.4 - 0.8 Å range. By comparison, distances in the 4 Å regime measured using FSR had typical uncertainties on the order of 0.1-0.2 Å.⁴⁴ The 3D TEDOR experiments, however, provide a more general approach to the determination of multiple structural constraints in uniformly ^{13}C , ^{15}N labeled systems.

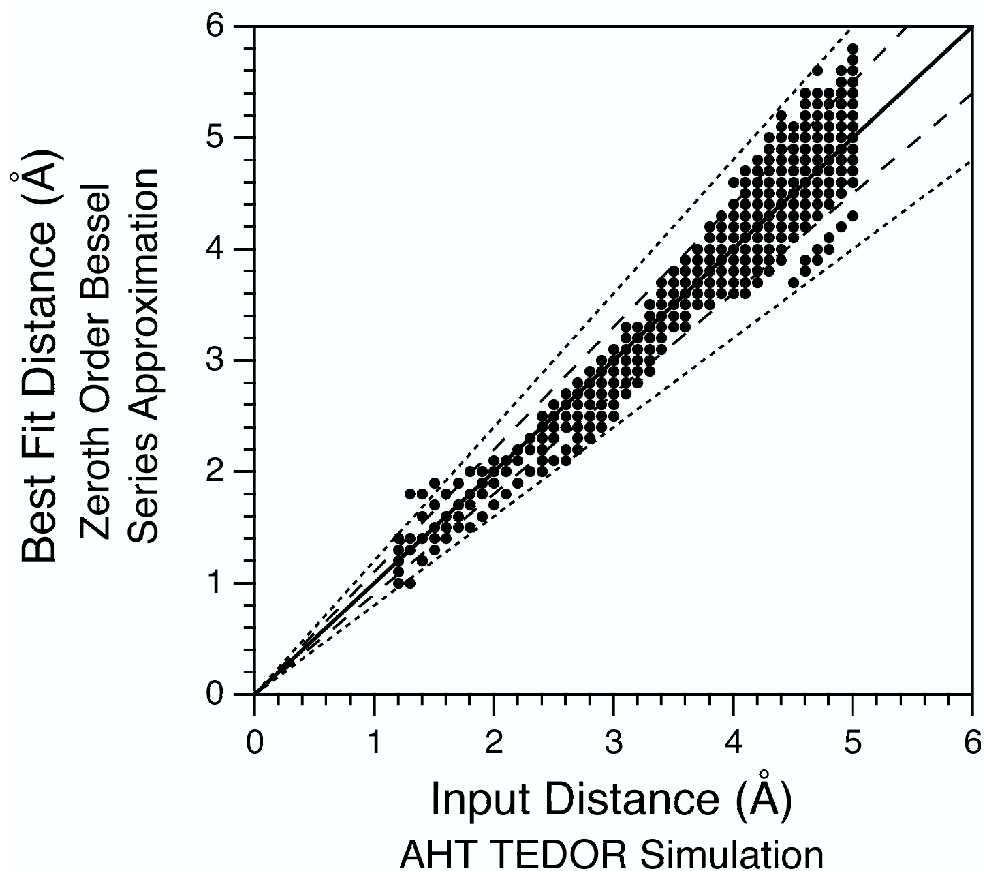


Figure 6-3. Comparison of the approximate simulation model with average Hamiltonian simulations for an $I-S_2$ spin system.

A grid of TEDOR buildup curves based on average Hamiltonian theory was generated using eq 8 for pairs of dipolar couplings with different magnitudes and relative orientations (see text for details). The AHT TEDOR simulations were subsequently fit using the approximate analytical model in eq 10. Perfect agreement between the input distances used for the AHT calculations and best-fit distances obtained using the approximate model is indicated by the solid line of slope 1.0. Discrepancies between the input and best-fit distances of $\pm 10\%$ and $\pm 20\%$ are indicated by the dashed and dotted lines, respectively.

6.4 Results and Discussion

6.4.1 Distance Measurements in $[U-^{13}\text{C}, ^{15}\text{N}]$ N-acetyl-Val-Leu

In the following we apply the 3D TEDOR experiments to the simultaneous measurement of multiple carbon-nitrogen distances in $U-^{13}\text{C}, ^{15}\text{N}$ labeled peptides, N-acetyl-L-Val-L-Leu (N-ac-VL) and N-formyl-L-Met-L-Leu-L-Phe (N-f-MLF).

N-acetyl-L-Val-L-Leu represents an excellent model system for the 3D TEDOR experiments. The three-dimensional structure of the peptide (see Figure 6-4) has been determined using X-ray crystallography.⁷⁰ Furthermore, various SSNMR structural studies, which include complete ^{13}C and ^{15}N resonance assignments and carbon-nitrogen distance measurements,⁴⁴ have been performed for N-ac-VL.

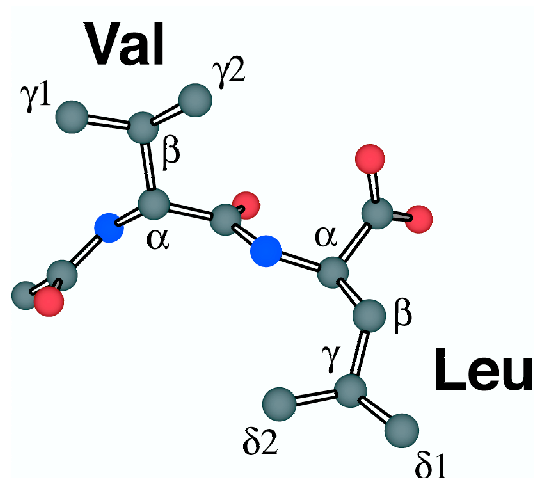


Figure 6-4. X-ray crystal structure of N-acetyl-L-Val-L-Leu.

In Figure 6-5 we show representative two-dimensional slices from the broadband 3D TEDOR experiments corresponding to mixing times in the range $t_{mix} \approx 4-16$ ms. The spectra in Figures 6-5a – 6-5c and Figures 6-5d – 6-5f were acquired using the pulse

sequence in Figure 6-1a with the z -filter periods (highlighted by gray rectangles) omitted and included, respectively. For clarity only the aliphatic ^{13}C resonances are shown, where the cross-peak assignments are based on previous studies.⁴⁴ While for short mixing times ($t_{mix} \approx 1\text{-}2$ ms), which reveal correlations between directly bonded ^{13}C and ^{15}N nuclei, the 2D spectra with and without the z -filter periods are nearly identical, for longer mixing times the spectra are clearly degraded due to ^{13}C - ^{13}C J-evolution as described in detail in the Appendix. The essential spectral features due to the J-couplings in the form of spurious cross-peaks and phase-twisted lines are observed experimentally (Figures 6-5a – 6-5c). These artifacts can be suppressed using the z -filter periods resulting in 2D spectra with pure absorption mode peaks (Figures 6-5d – 6-5f), and hence optimal resolution and sensitivity.

For N-acetyl-L-Val-L-Leu a number of ^{13}C - ^{15}N correlations are observed in Figure 6-5. Each cross-peak is labeled with the ^{13}C and ^{15}N frequencies characteristic of the dipolar coupled nuclei, and can be used to obtain internuclear distance information. In Figure 6-6 we demonstrate the 3D TEDOR distance measurements from Val C^{β} and both Val C^{γ} carbons to the Val and Leu nitrogens. The cross-peak intensities, corresponding to carbon-nitrogen distances in the 2.5-4.7 Å range, are plotted in Figures 6-6a - 6-6c as a function of the TEDOR mixing time, t_{mix} . The internuclear distances were determined by fitting the experimental buildup curves using the analytical model described in the Theoretical Background section (c.f. eq 10).

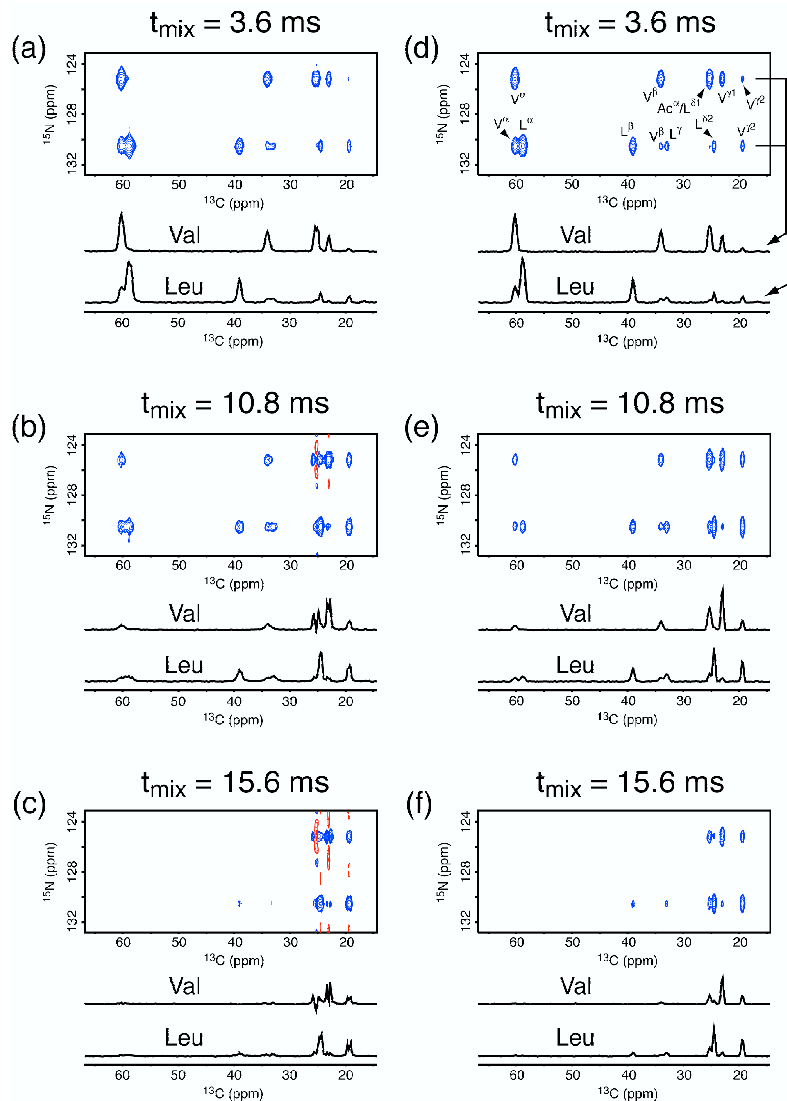


Figure 6-5. Representative two-dimensional slices from broadband 3D TEDOR experiments in [U- ^{13}C , ^{15}N]N-acetyl-L-Val-L-Leu.

Spectra were recorded using the pulse sequence in Figure 6-1a without (a)-(c) and with (d)-(f) z -filters. The experiments demonstrate that the use of z -filters eliminates the detrimental effects of ^{13}C - ^{13}C J-couplings and leads to pure absorption mode spectra (see text for details). Positive and negative contours are shown in black and grey, respectively. The experiments were performed at 500 MHz ^1H frequency, $\omega_r/2\pi = 10 \text{ kHz} \pm 5 \text{ Hz}$ and the z -filter delays of $\Delta = 200 \mu\text{s}$ were used. Additional experimental parameters are described in the text. The 3D data set used to extract carbon-nitrogen distances was recorded using the z -filtered sequence as (11, 1024, 16) points in $(t_1, t_2, t_{\text{mix}})$, with time increments of (2.0, 0.02, 1.2) ms resulting in acquisition times of (20.0, 20.5, 18.0) ms. Each FID was 64 scans, the recycle delay was 3 s, and (t_1, t_2) points were acquired as complex pairs for phase sensitive detection,⁵⁹ yielding a total measurement time of ~ 20 h.

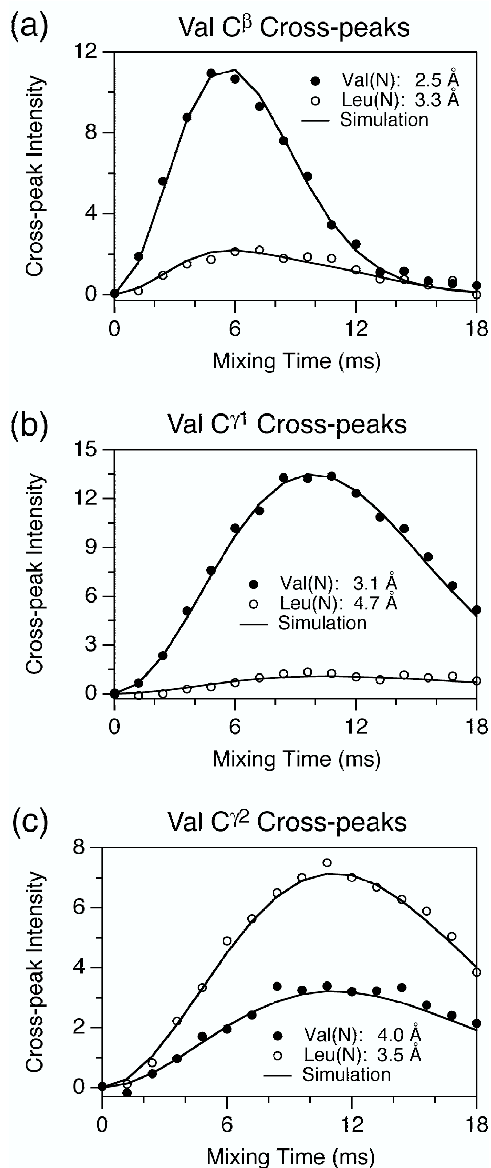


Figure 6-6. 3D ZF TEDOR cross-peak buildup curves in [U- ^{13}C , ^{15}N]N-acetyl-L-Val-L-Leu.

The buildup curves were acquired using the pulse sequence in Figure 6-1a and correspond to cross-peaks observed for the Val C β (a), Val C γ^1 (b) and Val C γ^2 (c) resonances in the 2D correlation spectra in Figures 6-5d – 6-5f. For each ^{13}C the experimental buildup curves corresponding to the Val (●) and Leu (○) ^{15}N sites were fit (—) using analytical expressions in eq 10 based on the zeroth order Bessel function approximation. The ^{13}C - ^{13}C J-coupling constants used in the fits were measured in a separate experiment (see Table 6-1). The cross-peak buildup curves shown correspond to carbon-nitrogen distances in the 2.5-4.7 Å regime (the actual distances measured are noted in the insets). Similar simulations were performed for the remaining cross-peaks (c.f. Figure 6-5) and the resulting ^{13}C - ^{15}N internuclear distances are summarized in Table 6-2.

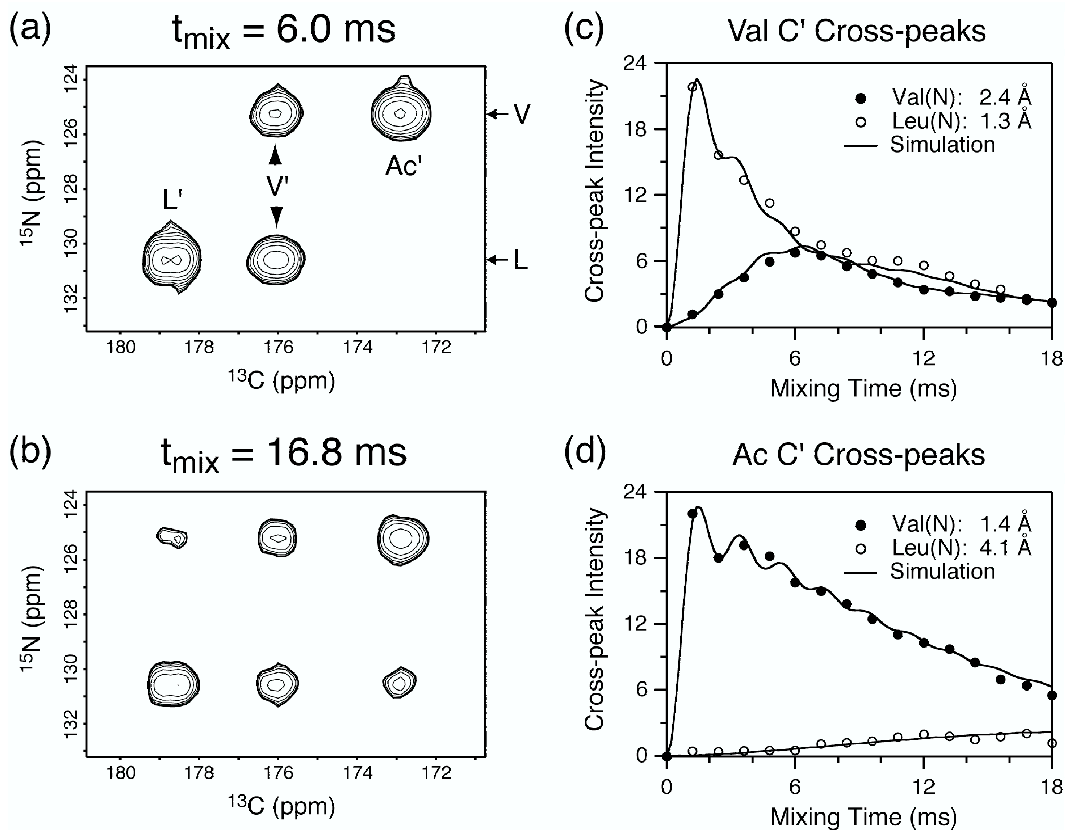


Figure 6-7. Representative two-dimensional slices from the 3D BASE TEDOR experiment for ^{13}C nuclei and cross-peak buildup curves in $[\text{U-}^{13}\text{C}, ^{15}\text{N}]\text{N-acetyl-L-Val-L-Leu}$.

The pulse sequence in Figure 6-1b was used with the carrier placed in the carbonyl region and a Gaussian band-selective ^{13}C refocusing pulse of 0.4 ms. Experimental parameters are described in the text and the 3D data set was recorded as described in Figure 6-5. For the relatively short TEDOR mixing time (a) only the trivial one- and two-bond ^{13}C - ^{15}N correlations are observed. However, with a longer mixing period (b) all cross-peaks expected in the CO region are detected (we note that cross-peaks corresponding to the weakest dipolar couplings were at the limit of detection using the 3D ZF TEDOR sequence). The buildup curves for Val C' (c) and Ac C' (d) corresponding to the Val (●) and Leu (○) ^{15}N sites were fit (—) using analytical expressions in eq 10 and the distances measured are found in the insets. All ^{13}C - ^{15}N internuclear distances measured in N-ac-VL are summarized in Table 6-2.

For ^{13}C nuclei having relatively strong J-couplings to other ^{13}C spins, such as CO and C^α , cross-peaks corresponding to approximately 4 Å and longer distances were found to be at the limit of detection using 3D ZF TEDOR even for the simple spin system of two ^{15}N nuclei represented by N-acetyl-L-Val-L-Leu. Specifically, the Ac(C')-Leu(N)

and Leu(C')-Val(N) cross-peaks had very poor signal-to-noise ratios and the corresponding distances were difficult to quantify. Using the band-selective pulse sequence (3D BASE TEDOR) shown in Figure 6-1b, which refocuses the homonuclear J-couplings, cross-peaks corresponding to the weak dipolar couplings could be easily detected (Figure 6-7). Their buildup curves were used to measure the ^{13}C - ^{15}N internuclear distances.

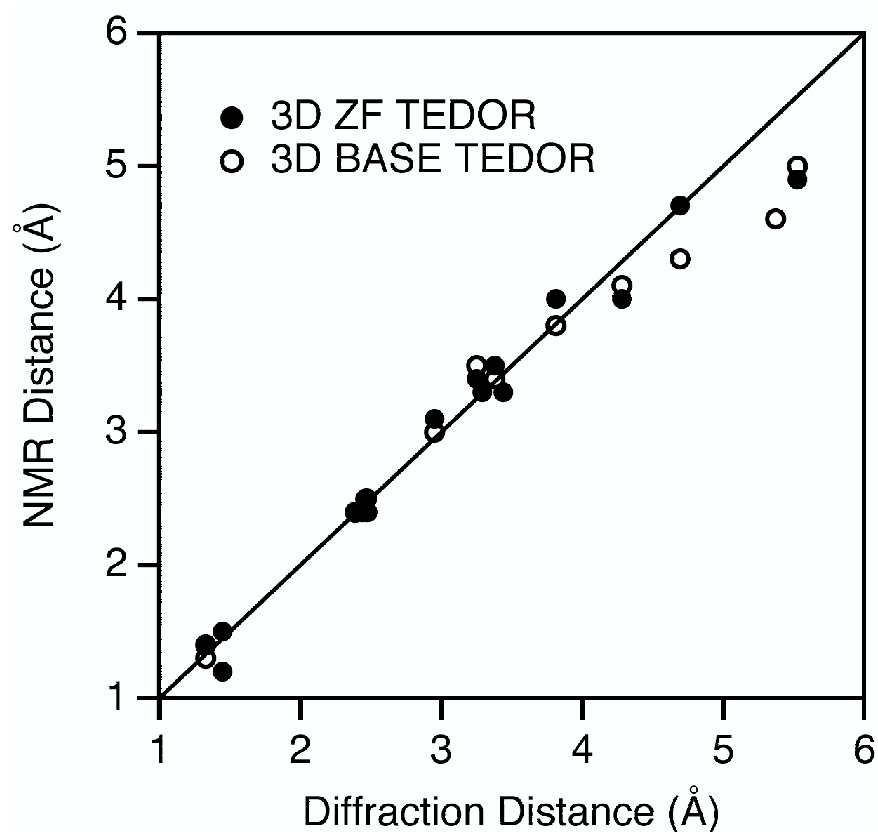


Figure 6-8. Summary of distance measurements in N-acetyl-L-Val-L-Leu.

Comparison of carbon-nitrogen distances in N-acetyl-L-Val-L-Leu measured using X-ray diffraction⁷⁰ and 3D ZF TEDOR (●) and 3D BASE TEDOR (○) experiments (see text for discussion of uncertainties in measured distances).

The carbon-nitrogen distance measurements in N-acetyl-L-Val-L-Leu are summarized in Figure 6-8 and Table 6-2. A total of 20 distances between ~ 1.3 - 5 Å were

measured in the peptide using 3D ZF TEDOR and 3D BASE TEDOR. The measured distances are in good agreement with the X-ray crystal structure⁷⁰ and previous SSNMR studies.⁴⁴ Note that the slight systematic discrepancy between X-ray and NMR results for the longest distances measured ($r > \sim 4.5$ Å) is most likely caused by residual intermolecular dipolar couplings resulting from the insufficient dilution of [U-¹³C, ¹⁵N]N-ac-VL in natural abundance N-ac-VL.

Table 6-2. Internuclear Distances in N-acetyl-L-Val-L-Leu

atoms		r_{C-N} (Å) ^a		
		3D ZF TEDOR	3D BASE TEDOR ^b	X-ray ^c
Val(N)	Ac(C')	1.4	1.4	1.33
	Ac(C ^α)	2.4	2.4	2.39
	Val(C')	2.4	2.4	2.39
	Val(C ^α)	1.5	—	1.45
	Val(C ^β)	2.5	—	2.46
	Val(C ^{γ1})	3.1	3.0	2.95
	Val(C ^{γ2})	4.0	3.8	3.81
	Leu(C')	—	4.6	5.37
Leu(N)	Leu(C ^{δ2})	4.9	5.0	5.52
	Ac(C')	4.0	4.1	4.28
	Val(C')	1.4	1.3	1.33
	Val(C ^α)	2.4	—	2.44
	Val(C ^β)	3.3	—	3.44
	Val(C ^{γ1})	4.7	4.3	4.69
	Val(C ^{γ2})	3.5	3.4	3.38
	Leu(C')	2.4	2.5	2.47
	Leu(C ^α)	1.2	—	1.45
	Leu(C ^β)	2.4	—	2.48
	Leu(C ^γ)	3.3	—	3.29
	Leu(C ^{δ2})	3.4	3.5	3.25

^aSee text for a detailed discussion of uncertainties associated with the NMR distance measurements. ^bMeasurements of distances marked with a (—) for 3D BASE TEDOR were not attempted. ^cRef 70.

6.4.2 Distance Measurements in N-formyl-[U- ^{13}C , ^{15}N]Met-Leu-Phe

N-formyl-L-Met-L-Leu-L-Phe represents a more complicated spin system, where each ^{13}C can interact with up to three ^{15}N nuclei. Figure 6-9 shows the X-ray crystal structure of the methyl ester analogue of N-f-MLF, N-formyl-L-Met-L-Leu-L-Phe-OMe (N-f-MLF-OMe).⁷¹ A number of ^{13}C - ^{15}N distances in N-f-MLF were determined previously using frequency selective REDOR and found to be in good agreement with the corresponding distances in N-f-MLF-OMe.⁴⁴ In fact, the overall three-dimensional structure of N-f-MLF determined recently using SSNMR methods,⁵⁰ is in close agreement with the N-f-MLF-OMe X-ray structure.

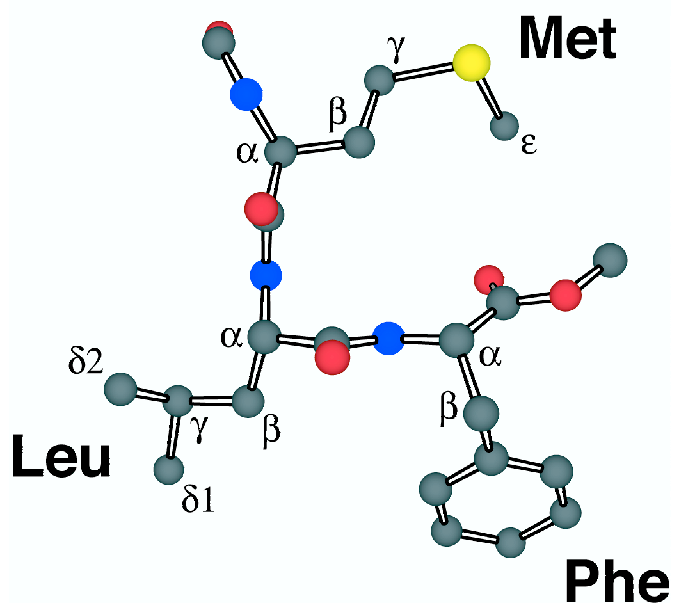


Figure 6-9. X-ray crystal structure of N-formyl-L-Met-L-Leu-L-Phe-OMe.

Figure 6-10 shows representative 2D ^{15}N - ^{13}C correlation spectra in N-formyl-[U- ^{13}C , ^{15}N]L-Met-L-Leu-L-Phe recorded using 3D ZF TEDOR. A large number of dipolar correlations (~ 20) are observed in the aliphatic ^{13}C region for the spectrum acquired with

10 ms of TEDOR mixing (Figure 6-10c), and each cross-peak carries information about ^{13}C - ^{15}N internuclear distances. The ^{13}C and ^{15}N resonance assignments for N-f-MLF have been presented in previous studies.^{4,44,72} The 3D ZF TEDOR cross-peak buildup curves for selected ^{13}C sites corresponding to distances in the 2.5-5.8 Å range are shown in Figure 6-11.

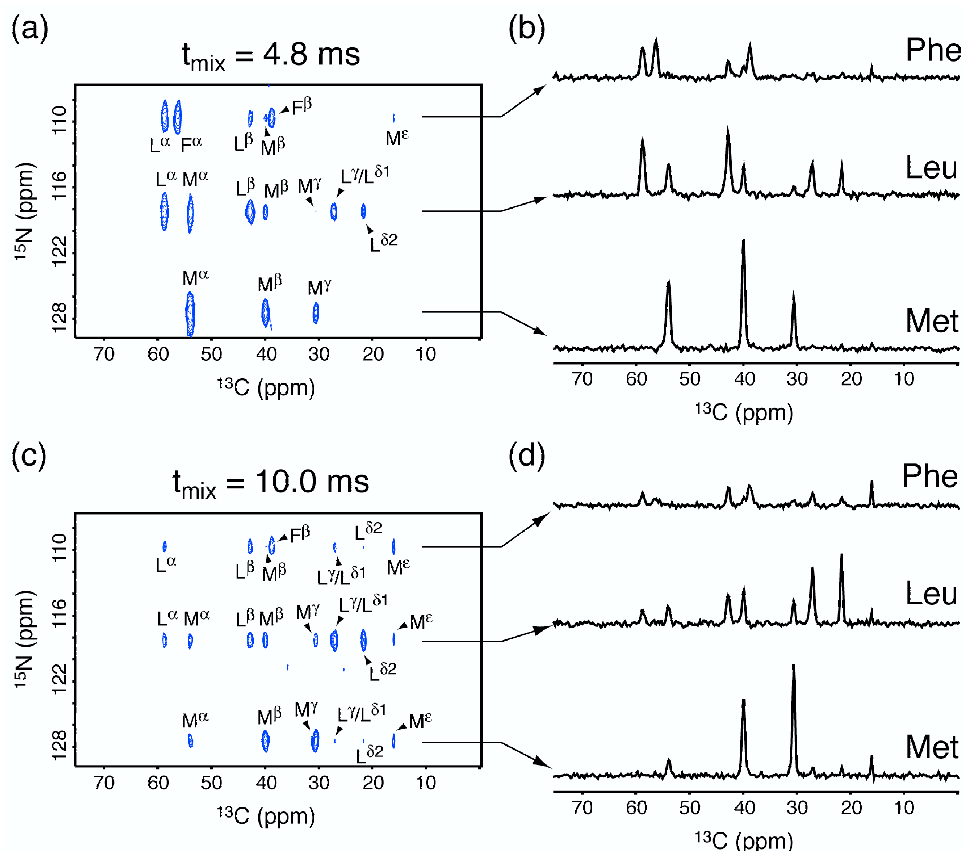


Figure 6-10. Representative two-dimensional slices for the 3D ZF TEDOR experiment in N-formyl-[U- ^{13}C , ^{15}N]L-Met-L-Leu-L-Phe.

The 2D spectra shown in (a) and (c) (with the 1D slices corresponding to Met, Leu and Phe ^{15}N resonances shown in (b) and (d)) were recorded at 500 MHz ^1H frequency and $\omega_r/2\pi = 10 \text{ kHz} \pm 5 \text{ Hz}$ using the pulse sequence in Figure 6-1a with the z -filter delays of $\Delta = 200 \mu\text{s}$. Additional experimental parameters are described in the text. The 3D data set consisted of 16 2D spectra acquired for TEDOR mixing times up to 18 ms and incremented in a non-linear fashion in order to maximize the information content and minimize the duration of the experiment. Each 2D spectrum was acquired as (19, 1024) complex points in (t_1, t_2) , with time increments of (800, 20) μs resulting in acquisition times of (14.4, 20.5) ms. Each FID was 128 scans, with a 3 s recycle delay, yielding a total measurement time of $\sim 67 \text{ h}$.

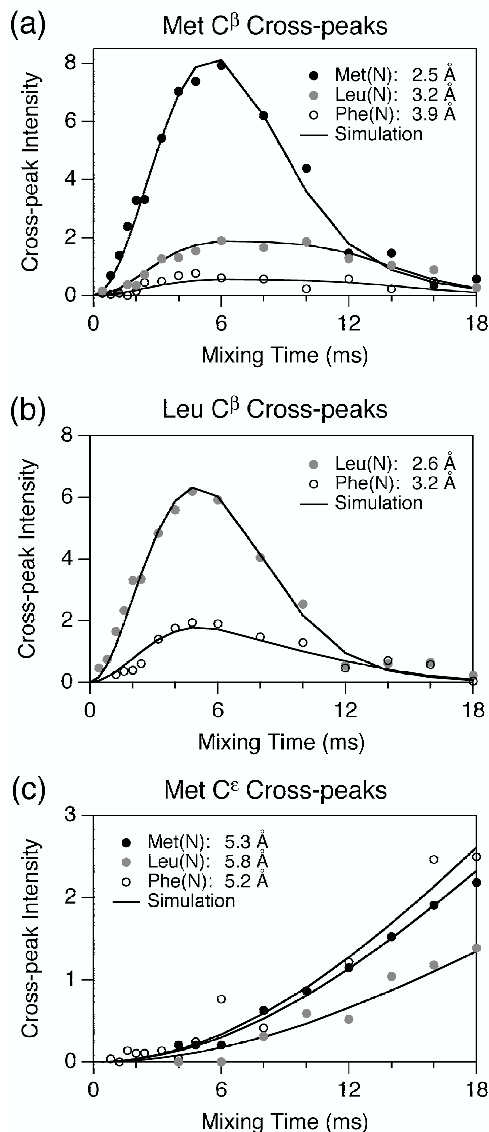


Figure 6-11. 3D ZF TEDOR cross-peak buildup curves in N-formyl-[U- ^{13}C , ^{15}N]L-Met-L-Leu-L-Phe.

The buildup curves were acquired using the pulse sequence in Figure 6-1a and correspond to cross-peaks observed for the Met C^β (a), Leu C^β (b) and Met C^ϵ (c) resonances in the 2D correlation spectra in Figure 6-10. For each ^{13}C the experimental buildup curves corresponding to the Met (\bullet), Leu(\bullet) and Phe (\circ) ^{15}N sites were fit (—) using analytical expressions in eq 10 based on the zeroth order Bessel function approximation. The values of ^{13}C - ^{13}C J-coupling constants used in the fits were 55 Hz for $^1J_{\text{CO}-\text{C}^\alpha}$ and 34 Hz for all other J-couplings. The cross-peak buildup curves shown in the figure correspond to carbon-nitrogen distances in the 2.5-5.8 Å regime (actual distances measured are found in the insets). Similar simulations were performed for the remaining cross-peaks (c.f. Figure 6-10) and the ^{13}C - ^{15}N internuclear distances are summarized in Table 6-3.

The 3D BASE TEDOR experiment is demonstrated in Figure 6-12 for distance measurements in N-f-MLF involving ^{13}C O sites. Here, the dipolar coupling between Met(C') and Phe(N) is of most interest. It corresponds to an internuclear distance of 3.4 Å and provides direct information about backbone conformation. The Met(C')-Phe(N) cross-peak (at the limit of detection using 3D ZF TEDOR) is easily detected (Figure 6-12b) and its buildup can be used to determine the internuclear distance (Figure 6-12c).

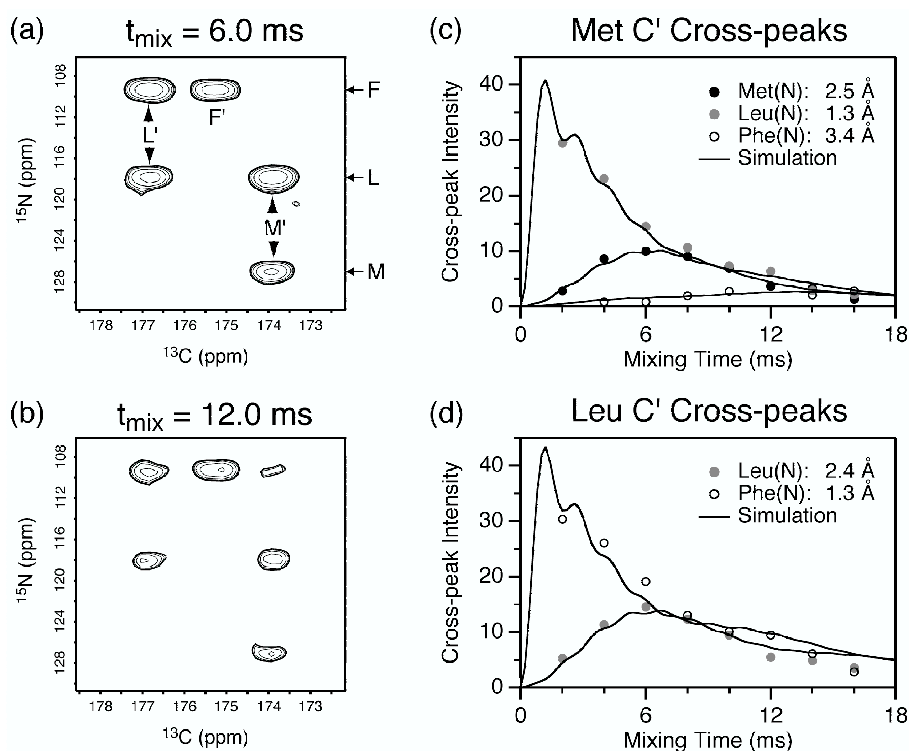


Figure 6-12. Representative two-dimensional slices from the 3D BASE TEDOR experiment for ^{13}C O nuclei and cross-peak buildup curves in N-formyl-[U- ^{13}C , ^{15}N]L-Met-L-Leu-L-Phe.

The pulse sequence in Figure 6-1b was used with the carrier frequency on resonance with the carbonyl region of the spectrum and a Gaussian band-selective ^{13}C refocusing pulse of 0.4 ms. Experimental parameters are described in the text. The 3D data set was recorded as (12, 1024, 8) points in (t_1, t_2, t_{mix}) , with time increments of (0.8, 0.02, 2.0) ms resulting in acquisition times of (8.8, 20.5, 16.0) ms. Each FID was 256 scans, the recycle delay was 3 s, and (t_1, t_2) points were acquired as complex pairs yielding a total measurement time of ~42 h. The buildup curves for Met C' (c) and Leu C' (d) corresponding to the Met (●), Leu (●) and Phe (○) ^{15}N sites were fit (—) using analytical expressions in eq 10 and the distances determined are indicated in the insets. All ^{13}C - ^{15}N internuclear distances measured in N-f-MLF are summarized in Table 6-3.

The carbon-nitrogen distance measurements in N-formyl-L-Met-L-Leu-L-Phe are summarized in Figure 6-13 and Table 6-3. A total of 26 distances between ~ 1.3 -6 Å were measured in N-f-MLF using 3D ZF TEDOR and 3D BASE TEDOR. The measured distances are in good agreement with the corresponding X-ray diffraction distances in N-f-MLF-OMe⁷¹ and previous SSNMR studies.⁴⁴ We note here, that for demonstration purposes we have applied 3D BASE TEDOR to distance measurements involving ¹³C resonances other than ¹³CO in both peptides (buildup curves are not shown). The ¹³C-¹⁵N distances measured using the band-selective experiments in the methyl region of N-ac-VL and C^β region in N-f-MLF corresponded closely to the distances determined using 3D ZF TEDOR (see Tables 6-2 and 6-3).

Finally, we note that many dipolar couplings measured in N-ac-VL and N-f-MLF using the 3D TEDOR techniques corresponded to the trivial one- and two-bond ¹³C-¹⁵N distances, which do not restrain the peptide structure, and served as control experiments. In N-ac-VL, 10 structurally interesting distances ($r > \sim 3$ Å) were measured, and in N-f-MLF, 13 such distances were determined. A number of distances in the 3-4 Å regime (e.g., Val(C^β)-Leu(N), Val(C^{γ1})-Val(N), Leu(C^γ)-Leu(N) in N-ac-VL and Met(C^β)-Leu(N), Met(C^γ)-Met(N), Leu(C^β)-Phe(N) in N-f-MLF) depend on a single ψ or χ torsion angle (assuming standard values for the bond angles), and the longer distances in the 4-6 Å range contain information about multiple ϕ , ψ , and χ torsion angles. These ¹³C-¹⁵N distance measurements place very strong constraints on the overall peptide structure (particularly on the sidechain conformations), but in general they should be used in combination with other structure determination methods, such as chemical shift assignments, and direct measurements of torsion angles, to uniquely define a three-

dimensional peptide structure. This approach was used for N-f-MLF, where long-range ^{13}C - ^{15}N distance measurements⁴⁴ were combined with measurements of 10 ϕ , ψ , and χ torsion angles from dipolar tensor correlation experiments,⁴⁹ and used as constraints in the calculation of a three-dimensional SSNMR structure for the tripeptide.⁵⁰

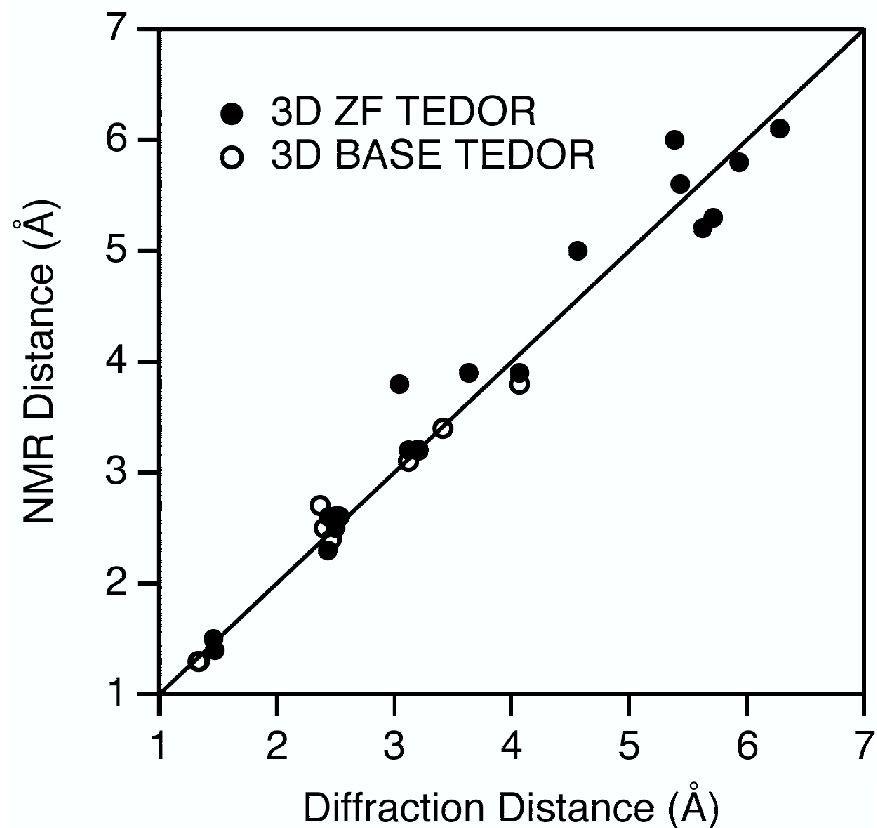


Figure 6-13. Summary of distance measurements in N-formyl-L-Met-L-Leu-L-Phe. Comparison of carbon-nitrogen distances in N-formyl-L-Met-L-Leu-L-Phe measured using 3D ZF TEDOR (●) and 3D BASE TEDOR (○) with the corresponding X-ray diffraction distances determined for N-f-MLF-OMe⁷¹ (see text for discussion of uncertainties in measured distances).

Table 6-3. Internuclear Distances in N-formyl-L-Met-L-Leu-L-Phe

atoms		r_{C-N} (Å) ^a		
		3D ZF TEDOR	3D BASE TEDOR ^b	X-ray ^c
Met(N)	Met(C')	—	2.5	2.40
	Met(C ^α)	1.5	—	1.46
	Met(C ^β)	2.5	2.6	2.50
	Met(C ^γ)	3.8	—	3.04
	Met(C ^ε)	5.3	—	5.71
	Leu(C ^{δ2})	6.1	—	6.28
Leu(N)	Met(C')	—	1.3	1.33
	Met(C ^α)	2.6	—	2.44
	Met(C ^β)	3.2	3.2	3.20
	Met(C ^γ)	5.0	—	4.56
	Met(C ^ε)	5.8	—	5.93
	Leu(C')	—	2.4	2.46
	Leu(C ^α)	1.5	—	1.46
	Leu(C ^β)	2.6	2.6	2.50
Phe(N)	Leu(C ^{δ2})	3.9	—	3.63
	Met(C')	—	3.4	3.41
	Met(C ^β)	3.9	3.8	4.06
	Met(C ^γ)	5.6	—	5.43
	Met(C ^ε)	5.2	—	5.62
	Leu(C')	—	1.3	1.34
	Leu(C ^α)	2.3	—	2.43
	Leu(C ^β)	3.2	3.1	3.12
	Leu(C ^{δ2})	6.0	—	5.38
	Phe(C')	—	2.7	2.37
Phe(C ^α)	1.4	—	1.47	
Phe(C ^β)	2.6	2.6	2.53	

^aSee text for a detailed discussion of uncertainties associated with the NMR distance measurements. ^bMeasurements of distances marked with a (—) for 3D BASE TEDOR were not attempted. ^cRef 71.

6.5 Conclusions

In conclusion we have presented two 3D TEDOR NMR experiments for the simultaneous measurement of multiple carbon-nitrogen distances in uniformly ¹³C,¹⁵N labeled solids in site-specific fashion. The novel feature of the experiments is that they are specifically compensated for the detrimental effects of ¹³C-¹³C J-couplings on the

measurements of long-range carbon-nitrogen distances. The experiments are robust and straightforward to implement. Qualitatively, the presence of ^{13}C - ^{15}N correlations in the 2D spectra itself provides direct information about three-dimensional structure, and quantitative distance measurements were performed using a simple analytical simulation model, which accounts explicitly for multiple spin-spin couplings contributing to cross-peak buildup. The utility of the experiments for structural studies was demonstrated by measurements of 20 and 26 carbon-nitrogen distances up to $\sim 5\text{-}6$ Å in two uniformly ^{13}C , ^{15}N labeled peptides. Specifically, 10 ^{13}C - ^{15}N distances measured in N-ac-VL, and 13 distances in N-f-MLF are greater than 3 Å and provide valuable structural constraints. We expect the 3D TEDOR experiments demonstrated here on microcrystalline peptides to be applicable to structural measurements in non-crystalline biological systems, such as amyloid fibrils and membrane proteins. We have recently used 3D ZF TEDOR to simultaneously measure multiple ^{13}C - ^{15}N distances in the 3-5 Å range in a U- ^{13}C , ^{15}N -labeled amyloid fibril-forming peptide, and applications to distance measurements in the bacteriorhodopsin active site⁴⁸ can be envisaged.

Acknowledgments

The authors thank Dr. Vladimir Ladizhansky, Dr. Chad Rienstra, Dr. David Ruben and Dr. Jonathan Lansing for stimulating discussions during the course of this work, and Dr. Bernd Reif for a careful reading of the manuscript. C.P.J. thanks the NSF for a Predoctoral Fellowship. This research was supported by NIH grants GM-23403, GM-23289, and RR-00995.

Appendix

In this section we calculate the 3D TEDOR spin dynamics in the simplest multiple spin system (I_2 - S) having heteronuclear dipolar and homonuclear J couplings. Although this is much simpler than the spin systems represented by the uniformly ^{13}C , ^{15}N labeled peptides, it is sufficient to demonstrate the detrimental effects due to homonuclear J-couplings and explain the main features observed in the experimental 2D correlation spectra shown in Figures 6-5a – 6-5c. We consider the 3D TEDOR pulse sequence shown in the Figure 6-1a, where the z -filter periods, Δ , are set to zero (i.e., the homonuclear J-coupling is active throughout the entire experiment). In the analysis it is sufficient to follow the evolution of the transverse magnetization corresponding to one of the spins, for instance I_{1x} . The results can be extended to the second spin by simply interchanging the labels 1 and 2. For consistency, in the following derivations we use the notation introduced in eqs 1-5 of the Theoretical Background section.

For the model I_2 - S spin system the effective Hamiltonian during the REDOR mixing periods is given by

$$H = \sum_{k=1,2} \omega_k I_{kz} S_z + \pi J 2 I_{1z} I_{2z}. \quad (\text{A1})$$

Therefore, after the first REDOR mixing period followed by the 90° pulses applied on the I and S channels, I_{1x} transforms to

$$I_{1x} \rightarrow (I_{1x} c_J - 2 I_{1z} I_{2y} s_J) c_{\omega 1} - 2 (I_{1z} c_J + 2 I_{1x} I_{2y} s_J) S_y s_{\omega 1}. \quad (\text{A2})$$

The applied phase cycle eliminates all coherences, which contain only I -spin operators after the first REDOR mixing period, and retains terms, which depend on transverse S -spin operators:

$$I_{1x} \rightarrow -2(I_{1z}c_J + 2I_{1x}I_{2y}S_J)S_yS_{\omega 1}. \quad (\text{A3})$$

Thus, in addition to the desired anti-phase coherence ($\sim I_{1z}S_y$), which reflects I - S dipolar correlations and carries I - S distance information, an additional term ($\sim I_{1x}I_{2y}S_y$) is also generated, which depends on I - I correlations and is represented by a combination of zero-quantum (ZQ) and double-quantum (DQ) spin coherences with respect to I -spin operators.

The REDOR excitation is followed by a free evolution period (t_1) under the Hamiltonian

$$H = \sum_{k=1,2} \Omega_{Ik} I_{kz} + \Omega_S S_z + \pi J 2I_{1z}I_{2z}. \quad (\text{A4})$$

This leads to

$$\begin{aligned} I_{1x} \rightarrow & -2I_{1z}S_yS_{\omega 1}c_J \cos(\Omega_S t_1) \\ & -ZQ_x S_x S_{\omega 1} S_J \left\{ \cos[(\Omega_{I1} - \Omega_{I2} + \Omega_S) t_1] - \cos[(\Omega_{I1} - \Omega_{I2} - \Omega_S) t_1] \right\} \\ & +ZQ_y S_y S_{\omega 1} S_J \left\{ \cos[(\Omega_{I1} - \Omega_{I2} + \Omega_S) t_1] + \cos[(\Omega_{I1} - \Omega_{I2} - \Omega_S) t_1] \right\}, \quad (\text{A5}) \\ & +DQ_x S_x S_{\omega 1} S_J \left\{ \cos[(\Omega_{I1} + \Omega_{I2} + \Omega_S) t_1] - \cos[(\Omega_{I1} + \Omega_{I2} - \Omega_S) t_1] \right\} \\ & +DQ_y S_y S_{\omega 1} S_J \left\{ \cos[(\Omega_{I1} + \Omega_{I2} + \Omega_S) t_1] + \cos[(\Omega_{I1} + \Omega_{I2} - \Omega_S) t_1] \right\} \end{aligned}$$

where we have retained only the cosine modulated chemical shift terms and the following notation for the ZQ and DQ coherences was used:⁵³

$$\begin{aligned} ZQ_x &= I_{1x}I_{2x} + I_{1y}I_{2y}, & ZQ_y &= I_{1y}I_{2x} - I_{1x}I_{2y} \\ DQ_x &= I_{1x}I_{2x} - I_{1y}I_{2y}, & DQ_y &= I_{1x}I_{2y} + I_{1y}I_{2x}. \end{aligned} \quad (\text{A6})$$

The $I_{1z}S_y$ coherence in eq A5 is modulated by the S -spin chemical shift, Ω_S , and gives rise to the desired cross-peaks located at (Ω_S, Ω_I) in the 2D spectra. The zero- and double-quantum coherences evolve in the indirect dimension with frequencies $\Omega_{I1} \pm \Omega_{I2} \pm \Omega_S$, giving rise to spurious cross-peaks. For the simple I_2 - S spin system only the isotropic

chemical shift terms in the Hamiltonian in eq A4 contribute to the spin dynamics during t_1 . For larger spin systems having multiple I - I J-couplings, the scalar interactions would also contribute to the evolution resulting in more complicated dynamics.

The second pair of 90° pulses followed by the REDOR mixing period generates I -spin coherences, which are subsequently detected during the acquisition of the FID in t_2 . The coherences are represented by both, in-phase ($\sim I_x$) and anti-phase ($\sim I_y I_z$) terms

$$\begin{aligned}
 I_{1x} \rightarrow & -\left(I_{1x}c_J^2 - 2I_{1y}I_{2z}s_Jc_J\right)s_{\omega_1}^2 \cos(\Omega_S t_1) \\
 & -\left(I_{1x}c_J^2 + 2I_{1y}I_{2z}s_Jc_J\right)s_{\omega_1}^2 \left\{ \cos[(\Omega_{I1} - \Omega_{I2} + \Omega_S)t_1] + \cos[(\Omega_{I1} - \Omega_{I2} - \Omega_S)t_1] \right\} \\
 & -\left(I_{2x}c_J^2 + 2I_{2y}I_{1z}s_Jc_J\right)s_{\omega_1}s_{\omega_2} \left\{ \cos[(\Omega_{I1} - \Omega_{I2} + \Omega_S)t_1] - \cos[(\Omega_{I1} - \Omega_{I2} - \Omega_S)t_1] \right\}
 \end{aligned} \quad (A7)$$

Under the chemical shift and homonuclear J-coupling interactions, the in-phase terms ($\sim I_x$) in eq A7 give rise to purely absorptive doublets split by the J-coupling

$$I_{1x} \rightarrow I_{1+} \left(e^{i\left(\Omega_{I1} - \frac{J}{2}\right)t_2} + e^{i\left(\Omega_{I1} + \frac{J}{2}\right)t_2} \right), \quad (A8)$$

while the anti-phase terms ($\sim I_y I_z$) generate purely dispersive doublets with anti-phase components

$$2I_{1y}I_{2z} \rightarrow iI_{1+} \left(e^{i\left(\Omega_{I1} - \frac{J}{2}\right)t_2} - e^{i\left(\Omega_{I1} + \frac{J}{2}\right)t_2} \right). \quad (A9)$$

The superposition of these signals results in phase-twisted lines in the direct dimension and prohibits the extraction of reliable cross-peak intensities.

In summary, even for relatively simple multiple spin systems the presence of homonuclear J-couplings leads to quite complicated spin dynamics. The J-couplings generate artifacts in the 2D correlation spectra in the form of spurious cross-peaks and phase-twisted lines, which degrade the resolution and prohibit the extraction of reliable cross-peak intensities. The J-coupling effects become more severe as the mixing time

increases, since the anti-phase components are modulated by $\sin(\pi J t_{mix}/2)$. This is clearly a problem for the measurements of weak dipolar couplings, which typically employ relatively long mixing times.

The modified 3D TEDOR pulse sequences presented here make use of z -filter periods and band-selective refocusing pulses to suppress the ZQ and DQ spin coherences and refocus the J-couplings altogether, respectively. Both experiments generate pure absorption mode 2D spectra, where the cross-peaks located at (Ω_S, Ω_I) depend primarily on dipolar I - S correlations and can be used to determine internuclear distances.

References

- (1) A. E. Bennett, R. G. Griffin and S. Vega. in *Solid State NMR IV: Methods and Applications of Solid-State NMR* (ed. B. Blumich) 1-77 (Springer-Verlag, Berlin, 1994).
- (2) R. G. Griffin, "Dipolar recoupling in MAS spectra of biological solids," *Nature Struct. Biol.* **5**, 508-512 (1998).
- (3) S. Dusold and A. Sebald, "Dipolar recoupling under magic-angle spinning conditions," *Annu. Rep. Nucl. Magn. Reson. Spectr.* **41**, 185-264 (2000).
- (4) C. M. Rienstra, M. Hohwy, M. Hong and R. G. Griffin, "2D and 3D ^{15}N - ^{13}C - ^{13}C NMR chemical shift correlation spectroscopy of solids: assignment of MAS spectra of peptides," *J. Am. Chem. Soc.* **122**, 10979-10990 (2000).
- (5) A. Detken, E. H. Hardy, M. Ernst, M. Kainosho, T. Kawakami, S. Aimoto and B. H. Meier, "Methods for sequential resonance assignment in solid, uniformly ^{13}C , ^{15}N labelled peptides: Quantification and application to antamanide," *J. Biomol. NMR* **20**, 203-221 (2001).
- (6) J. J. Balbach, Y. Ishii, O. N. Antzutkin, R. D. Leapman, N. W. Rizzo, F. Dyda, J. Reed and R. Tycko, "Amyloid fibril formation by A β 16-22, a seven-residue fragment of the Alzheimer's β -amyloid peptide, and structural characterization by solid state NMR," *Biochemistry* **39**, 13748-13759 (2000).
- (7) C. P. Jaroniec, C. E. MacPhee, N. S. Astrof, J. Zurdo, C. M. Dobson and R. G. Griffin. in *43rd Experimental NMR Conference* (Asilomar, CA, 2002).

- (8) C. P. Jaroniec, C. E. MacPhee, N. S. Astrof, C. M. Dobson and R. G. Griffin, "Molecular conformation of a peptide fragment of transthyretin in an amyloid fibril," *Proc. Natl. Acad. Sci. USA*, in press (2002).
- (9) S. K. Straus, T. Bremi and R. R. Ernst, "Experiments and strategies for the assignment of fully $^{13}\text{C}/^{15}\text{N}$ -labelled polypeptides by solid state NMR," *J. Biomol. NMR* **12**, 39-50 (1998).
- (10) M. Hong, "Resonance assignment of $^{13}\text{C}/^{15}\text{N}$ labeled solid proteins by two- and three-dimensional magic-angle-spinning NMR," *J. Biomol. NMR* **15**, 1-14 (1999).
- (11) A. McDermott, T. Polenova, A. Bockmann, K. W. Zilm, E. K. Paulsen, R. W. Martin and G. T. Montelione, "Partial NMR assignments for uniformly ($^{13}\text{C},^{15}\text{N}$)-enriched BPTI in the solid state," *J. Biomol. NMR* **16**, 209-219 (2000).
- (12) T. A. Egorova-Zachernyuk, J. Hollander, N. Fraser, P. Gast, A. J. Hoff, R. Cogdell, H. J. M. de Groot and M. Baldus, "Heteronuclear 2D-correlations in a uniformly [$^{13}\text{C},^{15}\text{N}$] labeled membrane-protein complex at ultra-high magnetic fields," *J. Biomol. NMR* **19**, 243-253 (2001).
- (13) J. Pauli, M. Baldus, B. van Rossum, H. de Groot and H. Oschkinat, "Backbone and side-chain ^{13}C and ^{15}N signal assignments of the α -spectrin SH3 domain by magic angle spinning solid-state NMR at 17.6 Tesla," *ChemBiochem* **2**, 272-281 (2001).
- (14) B. J. van Rossum, F. Castellani, K. Rehbein, J. Pauli and H. Oschkinat, "Assignment of the nonexchanging protons of the alpha-spectrin SH3 domain by two- and three-dimensional ^1H - ^{13}C solid-state magic-angle spinning NMR and comparison of solution and solid-state proton chemical shifts," *ChemBiochem* **2**, 906-914 (2001).

- (15) S. Spera and A. Bax, "Empirical correlation between protein backbone conformation and C α and C β ^{13}C nuclear magnetic resonance chemical shifts," *J. Am. Chem. Soc.* **113**, 5490-5492 (1991).
- (16) D. S. Wishart and B. D. Sykes, "Chemical shifts as a tool for structure determination," *Methods Enzymol.* **239**, 363-392 (1994).
- (17) D. S. Wishart, C. G. Bigam, A. Holm, R. S. Hodges and B. D. Sykes, " ^1H , ^{13}C and ^{15}N random coil NMR chemical shifts of the common amino acids. 1. Investigations of nearest neighbor effects," *J. Biomol. NMR* **5**, 67-81 (1995).
- (18) G. Cornilescu, F. Delaglio and A. Bax, "Protein backbone angle restraints from searching a database for chemical shift and sequence homology," *J. Biomol. NMR* **13**, 289-302 (1999).
- (19) H. Saito, "Conformation dependent ^{13}C chemical shifts: A new means of conformational characterization as obtained by high-resolution solid-state ^{13}C NMR," *Magn. Reson. Chem.* **24**, 835-852 (1986).
- (20) H. Saito, S. Tuzi and A. Naito, *Annu. Rep. Nucl. Magn. Reson. Spectr.* **36**, 79-121 (1998).
- (21) S. Luca, D. V. Filippov, J. H. van Boom, H. Oschkinat, H. J. M. de Groot and M. Baldus, "Secondary chemical shifts in immobilized peptides and proteins: A qualitative basis for structure refinement under Magic Angle Spinning," *J. Biomol. NMR* **20**, 325-331 (2001).
- (22) P. R. Costa, Ph. D. Thesis, Massachusetts Institute of Technology, 1996.

- (23) M. Hohwy, C. M. Rienstra, C. P. Jaroniec and R. G. Griffin, "Fivefold symmetric homonuclear dipolar recoupling in rotating solids: Application to double quantum spectroscopy," *J. Chem. Phys.* **110**, 7983-7992 (1999).
- (24) V. Ladizhansky and S. Vega, "Polarization transfer dynamics in Lee-Goldburg cross polarization nuclear magnetic resonance experiments on rotating solids," *J. Chem. Phys.* **112**, 7158-7168 (2000).
- (25) C. A. Fyfe and A. R. Lewis, "Investigation of the viability of solid-state NMR distance determinations in multiple spin systems of unknown structure," *J. Phys. Chem. B* **104**, 48-55 (2000).
- (26) P. Hodgkinson and L. Emsley, "The accuracy of distance measurements in solid-state NMR," *J. Magn. Reson.* **139**, 46-59 (1999).
- (27) T. Gullion and J. Schaefer, "Rotational-echo double-resonance NMR," *J. Magn. Reson.* **81**, 196-200 (1989).
- (28) T. Gullion and J. Schaefer, "Detection of weak heteronuclear dipolar coupling by rotational-echo double-resonance nuclear magnetic resonance," *Adv. Magn. Reson.* **13**, 57-83 (1989).
- (29) A. W. Hing, S. Vega and J. Schaefer, "Transferred-echo double-resonance NMR," *J. Magn. Reson.* **96**, 205-209 (1992).
- (30) A. W. Hing, S. Vega and J. Schaefer, "Measurement of heteronuclear dipolar coupling by transferred-echo double-resonance NMR," *J. Magn. Reson. A* **103**, 151-162 (1993).
- (31) L. M. McDowell and J. Schaefer, "High resolution NMR of biological solids," *Curr. Opin. Struct. Biol.* **6**, 624-629 (1996).

- (32) G. A. Morris and R. Freeman, "Enhancement of nuclear magnetic resonance signals by polarization transfer," *J. Am. Chem. Soc.* **101**, 760-762 (1979).
- (33) J. E. Roberts, S. Vega and R. G. Griffin, "Two-dimensional heteronuclear chemical shift correlation spectroscopy," *J. Am. Chem. Soc.* **106**, 2506-2512 (1984).
- (34) C. A. Fyfe, K. T. Mueller, H. Grondy and K. C. Wong-Moon, "Dipolar dephasing between quadrupolar and spin-1/2 nuclei. REDOR and TEDOR NMR experiments on VPI-5," *Chem. Phys. Lett.* **199**, 198-204 (1992).
- (35) E. R. H. van Eck and W. S. Veeman, "A solid-state NMR 3D heteronuclear dipolar-correlation experiment. The correlation of $\delta(^{13}\text{C})$, $\delta(^{15}\text{N})$, and $D_{(\text{C-N})}$," *J. Magn. Reson. A* **109**, 250-252 (1994).
- (36) C. A. Michal and L. W. Jelinski, "REDOR 3D: Heteronuclear distance measurements in uniformly labeled and natural abundance solids," *J. Am. Chem. Soc.* **119**, 9059-9060 (1997).
- (37) A. E. Bennett, L. R. Becerra and R. G. Griffin, "Frequency-selective heteronuclear recoupling in rotating solids," *J. Chem. Phys.* **100**, 812-814 (1994).
- (38) A. E. Bennett, C. M. Rienstra, P. T. Lansbury and R. G. Griffin, "Frequency-selective heteronuclear dephasing by dipole couplings in spinning and static solids," *J. Chem. Phys.* **105**, 10289-10299 (1996).
- (39) J. Schaefer, "REDOR-determined distances from heterospins to clusters of ^{13}C labels," *J. Magn. Reson.* **137**, 272-275 (1999).
- (40) T. Gullion and C. H. Pennington, " θ -REDOR: an MAS NMR method to simplify multiple coupled heteronuclear spin systems," *Chem. Phys. Lett.* **290**, 88-93 (1998).

- (41) O. Liivak and D. B. Zax, "Multiple simultaneous distance determinations: Application of rotational echo double resonance nuclear magnetic resonance to IS_2 spin networks," *J. Chem. Phys.* **113**, 1088-1096 (2000).
- (42) O. Liivak and D. B. Zax, "Rotational echo double resonance in IS_N spin networks: Deconvolution of multiple dipole-dipole couplings," *J. Chem. Phys.* **115**, 402-409 (2001).
- (43) C. P. Jaroniec, B. A. Tounge, C. M. Rienstra, J. Herzfeld and R. G. Griffin, "Measurement of ^{13}C - ^{15}N distances in uniformly ^{13}C labeled biomolecules: J-decoupled REDOR," *J. Am. Chem. Soc.* **121**, 10237-10238 (1999).
- (44) C. P. Jaroniec, B. A. Tounge, J. Herzfeld and R. G. Griffin, "Frequency selective heteronuclear dipolar recoupling in rotating solids: Accurate ^{13}C - ^{15}N distance measurements in uniformly ^{13}C , ^{15}N -labeled peptides," *J. Am. Chem. Soc.* **123**, 3507-3519 (2001).
- (45) J. C. C. Chan and H. Eckert, "Dipolar coupling information in multispin systems: Application of a compensated REDOR NMR approach to inorganic phosphates," *J. Magn. Reson.* **147**, 170-178 (2000).
- (46) J. C. C. Chan, "C-REDOR: rotational echo double resonance under very fast magic-angle spinning," *Chem. Phys. Lett.* **335**, 289-297 (2001).
- (47) J. C. C. Chan and H. Eckert, "C-rotational echo double resonance: Heteronuclear dipolar recoupling with homonuclear dipolar decoupling," *J. Chem. Phys.* **115**, 6095-6105 (2001).
- (48) C. P. Jaroniec, J. C. Lansing, B. A. Tounge, M. Belenky, J. Herzfeld and R. G. Griffin, "Measurement of dipolar couplings in a uniformly ^{13}C , ^{15}N -labeled

membrane protein: Distances between the Schiff base and aspartic acids in the active site of bacteriorhodopsin," *J. Am. Chem. Soc.* **123**, 12929-12930 (2001).

- (49) C. M. Rienstra, Ph. D. Thesis, Massachusetts Institute of Technology, 1999.
- (50) C. M. Rienstra, L. Tucker-Kellogg, C. P. Jaroniec, M. Hohwy, B. Reif, T. Lozano-Perez, B. Tidor and R. G. Griffin, "De novo determination of peptide structure with solid-state MAS NMR spectroscopy," *Proc. Natl. Acad. Sci. USA* **99**, 10260-10265 (2002).
- (51) M. Baldus, A. T. Petkova, J. Herzfeld and R. G. Griffin, "Cross polarization in the tilted frame: assignment and spectral simplification in heteronuclear spin systems," *Mol. Phys.* **95**, 1197-1207 (1998).
- (52) C. M. Rienstra. in *2nd Alpine Conference on Solid-State NMR* (Chamonix, France, 2001).
- (53) J. Cavanagh, W. J. Fairbrother, A. G. Palmer and N. J. Skelton, "Protein NMR Spectroscopy: Principles and Practice," Academic Press, San Diego (1996).
- (54) R. Brüschweiler, C. Griesinger, O. W. Sørensen and R. R. Ernst, "Combined use of hard and soft pulses for ω_1 decoupling in two-dimensional NMR spectroscopy," *J. Magn. Reson.* **78**, 178-185 (1988).
- (55) S. K. Straus, T. Bremi and R. R. Ernst, "Resolution enhancement by homonuclear J decoupling in solid-state MAS NMR," *Chem. Phys. Lett.* **262**, 709-715 (1996).
- (56) P. L. Stewart, R. Tycko and S. J. Opella, "Peptide backbone conformation by solid-state nuclear magnetic resonance spectroscopy," *J. Chem. Soc. Faraday Trans. I* **84**, 3803-3819 (1988).

- (57) T. Gullion, D. B. Baker and M. S. Conradi, "New, compensated Carr-Purcell sequences," *J. Magn. Reson.* **89**, 479-484 (1990).
- (58) T. G. Oas, R. G. Griffin and M. H. Levitt, "Rotary resonance recoupling of dipolar interactions in solid-state nuclear magnetic resonance spectroscopy," *J. Chem. Phys.* **89**, 692-695 (1988).
- (59) D. J. States, R. A. Haberkorn and D. J. Ruben, "A two-dimensional nuclear Overhauser experiment with pure absorption phase in four quadrants," *J. Magn. Reson.* **48**, 286-292 (1982).
- (60) G. Metz, X. Wu and S. O. Smith, "Ramped-amplitude cross-polarization in magic-angle-spinning NMR," *J. Magn. Reson. A* **110**, 219-227 (1994).
- (61) R. R. Ernst, G. Bodenhausen and A. Wokaun, "Principles of Nuclear Magnetic Resonance in One and Two Dimensions," Clarendon Press, Oxford (1991).
- (62) T. Gullion and S. Vega, "A simple magic angle spinning NMR experiment for the dephasing of rotational echoes of dipolar coupled homonuclear spin pairs," *Chem. Phys. Lett.* **194**, 423-428 (1992).
- (63) A. E. Bennett, J. H. Ok, R. G. Griffin and S. Vega, "Chemical shift correlation spectroscopy in rotating solids: Radio frequency driven dipolar recoupling and longitudinal exchange," *J. Chem. Phys.* **96**, 8624-8627 (1992).
- (64) A. E. Bennett, C. M. Rienstra, M. Auger, K. V. Lakshmi and R. G. Griffin, "Heteronuclear decoupling in rotating solids," *J. Chem. Phys.* **103**, 6951-6957 (1995).
- (65) D. P. Raleigh, M. H. Levitt and R. G. Griffin, "Rotational resonance in solid state NMR," *Chem. Phys. Lett.* **146**, 71-76 (1988).

- (66) O. W. Sørensen, G. W. Eich, M. H. Levitt, G. Bodenhausen and R. R. Ernst, "Product operator formalism for the description of NMR pulse experiments," *Prog. NMR Spect.* **16**, 163-192 (1983).
- (67) K. T. Mueller, "Analytic solutions for the time evolution of dipolar-dephasing NMR signals," *J. Magn. Reson. A* **113**, 81-93 (1995).
- (68) W. H. Press, S. A. Teukolsky, W. T. Vetterling and B. P. Flannery, "Numerical Recipes in C," Cambridge University Press, Cambridge (1996).
- (69) U. Haeberlen, "High-Resolution NMR in Solids: Selective Averaging," Academic Press, New York (1976).
- (70) P. J. Carroll, P. L. Stewart and S. J. Opella, "Structures of two model peptides: N-Acetyl-D,L-valine and N-Acetyl-L-valyl-L-leucine," *Acta Cryst.* **C46**, 243-246 (1990).
- (71) E. Gavuzzo, F. Mazza, G. Pochetti and A. Scatturin, "Crystal structure, conformation, and potential energy calculations of the chemotactic peptide N-formyl-L-Met-L-Leu-L-Phe-OMe," *Int. J. Peptide Protein Res.* **34**, 409-415 (1989).
- (72) M. Hong and R. G. Griffin, "Resonance assignments for solid peptides by dipolar-mediated $^{13}\text{C}/^{15}\text{N}$ correlation solid-state NMR," *J. Am. Chem. Soc.* **120**, 7113-7114 (1998).

CHAPTER 7. MOLECULAR CONFORMATION OF A PEPTIDE FRAGMENT OF TRANSTHYRETIN IN AN AMYLOID FIBRIL

Note: Reproduced with permission from C. P. Jaroniec, C. E. MacPhee, N. S. Astrof, C. M. Dobson and R. G. Griffin, "Molecular conformation of a peptide fragment of transthyretin in an amyloid fibril," Proc. Natl. Acad. Sci. USA, in press. Unpublished work copyright 2002 The National Academy of Sciences of the United States of America.

ABSTRACT

The molecular conformation of peptide fragment 105-115 of transthyretin, TTR(105-115), previously shown to form amyloid fibrils *in vitro*, has been determined by magic-angle spinning solid-state NMR spectroscopy. ^{13}C and ^{15}N linewidth measurements indicate that TTR(105-115) forms a highly ordered structure with each amino acid in a unique environment. Two-dimensional ^{13}C - ^{13}C and ^{15}N - ^{13}C - ^{13}C chemical shift correlation experiments, performed on three fibril samples uniformly ^{13}C , ^{15}N labeled in consecutive stretches of four amino acids, allowed the complete sequence specific backbone and side-chain ^{13}C and ^{15}N resonance assignments to be obtained for residues 105-114. Analysis of the ^{15}N , ^{13}CO , $^{13}\text{C}^{\alpha}$ and $^{13}\text{C}^{\beta}$ chemical shifts allowed quantitative predictions to be made for the backbone torsion angles ϕ and ψ . Furthermore, four backbone ^{13}C - ^{15}N distances were determined in two selectively ^{13}C , ^{15}N labeled fibril samples using rotational-echo double-resonance NMR. The results show that TTR(105-115) adopts an extended β -strand conformation that is remarkably similar to that found in the native protein, with the exception of the region surrounding the proline residue.

7.1 Introduction

Amyloid fibrils are highly organized aggregates formed by peptides and proteins with a wide variety of structures and functions. Fibril formation is associated with a number of protein deposition diseases including Alzheimer's disease, type II diabetes and the transmissible spongiform encephalopathies.^{1,2} In addition, many peptides and proteins not directly associated with disease have the propensity to self-assemble into amyloid fibrils *in vitro*.^{3,4} Although fibrils are formed by polypeptides with different amino acid sequences and lengths, they share a number of common characteristics. They exhibit similar morphologies under electron microscopy and a characteristic "cross- β " pattern in X-ray fiber diffraction experiments.^{1,2} The latter has been attributed to an extensive β -sheet structure in which the peptide strands are oriented perpendicular to the long fibril axis. The fibrils are assembled from a large number of molecules but do not form single crystals. Therefore, they are not amenable to characterization using solution-state nuclear magnetic resonance (NMR) or X-ray crystallography. Solid-state NMR (SSNMR) spectroscopy, however, can be used to obtain site-specific structural information at atomic resolution in non-crystalline biological solids such as amyloid fibrils. Indeed, recent developments in SSNMR instrumentation and methodology^{5,6} have enabled a number of structural details to be determined for various peptide fragments of the Alzheimer's β -peptide, ranging from 7 to 40 residues in length,⁷⁻¹³ for a peptide fragment of the human islet amyloid polypeptide,¹⁴ and for several peptides derived from prion proteins.^{15,16}

In this paper we describe the complete resonance assignments and determine the molecular conformation of an amyloid fibril-forming peptide fragment of transthyretin

(TTR) using magic-angle spinning (MAS) SSNMR spectroscopy. TTR is a 55 kDa protein, involved in the transport of thyroxine and retinol in plasma. The native protein is a homotetramer of 127-residue subunits and has extensive β -sheet structure.¹⁷ Wild-type (wt) TTR forms amyloid fibrils *in vivo* in a condition termed senile systemic amyloidosis,¹⁸ and a number of naturally occurring TTR variants are associated with familial amyloid polyneuropathy.¹⁹ Full length TTR,²⁰ TTR variants,^{1,2,21,22} and two 11-residue peptide fragments derived from the native sequence²⁰ have been previously shown readily to form amyloid fibrils *in vitro*. They are therefore important systems for the detailed investigations of the structure of amyloid fibrils and the mechanism of fibril formation.²³ The peptides, TTR(10-20) and TTR(105-115), correspond to the sequences that are found as β -strands A and G, respectively, in the native protein. Both strands are located at the surface of the thyroxine-binding channel formed by the homotetramer.²⁴ Oriented fibrils formed by TTR(10-20) and TTR(105-115) exhibit the characteristic “cross- β ” X-ray fiber diffraction patterns.²⁵ The monomeric peptides have been found to adopt essentially random conformations in aqueous solution.²⁶

In the present work we have used one- (1D) and two-dimensional (2D) MAS SSNMR to probe the molecular conformation of TTR(105-115) in the fibrillar state. ¹³C and ¹⁵N linewidth measurements indicate that the peptide forms highly-ordered fibrils in which there is a single unique environment for each residue. We have established the complete sequence specific backbone and side-chain ¹³C and ¹⁵N resonance assignments for residues 105-114 in fibrils prepared from peptides uniformly ¹³C,¹⁵N (U-¹³C,¹⁵N) labeled in consecutive stretches of four amino acids. The 2D ¹³C-¹³C and ¹⁵N-¹³C-¹³C chemical shift correlation techniques employed here are analogous to those used recently

to assign several (U- ^{13}C , ^{15}N)-labeled peptides and proteins^{12,27-32} and the complete resonance assignments represent the initial step in the determination of a high-resolution NMR structure for TTR(105-115) fibrils. The ^{15}N , ^{13}CO , $^{13}\text{C}^\alpha$ and $^{13}\text{C}^\beta$ chemical shifts have been used to predict the backbone torsion angles ϕ and ψ . Furthermore, we have measured four backbone ^{13}C - ^{15}N distances in the 4-5 Å regime in two selectively ^{13}C , ^{15}N labeled fibril samples using rotational-echo double resonance (REDOR) NMR (*vide infra*). The data indicate that the TTR(105-115) fibrils are extremely well-ordered, and that the fibrils represent an array of identical peptide molecules each of which is in a fully extended β -strand conformation.

7.2 Experimental

7.2.1 Preparation of Amyloid Fibrils

TTR(105-115) (YTIAALLSPYS) peptides for the resonance assignment experiments were synthesized using standard solid-phase methods and purified by HPLC (CS Bio Company, San Carlos, CA). The peptides used for the REDOR measurements were synthesized by Midwest Biotech (Fishers, IN) and the MIT Cancer Center Biopolymers Facility (Cambridge, MA). All ^{13}C , ^{15}N -labeled, protected amino acids used in the peptide synthesis were purchased directly from Cambridge Isotope Laboratories (CIL) (Andover, MA), with the exception of N-Fmoc, O-t-butyl ether protected (U- ^{13}C , ^{15}N)threonine, (U- ^{13}C , ^{15}N)serine, (1- ^{13}C , ^{15}N)serine, (2- ^{13}C , ^{15}N)serine and (^{15}N)tyrosine, which were synthesized by Midwest Biotech starting with isotopically labeled amino acids from CIL.

Three TTR(105-115) fibril samples were used for all resonance assignment experiments. The peptides contained four ($U\text{-}^{13}\text{C},^{15}\text{N}$)-labeled amino acids at positions (i) 105-108, (ii) 108-111, and (iii) 111-114; these samples are referred to as $\text{TTR}(105\text{-}115)_{\text{YTIA}}$, $\text{TTR}(105\text{-}115)_{\text{AALL}}$, and $\text{TTR}(105\text{-}115)_{\text{LSPY}}$, respectively (see Figure 7-1). Note that the C-terminal residue (S115) was not ($U\text{-}^{13}\text{C},^{15}\text{N}$)-labeled due to the expense associated with the coupling of that residue to the resin with high yield. Two additional TTR(105-115) samples containing selectively $^{13}\text{C},^{15}\text{N}$ labeled amino acids were used for REDOR $^{13}\text{C}\text{-}^{15}\text{N}$ distance measurements. The first sample contained the ^{13}C and ^{15}N labels at the A108 ^{13}CO , L111 $^{13}\text{C}^{\alpha}$ and L110 ^{15}N positions, and the second sample was labeled at S112 ^{13}CO , S115 $^{13}\text{C}^{\alpha}$ and Y114 ^{15}N .

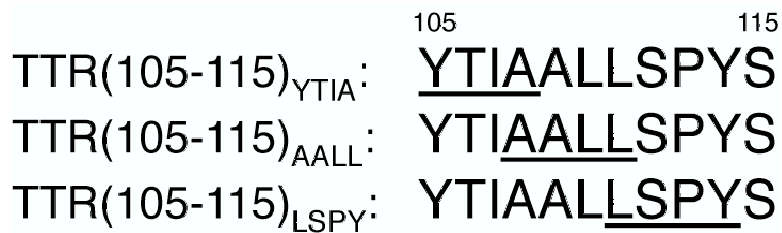


Figure 7-1. Amino acid sequence of TTR(105-115).

The labeling scheme used for the resonance assignments experiments is shown with ($U\text{-}^{13}\text{C},^{15}\text{N}$)-labeled residues are underlined.

Amyloid fibrils were prepared by dissolving TTR(105-115) in a 10% acetonitrile/water solution (adjusted to pH 2 with HCl) at ca. 15 mg/ml. The samples were incubated for 2 days at 37 °C followed by incubation for 14 days at room temperature. The samples were routinely characterized by transmission electron microscopy (TEM). After this period the clear, viscous gel containing the fibrils was transferred to a centrifuge tube and washed twice with ca. 2 ml of 10% acetonitrile/water at pH 2. Following each wash the sample was centrifuged for 2 h at 4 °C and ~320,000g.

After the second spin the pellet containing ~10 mg of fibrils was packed into a 4-mm zirconia NMR rotor (Varian-Chemagnetics, Fort Collins, CO). The top of the rotor was sealed with epoxy to prevent dehydration during the MAS NMR experiments.

7.2.2 NMR Experiments

NMR experiments were performed on a custom-designed spectrometer (courtesy of Dr. D. J. Ruben) operating at the frequencies of 500 MHz for ^1H , 125.7 MHz for ^{13}C and 50.7 MHz for ^{15}N , using a Varian-Chemagnetics (Fort Collins, CO) 500 MHz triple-resonance T3 probe equipped with a 4-mm spinner module. Spinning frequencies of ~9-11 kHz were used in all experiments, regulated to ± 5 Hz using a Doty Scientific (Columbia, SC) spinning frequency controller, and the sample temperature was maintained at 2 °C using a stream of cooled nitrogen gas.

The 1D ^{13}C and ^{15}N MAS spectra were recorded with ramped cross-polarization (CP).^{33,34} The ^1H radiofrequency (rf) field was set to 50 kHz, the ^{13}C field was ramped linearly through the $n = -1$ Hartmann-Hahn matching condition (between 38-42 kHz) and the contact time was 2 ms.

The 2D ^{13}C - ^{13}C proton-driven spin diffusion experiments³⁵ used 5 μs 90° ^{13}C pulses and a 10 ms spin diffusion period. A ^1H rf field matching the $n = 1$ rotary resonance condition³⁶ was applied during the mixing period to facilitate efficient ^{13}C - ^{13}C magnetization transfer.

The 2D ^{15}N - ^{13}C - ^{13}C spectra were recorded using the NCOCX and NCACX pulse sequences described elsewhere.^{31,32} Following ^1H - ^{15}N CP and ^{15}N chemical shift evolution period (t_1), band-selective SPECIFIC ramped cross-polarization³⁷ was used to transfer the

^{15}N magnetization selectively to ^{13}CO or $^{13}\text{C}^\alpha$ by placing the ^{13}C carrier frequency $\sim 10\text{-}15$ ppm outside the CO (for $\text{N}\rightarrow\text{CO}$ transfer) and C^α (for $\text{N}\rightarrow\text{C}^\alpha$ transfer) regions. The ^{15}N rf field strength was ~ 35 kHz, the ^{13}C field was ramped linearly between ~ 1 kHz below and ~ 1 kHz above the $n = -1$ Hartmann-Hahn matching condition, and the mixing time was 3 ms. Immediately following the $^{15}\text{N}\text{-}^{13}\text{C}$ CP, a 10-20 ms ^1H -driven $^{13}\text{C}\text{-}^{13}\text{C}$ spin diffusion period was used to establish the intraresidue $^{13}\text{C}\text{-}^{13}\text{C}$ correlations.

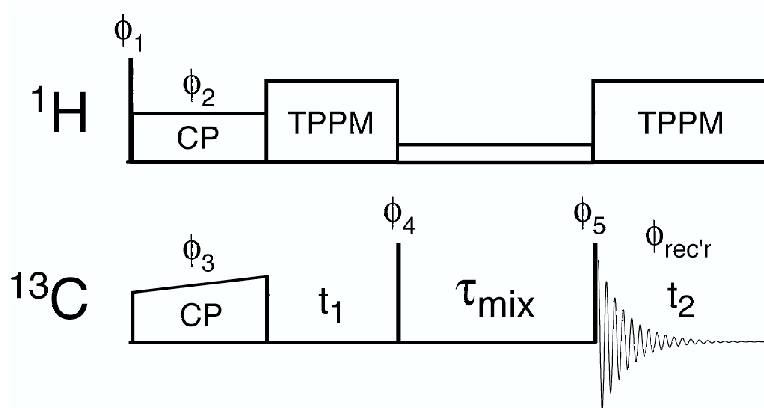


Figure 7-2. Two-dimensional spin diffusion pulse sequence.

Narrow solid rectangles represent $\pi/2$ pulses. During the spin diffusion period a weak proton rf field, $\omega_{rf} \approx \omega_r$, was applied³⁶ to facilitate efficient $^{13}\text{C}\text{-}^{13}\text{C}$ mixing. Phase cycle: $\phi_1 = 8 \times (1) \ 8 \times (3)$, $\phi_2 = 16 \times (2)$, $\phi_3 = 8 \times (13)$, $\phi_4 = 16 \times (2)$, $\phi_5 = 2 \times (11223344)$, $\phi_{\text{rec'r}} = 13243142 \ 31421324$, where $1 = x$, $2 = y$, $3 = -x$, $4 = -y$. Hypercomplex data were acquired by shifting ϕ_3 according to Ruben and co-workers.³⁸

Backbone $^{13}\text{C}\text{-}^{15}\text{N}$ distances were measured using the REDOR experiment.³⁹ The initial ^{13}C magnetization created via CP was observed as a spin-echo and dephased during the REDOR mixing period using a train of rotor-synchronized 180° ^{15}N pulses. For each REDOR curve, S , a reference curve, S_0 , was recorded in the absence of ^{15}N pulses to account for relaxation effects. The internuclear $^{13}\text{C}\text{-}^{15}\text{N}$ distances were extracted by fitting the quantity S/S_0 as a function of the REDOR mixing time to the analytical expression describing the dipolar dephasing.³⁹

During ^{15}N - ^{13}C CP and REDOR mixing, 100 kHz continuous wave proton decoupling was used and 70-80 kHz TPPM decoupling⁴⁰ was employed during all chemical shift evolution periods.

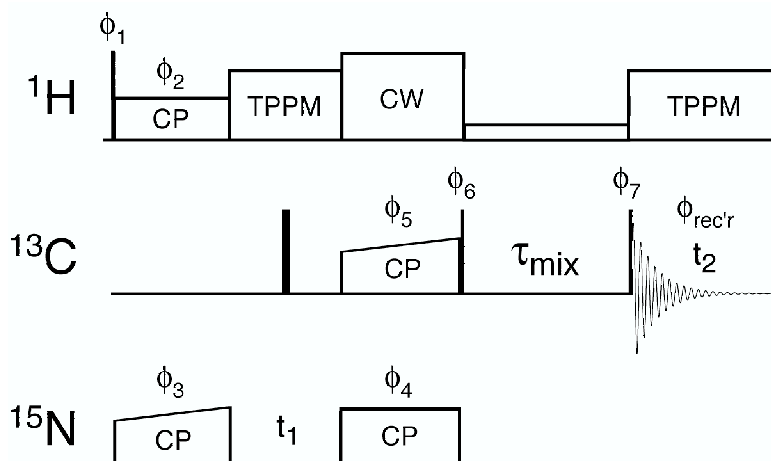


Figure 7-3. Two-dimensional N-C-C pulse sequence.

Narrow and wide solid rectangles represent $\pi/2$ and π pulses, respectively. The ^{15}N - ^{13}C CP band-selective SPECIFIC CP³⁷ is adjusted appropriately (see text for details) to transfer the ^{15}N coherence selectively to $^{13}\text{C}^\alpha$ (NCACX experiment) or ^{13}CO (NCOX experiment). During the spin diffusion period a weak proton rf field, $\omega_{rf} \approx \omega_r$, is applied³⁶ to facilitate efficient ^{13}C - ^{13}C mixing. Phase cycle: $\phi_1 = 16 \times (1) 16 \times (3)$, $\phi_2 = 32 \times (2)$, $\phi_3 = 16 \times (13)$, $\phi_4 = 32 \times (1)$, $\phi_5 = 8 \times (1) 8 \times (3) 8 \times (1) 8 \times (3)$, $\phi_6 = 32 \times (2)$, $\phi_7 = 4 \times (11223344)$, $\phi_{\text{rec'r}} = 13243142 31421324 31421324 13243142$, where $1 = x$, $2 = y$, $3 = -x$, $4 = -y$. Hypercomplex data were acquired by shifting ϕ_3 according to Ruben and co-workers.³⁸

7.3 Results and Discussion

An electron micrograph of the fibrils formed by TTR(105-115) is shown in Figure 7-4. The fibrils have variable lengths and are approximately 10 nm wide, and are similar in appearance to those observed in disease associated systems.^{1,2}

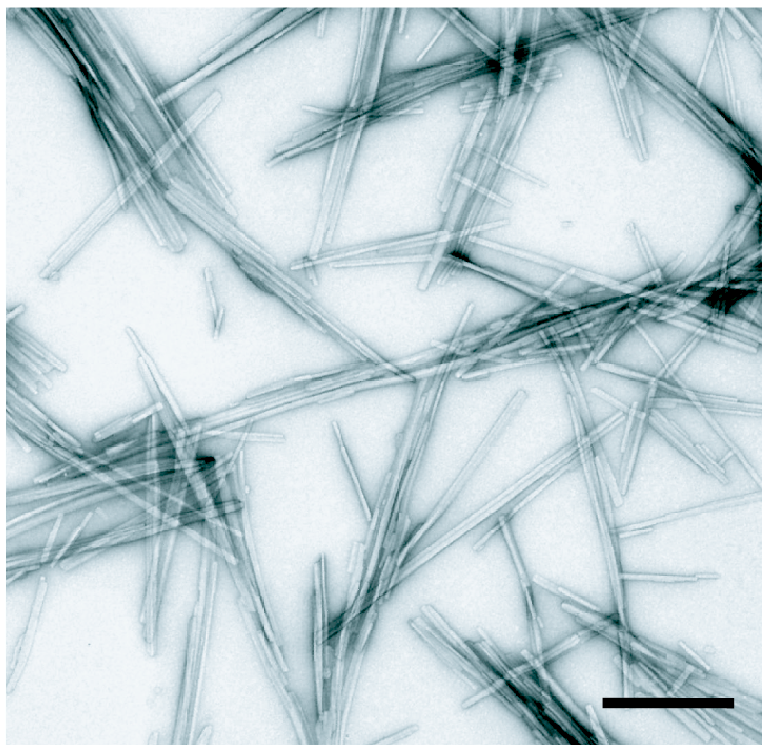


Figure 7-4. Electron micrograph of TTR(105-115) fibrils.

Amyloid fibrils were diluted to 100-200 $\mu\text{g/ml}$ and negatively stained using 2% w/v uranyl acetate. Fibrils were viewed in a Jeol 1200EX TEM, using an accelerating voltage of 80 kV. The scale bar represents 200 nm.

The 1D ^{13}C and ^{15}N MAS spectra of ($U\text{-}^{13}\text{C},^{15}\text{N}$)-labeled TTR(105-115) fibrils (Figure 7-5) are extremely well-resolved, with virtually all sites giving rise to narrow, single resonances. The spectral assignments indicated in Figure 7-5 and listed in Table 7-1 were established using 2D $^{13}\text{C}\text{-}^{13}\text{C}$ and $^{15}\text{N}\text{-}^{13}\text{C}\text{-}^{13}\text{C}$ correlation techniques which are discussed in detail below. Widths at half height of ca. 0.6-1.8 ppm and 0.7-1.5 ppm were observed for ^{13}C and ^{15}N resonances, respectively, with the majority of sites having linewidths of < 1.0 ppm for ^{13}C and < 1.3 ppm for ^{15}N (see Table 7-2). The ^{13}C and ^{15}N resonances in TTR(105-115) fibrils are significantly narrower than those characteristic of amorphous or disordered systems, and the linewidths compare favorably with those

observed in (U - ^{13}C , ^{15}N)-labeled microcrystalline amino acids and peptides.²⁷⁻²⁹ This implies that the inhomogeneous line broadening due to disorder is minimal. This observation is remarkable given the fact that the fibrils are non-crystalline and indicates on the atomic level a highly ordered fibrillar structure with a narrow distribution of peptide conformations. The ^{13}C and ^{15}N chemical shift anisotropies and ^1H - ^{13}C , ^1H - ^{15}N , and ^{13}C - ^{15}N dipolar interactions involving backbone resonances measured in TTR(105-115) fibrils (unpublished data) correspond to the rigid limit values and indicate the absence of appreciable dynamics along the peptide backbone.

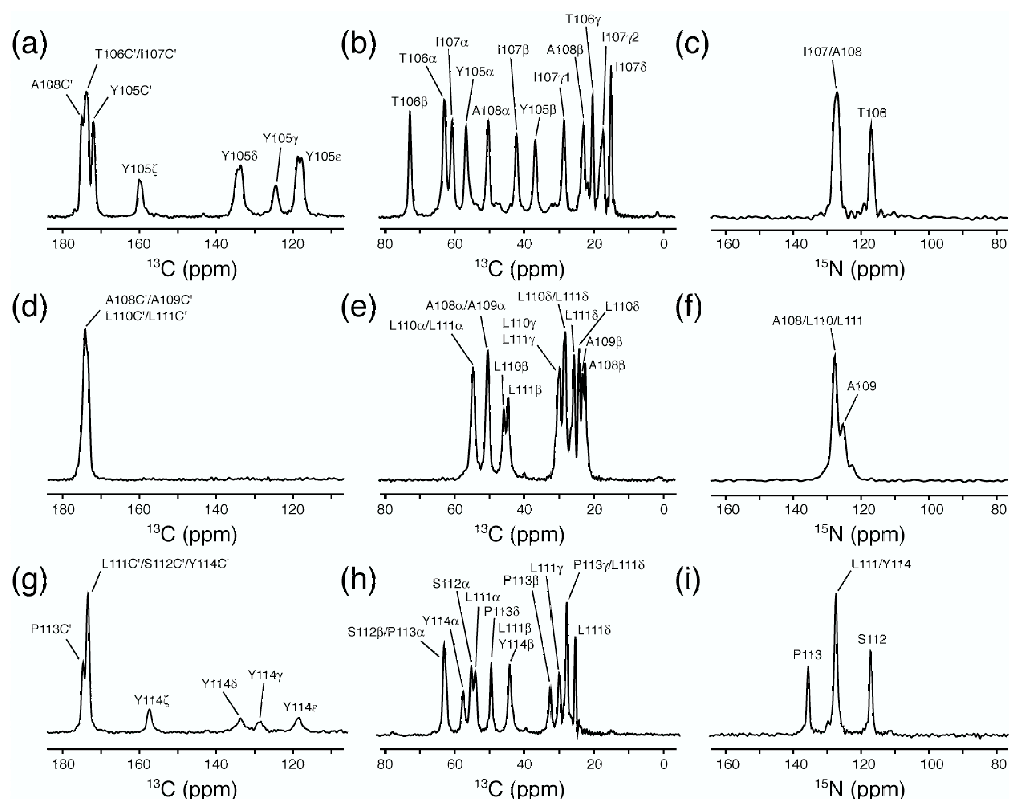


Figure 7-5. 1D ^{13}C and ^{15}N MAS NMR spectra of (U - ^{13}C , ^{15}N)-labeled TTR(105-115) fibrils.

^{13}C carbonyl and aromatic (a), (d), (g), ^{13}C aliphatic (b), (e), (h), and ^{15}N amide (c), (f), (i) spectral regions are shown for the TTR(105-115)_{YTIA} (a)-(c), TTR(105-115)_{AALL} (d)-(f), and TTR(105-115)_{LSPY} (g)-(i) samples. ^{13}C and ^{15}N spectra were acquired using the ramped CP pulse sequence^{33,34} (see text) with 128 and 512 scans, respectively, a 3 s recycle delay, and spinning frequencies of 8.929 kHz (a)-(c), 10.87 kHz (d)-(e), and 10.0 kHz (g)-(i).

Table 7-1. ^{13}C and ^{15}N Chemical Shifts Measured in TTR(105-115) Fibrils

Residue	^{15}N	^{13}CO	$^{13}\text{C}^{\alpha}$	$^{13}\text{C}^{\beta}$	$^{13}\text{C}^{\gamma}$	$^{13}\text{C}^{\delta}$	$^{13}\text{C}^{\epsilon}$	$^{13}\text{C}^{\zeta}$
Y105	39.2	172.0	56.3	36.5	124.5	134.5/133.4	118.7/117.8	160.0
T106	117.0	173.5	62.6	72.5	20.0	—	—	—
I107	127.0	174.1	60.2	41.8	28.2/17.0	14.6	—	—
A108	128.0	174.5	49.9	22.1	—	—	—	—
A109	125.1	173.3	50.3	22.9	—	—	—	—
L110	127.0	174.2	54.4	45.5	29.4	28.2/23.9	—	—
L111	127.5	173.9	54.1	44.3	29.9	27.7/25.3	—	—
S112	117.2	173.6	55.4	63.2	—	—	—	—
P113	135.8	174.8	62.6	32.6	28.0	49.6	—	—
Y114	127.3	173.6	57.7	43.8	128.7	133.6	118.3	157.4
S115	—	—	57.8*	—	—	—	—	—

All chemical shifts are in ppm, referenced indirectly to the methyl ^1H resonance of DSS.⁴¹

*S115 $^{13}\text{C}^{\alpha}$ chemical shift was measured in a selectively labeled fibril sample.

Table 7-2. ^{13}C and ^{15}N Linewidths Measured in TTR(105-115) Fibrils

Residue	^{15}N	^{13}CO	$^{13}\text{C}^{\alpha}$	$^{13}\text{C}^{\beta}$	$^{13}\text{C}^{\gamma}$	$^{13}\text{C}^{\delta}$	$^{13}\text{C}^{\epsilon}$	$^{13}\text{C}^{\zeta}$
Y105	0.73	0.87	1.11	1.11	1.50	—	—	1.45
T106	1.14	0.93	1.10	0.88	0.76	—	—	—
I107	1.48	0.94	1.10	1.02	1.03/1.48	0.70	—	—
A108	1.30	0.85	0.96	0.81	—	—	—	—
A109	1.34	0.85	0.94	0.87	—	—	—	—
L110	1.40	1.03	0.96	0.97	0.80	0.83/0.60	—	—
L111	1.02	1.01	1.04	0.86	0.85	0.58/0.60	—	—
S112	0.98	1.06	0.90	0.81	—	—	—	—
P113	0.91	0.92	0.98	0.88	0.82	0.76	—	—
Y114	1.30	0.98	1.07	1.86	1.74	—	—	1.33

Linewidths in ppm are obtained from 1D and 2D NMR spectra described in the text.

2D ^{13}C - ^{13}C and ^{15}N - ^{13}C - ^{13}C correlation spectra used to establish the sequence specific backbone and side-chain ^{13}C and ^{15}N resonance assignments for TTR(105-115) are shown in Figures 7-6 and 7-7. The 2D ^{13}C - ^{13}C experiments (Figure 7-6) employed proton-driven spin diffusion to establish the intraresidue ^{13}C - ^{13}C correlations and identify amino-acid types. In the aliphatic regions of the 2D spectra most cross-peaks corresponding to the one-bond correlations (indicated by dotted lines in Figure 7-6) are well-resolved, which enables the straightforward identification of the cross-peak patterns

for all residues. A number of correlations with increasingly weaker intensities extending over two or more bonds and corresponding to multiple relayed one-bond transfers are also observed. Most remarkable is the fact that for TTR(105-115)_{AALL}, where two alanine and two leucine residues are (U - ^{13}C , ^{15}N)-labeled, the C^α - C^β , C^β - C^γ and C^γ - C^δ correlations for each residue can be readily identified, with the most significant overlap occurring in the Leu C^δ region.

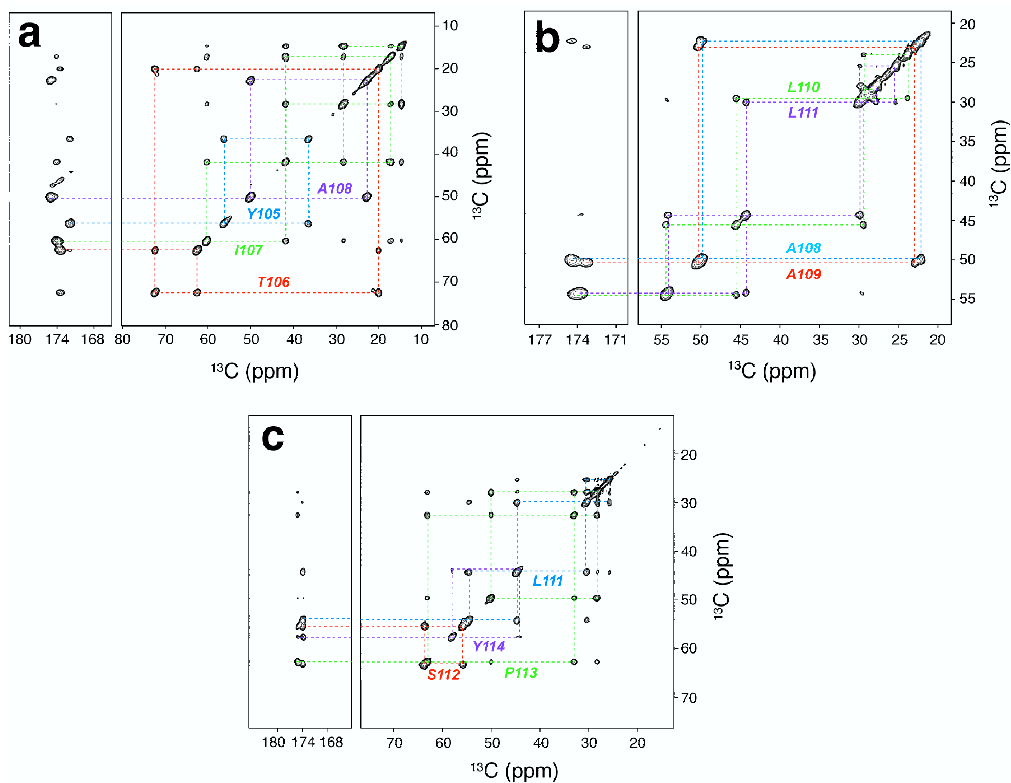


Figure 7-6. 2D ^{13}C - ^{13}C correlation spectra of TTR(105-115) fibrils.

2D ^{13}C - ^{13}C correlation spectra of TTR(105-115)_{YTHA} (a), TTR(105-115)_{AALL} (b), and TTR(105-115)_{LSPY} (c) fibrils. Spectra were acquired at the spinning frequencies of 8.929 kHz (a), 10.87 kHz (b), and 10.0 kHz (c), using the proton-driven spin diffusion pulse sequence³⁵ with a 10 ms ^{13}C - ^{13}C mixing time (see text). 2D data sets were acquired according to Ruben and co-workers,³⁸ with 100-250 complex points in the indirect dimension and increments of 40-92 μs , resulting in the total t_1 evolution times of 8-10 ms. 64 transients were averaged per point with a 3 s recycle delay, resulting in the total 2D acquisition times of \sim 11-27 h. The intraresidue one-bond correlations are indicated in the spectra by dotted lines.

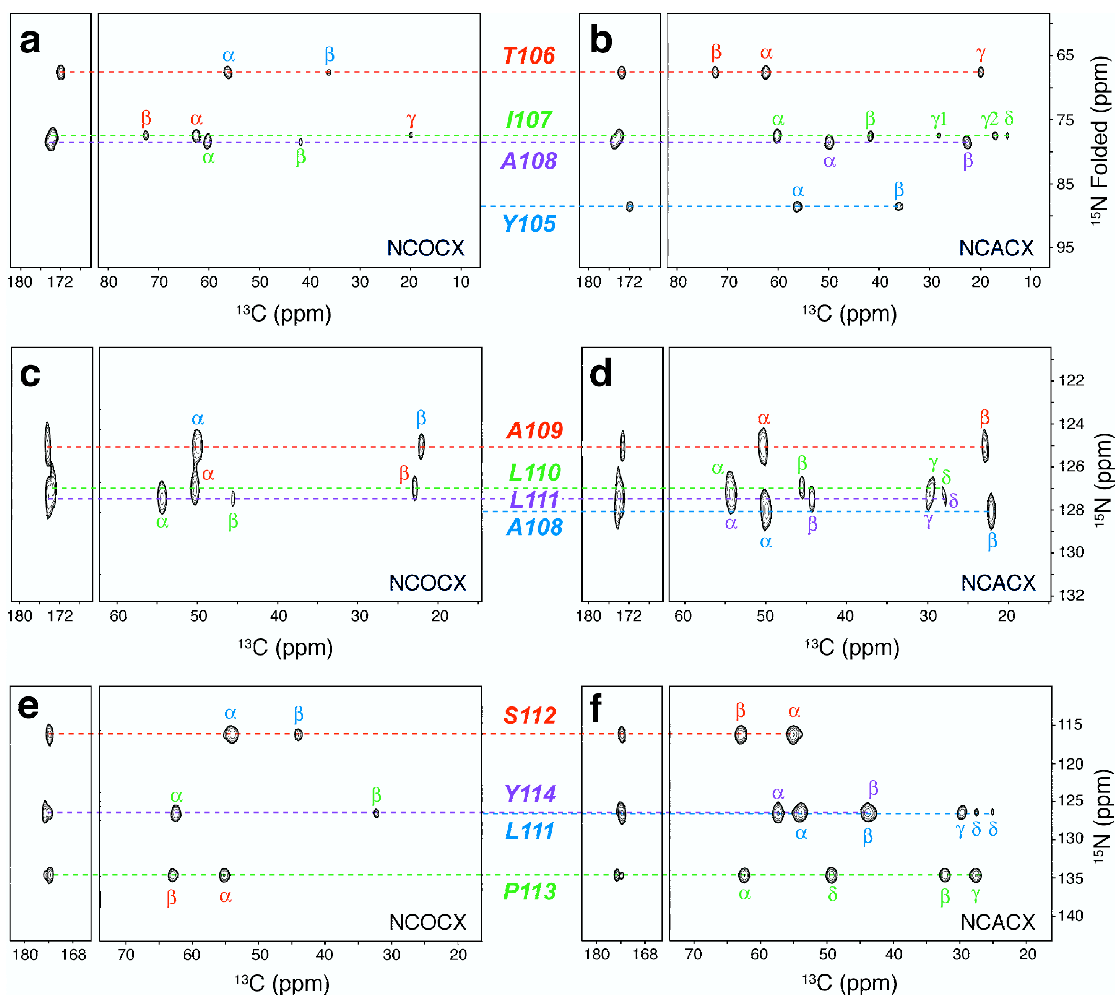


Figure 7-7. 2D ^{15}N - ^{13}C - ^{13}C correlation spectra of TTR(105-115) fibrils.

2D ^{15}N - ^{13}C - ^{13}C correlation spectra of TTR(105-115)_{Y71A} (a)-(b), TTR(105-115)_{A111L} (c)-(d), and TTR(105-115)_{L50P} (e)-(f) fibrils. The NCOCX spectra (a), (c), (e) correlate the $^{15}\text{N}_{i-1}$ and $^{13}\text{C}_{i-1}$ resonances, and the NCACX spectra (b), (d), (f) correlate the $^{15}\text{N}_i$ and $^{13}\text{C}_i$ resonances. The spectra were acquired using the NCOCX and NCACX pulse sequences,^{31,32} with a 3 ms ^{15}N - ^{13}C CO or ^{15}N - C^α band-selective CP transfer³⁷ followed by a 10-20 ms ^1H -driven spin-diffusion ^{13}C - ^{13}C mixing (see text), and the spinning frequencies of 8.929 kHz (a)-(b), 10.87 kHz (c)-(d), and 10.0 kHz (e)-(f). 2D data sets were acquired according to Ruben and co-workers,³⁸ with 7-21 complex points in the indirect dimension and increments of 0.4-1.656 ms, resulting in the total t_1 evolution times of 8-12 ms. 256-768 transients were averaged per point and a 3 s recycle delay was used, resulting in the total 2D acquisition time of ~10 h. For each pair of NCOCX and NCACX spectra the residues participating in the ^{15}N - ^{13}C correlations are labeled.

The ^{15}N resonances were assigned using 2D NCACX experiments (Figure 7-7b) analogous to those described in the literature,^{31,32} which establish the intraresidue ^{15}N - ^{13}C correlations. All N- C^α correlations except Leu 110 and Leu 111 are well-resolved in the 2D spectra and enable the unambiguous assignment of the amide ^{15}N resonances (Leu 110 and Leu 111 ^{15}N chemical shifts were obtained from N- C^β correlations generated using ^{13}C - ^{13}C proton-driven spin diffusion). 2D NCOCX experiments^{31,32} (Figure 7-7a) were used to establish the interresidue correlations (between the ^{15}N resonance of residue i and ^{13}C resonances of residue $i-1$) required for sequence specific assignments. Note that due to the isotope labeling scheme employed, the sequence specific ^{13}C and ^{15}N assignments for the TTR(105-115)_{YTTA} and TTR(105-115)_{LSPY} samples would be obtained using only the 2D ^{13}C - ^{13}C and NCACX experiments, while all three experiments are necessary to assign the spectra of TTR(105-115)_{AALL} fibrils. Furthermore, we note that although three (U- ^{13}C , ^{15}N)-labeled TTR(105-115) fibril samples were used to assign the ^{13}C and ^{15}N chemical shifts in this work, inspection of the 2D correlation spectra indicates that complete sequence specific resonance assignments could be established using a single uniformly isotope labeled fibril sample.

Site-specific ^1H , ^{13}C and ^{15}N resonance assignments are in themselves a source of valuable structural information in solution- and solid-state NMR studies of peptides and proteins because the secondary shifts (i.e., differences between the experimentally observed isotropic chemical shifts and the corresponding random coil values) can be used reliably to predict the conformation of the protein backbone.⁴²⁻⁴⁶ Figure 7-8 shows the ^{13}CO , $^{13}\text{C}^\alpha$, $^{13}\text{C}^\beta$ and ^{15}N secondary shifts for the TTR(105-115) fibrils, which strongly indicate that the peptide adopts a β -strand conformation in the fibrillar state.

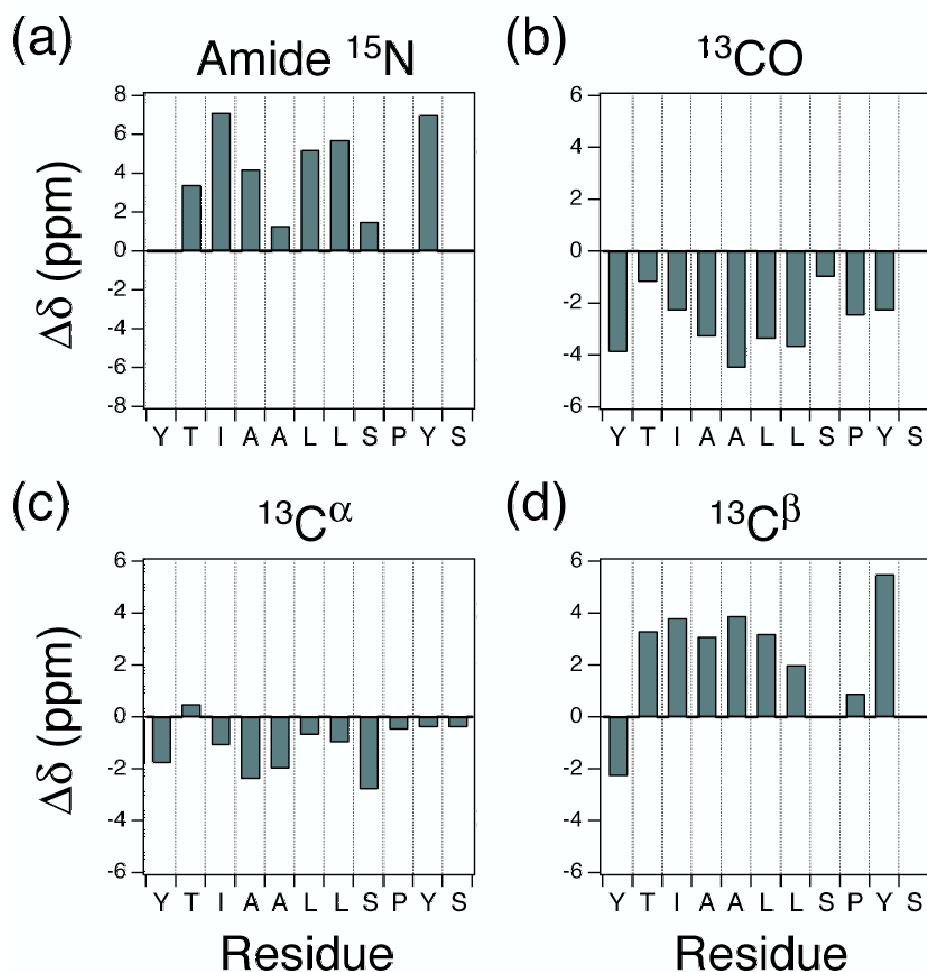


Figure 7-8. Secondary ^{15}N and ^{13}C chemical shifts in TTR(105-115) fibrils.

The secondary shifts ($\Delta\delta$) for amide ^{15}N (a), ^{13}C carbonyl (b), $^{13}\text{C}\alpha$ (c) and $^{13}\text{C}\beta$ (d) resonances were calculated as $\Delta\delta = \delta_{\text{EXP}} - \delta_{\text{RC}}$, where δ_{EXP} and δ_{RC} are the experimentally observed and random coil chemical shifts in ppm, respectively. The random coil shifts used have been reported previously^{42,47} and correspond to the values used by the TALOS program⁴³ to provide quantitative predictions for the torsion angles ϕ and ψ (c.f. Table 7-3). The secondary shifts for Y105 ^{15}N , S115 ^{15}N , S115 $^{13}\text{C}\text{O}$ and S115 $^{13}\text{C}\beta$ could not be calculated; Y105 is the N-terminal residue and S115 was not (^{13}C , ^{15}N)-labeled in any of the samples (S115 $^{13}\text{C}\alpha$ chemical shift was obtained using a selectively labeled sample).

Quantitative predictions for backbone torsion angles ϕ and ψ in TTR(105-115) fibrils were made using the TALOS program⁴³ (Table 7-3). Satisfactory convergence is obtained for eight out of the nine residues, for which the program can predict ϕ and ψ .

The torsion angles with estimated uncertainties of approximately $\pm 20^\circ$ are all between ca. -80° – -130° for ϕ and ca. 125° – 145° for ψ . These angles are in the β -strand region of the Ramachandran plot. The conformation of the peptide bond between S112 and P113 could, in addition, be determined from the chemical shift data. The difference of 4.6 ppm between the $^{13}\text{C}^\beta$ and $^{13}\text{C}^\gamma$ chemical shifts for Pro-113 in TTR(105-115) fibrils indicates that the S112-P113 peptide bond exists in a *trans* conformation.⁴⁸ This conformation is the more common one in peptides and globular proteins, and indeed the S112-P113 peptide bond in native TTR is *trans*.¹⁷

Table 7-3. Backbone Torsion Angles ϕ and ψ in TTR(105-115) Fibrils and in wt TTR

Residue	Predicted TALOS ϕ Angle in Fibrils (deg)	Predicted TALOS ψ Angle in Fibrils (deg)	X-ray ϕ Angle in wt TTR (deg) [‡]	X-ray ψ Angle in wt TTR (deg) [‡]
Y105	— [*]	— [*]	-117/-116	127/129
T106	— [†]	— [†]	-120/-124	115/114
I107	-125 ± 20	143 ± 12	-105/-102	119/126
A108	-117 ± 22	133 ± 13	-104/-112	138/147
A109	-131 ± 14	129 ± 18	-126/-140	141/131
L110	-112 ± 18	120 ± 16	-124/-112	111/113
L111	-118 ± 22	137 ± 15	-99/-98	145/132
S112	-109 ± 22	136 ± 27	-140/-130	160/161
P113	-81 ± 31	126 ± 19	-50/-61	-49/-40
Y114	-112 ± 27	138 ± 15	-113/-115	20/14
S115	— [*]	— [*]	-155/-156	149/147

Backbone torsion angles ϕ and ψ obtained for TTR(105-115) fibrils using the TALOS program⁴³ are compared with the corresponding angles in the wt TTR X-ray structure.¹⁷ TALOS uses experimental ^{13}C and ^{15}N chemical shifts (c.f. Table 7-1) and sequence homology to predict the most likely values for ϕ and ψ .
*Torsion angles for the N- and C-terminal residues are not accessible because TALOS compares chemical shifts for three residues at-a-time to predict ϕ and ψ for the central residue in each triplet.

[†]No satisfactory convergence was obtained for T106.

[‡]Entries correspond to the two subunits of the crystallographic dimer.¹⁷

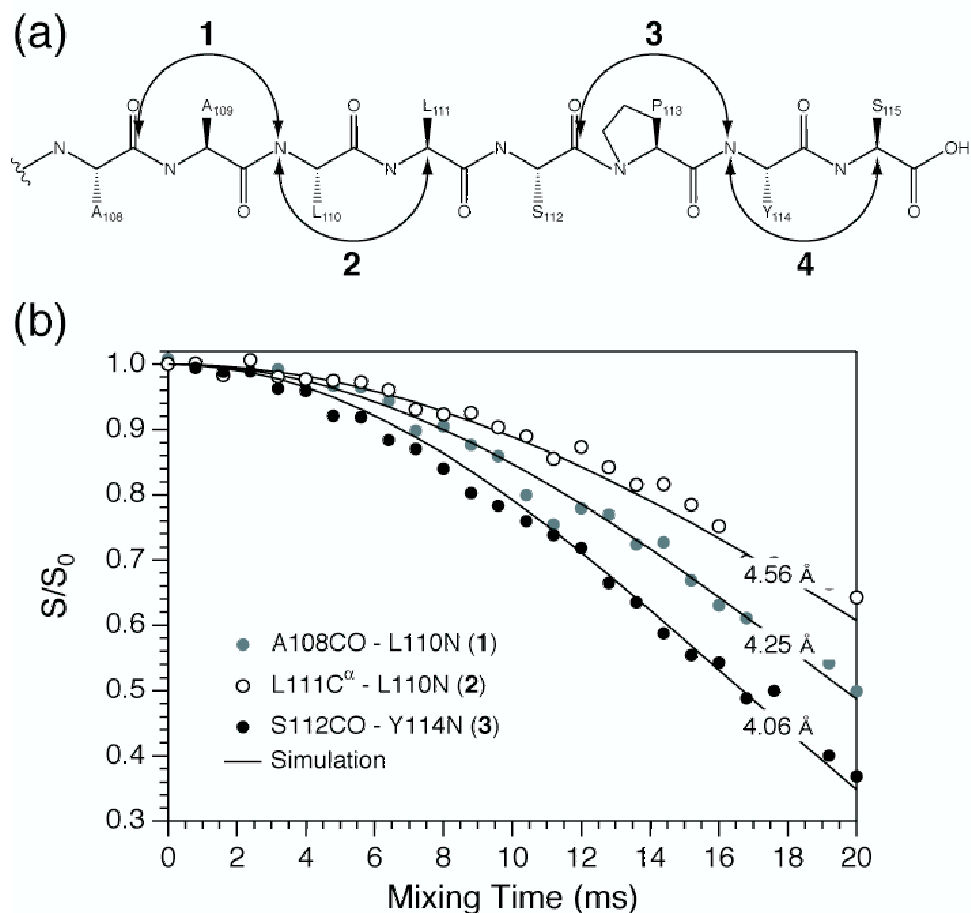


Figure 7-9. Backbone ^{13}C - ^{15}N distances measured in selectively labeled TTR(105-115) fibrils using REDOR.

The schematic of the peptide backbone and the specific distances measured are shown in (a). Distances indicated in (a) as **1** and **2** were measured in fibrils isotopically labeled at A108 ^{13}C O, L111 $^{13}\text{C}^\alpha$ and L110 ^{15}N and distances indicated as **3** and **4** were measured in fibrils labeled at S112 ^{13}C O, S115 $^{13}\text{C}^\alpha$ and Y114 ^{15}N . Experimental (circles) and simulated (lines) REDOR S/S_0 curves are shown in (b). The experimental curves correspond to the distances: A108 CO-L110 N (●), L111 C $^\alpha$ -L110 N (○) and S112 CO-Y114 N (●). The measured distances are indicated directly in (b) and summarized in Table 7-4 (the S115 C $^\alpha$ -Y114 N measurement was omitted for clarity). The S and S_0 spectra were acquired using the REDOR pulse sequence³⁹ with 320-384 transients and the spinning frequency of 10.0 kHz \pm 5 Hz.

We next performed REDOR experiments³⁹ on selectively ^{13}C , ^{15}N labeled TTR(105-115) fibrils to determine several carbon-nitrogen distances along the peptide backbone (Figure 7-9). The measured distances (Table 7-4) are in good agreement (i.e.,

within $\sim 0.05\text{-}0.2$ Å) with those found in a TTR(105-115) backbone model constructed using the ϕ and ψ angles obtained from TALOS (*vide infra*). Furthermore, the distances in the central region of the peptide (A108 CO-L110 N and L111 C $^{\alpha}$ -L110 N) are consistent with the wt TTR X-ray structure,¹⁷ whereas the S112 CO-Y114 N and S115 C $^{\alpha}$ -Y114 N distances in the fibril are significantly longer than the corresponding distances in native TTR.¹⁷ Despite the potential presence of non-negligible intermolecular dipolar couplings, a simple two-spin model was used to analyze the REDOR dephasing data. The rationale for this is that no information is available about the supramolecular organization of peptides in the fibril, and hence about the magnitude of the intermolecular couplings. The influence of these couplings on the dipolar dephasing was investigated via simulations of multiple spin systems resulting from canonical in-register parallel and antiparallel β -strand topologies. For the parallel arrangement we found that the intramolecular distances obtained using the two-spin model are underestimated by $\sim 0.1\text{-}0.3$ Å. For the antiparallel arrangement the L111 C $^{\alpha}$ -L110N distance is underestimated by ca. 0.5 Å and all other measurements are unaffected. In summary, the use of the two-spin model does not lead to significant systematic errors for most of the intramolecular distances measured, regardless of the arrangement of the peptides in the fibril, and it does not alter the conclusion that TTR(105-115) adopts an extended β -strand conformation in the fibril.

Table 7-4. Backbone Carbon-Nitrogen Distances in TTR(105-115) Fibrils and in wt TTR

Atoms		Measured REDOR Distance in Fibrils (Å)*	Predicted TALOS Distance in Fibrils (Å)	X-ray Distance in wt TTR (Å)†
A108 CO	L110 N	4.25 ± 0.15	4.28	4.34/4.36
L111 C ^α	L110 N	4.56 ± 0.12	4.60	4.54/4.56
S112 CO	Y114 N	4.06 ± 0.06	3.94	3.26/3.29
S115 C ^α	Y114 N	5.0 ^{+1.5} _{-0.5}	4.80	4.11/4.17

Distances measured in selectively ¹³C, ¹⁵N labeled fibrils using REDOR³⁹ are compared with the corresponding distances in a TTR(105-115) backbone model constructed according to the TALOS⁴³ predictions for ϕ and ψ (c.f. Table 7-3) and in the wt TTR X-ray structure.¹⁷

*REDOR dephasing data were analyzed using a two-spin model (see text) and the uncertainties correspond to the 95% confidence limit.

†Entries correspond to the two subunits of the crystallographic dimer.¹⁷

Figure 7-10 compares the structure of the peptide fragment corresponding to residues 105-115 in wt TTR¹⁷ and the backbone model for TTR(105-115) in the fibrillar state constructed using the torsion angles in Table 7-3. In wt TTR residues 105-111 have typical β -strand ϕ and ψ angles and residues 112-114 form a turn, with Pro-113 torsion angles in the helical region of the Ramachandran plot (Table 7-3). The comparison of torsion angles and distances for wt TTR and TTR(105-115) peptide in the fibrils reveals remarkable similarity in the backbone conformation of residues 107-111. However the backbone turn involving residues 112-114, characterized in wt TTR¹⁷ by the relatively short S112 CO-Y114 N distance (Table 7-4), is absent in TTR(105-115) fibrils where we find typical β -strand ϕ and ψ values for residues 112-114. In the native structure, Pro-113 promotes interactions with adjacent strands and dictates tertiary contacts, preventing self-association. In the absence of this greater context, and despite its inability to participate in a hydrogen-bonding network, the proline is instead fully incorporated into the β -strand and possibly also into the β -sheet fibrillar array. This observation illustrates the importance of three-dimensional context in the adoption of secondary structure, but also

represents one way in which nature neatly manipulates folding propensity to prevent aggregation.

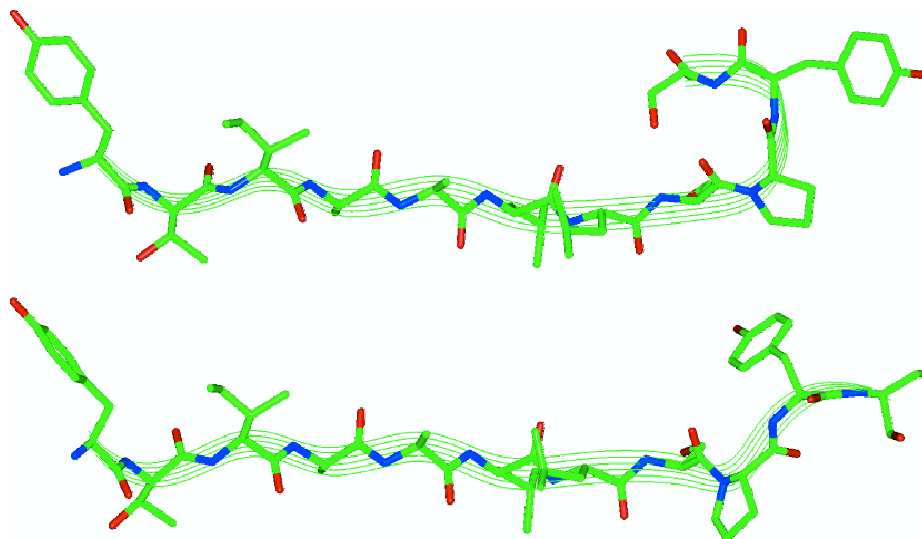


Figure 7-10. X-ray structure of the peptide fragment corresponding to residues 105-115 in wt TTR and the backbone model for the TTR(105-115) peptide in the fibrillar state.

X-ray structure of the peptide fragment corresponding to residues 105-115 in wt TTR¹⁷ (top) and the backbone model for the TTR(105-115) peptide in the fibrillar state constructed using the ϕ and ψ angles in Table 7-3 (bottom). The Y105 and T106 backbone torsion angles used in the model were obtained using preliminary SSNMR measurements of internuclear distances and torsion angles (unpublished data) analogous to those published previously.^{28,49-51} No constraints are available for ψ_{S115} and the experiments designed to probe side-chain χ angles are currently in progress (unpublished data). These moieties are present for illustration purposes only and their conformations in the model correspond to those found in wt TTR.¹⁷ The figure was prepared using the program Insight II version 2000 (Accelrys Inc., San Diego, CA).

7.4 Conclusions

We have carried out the initial step in the determination of the complete atomic-resolution structure of an amyloid fibril, by characterizing the molecular conformation of a peptide fragment of transthyretin using 1D and 2D ¹³C and ¹⁵N MAS NMR techniques. The present results show that exceptionally high-quality NMR data can be obtained for

amyloid fibrils. The ^{13}C and ^{15}N linewidth measurements indicate that TTR(105-115) forms a highly ordered structure with each amino acid in a unique environment. This observation is consistent with the concept that the amyloid core structure is generic and can override the properties of individual sequences that define the structures of globular proteins. Quantitative predictions for the backbone torsion angles were obtained using the sequence specific ^{13}C and ^{15}N backbone and side-chain chemical shifts. Furthermore, four backbone ^{13}C - ^{15}N distances in the 4-5 Å range were measured using REDOR NMR. The results indicate that TTR(105-115) adopts a β -strand conformation in the fibrillar state in a structure remarkably similar to that found in the native protein, with the exception of the region surrounding the proline residue. Although we as yet have no information about the three-dimensional organization of the peptides, the quality of the NMR data will enable us to probe the higher order architecture and determine the complete structure of an amyloid fibril to atomic-resolution. These experiments are currently underway.

Acknowledgments

We would like to thank Dr. Jesús Zurdo, Vikram Bajaj, and Dr. Michael McMahon for stimulating discussions. C. P. J. is a National Science Foundation Predoctoral Fellow. C. E. M. is a Royal Society Dorothy Hodgkin Research Fellow. N. S. A. is a National Institutes of Health Postdoctoral Fellow (1 F32 NS10964-01). The research of C. M. D. is supported in part by the Wellcome Trust and the research of R. G. G. was supported by National Institutes of Health grants GM-23403 and RR-00995.

References

- (1) M. Sunde and C. C. F. Blake, "From the globular to the fibrous state: protein structure and structural conversion in amyloid formation," *Q. Rev. Biophys.* **31**, 1-39 (1998).
- (2) J. W. Kelly, "The alternative conformations of amyloidogenic proteins and their multi-step assembly pathways," *Curr. Opin. Struct. Biol.* **8**, 101-106 (1998).
- (3) J. I. Guijarro, M. Sunde, J. A. Jones, I. D. Campbell and C. M. Dobson, "Amyloid fibril formation by an SH3 domain," *Proc. Natl. Acad. Sci. USA* **95**, 4224-4228 (1998).
- (4) F. Chiti, P. Webster, N. Taddei, A. Clark, M. Stefani, G. Ramponi and C. M. Dobson, "Designing conditions for in vitro formation of amyloid protofilaments and fibrils," *Proc. Natl. Acad. Sci. USA* **96**, 3590-3594 (1999).
- (5) R. G. Griffin, "Dipolar recoupling in MAS spectra of biological solids," *Nature Struct. Biol.* **5**, 508-512 (1998).
- (6) S. Dusold and A. Sebald, "Dipolar recoupling under magic-angle spinning conditions," *Annu. Rep. Nucl. Magn. Reson. Spectr.* **41**, 185-264 (2000).
- (7) R. G. S. Spencer, K. J. Halverson, M. Auger, A. E. McDermott, R. G. Griffin and P. T. Lansbury, "An unusual peptide conformation may precipitate amyloid formation in Alzheimer's disease: Application of solid-state NMR to the determination of protein secondary structure," *Biochemistry* **30**, 10382-10387 (1991).
- (8) P. T. Lansbury, P. R. Costa, J. M. Griffiths, E. J. Simon, M. Auger, K. J. Halverson, D. A. Kocisko, Z. S. Hendsch, T. T. Ashburn, R. G. S. Spencer, B. Tidor and R. G. Griffin, "Structural model for the β -amyloid fibril based on interstrand alignment of

- an antiparallel-sheet comprising a C-terminal peptide," *Nature Struct. Biol.* **2**, 990-998 (1995).
- (9) T. L. S. Benzinger, D. M. Gregory, T. S. Burkoth, H. Miller-Auer, D. G. Lynn, R. E. Botto and S. C. Meredith, "Propagating structure of Alzheimer's β -amyloid₍₁₀₋₃₅₎ is parallel β -sheet with residues in exact register," *Proc. Natl. Acad. Sci. USA* **95**, 13407-13412 (1998).
- (10) D. M. Gregory, T. L. S. Benzinger, T. S. Burkoth, H. Miller-Auer, D. G. Lynn, S. C. Meredith and R. E. Botto, "Dipolar recoupling NMR of biomolecular self-assemblies: determining inter- and intrastrand distances in fibrilized Alzheimer's β -amyloid peptide," *Solid State Nucl. Magn. Reson.* **13**, 149-166 (1998).
- (11) T. L. S. Benzinger, D. M. Gregory, T. S. Burkoth, H. Miller-Auer, D. G. Lynn, R. E. Botto and S. C. Meredith, "Two-dimensional structure of β -amyloid(10-35) fibrils," *Biochemistry* **39**, 3491-3499 (2000).
- (12) J. J. Balbach, Y. Ishii, O. N. Antzutkin, R. D. Leapman, N. W. Rizzo, F. Dyda, J. Reed and R. Tycko, "Amyloid fibril formation by A β 16-22, a seven-residue fragment of the Alzheimer's β -amyloid peptide, and structural characterization by solid state NMR," *Biochemistry* **39**, 13748-13759 (2000).
- (13) O. N. Antzutkin, J. J. Balbach, R. D. Leapman, N. W. Rizzo, J. Reed and R. Tycko, "Multiple quantum solid-state NMR indicates a parallel, not antiparallel, organization of β -sheets in Alzheimer's β -amyloid fibrils," *Proc. Natl. Acad. Sci. USA* **97**, 13045-13050 (2000).

- (14) J. M. Griffiths, T. T. Ashburn, M. Auger, P. R. Costa, R. G. Griffin and P. T. Lansbury, "Rotational resonance solid-state NMR elucidates a structural model of pancreatic amyloid," *J. Am. Chem. Soc.* **117**, 3539-3546 (1995).
- (15) J. Heller, A. C. Kolbert, R. Larsen, M. Ernst, T. Bekker, M. Baldwin, S. B. Prusiner, A. Pines and D. E. Wemmer, "Solid-state NMR studies of the prion protein H1 fragment," *Protein Sci.* **5**, 1655-1661 (1996).
- (16) D. D. Laws, H. L. Bitter, K. Liu, H. L. Ball, K. Kaneko, H. Wille, F. E. Cohen, S. B. Prusiner, A. Pines and D. E. Wemmer, "Solid-state NMR studies of the secondary structure of a mutant prion protein fragment of 55 residues that induces neurodegeneration," *Proc. Natl. Acad. Sci. USA* **98**, 11686-11690 (2001).
- (17) C. C. F. Blake, M. J. Geisow, S. J. Oatley, B. Rerat and C. Rerat, "Structure of prealbumin: secondary, tertiary and quaternary interactions determined by Fourier refinement at 1.8 Å," *J. Mol. Biol.* **121**, 339-356 (1978).
- (18) P. Westermark, K. Sletten, B. Johansson and G. G. Cornwell, "Fibril in senile systemic amyloidosis is derived from normal transthyretin," *Proc. Natl. Acad. Sci. USA* **87**, 2843-2845 (1990).
- (19) M. J. M. Saraiva, "Transthyretin mutations in hyperthyroxinemia and amyloid diseases," *Hum. Mutat.* **17**, 493-503 (2001).
- (20) A. Gustavsson, U. Engstrom and P. Westermark, "Normal transthyretin and synthetic fragments form amyloid-like fibrils in vitro," *Biochem. Biophys. Res. Commun.* **175**, 1159-1164 (1991).
- (21) W. Colon and J. W. Kelly, "Partial denaturation of transthyretin is sufficient for amyloid fibril formation in vitro," *Biochemistry* **31**, 8654-8660 (1992).

- (22) M. J. Bonifacio, Y. Sakaki and M. J. Saraiva, "In vitro amyloid fibril formation from transthyretin: The influence of ions and the amyloidogenicity of TTR variants," *Biochim. Biophys. Acta* **1316**, 35-42 (1996).
- (23) C. E. MacPhee and C. M. Dobson, "Chemical dissection and reassembly of amyloid fibrils formed by a peptide fragment of transthyretin," *J. Mol. Biol.* **297**, 1203-1215 (2000).
- (24) C. C. F. Blake and S. J. Oatley, "Protein-DNA and protein-hormone interactions in prealbumin," *Nature* **268**, 115-120 (1977).
- (25) J. A. Jarvis, D. J. Craik and M. C. J. Wilce, "X-ray diffraction studies of fibrils formed from peptide fragments of transthyretin," *Biochem. Biophys. Res. Commun.* **192**, 991-998 (1993).
- (26) J. A. Jarvis, A. Kirkpatrick and D. J. Craik, "¹H NMR analysis of fibril-forming peptide fragments of transthyretin," *Int. J. Peptide Protein Res.* **44**, 388-398 (1994).
- (27) C. M. Rienstra, M. Hohwy, M. Hong and R. G. Griffin, "2D and 3D ¹⁵N-¹³C-¹³C NMR chemical shift correlation spectroscopy of solids: assignment of MAS spectra of peptides," *J. Am. Chem. Soc.* **122**, 10979-10990 (2000).
- (28) C. P. Jaroniec, B. A. Tounge, J. Herzfeld and R. G. Griffin, "Frequency selective heteronuclear dipolar recoupling in rotating solids: Accurate ¹³C-¹⁵N distance measurements in uniformly ¹³C, ¹⁵N-labeled peptides," *J. Am. Chem. Soc.* **123**, 3507-3519 (2001).
- (29) A. Detken, E. H. Hardy, M. Ernst, M. Kainosho, T. Kawakami, S. Aimoto and B. H. Meier, "Methods for sequential resonance assignment in solid, uniformly ¹³C, ¹⁵N

- labelled peptides: Quantification and application to antamanide," *J. Biomol. NMR* **20**, 203-221 (2001).
- (30) A. McDermott, T. Polenova, A. Bockmann, K. W. Zilm, E. K. Paulsen, R. W. Martin and G. T. Montelione, "Partial NMR assignments for uniformly (^{13}C , ^{15}N)-enriched BPTI in the solid state," *J. Biomol. NMR* **16**, 209-219 (2000).
- (31) T. A. Egorova-Zachernyuk, J. Hollander, N. Fraser, P. Gast, A. J. Hoff, R. Cogdell, H. J. M. de Groot and M. Baldus, "Heteronuclear 2D-correlations in a uniformly [^{13}C , ^{15}N] labeled membrane-protein complex at ultra-high magnetic fields," *J. Biomol. NMR* **19**, 243-253 (2001).
- (32) J. Pauli, M. Baldus, B. van Rossum, H. de Groot and H. Oschkinat, "Backbone and side-chain ^{13}C and ^{15}N signal assignments of the α -spectrin SH3 domain by magic angle spinning solid-state NMR at 17.6 Tesla," *ChemBiochem* **2**, 272-281 (2001).
- (33) A. Pines, M. G. Gibby and J. S. Waugh, "Proton-enhanced NMR of dilute spins in solids," *J. Chem. Phys.* **59**, 569-590 (1973).
- (34) G. Metz, X. Wu and S. O. Smith, "Ramped-amplitude cross-polarization in magic-angle-spinning NMR," *J. Magn. Reson. A* **110**, 219-227 (1994).
- (35) D. Suter and R. R. Ernst, "Spin diffusion in resolved solid-state NMR spectra," *Phys. Rev. B* **32**, 5608-5627 (1985).
- (36) T. G. Oas, R. G. Griffin and M. H. Levitt, "Rotary resonance recoupling of dipolar interactions in solid-state nuclear magnetic resonance spectroscopy," *J. Chem. Phys.* **89**, 692-695 (1988).

- (37) M. Baldus, A. T. Petkova, J. Herzfeld and R. G. Griffin, "Cross polarization in the tilted frame: assignment and spectral simplification in heteronuclear spin systems," *Mol. Phys.* **95**, 1197-1207 (1998).
- (38) D. J. States, R. A. Haberkorn and D. J. Ruben, "A two-dimensional nuclear Overhauser experiment with pure absorption phase in four quadrants," *J. Magn. Reson.* **48**, 286-292 (1982).
- (39) T. Gullion and J. Schaefer, "Detection of weak heteronuclear dipolar coupling by rotational-echo double-resonance nuclear magnetic resonance," *Adv. Magn. Reson.* **13**, 57-83 (1989).
- (40) A. E. Bennett, C. M. Rienstra, M. Auger, K. V. Lakshmi and R. G. Griffin, "Heteronuclear decoupling in rotating solids," *J. Chem. Phys.* **103**, 6951-6957 (1995).
- (41) D. S. Wishart, C. G. Bigam, J. Yao, F. Abildgaard, H. J. Dyson, E. Oldfield, J. L. Markley and B. D. Sykes, "¹H, ¹³C and ¹⁵N chemical shift referencing in biomolecular NMR," *J. Biomol. NMR* **6**, 135-140 (1995).
- (42) S. Spera and A. Bax, "Empirical correlation between protein backbone conformation and C α and C β ¹³C nuclear magnetic resonance chemical shifts," *J. Am. Chem. Soc.* **113**, 5490-5492 (1991).
- (43) G. Cornilescu, F. Delaglio and A. Bax, "Protein backbone angle restraints from searching a database for chemical shift and sequence homology," *J. Biomol. NMR* **13**, 289-302 (1999).
- (44) D. S. Wishart and B. D. Sykes, "Chemical shifts as a tool for structure determination," *Methods Enzymol.* **239**, 363-392 (1994).

- (45) D. S. Wishart and D. A. Case, "Use of chemical shifts in macromolecular structure determination," *Methods Enzymol.* **338**, 3-34 (2001).
- (46) H. Saito, "Conformation dependent ^{13}C chemical shifts: A new means of conformational characterization as obtained by high-resolution solid-state ^{13}C NMR," *Magn. Reson. Chem.* **24**, 835-852 (1986).
- (47) D. S. Wishart, C. G. Bigam, A. Holm, R. S. Hodges and B. D. Sykes, " ^1H , ^{13}C and ^{15}N random coil NMR chemical shifts of the common amino acids. 1. Investigations of nearest neighbor effects," *J. Biomol. NMR* **5**, 67-81 (1995).
- (48) S. K. Sarkar, D. A. Torchia, K. D. Kopple and D. L. VanderHart, "Study of proline peptide bond conformation and ring dynamics in crystalline cyclic peptides using ^{13}C MAS NMR," *J. Am. Chem. Soc.* **106**, 3328-3331 (1984).
- (49) C. M. Rienstra, L. Tucker-Kellogg, C. P. Jaroniec, M. Hohwy, B. Reif, T. Lozano-Perez, B. Tidor and R. G. Griffin, "*De novo* determination of peptide structure with solid-state MAS NMR spectroscopy," *Proc. Natl. Acad. Sci. USA* **99**, 10260-10265 (2002).
- (50) C.P. Jaroniec, C. Filip, R.G. Griffin, "3D TEDOR NMR experiments for the simultaneous measurement of multiple carbon-nitrogen distances in uniformly ^{13}C , ^{15}N labeled solids," *J. Am. Chem. Soc.* **124**, 10728-10742 (2002).
- (51) C.M. Rienstra, M. Hohwy, L.J. Mueller, C.P. Jaroniec, B. Reif, R.G. Griffin, "Determination of multiple torsion-angle constraints in U- ^{13}C , ^{15}N -labeled peptides: 3D ^1H - ^{15}N - ^{13}C - ^1H dipolar-chemical shift NMR spectroscopy in rotating solids," *J. Am. Chem. Soc.* **124**, 11908-11922 (2002).

CHAPTER 8. STRUCTURE OF TTR(105-115) IN AN AMYLOID FIBRIL AT ATOMIC RESOLUTION

ABSTRACT

In Chapter 7 magic-angle spinning solid-state NMR spectroscopy was used to investigate an 11-residue fragment of transthyretin, TTR(105-115), in an amyloid fibril. The peptide was shown to form a well-ordered fibrillar structure, and the ^{13}C and ^{15}N resonance assignments, obtained using two-dimensional ^{13}C - ^{13}C and ^{15}N - ^{13}C - ^{13}C correlation experiments, indicate that it adopts an extended β -strand conformation when incorporated into the fibril. The complete resonance assignments permit the acquisition of site-specific structural constraints such as internuclear distances and torsion angles, which are required for the determination of an atomic-resolution structure of the peptide. The measurements of these structural constraints are presented in this chapter. The backbone torsion angles ϕ and ψ are determined using a series of three-dimensional dipolar-chemical shift correlation experiments, which report on the relative orientations of ^{13}C - ^{15}N , ^{13}C - ^1H and ^{15}N - ^1H dipolar tensors and intramolecular carbon-nitrogen distances in the 3-5 Å range are determined using 3D TEDOR methods introduced in Chapter 6, resulting in a total of about 60 structural constraints. An ensemble of atomic-resolution structures of TTR(105-115) in the fibril consistent with the structural constraints is calculated using simulated annealing molecular dynamics. The majority of torsion angles in the ensemble of calculated structures are uniquely defined by the solid-state NMR constraints and the results indicate that the peptide adopts an extended β -strand conformation in the fibril.

8.1 Torsion Angle Measurements

The dipolar and chemical shielding interactions are anisotropic and hence depend on the relative orientation of the molecular segment with respect to the external magnetic field. This dependence can be exploited to provide the relative orientations of the nuclear spin interaction tensors, which can subsequently be related to molecular torsion angles. A number of multidimensional NMR techniques have been described in the literature for measuring relative tensor orientations in static^{1,2} and spinning solids,³⁻¹⁵ as well as in solution.^{16,17} Briefly, in all of the above methods a correlated state between a pair of coupled nuclear spins is created either via a polarization transfer or the excitation of a multiple quantum coherence and evolves under the local fields due to the interactions with electrons or other nuclear spins. The time evolution of this correlated spin state depends on the relative orientation of the tensorial interactions, and can be related directly to molecular torsion angles.

In this thesis we limit our discussion to the measurements of relative orientations of dipolar interactions, such as $^{13}\text{C}-^{15}\text{N}$, $^{13}\text{C}-^1\text{H}$ and $^{15}\text{N}-^1\text{H}$. For a model system of four coupled spins A—B—C—D the evolution of a correlated state between spins B and C under the local dipolar fields is dominated by the strongest couplings, A—B and C—D, and for individual crystallites the observable signal is to a good approximation given by:

$$S(t_1, t_2, \tau_{mix}) = f_{BC}(\omega_{BC}, \tau_{mix}) \cos(\omega_{AB} t_1) \cos(\omega_{CD} t_2) \quad (1)$$

where ω_{AB} , ω_{BC} , and ω_{CD} are the orientation dependent dipolar couplings reintroduced under MAS by appropriate recoupling pulse sequences and t_1 and t_2 are the dipolar evolution times for the ω_{AB} and ω_{CD} couplings, respectively. f_{BC} describes the polarization transfer or the excitation of multiple quantum coherence between spins B and C, and it is

in general a function of the dipolar coupling ω_{BC} and mixing time τ_{mix} . Although, f_{BC} formally depends on the orientation of the molecular segment with respect to \mathbf{B}_0 , in many applications to peptides and proteins (particularly in the measurements of backbone torsion angles) an isotropic transfer function can be assumed (i.e., $f_{BC} = 1$),^{13,15} and the observable signal is to a good approximation given simply by the product of the cosine functions describing the dephasing under the dipolar couplings. Furthermore, for experiments in (U - ^{13}C , ^{15}N)-labeled molecules three-dimensional NMR experiments are typically employed to measure multiple torsion angles simultaneously, where two chemical shift dimensions are used for site-specific resolution and the information about the relative orientation of the interaction tensors is encoded in the third dimension.^{13,15} The observable signal in eq 1 displays very distinctive features¹⁸ when the arguments of the cosine functions have roughly the same magnitude for each crystallite, i.e.,:

$$\omega_{AB}t_1 \approx \omega_{CD}t_2 \quad (2)$$

This can occur when the dipolar vectors are nearly co-linear (i.e., the projection angle between the vectors is $\Theta \approx 0^\circ$ or 180°), and consequently the most dramatic deviations in the observable signal occur for small deviations (up to $\sim 30^\circ$) from the co-linear topology. For the molecular topologies in this region the torsion angle experiments will have optimum sensitivity and angular resolution. For example, for the peptide backbone (Figure 8-1) the projection angle between the $^1\text{H}_i^{\text{N}}-^{15}\text{N}_i$ and $^1\text{H}_i^\alpha-^{13}\text{C}_i^\alpha$ dipolar couplings depends on the torsion angle ϕ_i , and the corresponding $^1\text{H}_i^{\text{N}}-^{15}\text{N}_i-^{13}\text{C}_i^\alpha-^1\text{H}_i^\alpha$ experiment has the region of optimum angular resolution and sensitivity around $\phi_i = -120^\circ$, in the β -sheet region of the Ramachandran space.⁶

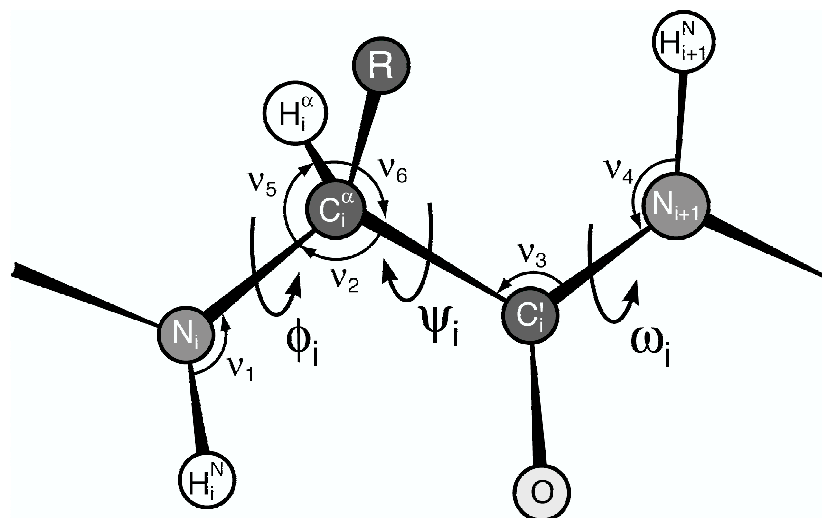


Figure 8-1. Model of the peptide backbone.

Backbone torsion angles ϕ_i , ψ_i and ω_i are indicated. The average values for the three-atom bond angles are: $\nu_1 = 118^\circ$, $\nu_2 = 111^\circ$, $\nu_3 = 116^\circ$, $\nu_4 = 120^\circ$, $\nu_5 = 108^\circ$, $\nu_6 = 109.5^\circ$. The three-atom angles involving heavy atoms are based on the survey of the Cambridge crystallographic database by Engh and Huber.¹⁹ The H^N-N-C^α (ν_1) and $N-C^\alpha-H^\alpha$ (ν_5) angles are based on the survey of the Cambridge crystallographic database by Ishii et al.¹⁰ and the $CO-C^\alpha-H^\alpha$ angle (ν_6) was assumed to be tetrahedral. According to Engh and Huber¹⁹ the three-atom bond angles involving heavy atoms can vary by ca. $1-3^\circ$ in peptides and proteins. Since a large dataset is not available for the three-atom bond angles involving protons, we have assumed similar potential variations in the subsequent analysis of the torsion angle experiments.

In this thesis, we have used three-dimensional dipolar-chemical shift correlation experiments to measure backbone torsion angles ϕ and ψ and constrain the structure of TTR(105-115) while incorporated into the amyloid fibril. The 3D $^1H_i^N-^{15}N_i-^{13}C_i^\alpha-^1H_i^\alpha$ experiment⁶ was used to determine the angles ϕ_i and the combination of 3D $^1H_{i+1}^N-^{15}N_{i+1}-^{13}C_i^\alpha-^1H_i^\alpha$ ^{13,15} and 3D $^{15}N_i-^{13}C_i^\alpha-^{13}CO_i-^{15}N_{i+1}$ ^{7,8} experiments was used to measure ψ_i . In the following sections the results of these experiments are presented, with a focus on the measurements of ψ .

8.1.1 3D $^{15}\text{N}_i\text{-}^{13}\text{C}_i^\alpha\text{-}^{13}\text{CO}_i\text{-}^{15}\text{N}_{i+1}$ Spectroscopy

The $^{15}\text{N}_i\text{-}^{13}\text{C}_i^\alpha\text{-}^{13}\text{CO}_i\text{-}^{15}\text{N}_{i+1}$ experiment for the measurement of ψ_i has been described in detail elsewhere.^{7,8} Here we provide a brief summary of the experiment and present representative measurements of ψ in TTR(105-115) fibrils. Figure 8-2 shows the molecular segment of interest, indicating the projection angle Θ and torsion angle ψ , as well as a plot showing the dependence of Θ on ψ . A well-known feature of all torsion angle experiments is apparent in Figure 8-2, namely that the same value of the projection angle is obtained for two distinct torsion angles (furthermore torsion angle experiments are symmetric about $\Theta = 90^\circ$, thus always resulting in at least two degenerate solutions).

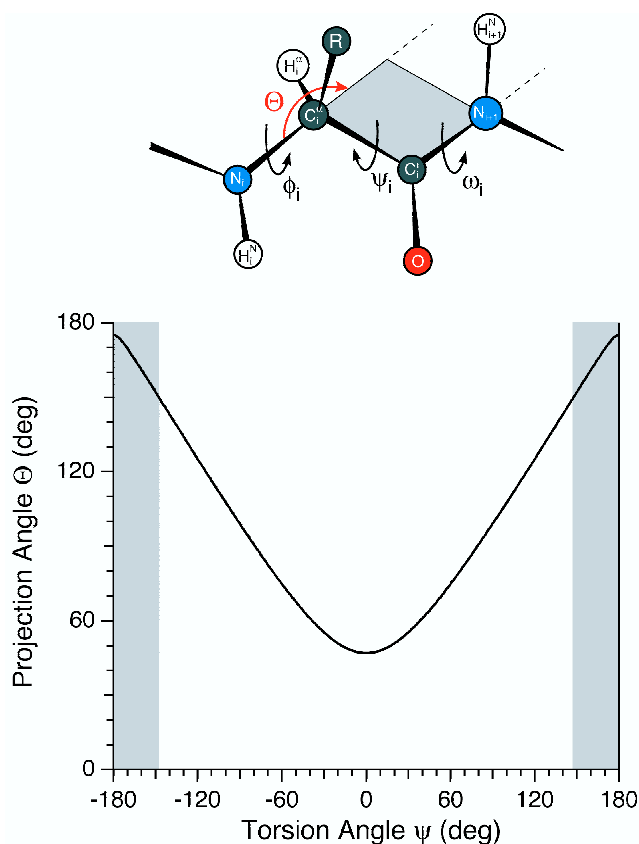


Figure 8-2. Dependence of the projection angle Θ between $^{15}\text{N}_i\text{-}^{13}\text{C}_i^\alpha$ and $^{13}\text{CO}_i\text{-}^{15}\text{N}_{i+1}$ bond vectors on the molecular torsion angle ψ .

Regions of high angular resolution and sensitivity of the $^{15}\text{N}_i\text{-}^{13}\text{C}_i^\alpha\text{-}^{13}\text{CO}_i\text{-}^{15}\text{N}_{i+1}$ experiment (i.e., where Θ is within $\sim 30^\circ$ of the co-linear topology) are indicated by gray rectangles.

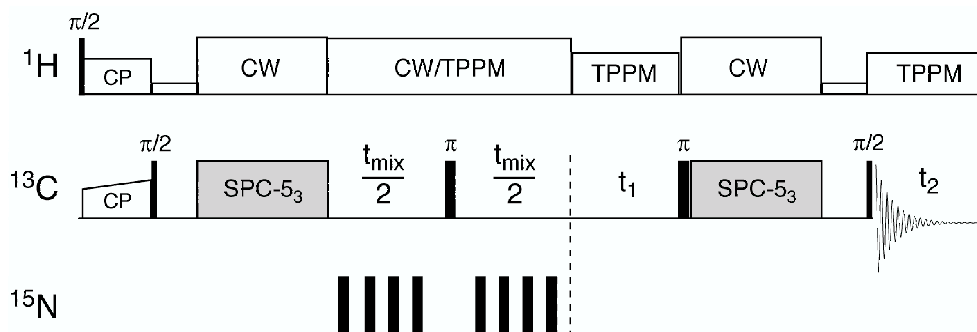


Figure 8-3. 3D $^{15}\text{N}_i$ - $^{13}\text{C}_i^\alpha$ - $^{13}\text{CO}_i$ - $^{15}\text{N}_{i+1}$ pulse sequence for the measurement of ψ_i .

The 3D $^{15}\text{N}_i$ - $^{13}\text{C}_i^\alpha$ - $^{13}\text{CO}_i$ - $^{15}\text{N}_{i+1}$ pulse sequence is shown in Figure 8-3. Following cross-polarization^{20,21} from ^1H to ^{13}C , sum ^{13}C polarization is created by the $\pi/2$ pulse. The SPC-5₃ sequence (see references^{22,23} for the details of the pulse scheme) generates ^{13}C - ^{13}C double quantum (DQ) coherences ($\sim I_1^+ I_2^+ + I_1^- I_2^-$) with high efficiency (~ 50 - 55% DQ filtering efficiency was achieved in a two-spin model system at 500 MHz ^1H Larmor frequency and 10 kHz MAS frequency, compared with the theoretical maximum of $\sim 73\%$). For the measurement of the torsion angle ψ , ^{13}CO - $^{13}\text{C}^\alpha$ coherences are of particular importance. These DQ coherences are frequency labeled during the evolution period t_1 in order to achieve site-specific resolution, resulting in an INADEQUATE²⁴ type 2D double quantum-single quantum (DQ-SQ) correlation spectrum²² shown in Figure 8-4 for the TTR(105-115)_{Y_{TIA}} sample (see Chapter 7 for the details of sample preparation and isotopic labeling schemes).

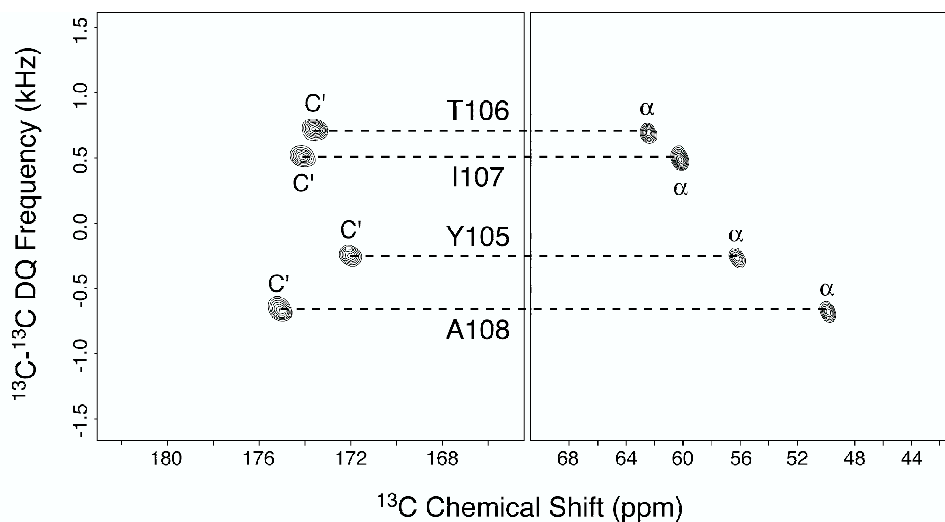


Figure 8-4. Double quantum-single quantum correlation spectrum of TTR(105-115)_{YTA}.

The four ^{13}CO - $^{13}\text{C}^\alpha$ correlations indicated in the spectra are based on resonance assignments²⁵ presented in Chapter 7. The spectrum was acquired at 11.7 T and 10 kHz MAS.

The REDOR²⁶ sequence applied during the period t_{mix} , reintroduces all ^{13}C - ^{15}N couplings simultaneously, which leads to the dephasing of the ^{13}C - ^{13}C DQ coherences. The dipolar dephasing formally depends on the relative orientation of all ^{13}C - ^{15}N couplings. However as noted above,^{7,8} the dephasing is dominated by the strongest dipolar couplings, $^{13}\text{CO}_i$ - $^{15}\text{N}_{i+1}$ and $^{13}\text{C}^\alpha_i$ - $^{15}\text{N}_i$, resulting in the simple analytical expression describing the powder averaged observable signal:

$$S(t_{\text{mix}}, \tau_{\text{DQ}}) \approx \langle f_{\text{DQ}}(\tau_{\text{DQ}}) \cos(\omega_1 t_{\text{mix}}) \cos(\omega_2 t_{\text{mix}}) \rangle \quad (3)$$

where $\langle \dots \rangle$ represents the powder average. Assuming that the z-axis of the crystallite fixed frame (see Chapter 1) coincides with the CO-C $^\alpha$ bond the excitation of the double quantum coherence is given by the analytical AHT expression:^{22,23,27}

$$f_{\text{DQ}} = \sin^2\left(\frac{1}{2\sqrt{2}} kb_{\text{CC}} \sin(2\beta_{\text{CR}}) \tau_{\text{DQ}}\right) \quad (4)$$

where b_{CC} is the ^{13}CO - $^{13}\text{C}^\alpha$ dipolar coupling constant, κ is the dipolar scaling factor for the SPC-5₃ pulse sequence²³ ($\kappa \approx 0.13$), and τ_{DQ} is the total DQ mixing time. The formal orientational dependence of the DQ excitation is contained entirely in the $\sin(2\beta_{\text{CR}})$ term, because SPC-5₃ is a γ -encoded sequence²⁸ (i.e., a pulse sequence for which the magnitude of the recoupled dipolar interaction is independent of the Euler angle γ). The expressions for the $^{13}\text{CO}_i$ - $^{15}\text{N}_{i+1}$ and $^{13}\text{C}_i^\alpha$ - $^{15}\text{N}_i$ dipolar interactions recoupled by REDOR are given by:

$$\omega_i \approx -\frac{4}{\pi} \text{Im}\{\omega_i^{(1)}(\Omega_{\text{PR}}^i)\} \quad i = 1, 2 \quad (5)$$

with

$$\omega_i^{(1)}(\Omega_{\text{PR}}^i) = -b_i \left\{ \sum_{m=-2}^2 D_{0,m}^{(2)}(\Omega_{\text{PC}}^i) D_{m,-1}^{(2)}(\Omega_{\text{CR}}^i) \right\} d_{-1,0}^{(2)}(\beta_{\text{RL}}) \quad (6)$$

where b_i are the $^{13}\text{CO}_i$ - $^{15}\text{N}_{i+1}$ and $^{13}\text{C}_i^\alpha$ - $^{15}\text{N}_i$ dipolar coupling constants (Wigner and reduced Wigner rotation matrices have been defined in Chapter 1). Note that under the experimental conditions employed here the finite pulse effects during REDOR are negligible²⁹ and have been ignored in eq 5.

A series of $^{15}\text{N}_i$ - $^{13}\text{C}_i^\alpha$ - $^{13}\text{CO}_i$ - $^{15}\text{N}_{i+1}$ DQ dephasing curves as a function of the REDOR mixing time were simulated according to eq 3 and are shown in Figure 8-5. The same simulations in the frequency domain are shown in Figure 8-6. The $|\psi| \approx 180^\circ$ simulation displays very distinctive features, and the simulations indicate that the region of optimal angular resolution and sensitivity occurs for small deviations from the *trans* conformation (i.e., $150^\circ < |\psi| < 180^\circ$).

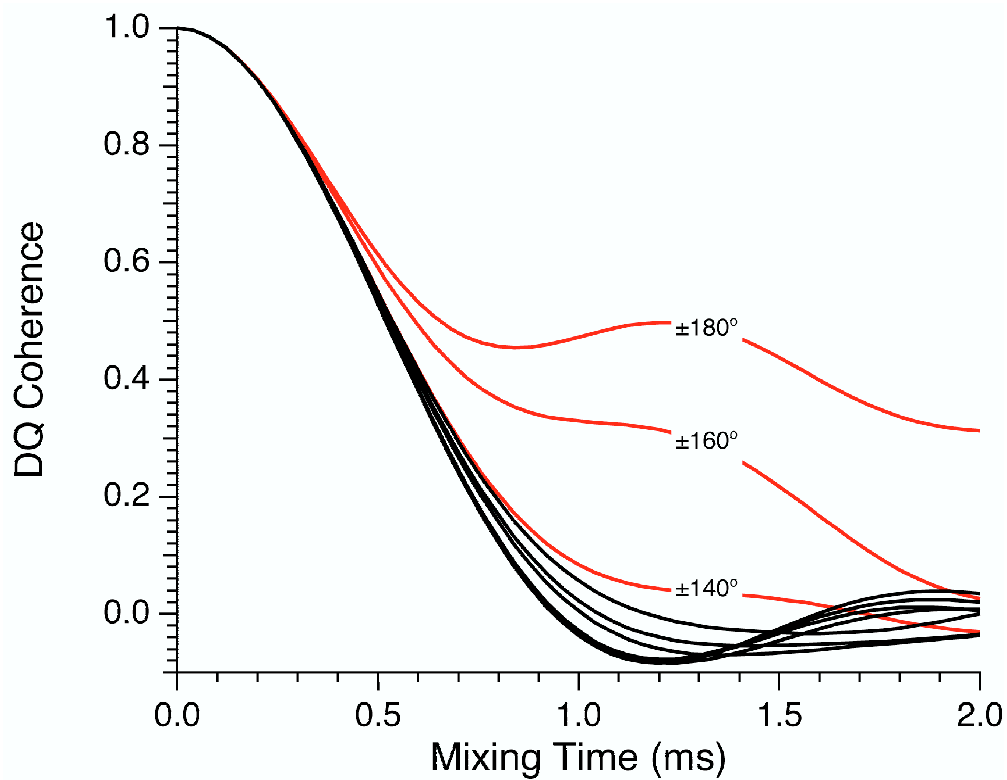


Figure 8-5. Simulated $^{15}\text{N}_i$ - $^{13}\text{C}_i^\alpha$ - $^{13}\text{CO}_i$ - $^{15}\text{N}_{i+1}$ DQ dephasing curves. Dephasing curves were calculated using eq 3 and are shown for $0^\circ < |\psi| < 180^\circ$ in steps of 20° . Note the large dynamic range for torsion angles in the region $150^\circ < |\psi| < 180^\circ$.

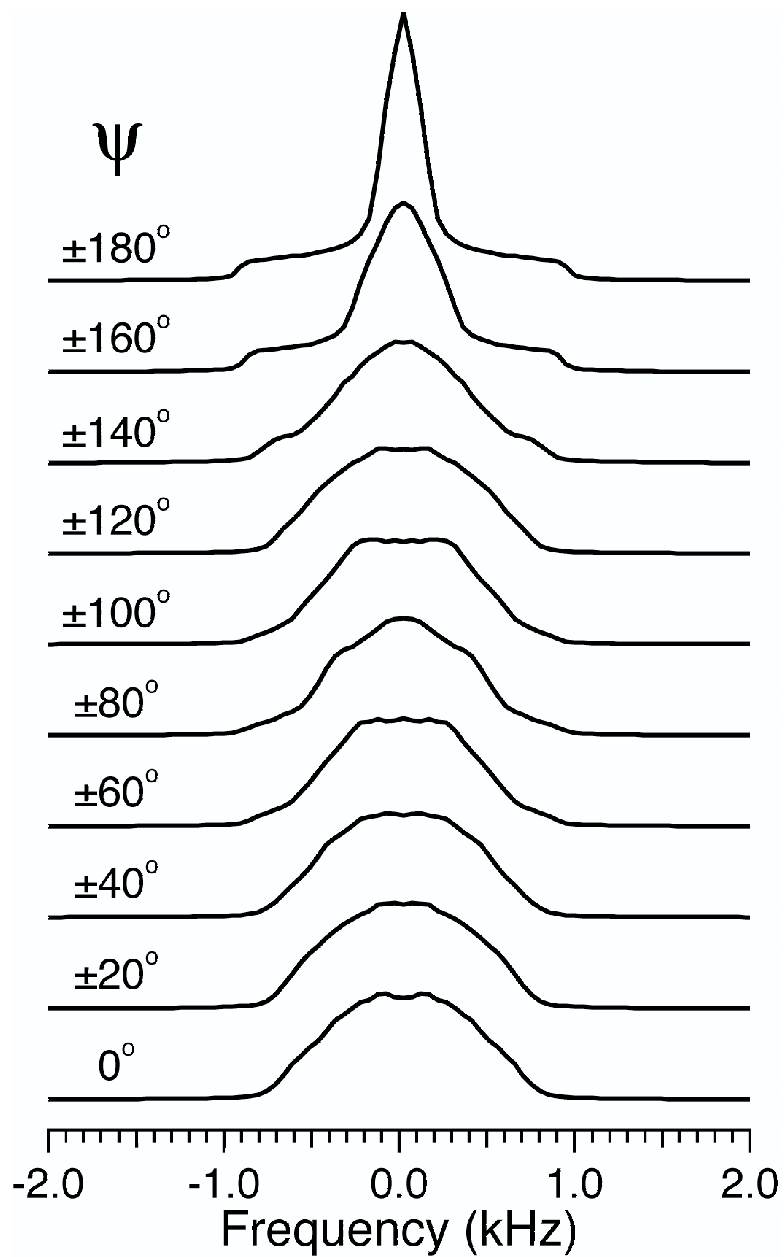


Figure 8-6. $^{15}\text{N}_i\text{-}^{13}\text{C}_i\text{-}^{13}\text{CO}_i\text{-}^{15}\text{N}_{i+1}$ simulations in the frequency domain. Frequency domain simulations shown correspond to the time-domain DQ dephasing curves in Figure 8-5.

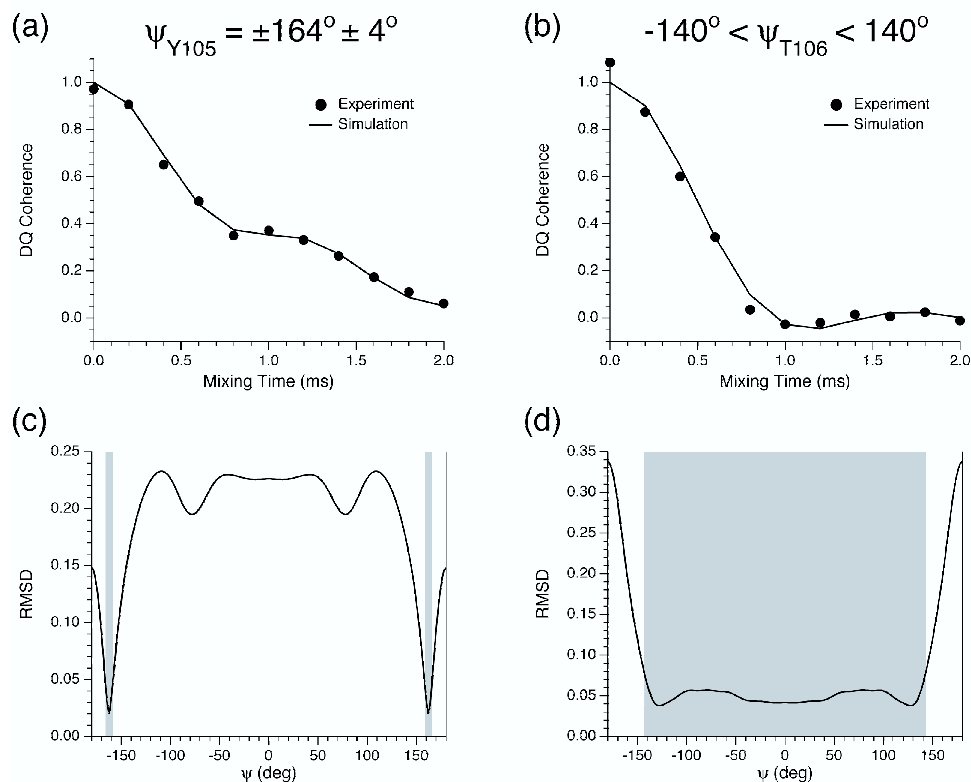


Figure 8-7. $^{15}\text{N}_i\text{-}^{13}\text{C}_i^\alpha\text{-}^{13}\text{CO}_i\text{-}^{15}\text{N}_{i+1}$ measurement of ψ for residues Y105 and T106 in TTR(105-115)_{YTIA} fibrils.

Experimental (●) and simulated (—) DQ dephasing curves are shown for Y105 (a) and T106 (b) residues (each experimental point in (a) and (b) corresponds to the intensity of the CO cross-peak for Y105 and T106, respectively, in the 2D DQ-SQ correlation spectrum shown in Figure 8-4). Also shown are plots of the root-mean-square-deviation (RMSD) as a function of torsion angle ψ for Y105 (c) and T106 (d). The gray rectangles indicate the allowed regions of the torsion angle space based on the $^{15}\text{N}_i\text{-}^{13}\text{C}_i^\alpha\text{-}^{13}\text{CO}_i\text{-}^{15}\text{N}_{i+1}$ measurements (i.e., ψ_{Y105} is confined to two narrow regions around $\psi = \pm 164^\circ$, whereas all solutions between -140° and 140° are permitted for ψ_{T106}). The experiments were performed at 11.7 T and 10 kHz MAS.

Figure 8-7 shows representative results of the $^{15}\text{N}_i\text{-}^{13}\text{C}_i^\alpha\text{-}^{13}\text{CO}_i\text{-}^{15}\text{N}_{i+1}$ experiment for TTR(105-115)_{YTIA} fibrils. The measurements indicate that the N-terminal Y105 residue is close to the fully extended (i.e., $\psi = 180^\circ$) conformation. For the T106 residue the ψ torsion angle ($|\psi| < 140^\circ$) is outside of the region of optimum angular resolution and sensitivity for the $^{15}\text{N}_i\text{-}^{13}\text{C}_i^\alpha\text{-}^{13}\text{CO}_i\text{-}^{15}\text{N}_{i+1}$ experiment (i.e., $150^\circ < |\psi| < 180^\circ$), and hence

could not be precisely defined for this particular system (note that in studies of small peptides with exceptionally high signal-to-noise ratios,^{13,15} a number of torsion angles could be measured with relatively high precision even when the angles were not in the most favorable regions for the particular experiment employed). The $^{15}\text{N}_i\text{-}^{13}\text{C}_i^\alpha\text{-}^{13}\text{CO}_i\text{-}^{15}\text{N}_{i+1}$ experiments indicate that ψ angles for all residues in TTR(105-115) fibrils except Y105 are $< \sim 140^\circ\text{-}150^\circ$ (the torsion angle measurements are summarized in Table 8-1 below). These observations are consistent with the chemical-shift based TALOS³⁰ predictions for the torsion angles presented in Chapter 7,²⁵ which indicate that peptide adopts an extended β -strand conformation in the fibril, characterized by torsion angles $\psi \approx 120^\circ$. Therefore, in order to obtain quantitative measurements for the remaining ψ angles in TTR(105-115) fibrils we have employed a 3D dipolar-chemical shift experiment, which generates correlations between $^{15}\text{N}_{i+1}$ and $^{13}\text{C}_i^\alpha$ sites along the peptide backbone and reports on ψ_i by measuring the relative orientations of the $^1\text{H}_{i+1}^{\text{N}}\text{-}^{15}\text{N}_{i+1}$ and $^{13}\text{C}_i^\alpha\text{-}^1\text{H}_i^\alpha$ dipolar tensors. As will be shown in the following section, the 3D $^1\text{H}_{i+1}^{\text{N}}\text{-}^{15}\text{N}_{i+1}\text{-}^{13}\text{C}_i^\alpha\text{-}^1\text{H}_i^\alpha$ experiment has the region of optimum resolution and sensitivity for $\psi \approx 120^\circ$, in the β -sheet region of the Ramachandran space, and hence is ideally suited for the application to TTR(105-115) fibrils.

8.1.2 3D $^1\text{H}_{i+1}^{\text{N}}\text{-}^{15}\text{N}_{i+1}\text{-}^{13}\text{C}_i^\alpha\text{-}^1\text{H}_i^\alpha$ Spectroscopy

The measurement of the projection angle between $^1\text{H}_{i+1}^{\text{N}}\text{-}^{15}\text{N}_{i+1}$ and $^{13}\text{C}_i^\alpha\text{-}^1\text{H}_i^\alpha$ dipole vectors reports on the ψ_i torsion angle^{13,15,16} and the resulting $^1\text{H}_{i+1}^{\text{N}}\text{-}^{15}\text{N}_{i+1}\text{-}^{13}\text{C}_i^\alpha\text{-}^1\text{H}_i^\alpha$ experiment has the region of optimum resolution and sensitivity for ψ angles in the β -

sheet region of the Ramachandran space. This is apparent in Figure 8-8, which shows the peptide backbone as well as a plot depicting the dependence of the projection angle Θ on the molecular torsion angle ψ . For torsion angles in the range $90^\circ < \psi < 150^\circ$ the projection angle is $\Theta < 30^\circ$, which translates into high angular resolution and sensitivity as described above.

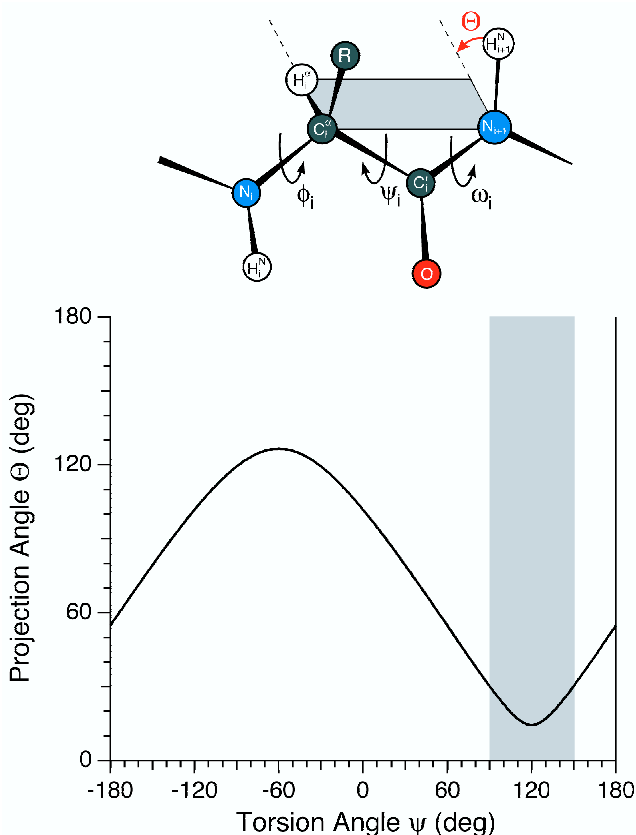


Figure 8-8. Dependence of the projection angle Θ between the $^1\text{H}_{i+1}^{\text{N}}$ - $^{15}\text{N}_{i+1}$ and $^{13}\text{C}_i^{\alpha}$ - $^1\text{H}_i^{\alpha}$ bond vectors on the molecular torsion angle ψ .

The region of high angular resolution and sensitivity of the $^1\text{H}_{i+1}^{\text{N}}$ - $^{15}\text{N}_{i+1}$ - $^{13}\text{C}_i^{\alpha}$ - $^1\text{H}_i^{\alpha}$ experiment (i.e., where Θ is within $\sim 30^\circ$ of the co-linear topology) is indicated by the gray rectangle.

The 3D $^1\text{H}_{i+1}^{\text{N}}$ - $^{15}\text{N}_{i+1}$ - $^{13}\text{C}_i^{\alpha}$ - $^1\text{H}_i^{\alpha}$ pulse sequence used for measurements in TTR(105-115) amyloid fibrils is shown in Figure 8-9. Following ^1H - ^{15}N CP^{20,21} the ^{15}N - ^1H dipolar interactions are reintroduced during MAS using a constant-time transverse MREV (T-

MREV) pulse sequence element¹¹ (in our implementation we have used T-MREV-4 with four C elements per rotor period).^{11-13,15} Subsequently the ^{15}N magnetization is frequency labeled with the isotropic chemical shift in t_1 and transferred to ^{13}CO using band-selective SPECIFIC CP.³¹ The relatively short 3-ms ^{15}N - ^{13}C CP mixing time favors $^{15}\text{N}_{i+1}$ - $^{13}\text{CO}_i$ transfers. Proton-driven ^{13}C - ^{13}C spin-diffusion is used to transfer the ^{13}CO magnetization to ^{13}C nuclei within each residue. The spin-diffusion mixing time is also relatively short (7-ms), which favors ^{13}CO - $^{13}\text{C}^\alpha$ transfers. A second constant-time T-MREV-4 sequence reintroduces ^{13}C - ^1H dipolar interactions, and finally the ^{13}C magnetization is detected in t_2 . The resulting 3D experiment consists of a series of 2D ^{15}N - ^{13}C correlation spectra (not shown), similar to the 2D NCOCX spectra presented in Chapter 7.²⁵ The cross-peaks of interest involve the $^{15}\text{N}_{i+1}$ and $^{13}\text{C}_i^\alpha$ sites, and these cross-peaks are dephased during the period τ , under the local fields due to dipolar couplings to ^1H nuclei. Note that the constant-time period and T-MREV evolution time on the ^{15}N and ^{13}C channels are not independently adjusted. The ^{15}N channel parameters are twice as long as the corresponding ^{13}C parameters due to the fact that the magnitude of the $^{13}\text{C}^\alpha$ - $^1\text{H}^\alpha$ dipolar coupling is approximately twice as large as the ^{15}N - $^1\text{H}^\text{N}$ coupling. This generates the largest interference effects between the $^{13}\text{C}^\alpha$ - $^1\text{H}^\alpha$ and ^{15}N - $^1\text{H}^\text{N}$ couplings in the dipolar dephasing curves and translates into optimum sensitivity.^{13,15} Although the implementation of the 3D $^1\text{H}_{i+1}^\text{N}$ - $^{15}\text{N}_{i+1}$ - $^{13}\text{C}_i^\alpha$ - $^1\text{H}_i^\alpha$ pulse sequence shown in Figure 8-9 has not been described previously to our knowledge, the scheme is a simple modification of previously described 3D ^1H - ^{15}N - ^{13}C - ^1H experiments,^{6,13,15} and is particularly advantageous for the application to TTR(105-115) fibrils because it reduces the congestion in the $^{13}\text{C}^\alpha$ spectral region. An essentially identical pulse sequence (where band-selective SPECIFIC

CP³¹ is used to transfer ¹⁵N magnetization to ¹³C^α instead of ¹³CO and the ¹H-driven ¹³C-¹³C spin-diffusion period is omitted) is used to measure the projection angle between the ¹H_i^N-¹⁵N_i and ¹³C_i^α-¹H_i^α dipole vectors,^{13,15} which can be subsequently related to the torsion angle ϕ_i .^{6,13,15} It can be easily shown⁶ that the resulting ¹H_i^N-¹⁵N_i-¹³C_i^α-¹H_i^α experiment has the region of optimum angular resolution and sensitivity around $\phi_i = -120^\circ$, in the β -sheet region of the Ramachandran space.⁶

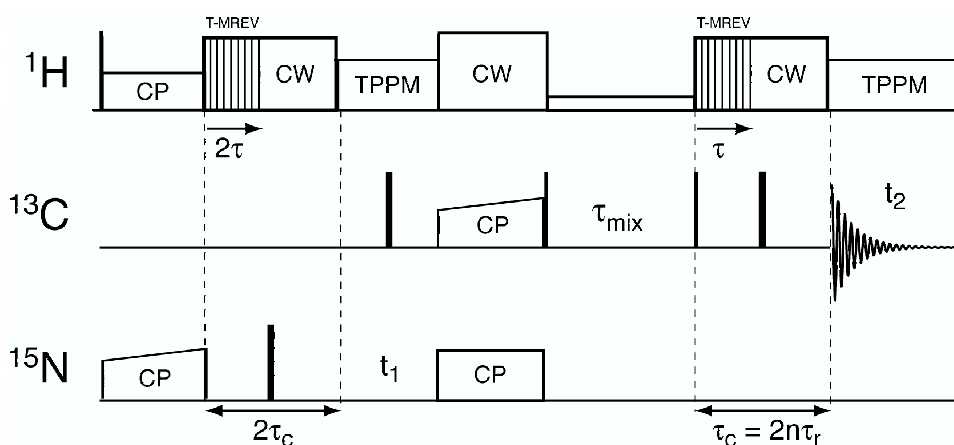


Figure 8-9. 3D ¹H_{i+1}^N-¹⁵N_{i+1}-¹³C_i^α-¹H_i^α pulse sequence for the measurement of ψ_i .

Representative results of the ¹H_{i+1}^N-¹⁵N_{i+1}-¹³C_i^α-¹H_i^α experiment for TTR(105-115)_{Y_{TIA}} fibrils are shown in Figure 8-10. The measurements indicate that ψ_{Y105} is not in the sensitive region of the ¹H_{i+1}^N-¹⁵N_{i+1}-¹³C_i^α-¹H_i^α experiment, which is consistent with the ¹⁵N_i-¹³C_i^α-¹³CO_i-¹⁵N_{i+1} measurement (c.f. Figure 8-7). However, more importantly the dephasing curve for the T106 residue is very characteristic of the ψ angle in the region $90^\circ < \psi < 150^\circ$, expected for an extended β -strand. ¹H_{i+1}^N-¹⁵N_{i+1}-¹³C_i^α-¹H_i^α dephasing curves similar to that for T106, were observed for all remaining residues for which the experiment could be performed, confirming directly that the peptide indeed adopts an extended β -strand conformation in the fibril. The ¹H_{i+1}^N-¹⁵N_{i+1}-¹³C_i^α-¹H_i^α experiment could

not be performed for S112 because it is followed by a Pro residue and for Y114 because S115 was not isotopically labeled. Analogous $^1\text{H}_i^{\text{N}}-^{15}\text{N}_i-^{13}\text{C}_i^{\alpha}-^1\text{H}_i^{\alpha}$ experiments were used to measure the ϕ torsion angles in TTR(105-115) (data not shown), and again indicate an extended β -strand with ϕ angles between $-150^\circ < \phi < -90^\circ$. The torsion angles measurements in TTR(105-115) fibrils are summarized in Table 8-1. The $^1\text{H}-^{15}\text{N}-^{13}\text{C}-^1\text{H}$ simulations have been described elsewhere,^{11,13,15,32} and are not discussed here in detail. In summary, we note that an isotropic $^{15}\text{N}-^{13}\text{C}$ polarization transfer model was assumed, the strongest $^1\text{H}^{\text{N}}-^{15}\text{N}$ and $^{13}\text{C}^{\alpha}-^1\text{H}^{\alpha}$ dipolar interactions were considered, and the simulations included the differential relaxation effects characteristic of T-MREV experiments and described in detail elsewhere.^{11,13,15,32} Furthermore, in the simulations of all torsion angle experiments we have taken into account the potential deviations of the three-atom bond angles from their average values (c.f. Figure 8-1).

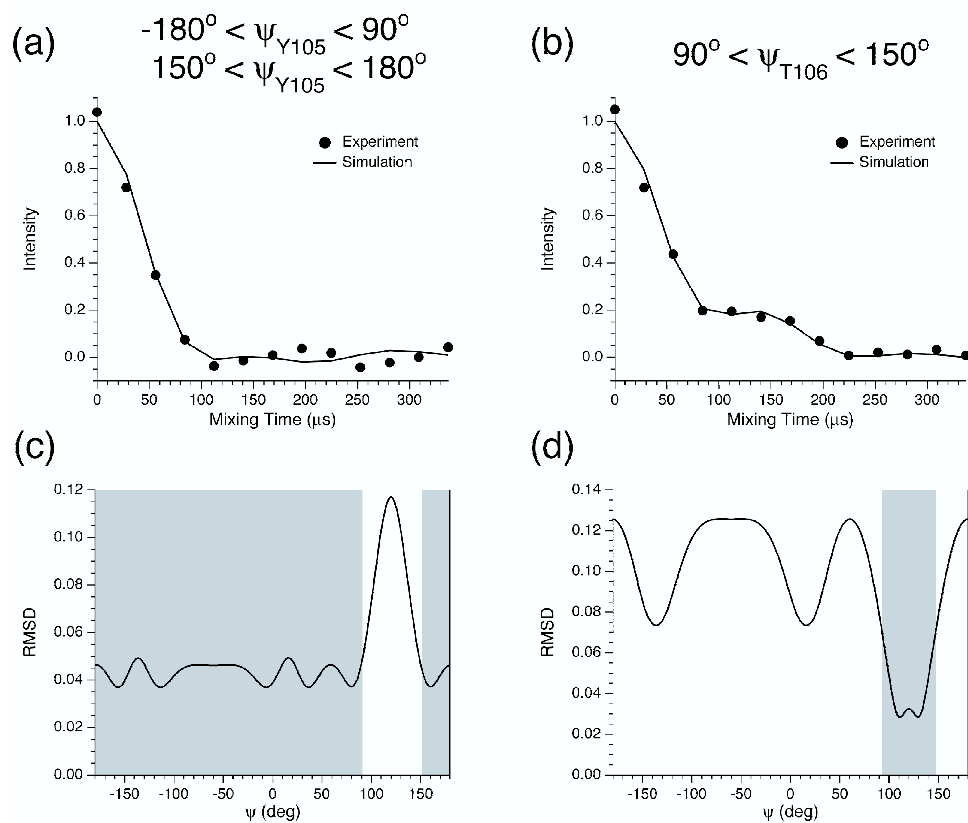


Figure 8-10. ${}^1\text{H}_{i+1}^{\text{N}}-{}^{15}\text{N}_{i+1}-{}^{13}\text{C}_i^{\alpha}-{}^1\text{H}_i^{\alpha}$ measurement of ψ for residues Y105 and T106 in $\text{TTR}(105-115)_{\text{YTTA}}$ fibrils.

Experimental (●) and simulated (—) dephasing curves are shown for Y105 (a) and T106 (b) residues (each experimental point in (a) and (b) corresponds to the intensity of the ${}^{15}\text{N}_{i+1}-{}^{13}\text{C}_i^{\alpha}$ cross-peak in the 2D correlation spectrum). Also shown are plots of the root-mean-square-deviation (RMSD) as a function of torsion angle ψ for Y105 (c) and T106 (d). The gray rectangles indicate the allowed regions of the torsion angle space based on the ${}^1\text{H}_{i+1}^{\text{N}}-{}^{15}\text{N}_{i+1}-{}^{13}\text{C}_i^{\alpha}-{}^1\text{H}_i^{\alpha}$ measurements. The experiments were performed at 11.7 T and 8.903 kHz MAS.

Table 8-1. Backbone torsion angles ϕ and ψ in TTR(105-115) fibrils predicted using TALOS and measured using 3D dipolar-chemical shift correlation experiments.

Residue	ϕ (deg)		ψ (deg)		
	TALOS	H-N _i -C ^α _i -H	TALOS	H-N _{i+1} -C ^α _i -H	N-C ^α _i -CO _i -N
Y105	—	—	—	-180 – 90 150 – 180	-168 – -160 160 – 168
T106	—	-139 – -101	—	90 – 150	-140 – 140
I107	-145 – -105	-143 – -97	131 – 155	90 – 150	-137 – 137
A108	-139 – -95	-142 – -98	120 – 146	92 – 148	-140 – 140
A109	-145 – -117	-141 – -99	111 – 147	90 – 150	-139 – 139
L110	-130 – -94	-139 – -101	104 – 136	90 – 150	-144 – 144
L111	-140 – -96	-140 – -100	122 – 152	90 – 150	-153 – 153
S112	-131 – -87	-139 – -101	109 – 163	—	-146 – 146
P113	-112 – -50	—	107 – 145	90 – 150	-157 – 157
Y114	-139 – -85	-139 – -101	123 – 153	—	—
S115	—	—	—	—	—

Most torsion angles in TTR(105-115) were determined using H-N_i-C^α_i-H (ϕ) and H-N_{i+1}-C^α_i-H (ψ) experiments, which are highly sensitive to variations in the torsion angle for angles in the β -sheet region of the Ramachandran space. Uncertainties for torsion angles determined using H-N_i-C^α_i-H, H-N_{i+1}-C^α_i-H and N-C^α_i-CO_i-N correlation experiments reflect the systematic contributions due to the potential 2-3° variations in the three-atom bond angles¹⁹ (c.f. Figure 8-1), as well as contributions due to random noise (the random contributions are obtained using an *F*-test approach with a 90% confidence limit). For the H-N_i-C^α_i-H and H-N_{i+1}-C^α_i-H experiments these uncertainties lead to the coalescence of pairs of degenerate solutions (about $\phi = -120^\circ$ for H-N_i-C^α_i-H and $\psi = 120^\circ$ for H-N_{i+1}-C^α_i-H) into single minima. The H-N_{i+1}-C^α_i-H in addition assume that $\omega_i = 180^\circ$.

8.2 Carbon-Nitrogen Distance Measurements

About 40 intramolecular carbon-nitrogen distances have been determined in TTR(105-115) fibrils. The majority of the distances were measured in three (U-¹³C,¹⁵N)-labeled fibril samples (c.f. Chapter 7) using the 3D ZF TEDOR experiment,³³ and several

distances were determined using frequency selective REDOR method.³⁴ The majority of the measured distances are in the 2.5-5 Å range, and correspond to correlations between the side-chain ¹³C sites of residue *i* and backbone amide ¹⁵N groups of residues *i* and *i*+1. Since many of these correlations depend on at least one torsion angle they provide important constraints on both the side-chain and the backbone conformations. In Figure 8-11 we show representative 3D ZF TEDOR spectra for TTR(105-115)_{YTIA} fibrils and the buildup curves for cross-peaks between T106 C^β and C^γ and T106 and I107 ¹⁵N. The details of the 3D ZF TEDOR simulations are provided in Chapter 6. The distance measurements are listed in Table 8-2 and displayed in Figure 8-12. Note the relatively low density of distance restraints for the N- and C-terminal residues.

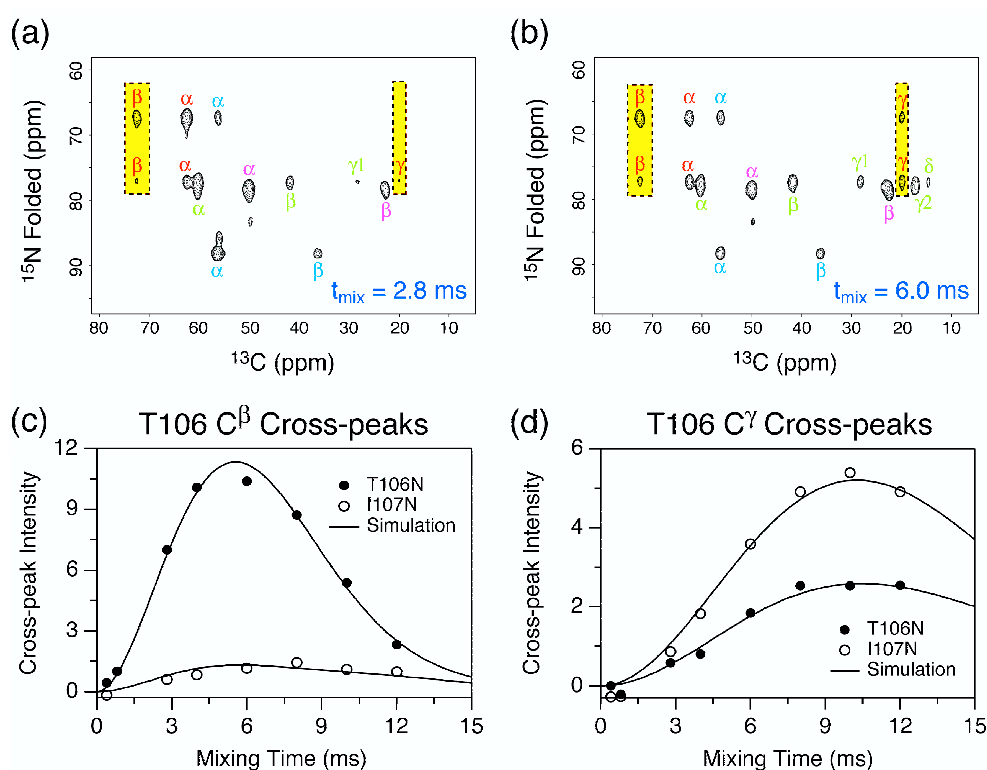


Figure 8-11. 3D ZF TEDOR spectra and buildup curves in TTR(105-115)_{YTIA} fibrils. 2D ¹⁵N-¹³C spectra are shown for TEDOR mixing times of 2.8 (a) and 6.0 ms (b), and experimental (●,○) and simulated (—) buildup curves are shown for T106 C^β (c) and T106 C^γ (d) sites. The experiments were performed at 11.7 T and 10.0 kHz MAS.

Table 8-2. Carbon-nitrogen distances in TTR(105-115) fibrils

Atoms		Distance (Å)	Atoms		Distance (Å)
Y105β	Y105N	2.5 ± 0.25	L110β	L111N	3.6 ± 0.36
	T106N	3.3 ± 0.33	L110δ2*	L110N	4.2 ± 0.42
Y105γ	Y105N	3.18 ± 0.2 [†]		L111N	3.4 ± 0.34
	T106N	> 3.5 [†]	L111β	L111N	2.4 ± 0.24
T106β	T106N	2.6 ± 0.26	L111γ	L111N	3.0 ± 0.3
	I107N	3.5 ± 0.35		S112N	4.6 ± 0.46
T106γ	T106N	3.6 ± 0.36	L111δ1*	L111N	> 3.5
	I107N	3.2 ± 0.32		S112N	> 3.5
I107β	I107N	2.8 ± 0.28	L111δ2*	L111N	3.2 ± 0.32
	A108N	3.4 ± 0.34		S112N	5.5 ± 0.55
I107γ1	I107N	3.1 ± 0.31	P113β	P113N	2.4 ± 0.24
	A108N	4.0 ± 0.4		Y114N	3.7 ± 0.37
I107γ2	I107N	3.8 ± 0.38	P113γ	P113N	2.3 ± 0.23
	A108N	3.1 ± 0.31		Y114N	> 3.5
I107δ	I107N	4.6 ± 0.46	P113δ	S112N	3.2 ± 0.32
	A108N	5.7 ± 0.57		P113N	1.5 ± 0.15
A108β	A108N	2.5 ± 0.25	Y114γ	Y114N	> 2.8 [†]
	A109N	3.5 ± 0.35	A108CO	L110N	4.25 ± 0.15 [‡]
A109β	A109N	2.6 ± 0.26	L111α	L110N	4.56 ± 0.12 [‡]
	L110N	3.3 ± 0.33	S112CO	Y114N	4.06 ± 0.06 [‡]
L110β	L110N	2.7 ± 0.27	S115α	Y114N	5.0 ^{+1.5[‡]} _{-0.5}

Distances were determined using 3D ZF TEDOR³³ unless indicated otherwise. A total of 42 distances were measured (38 sidechain-backbone and 4 backbone-backbone), and 34 distances depend on at least one torsion angle.

*For Leu110 and Leu111, C^{δ1} and C^{δ2} were arbitrarily assigned to the downfield and upfield resonances, respectively.

[†]Y105γ and Y114γ distances were determined using frequency selective REDOR.

[‡]Backbone-to-backbone distances were measured using REDOR in selectively ¹³C, ¹⁵N labeled fibrils.²⁵

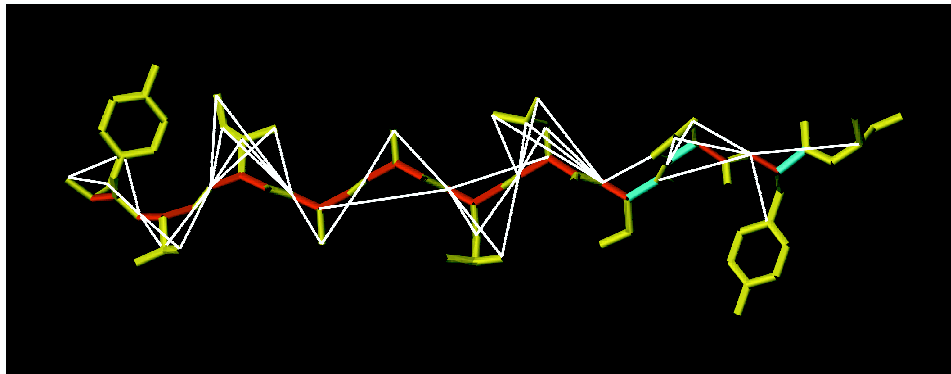


Figure 8-12. Summary of carbon-nitrogen distance restraints in TTR(105-115) fibrils.

A model of the peptide is shown with the measured carbon-nitrogen distances indicated by solid white lines. The majority of the measured distances are in the 2.5-5 Å range (c.f. Table 8-2), and correspond to correlations between the side-chain ^{13}C sites of residue i and backbone amide ^{15}N groups of residues i and $i+1$. Note the relatively low density of distance restraints for the N- and C-terminal residues.

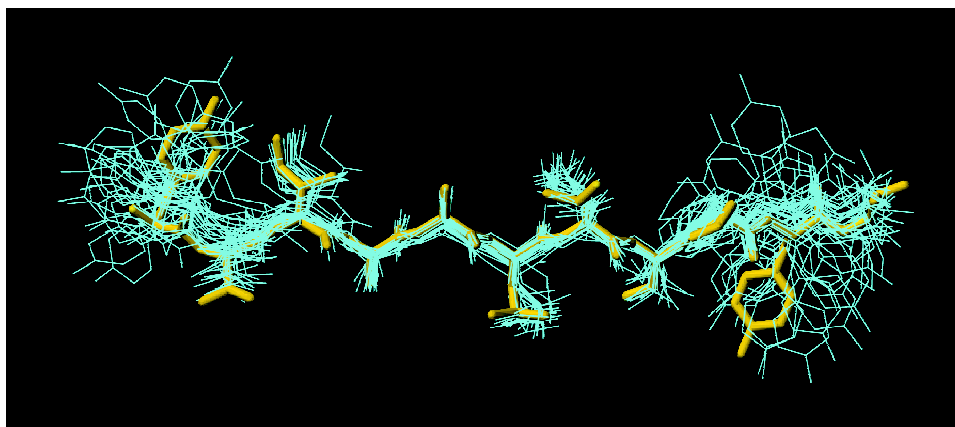


Figure 8-13. Ensemble of 30 atomic-resolution structures of TTR(105-115) in the amyloid fibril consistent with the NMR restraints.

The structures were calculated using a standard simulated annealing molecular dynamics protocol within the CNS program.³⁵ The structures are displayed by aligning the backbone atoms for residues 3-9, and a representative structure is highlighted using thicker bonds. Note that the central region of the peptide, where the density of the NMR restraints is the highest, is most well defined. For the ensemble of structures shown, the RMSD values for all 11 residues are 0.85 Å for the backbone atoms and 1.80 Å for all heavy atoms. For residues 3-9 the corresponding RMSD values are 0.51 Å (backbone) and 0.84 Å (heavy). The figure was prepared using the program MOLMOL.³⁶

8.3 Atomic-Resolution Structure of TTR(105-115)

An ensemble of atomic-resolution structures of TTR(105-115) in the amyloid fibril consistent with the NMR restraints (summarized in Tables 8-1 and 8-2) was calculated using a standard simulated annealing molecular dynamics protocol within the CNS program,³⁵ and is shown in Figure 8-13. We note here that analogous solid-state MAS NMR experiments combined with simulated annealing molecular dynamics were recently used to obtain the atomic-resolution structures of a microcrystalline tripeptide, N-formyl-L-Met-L-Leu-L-Phe,³⁷ and a microcrystalline 62-residue protein, α -spectrin SH3 domain.³⁸ For the ensemble of structures shown in Figure 8-13 the RMSD for all 11 residues is 0.85 Å for the backbone atoms and 1.80 Å for all heavy atoms. For residues 3-9 the corresponding RMSD values are 0.51 Å for the backbone and 0.84 Å for the heavy atoms. The calculated RMSD values are consistent with the fact that the density of NMR restraints is the highest in the central region of the peptide.

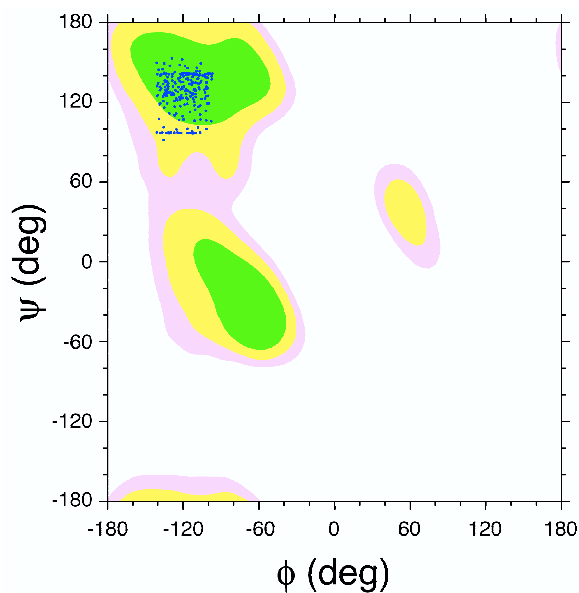


Figure 8-14. Ramachandran plot with (ϕ , ψ) pairs for all residues in the ensemble of 30 calculated structures superimposed.

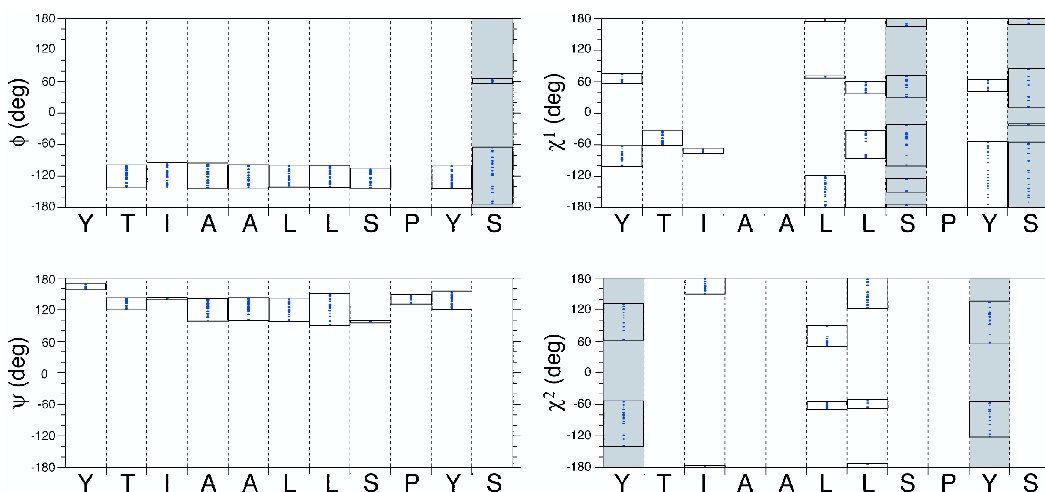


Figure 8-15. Distributions of backbone and side-chain torsion angles for the ensemble of 30 calculated TTR(105-115) structures.

The distributions indicate that the majority of the torsion angles are uniquely defined by the combination of the solid-state NMR measurements and the van der Waals restraints. The gray rectangles indicate torsion angles restrained for which no NMR measurements are available.

Based on all solid-state NMR measurements TTR(105-115) adopts an extended β -strand conformation when incorporated into the amyloid fibril, and the peptide structure appears to be very well-defined. This is summarized in Figure 8-14, which shows the Ramachandran plot with (ϕ, ψ) pairs for all residues in the ensemble superimposed. Distributions of the backbone and side-chain torsion angles for each residue in the ensemble of 30 calculated structures are shown in Figure 8-15. These distributions reflect the experimental uncertainties in the torsion angle measurements and indicate that the majority of the torsion angles are uniquely defined by the combination of the solid-state NMR measurements and van der Waals restraints. Furthermore, for several side-chain torsion angles, which are constrained by a single distance measurement (e.g., χ^1_{Y105}), bimodal angle distributions are observed in the calculated structures. In some of these cases it should be possible to predict the most likely side-chain conformation based on

information from rotamer libraries,³⁹ and these studies are currently in progress. Finally, in Figure 8-16 we compare the measured carbon-nitrogen distances with the distances observed in the ensemble of the calculated structures (for the calculated distances the average between the extremes observed in the ensemble was used). No violations of the experimental distance restraints are observed, and overall the measured and calculated distances are in good agreement (correlation coefficient $R \approx 0.98$). Note that all distances observed in the ensemble of calculated structures are within the experimental error of the measured distances.

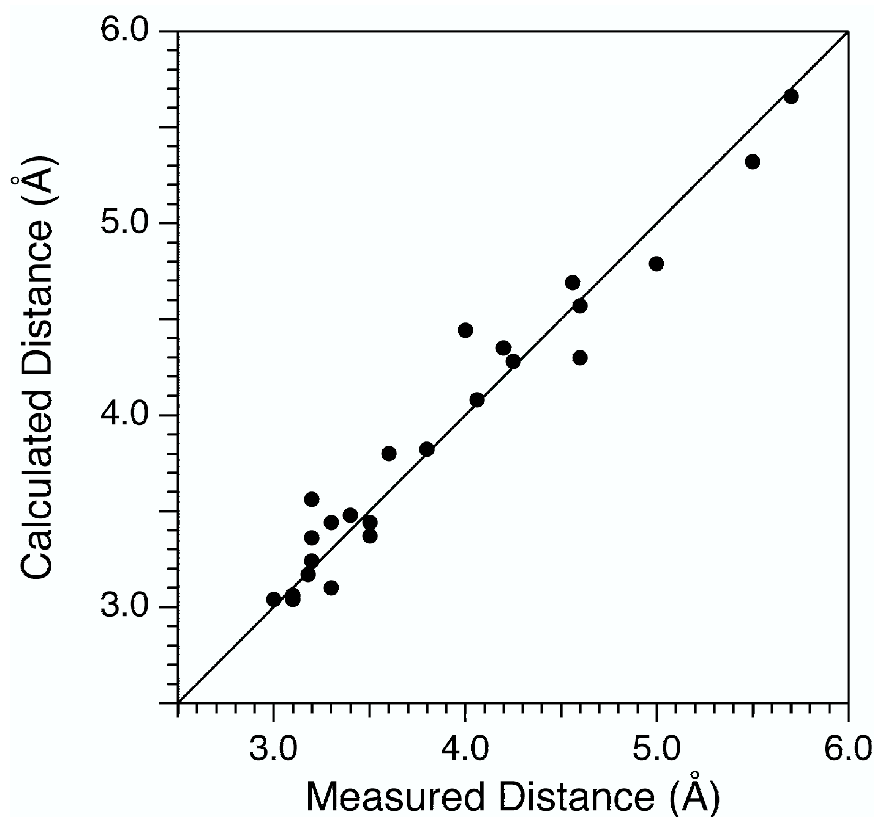


Figure 8-16. Comparison of experimentally determined carbon-nitrogen distances with the corresponding distances observed in the ensemble of 30 calculated TTR(105-115) structures.

8.4 Conclusions

We have determined the atomic-resolution structure of an 11-residue peptide fragment of transthyretin, TTR(105-115), in an amyloid fibril using solid-state MAS NMR spectroscopy and simulated annealing molecular dynamics. A total of about 60 site-specific structural NMR constraints were measured, which consisted of backbone torsion angles ϕ and ψ and carbon-nitrogen distances. The backbone torsion angles were determined using a series of three-dimensional dipolar-chemical shift correlation experiments, which report on the relative orientations of ^{13}C - ^{15}N , ^{13}C - ^1H and ^{15}N - ^1H dipolar tensors. The carbon-nitrogen distances in the 3-5 Å range were determined using REDOR based methods described in this thesis (mainly 3D ZF TEDOR). The results indicate that the peptide adopts an extended β -strand conformation when incorporated into the amyloid fibril.

Acknowledgments

This work was performed in collaboration with Cait MacPhee, Vikram Bajaj, Michel McMahon and Prof. Christopher Dobson. We thank Nathan Astrof, John Gross, Morten Hohwy and Vladimir Ladizhansky for stimulating discussions.

References

- (1) K. Schmidt-Rohr, "A double-quantum solid-state NMR technique for determining torsion angles in polymers," *Macromolecules* **29**, 3975-3981 (1996).
- (2) K. Schmidt-Rohr, "Torsion angle determination in solid ^{13}C -labeled amino acids and peptides by separated-local-field double-quantum NMR," *J. Am. Chem. Soc.* **118**, 7601-7603 (1996).
- (3) R. Tycko, D. P. Weliky and A. E. Berger, "Investigation of molecular structure in solids by two-dimensional NMR exchange spectroscopy with magic angle spinning," *J. Chem. Phys.* **105**, 7915-7930 (1996).
- (4) Y. Ishii, T. Terao and M. Kainosho, "Relayed anisotropy correlation NMR: determination of dihedral angles in solids," *Chem. Phys. Lett.* **256**, 133-140 (1996).
- (5) X. Feng, Y. K. Lee, D. Sandström, M. Eden, H. Maisel, A. Sebald and M. H. Levitt, "Direct determination of a molecular torsional angle by solid-state NMR," *Chem. Phys. Lett.* **257**, 314-320 (1996).
- (6) M. Hong, J. D. Gross and R. G. Griffin, "Site-resolved determination of peptide torsion angle ϕ from the relative orientations of backbone N-H and C-H bonds by solid-state NMR," *J. Phys. Chem. B* **101**, 5869-5874 (1997).
- (7) P. R. Costa, J. D. Gross, M. Hong and R. G. Griffin, "Solid-state NMR measurement of ψ in peptides: a NCCN 2Q-heteronuclear local field experiment," *Chem. Phys. Lett.* **280**, 95-103 (1997).
- (8) X. Feng, M. Eden, A. Brinkmann, H. Luthman, L. Eriksson, A. Gräslund, O. N. Antzutkin and M. H. Levitt, "Direct determination of a peptide torsional angle ψ by double-quantum solid-state NMR," *J. Am. Chem. Soc.* **119**, 12006-12007 (1997).

- (9) M. Hong, J. D. Gross, W. Hu and R. G. Griffin, "Determination of the peptide torsion angle ϕ by ^{15}N chemical shift and $^{13}\text{C}^{\alpha}$ - $^1\text{H}^{\alpha}$ dipolar tensor correlation in solid-state MAS NMR," *J. Magn. Reson.* **135**, 169-177 (1998).
- (10) Y. Ishii, K. Hirao, T. Terao, T. Terauchi, M. Oba, K. Nishiyama and M. Kainosho, "Determination of peptide ϕ angles in solids by relayed anisotropy correlation NMR," *Solid State Nucl. Magn. Reson.* **11**, 169-175 (1998).
- (11) M. Hohwy, C. P. Jaroniec, B. Reif, C. M. Rienstra and R. G. Griffin, "Local structure and relaxation in solid-state NMR: Accurate measurement of amide N-H bond lengths and H-N-H bond angles," *J. Am. Chem. Soc.* **122**, 3218-3219 (2000).
- (12) B. Reif, M. Hohwy, C. P. Jaroniec, C. M. Rienstra and R. G. Griffin, "NH-NH vector correlation in peptides by solid state NMR," *J. Magn. Reson.* **145**, 132-141 (2000).
- (13) C. M. Rienstra, M. Hohwy, L. J. Mueller, C. P. Jaroniec, B. Reif and R. G. Griffin, "Determination of Multiple Torsion-Angle Constraints in U- ^{13}C , ^{15}N -Labeled Peptides: 3D ^1H - ^{15}N - ^{13}C - ^1H Dipolar Chemical Shift NMR Spectroscopy in Rotating Solids," *J. Am. Chem. Soc.* **124**, 11908-11922 (2002).
- (14) V. Ladizhansky, M. Veshtort and R. G. Griffin, "NMR determination of the torsion angle ψ in α -helical peptides and proteins: The HCCN dipolar correlation experiment," *J. Magn. Reson.* **154**, 317-324 (2002).
- (15) C. M. Rienstra, Ph. D. Thesis, Massachusetts Institute of Technology (1999).
- (16) B. Reif, M. Hennig and C. Griesinger, "Direct measurement of angles between bond vectors in high-resolution NMR," *Science* **276**, 1230-1233 (1997).

- (17) D. Yang, R. Konrat and L. E. Kay, "A multidimensional NMR experiment for measurement of the protein dihedral angle ψ based on cross-correlated relaxation between $^1\text{H}^\alpha$ - $^{13}\text{C}^\alpha$ dipolar and $^{13}\text{C}'$ (carbonyl) chemical shift anisotropy mechanisms," *J. Am. Chem. Soc.* **119**, 11938-11940 (1997).
- (18) J. D. Gross, Ph. D. Thesis, Massachusetts Institute of Technology (1998).
- (19) R. A. Engh and R. Huber, "Accurate bond and angle parameters for X-ray protein structure refinement," *Acta Cryst.* **A47**, 392-400 (1991).
- (20) A. Pines, M. G. Gibby and J. S. Waugh, "Proton-enhanced NMR of dilute spins in solids," *J. Chem. Phys.* **59**, 569-590 (1973).
- (21) G. Metz, X. Wu and S. O. Smith, "Ramped-amplitude cross-polarization in magic-angle-spinning NMR," *J. Magn. Reson. A* **110**, 219-227 (1994).
- (22) M. Hohwy, C. M. Rienstra, C. P. Jaroniec and R. G. Griffin, "Fivefold symmetric homonuclear dipolar recoupling in rotating solids: Application to double quantum spectroscopy," *J. Chem. Phys.* **110**, 7983-7992 (1999).
- (23) M. Hohwy, C. M. Rienstra and R. G. Griffin, "Band-selective homonuclear dipolar recoupling in rotating solids," *J. Chem. Phys.* **117**, 4973-4987 (2002).
- (24) A. Bax, R. Freeman and S. P. Kempell, "Natural abundance ^{13}C - ^{13}C coupling observed via double-quantum coherence," *J. Am. Chem. Soc.* **102**, 4849-4851 (1980).
- (25) C. P. Jaroniec, C. E. MacPhee, N. S. Astrof, C. M. Dobson and R. G. Griffin, "Molecular conformation of a peptide fragment of transthyretin in an amyloid fibril," *Proc. Natl. Acad. Sci. USA*, in press (2002).

- (26) T. Gullion and J. Schaefer, "Rotational-echo double-resonance NMR," *J. Magn. Reson.* **81**, 196-200 (1989).
- (27) Y. K. Lee, N. D. Kurur, M. Helmle, O. G. Johannessen, N. C. Nielsen and M. H. Levitt, "Efficient dipolar recoupling in the NMR of rotating solids. A sevenfold symmetric radiofrequency pulse sequence," *Chem. Phys. Lett.* **242**, 304-309 (1995).
- (28) N. C. Nielsen, H. Bildsøe, H. J. Jakobsen and M. H. Levitt, "Double-quantum homonuclear rotary resonance: Efficient dipolar recovery in magic-angle spinning nuclear magnetic resonance," *J. Chem. Phys.* **101**, 1805-1812 (1994).
- (29) C. P. Jaroniec, B. A. Tounge, C. M. Rienstra, J. Herzfeld and R. G. Griffin, "Recoupling of heteronuclear dipolar interactions with rotational-echo double-resonance at high magic-angle spinning frequencies," *J. Magn. Reson.* **146**, 132-139 (2000).
- (30) G. Cornilescu, F. Delaglio and A. Bax, "Protein backbone angle restraints from searching a database for chemical shift and sequence homology," *J. Biomol. NMR* **13**, 289-302 (1999).
- (31) M. Baldus, A. T. Petkova, J. Herzfeld and R. G. Griffin, "Cross polarization in the tilted frame: assignment and spectral simplification in heteronuclear spin systems," *Mol. Phys.* **95**, 1197-1207 (1998).
- (32) M. Hohwy, Ph. D. Thesis, University of Aarhus (1999).
- (33) C. P. Jaroniec, C. Filip and R. G. Griffin, "3D TEDOR NMR experiments for the simultaneous measurement of multiple carbon-nitrogen distances in uniformly ^{13}C , ^{15}N -Labeled Solids," *J. Am. Chem. Soc.* **124**, 10728-10742 (2002).

- (34) C. P. Jaroniec, B. A. Tounge, J. Herzfeld and R. G. Griffin, "Frequency selective heteronuclear dipolar recoupling in rotating solids: Accurate ^{13}C - ^{15}N distance measurements in uniformly ^{13}C , ^{15}N -labeled peptides," *J. Am. Chem. Soc.* **123**, 3507-3519 (2001).
- (35) A. T. Brunger, P. D. Adams, G. M. Clore, W. L. DeLano, P. Gros, R. W. Grosse-Kunstleve, J. S. Jiang, J. Kuszewski, M. Nilges, N. S. Pannu, R. J. Read, L. M. Rice, T. Simonson and G. L. Warren, "Crystallography & NMR system: A new software suite for macromolecular structure determination," *Acta Cryst. D* **54**, 905-921 (1998).
- (36) R. Koradi, M. Billeter and K. Wuthrich, "MOLMOL: A program for display and analysis of macromolecular structures," *J. Mol. Graph.* **14**, 51-55 (1996).
- (37) C. M. Rienstra, L. Tucker-Kellogg, C. P. Jaroniec, M. Hohwy, B. Reif, T. Lozano-Perez, B. Tidor and R. G. Griffin, "De novo determination of peptide structure with solid-state MAS NMR spectroscopy," *Proc. Natl. Acad. Sci. USA* **99**, 10260-10265 (2002).
- (38) F. Castellani, B. van Rossum, A. Diehl, M. Schubert, K. Rehbein and H. Oschkinat, "Structure of a protein determined by solid-state magic-angle spinning NMR spectroscopy," *Nature* **420**, 98-102 (2002).
- (39) R. L. Dunbrack and M. Karplus, "Backbone-dependent rotamer library for proteins: Application to side-chain predictions," *J. Mol. Biol.* **230**, 543-574 (1993).

CURRICULUM VITAE

EDUCATION

Kent State University, B.S. Chemistry summa cum laude 1993-1997
Massachusetts Institute of Technology, Ph.D. Physical Chemistry 1997-2003

HONORS AND AWARDS

National Science Foundation Graduate Fellowship 1997-2000
Graduate Teaching Award, Department of Chemistry, MIT 1998
Phi Beta Kappa 1997

PUBLICATIONS

1. M. Hohwy, C.M. Rienstra, C.P. Jaroniec, R.G. Griffin, Fivefold symmetric homonuclear dipolar recoupling in rotating solids: Application to double quantum spectroscopy, *J. Chem. Phys.* 1999, 110, 7983-7992.
2. C.P. Jaroniec, B.A. Tounge, C.M. Rienstra, J. Herzfeld, R.G. Griffin, Measurement of ^{13}C - ^{15}N distances in uniformly ^{13}C labeled biomolecules: J-decoupled REDOR, *J. Am. Chem. Soc.* 1999, 121, 10237-10238.
3. M. Hohwy, C.P. Jaroniec, B. Reif, C.M. Rienstra, R.G. Griffin, Local structure and relaxation in solid-state NMR: Accurate measurement of amide N-H bond lengths and H-N-H bond angles, *J. Am. Chem. Soc.* 2000, 122, 3218-3219.
4. B. Reif, M. Hohwy, C.P. Jaroniec, C.M. Rienstra, R.G. Griffin, NH-NH vector correlation in peptides by solid-state NMR, *J. Magn. Reson.* 2000, 145, 132-141.
5. C.P. Jaroniec, B.A. Tounge, C.M. Rienstra, J. Herzfeld, R.G. Griffin, Recoupling of heteronuclear dipolar interactions with rotational-echo double-resonance at high magic-angle spinning frequencies, *J. Magn. Reson.* 2000, 146, 132-139.
6. C.P. Jaroniec, B.A. Tounge, J. Herzfeld, R.G. Griffin, Frequency selective heteronuclear dipolar recoupling in rotating solids: Accurate ^{13}C - ^{15}N distance measurements in uniformly ^{13}C , ^{15}N -labeled peptides, *J. Am. Chem. Soc.* 2001, 123, 3507-3519.
7. B. Reif, C.P. Jaroniec, C.M. Rienstra, M. Hohwy, R.G. Griffin, ^1H - ^1H MAS correlation spectroscopy and distance measurements in a deuterated peptide, *J. Magn. Reson.* 2001, 151, 320-327.
8. C.P. Jaroniec, B.A. Tounge, J. Herzfeld, R.G. Griffin, Accurate ^{13}C - ^{15}N distance measurements in uniformly ^{13}C , ^{15}N -labeled peptides, In "Perspectives on Solid State NMR in Biology," S. Kiihne, H.J.M. de Groot, (Eds.), Kluwer, Dordrecht, 2001, 15-21.
9. C.P. Jaroniec, J.C. Lansing, B.A. Tounge, M. Belenky, J. Herzfeld, R.G. Griffin, Measurement of dipolar couplings in a uniformly ^{13}C , ^{15}N labeled membrane protein: Distances between the Schiff base and aspartic acids in the active site of bacteriorhodopsin, *J. Am. Chem. Soc.* 2001, 123, 12929-12930.
10. J.C. Lansing, M. Hohwy, C.P. Jaroniec, A.F.L. Creemers, J. Lugtenburg, J. Herzfeld, R.G. Griffin, Chromophore distortions in the bacteriorhodopsin photocycle: Evolution of the H-C14-C15-H dihedral angle measured by solid-state NMR, *Biochemistry* 2002, 41, 431-438.
11. A.T. Petkova, M. Hatanaka, C.P. Jaroniec, J.G. Hu, M. Belenky, M. Verhoeven, J. Lugtenburg, R.G. Griffin, J. Herzfeld, Tryptophan interactions in bacteriorhodopsin: A heteronuclear solid-state NMR study, *Biochemistry* 2002, 41, 2429-2437.
12. C.M. Rienstra, L. Tucker-Kellogg, C.P. Jaroniec, M. Hohwy, B. Reif, M.T. McMahon, B. Tidor, T. Lozano-Perez, R.G. Griffin, De novo determination of peptide structure with solid-state magic-angle spinning NMR spectroscopy, *Proc. Natl. Acad. Sci. USA* 2002, 99, 10260-10265.
13. C.P. Jaroniec, C. Filip, R.G. Griffin, 3D TEDOR NMR experiments for the simultaneous measurement of multiple carbon-nitrogen distances in uniformly ^{13}C , ^{15}N labeled solids, *J. Am. Chem. Soc.* 2002, 124, 10728-10742.
14. C.M. Rienstra, M. Hohwy, L.J. Mueller, C.P. Jaroniec, B. Reif, R.G. Griffin, Determination of multiple torsion-angle constraints in U- ^{13}C , ^{15}N -labeled peptides: 3D ^1H - ^{15}N - ^{13}C - ^1H dipolar-chemical shift NMR spectroscopy in rotating solids, *J. Am. Chem. Soc.* 2002, 124, 11908-11922.
15. C.P. Jaroniec, C.E. MacPhee, N.S. Astrof, C.M. Dobson, R.G. Griffin, Molecular conformation of a peptide fragment of transthyretin in an amyloid fibril, *Proc. Natl. Acad. Sci. USA* 2002, in press.